Antibiotic permeation through membrane proteins

by

Harsha Bajaj

A Thesis submitted in partial fulfillment

of the requirements for the degree of

Doctor of Philosophy

in Biochemical Engineering

Approved, Dissertation Committee

_____

Prof. Dr. Mathias Winterhalter

_____

Prof. Dr. Roland Benz

_____

Prof. Dr. Matteo Ceccarelli

_____

Prof. Dr. Ulrich F. Keyser

_____

Prof. Dr. Ulrich Kleinekathöfer

Date of Defense: April 22nd , 2015

Statutory Declaration

I, **HARSHA BAJAJ** hereby declare that I have written this PhD thesis independently, unless where clearly stated otherwise. I have used only the sources, the data and the support that I have clearly mentioned. This PhD thesis has not been submitted for conferral of degree elsewhere.

I confirm that no rights of third parties will be infringed by the publication of this thesis.

Bremen, September 21, 2015

Signature _____

Acknowledgements

I would like to take the opportunity to express my gratitude to my supervisor Mathias Winterhalter for giving me a chance to work as a PhD student in his research group. I am grateful for his support and motivation throughout my PhD and Master's studies. I am thankful to him to introduce me to the field of biophysics and lay a foundation stone in my research career. I would like to thank Roland Benz for giving me the chance to work in his lab and for his support and insight on my projects. I am grateful to Matteo Ceccarelli for his collaboration, exciting discussions and assistance throughout my PhD studies. I sincerely thank Ulrich F. Keyser for his collaboration and to host me in his lab. I am thankful to Ulrich Kleinekathöfer for his support. I also extend my appreciation to the committee members for being part of my thesis committee and for their valuable inputs throughout my research.

I would like to thank the TRANSLOCATION consortium, the Innovative Medicines Joint Undertaking under grant agreement 115525, the European Union's seventh framework program (FP7/2007-2013) and Oxford Nanopore Technologies for the financial support.

I would like to thank Pratik Raj Singh for helping me in *Nocardia farcinica* project and for his critical comments and discussions. I thank Ivan Barcena, Satya Prathyusha, Usha Lamichhane, Fatma Dogan and all the wonderful previous and current members of the Winterhalter group for encouraging environment in the lab. I would also like to thank the members of Benz group. I thank all group members of Matteo Ceccarelli especially Igor Bodrenko, Andrea Scorciapino and Giuliano Malloci for being so accessible for scientific discussions. I thank also the members of Keyser group especially Jehangir Cama for his support for microfluidic project. I would like to thank Niraj Modi from Kleinekathöfer group for his collaboration in the *Nocardia farcinica* project. I would like to thank all other colleagues at Jacobs University Bremen. It's been a great pleasure working with all of you.

I would like to thank my friends; Shilpi, Divya, Jenice and Richa for their support and great times. I thank Frauke and Predrag for always being there for me since the time I have come to Bremen. Special thanks to Mahendran for all his support and great discussions.

I thank my grandparents, my uncle, my aunt and whole my family for their blessings. Finally I thank my parents and brother for their support and love, without them I wouldn't be the person I am.

Dedicated in memory of my grandfather (Hanuman Prasad Bajaj)

List of Publications during PhD thesis: 04/2013 – to date

1.   **Bajaj, H.**, Scorciapino, M. A., Moynie, L., Page, M., Naismith, J. H., Ceccarelli, M., Winterhalter, M., Molecular Basis of Filtering Carbapenems by Porins from β-Lactam-resistant Clinical Strains of *Escherichia coli* (submitted).

2.   Cama, J.[*], **Bajaj, H**.[*], Pagliara S, Maier T., Braun Y., Winterhalter, M., Keyser, U. F., Quantification of fluoroquinolone uptake through the outer membrane channel OmpF of *Escherichia coli* (submitted).

3.   Bodrenko, I., **Bajaj, H.**, Ruggerone, P., Winterhalter, M., and Ceccarelli, M. (2015) Analysis of fast channel blockage: revealing substrate binding in the microsecond range. Analyst.

4.   Weichbrodt, C., **Bajaj, H.**, Baaken, G., Wang, J., Guinot, S., Kreir, M., Behrends, J., Winterhalter, M., and Fertig, N. (2015) Antibiotic translocation through porins studied in planar lipid bilayers using parallel platforms. Analyst.

5.   Singh, P. R., **Bajaj, H.**, Benz, R., Winterhalter, M., and Mahendran, K. R. (2015) Transport across the outer membrane porin of mycolic acid containing actinomycetales: Nocardia farcinica. Biochim. Biophys. Acta - Biomembr. 1848, 654–661.

6.   Song, W., **Bajaj, H.**, Nasrallah, C., Jiang, H, Winterhalter, M., Colletier, J.-P., Xu, Y., (2015) Understanding Voltage Gating of Porins from Providencia Stuartii at Atomic Level. PLoS Comput Biol. 11, e1004255.

7.   **Bajaj, H**. Winterhalter, M., Ceccarelli, M. Revealing single antibiotic molecule translocation through biological nanopores (manuscript under preparation).

Publications during MSc study: 09/2011- 04/2013

8. **Bajaj, H.**, Tran, Q.-T., Mahendran, K. R., Nasrallah, C., Colletier, J.-P., Davin-Regli, A., Bolla, J.-M., Pagès, J.-M., and Winterhalter, M. (2012) Antibiotic uptake through membrane channels: role of Providencia stuartii OmpPst1 porin in carbapenem resistance. Biochemistry 51, 10244–9.

Table of Contents

Summary

The outer membrane of bacteria forms an effective barrier; hence hydrophilic antibiotics are known to use porin pathway to reach the target inside the bacterium. With the overuse of antibiotics in clinics, bacteria have evolved to become resistant and one of the ways to do so is to reduce the intake of antibiotics. Increasing antibiotic resistance is recognized as a major public health threat. Introduction of only two new classes of antimicrobials in the past 30 years have aggravated the situation. Antimicrobial drug discovery faces unique challenges, primarily to produce compounds which have sufficient permeation across outer membrane of bacteria. In this regard it becomes indispensable to measure the translocation rate and understand the molecular mechanism of antibiotic transport through porin channel.

In this thesis we investigate two aspects: one to study antibiotic transport across clinically relevant porins and understand their contribution in antibiotic resistance; Second, to elucidate the translocation mechanism of the relevant antibiotics across porins from Gram-negative and Gram-positive bacteria.

In the first part, we studied antibiotic translocation across, major **porin from pathogen *Providencia stuartii*** and **porin mutants from *Escherichia coli* clinical strain**. A multidisciplinary approach, including single channel electrophysiology, liposome permeation assay, microbiological assays and molecular dynamic simulations, provided an understanding of permeability from macro scale to atomic scale.

In the second part of the thesis, we mainly investigate the interaction of β-lactam and fluoroquinolone class of antibiotics with porins from *E. coli* and *Nocardia farcinica* at a single molecule level. An assay based on **fluorescence detection in vesicles in microfluidic chambers** is employed to obtain translocation rate of fluoroquinolone antibiotic across porins in a quantitative manner. Modulating parameters like pH significantly changes the kinetics of norfloxacin through OmpF in electrophysiology. **Voltage dependent transport of antibiotic norfloxacin through single OmpF** is reported and we discuss **different contributions involved in the translocation of antibiotic through channel.**

We conclude that altered permeability across porins contributes to reduced susceptibility. By varying different parameters, like effect of point mutations in antibiotic translocation through channels or varying the charge state of antibiotic, we decipher the rate limiting interactions which might be useful for rational drug designing.

Part 1

Motivation

1.1 Introduction

Antibiotics are one of the most successful forms of chemotherapy in modern medicine. Their use has reduced illness and mortality due to infectious diseases. They are crucial for treating hospital acquired infections mainly occurring during invasive surgery and transplantations in intensive care units. However, since the introduction of antibiotics in clinics; resistance against antibiotics has been a constant threat. For example, penicillin resistant strains of *Staphylococcus aureus* were isolated 2 years after the introduction of penicillin in the market[1]. In the last 50 years this phenomenon has dramatically escalated and today the crisis is epitomized by the spread of multidrug resistant 'ESKAPE' (comprises of *Enterococcus faecium, Staphylococcus aureus, Klebsiella pneumoniae, Acinetobacter baumannii, Pseudomonas aeruginosa, and Enterobacter species)* pathogens or the so called superbugs[2–4]. In some cases, 'ESKAPE' pathogens like *A. baumannii* are also resistant to last resort antibiotics like carbapenems jeopardizing the development of modern techniques in medicine[5–7]. The current situation of antibiotic resistance has worsened by the dearth of new drugs. Nearly all antibiotics in use today are compounds that were discovered during the 1940s to 1960s — the golden era of antibiotic discovery as shown in *Figure 1* [8]. This was followed by a huge innovation gap and by the mid-1990 there was little interest for making more improvements to existing antibiotics.
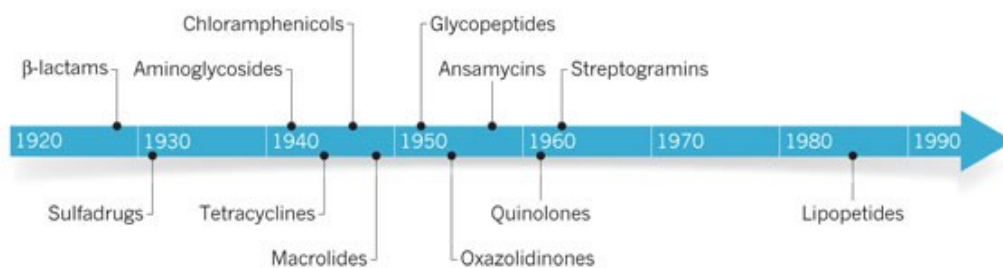

Figure 1: Timeline of the discovery of antibiotics (Reprinted by permission from Macmillan   Publishers Ltd: [Nature] (Lewis, K. Antibiotics: Recover the lost art of drug discovery. Nature 485, 439–40), copyright (2012)).

In 1995, the determination of the complete DNA sequence of a bacterial genome from *Haemophilus influenzae* presented the prospect to explore hundreds of new genes as possible targets. This revived a new interest in antibacterial discovery. Pharmaceutical giants like GlaxoSmithKline (GSK) spent 7 years, evaluating more than 300 genes looking for potential targets and 70 high-throughput screening (HTS) campaigns of individual targets were run[9]. Although inhibitors of targets were readily identified through *in vitro* HTS, it failed mainly due to challenges in identifying compounds that could effectively penetrate bacterial cell wall especially in Gram-negative species[9–12]. The latest discovery of a new antibiotic Teixobactin[13] is a respite which active against the Gram-positive pathogens including the resistance strains. However it is ineffective against most Gram-negative bacteria except for a strain of *E. coli* with a defective outer membrane barrier. This further emphasizes that the battle against antimicrobial resistance is not yet won. In this context, a more collaborative approach is called for to improve the success in antibacterial drug discovery (www.cdc.gov/drugresistance/threat-report-2013). Initiative like "New Drugs 4 Bad Bugs" (ND4BB) (http://www.nd4bb.eu) under the Innovative Medicines Initiative (IMI, www.imi.europa.eu) is launched to address challenges associated with antibacterial drug discovery and development[14].

Antibiotic resistance mechanisms

The main mechanisms by which bacteria gains resistance to antimicrobials are diverse and mainly classified into four fundamental mechanisms as shown in *Figure 2*[15]. A major mechanism of resistance involves the enzyme catalyzed inactivation of the antibiotics[16–18]. Target protection barrier forms another mechanism for resistance which is achieved through mutations that affect the intracellular target for a given antimicrobial drug[19–21]. Additionally, bacteria can evade the action of antibiotics by actively expelling the antibiotic out of the cells in a process termed efflux[22–25].
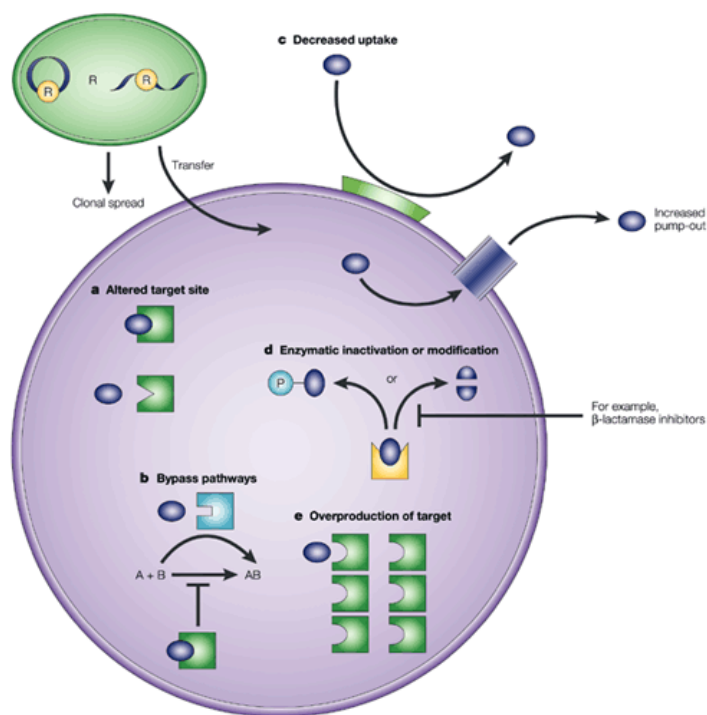
Figure 2: Mechanisms of antibiotic resistance[15] (Reprinted by permission from Macmillan Publishers Ltd: [Nature Reviews Drug Discovery] (Coates, A., Hu, Y., Bax, R. & Page, C. The future challenges facing the development of new antimicrobial drugs. Nat. Rev. Drug Discov. 1, 895-910), copyright (2002). http://www.nature.com/

Efflux mechanism together with reduced entry of the antibiotic into the bacterial cell due to porins comprises the membrane barrier mechanism[22,25,26]. One of the first reports on influx related resistance to β-lactams, is due to diminished levels of porin encoded by *ompF* gene from *Escherichia coli* [27].

The clinical evidence for the different strategies that are involved in reducing influx across the outer membrane is outlined in *Figure 3*[22,26,28]. Three kinds of bacterial responses have been documented as shown in *Figure 3*: One, Controlling the porin level in the outer membrane by changing the expression of porins; Two, Controlling the porin type by selecting the expressed porin which is more restricted; Three, Expressing a mutated porin with restricted channel activities.
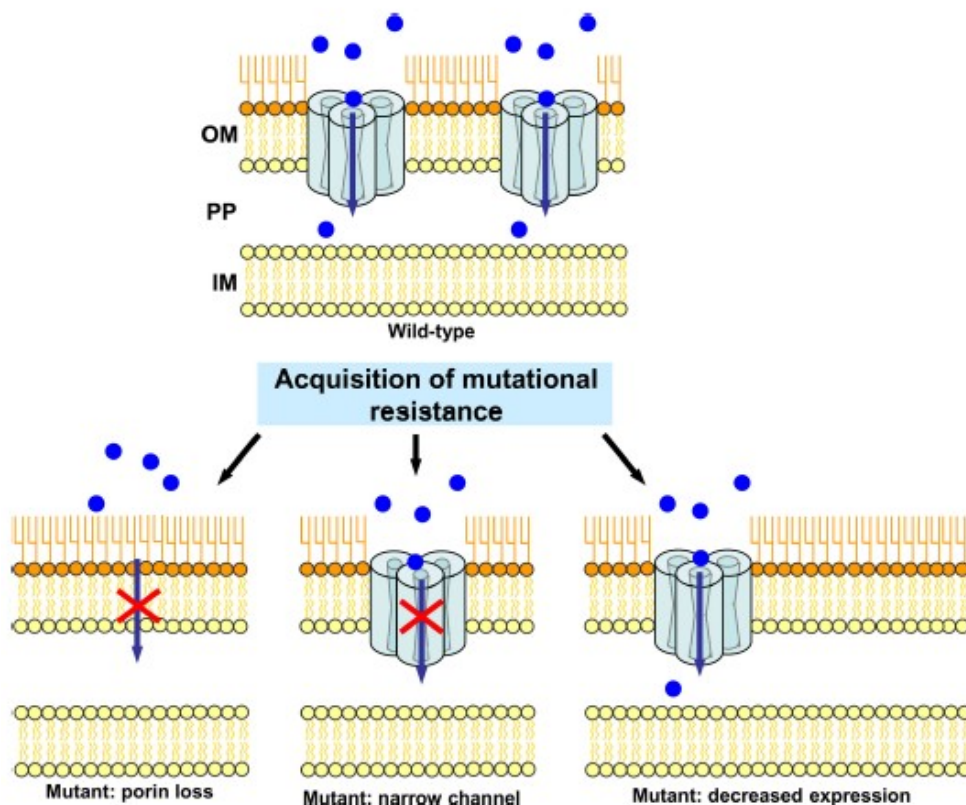
Figure 3: Various resistance mechanisms associated with porin modification[22]. (Reprinted by permission from American Society for Microbiology: [Clinical Microbiology Reviews] (Fernández, L. & Hancock, R. E. W. Adaptive and mutational resistance: role of porins and efflux pumps in drug resistance. Clin. Microbiol. Rev. 25, 661–81), copyright (2012)).

Porin-related mutations substantially affect resistance to β-lactams like in Enterobacteriaceae family. For example one study reported altered porin expression profile in the isolates of *Enterobacter aerogenes* collected over a 1-year period in which 6.4% were highly β-lactam-resistant (20 strains out of 311) [29]. Another mechanism used by Gram-negative bacteria to dodge the influx of antibiotic is the modulation of porin type synthesis. The expression of the narrow-channel like OmpC type porin is generally favored in the human body, with the in situ conditions of temperature and osmolarity. This porin naturally restricts the entry of large charged molecules which points to a major step in antibiotic uptake and leads to a decreased susceptibility [30,31]. Antibiotic resistance can also occur due to mutations that affect the proper function of porins. Modified porins have been identified in *E. coli, Neisseria gonorrhoeae, P. aeruginosa, E. aerogenes, K. pneumoniae* and *Haemophilus influenzae*[32–35]. For instance, a G-to-D mutation in a

putative loop3 of the OmpF/OmpC-like protein of *E. aerogenes* leads to a reduction of conductance of the pore and, additionally a decreased susceptibility to β-lactams[33]. This loop 3 is a characteristic feature of such channels(OmpF/C porins or homologs), which folds back into the lumen of the channel to form a constriction zone and is the narrowest part within the pore [36]. Several other modifications in the constriction zone have been reported to change the permeability of substrates like antibiotics[34,37].In this regard, it is very tempting to investigate the permeation of antibiotics across porins.

The pore forming properties of these porins and interactions with antibiotics are quantified by measuring ion current through channel inserted in a planar lipid bilayer[38–40]. Single porin channels are reconstituted into virtually solvent free lipid bilayer and ionic currents are generated through an open channel by applied transmembrane voltage. Addition of antibiotic to the system interrupts the passage of ions reflecting antibiotic-channel interactions[39]. Time resolved ion current blockages caused by antibiotics are interpreted as single-molecule event and the analysis helps to deduce the underlying kinetic parameters of antibiotic translocation[38].

In my thesis, we use **single channel electrophysiology** as a main technique to reveal porin-antibiotic interactions. We use permeation assays and microbiological assays together with molecular dynamics to get an idea on transport of antibiotics. We measure permeation of antibiotics across porin embedded giant unilamellar vesicles using fluorescence. Additionally we overcome the limitations of time resolution in electrophysiology by introduction of new analysis methods. In the next section we look at the scope of the thesis.

1.2 Scope of my thesis

In the first part of the thesis we elucidate the role of porins in uptake of β-lactam antibiotics and its relation to bacterial susceptibility.

In **chapter 1,** we mainly characterized two carbapenem molecules, imipenem and meropenem through major porin of an opportunistic pathogen *P. stuartii*. In **chapter 2**, porin mutants from clinical strains of *E. coli* were characterized for their permeability of carbapenem antibiotics. In both chapters, we employ an integrative approach to investigate the permeability of these antibiotics across porins. We study the interaction of antibiotics through porins at a single channel level using electrophysiology and together with molecular dynamics simulations reveal

the molecular pathway. To differentiate binding from translocation of antibiotics in the channel liposome swelling assay are performed. Microbiological assays provide information on the relation of permeability of antibiotic in the cell to its susceptibility.

In the second part of the thesis we investigate the translocation of antibiotics across porins from Gram-negative and Gram-positive bacteria. Novel aspects of antibiotic permeation through porins are revealed using electrophysiology and liposome based assays.

In **Chapter 3,** we investigate the transport of antibiotics across porins of *E. coli* and provide new insights. An alternate label-free fluorescence based detection assay is employed to measure the direct translocation rate of antibiotics through porins. Another major part of my work was to perform single channel electrophysiology measurements and screen the interaction of different classes of antibiotics through OmpF/C porins from *E. coli.* For the first time, we report voltage driven translocation of different charged forms of norfloxacin through OmpF. We modulated different parameters like pH and salt concentration to elucidate the translocation pathway of antibiotics.

In chapter 4, we deal with aspect of improving the time resolution of electrophysiology technique. Here, we introduced a modified power spectrum analysis method which can detect events in the range of a few microseconds. Additionally, a comparative study of three different bilayer systems is provided, to reveal an optimal setup in terms of their time and noise resolution.

Chapter 5 mainly deals with the transport properties of porin from Gram-positive *N. farcinica*. We mainly characterized the channel and solute transport like sugars and antibiotics through the pore. Mutations in *N. farcinica* porin were created to study extensively the effect on uptake of substrates like antibiotics.

References

1.   Kirby, W. M. Extraction of a highly potent Penicillin inactivator from Penicillin resistant Staphylococci. *Science* **99,** 452–3 (1944).

2.   Boucher, H. W. *et al.* Bad bugs, no drugs: no ESKAPE! An update from the Infectious Diseases Society of America. *Clin. Infect. Dis.* **48,** 1–12 (2009).

3.   Spellberg, B. *et al.* The epidemic of antibiotic-resistant infections: a call to action for the medical community from the Infectious Diseases Society of America. *Clin. Infect. Dis.* **46,** 155–64 (2008).

4.   Pablos-Méndez, A. *et al.* Global surveillance for antituberculosis-drug resistance, 1994-1997. World Health Organization-International Union against Tuberculosis and Lung Disease Working Group on Anti-Tuberculosis Drug Resistance Surveillance. *N. Engl. J. Med.* **338,** 1641–9 (1998).

5.   Higgins, P. G., Dammhayn, C., Hackel, M. & Seifert, H. Global spread of carbapenem-resistant Acinetobacter baumannii. *J. Antimicrob. Chemother.* **65,** 233–8 (2010).

6.   Johnson, A. P. & Woodford, N. Global spread of antibiotic resistance: the example of New Delhi metallo-β-lactamase (NDM)-mediated carbapenem resistance. *J. Med. Microbiol.* **62,** 499–513 (2013).

7.   Voulgari, E., Poulou, A., Koumaki, V. & Tsakris, A. Carbapenemase-producing Enterobacteriaceae: now that the storm is finally here, how will timely detection help us fight back? *Future Microbiol.* **8,** 27–39 (2013).

8.   Lewis, K. Antibiotics: Recover the lost art of drug discovery. *Nature* **485,** 439–40 (2012).

9.   Payne, D. J., Gwynn, M. N., Holmes, D. J. & Pompliano, D. L. Drugs for bad bugs: confronting the challenges of antibacterial discovery. *Nat. Rev. Drug Discov.* **6,** 29–40 (2007).

10.   Gwynn, M. N., Portnoy, A., Rittenhouse, S. F. & Payne, D. J. Challenges of antibacterial discovery revisited. *Ann. N. Y. Acad. Sci.* **1213,** 5–19 (2010).

11.   Lewis, K. Platforms for antibiotic discovery. *Nat. Rev. Drug Discov.* **12,** 371–87 (2013).

12.   Wright, G. D. The antibiotic resistome: the nexus of chemical and genetic diversity. *Nat. Rev. Microbiol.* **5,** 175–86 (2007).

13.   Ling, L. L. *et al.* A new antibiotic kills pathogens without detectable resistance. *Nature* **517,** 455–9 (2015).

14.   Stavenger, R. A. & Winterhalter, M. TRANSLOCATION project: how to get good drugs into bad bugs. *Sci. Transl. Med.* **6,** 228ed7 (2014).

15.   Coates, A., Hu, Y., Bax, R. & Page, C. The future challenges facing the development of new antimicrobial drugs. *Nat. Rev. Drug Discov.* **1,** 895–910 (2002).

16.   Redgrave, L. S., Sutton, S. B., Webber, M. A. & Piddock, L. J. V. Fluoroquinolone resistance: mechanisms, impact on bacteria, and role in evolutionary success. *Trends Microbiol.* **22,** 438–45 (2014).

17.   Nordmann, P., Dortet, L. & Poirel, L. Carbapenem resistance in Enterobacteriaceae: here is the storm! *Trends Mol. Med.* **18,** 263–72 (2012).

18.   Queenan, A. M. & Bush, K. Carbapenemases: the versatile beta-lactamases. *Clin. Microbiol. Rev.* **20,** 440–58, table of contents (2007).

19.   Blair, J. M. A., Webber, M. A., Baylay, A. J., Ogbolu, D. O. & Piddock, L. J. V. Molecular mechanisms of antibiotic resistance. *Nat. Rev. Microbiol.* **13,** 42–51 (2014).

20.   Unemo, M. *et al.* High-level cefixime- and ceftriaxone-resistant Neisseria gonorrhoeae in France: novel penA mosaic allele in a successful international clone causes treatment failure. *Antimicrob. Agents Chemother.* **56,** 1273–80 (2012).

21.   Leclercq, R. Mechanisms of resistance to macrolides and lincosamides: nature of the resistance elements and their clinical implications. *Clin. Infect. Dis.* **34,** 482–92 (2002).

22.   Fernández, L. & Hancock, R. E. W. Adaptive and mutational resistance: role of porins and efflux pumps in drug resistance. *Clin. Microbiol. Rev.* **25,** 661–81 (2012).

23.   Ball, P. R., Shales, S. W. & Chopra, I. Plasmid-mediated tetracycline resistance in Escherichia coli involves increased efflux of the antibiotic. *Biochem. Biophys. Res. Commun.* **93,** 74–81 (1980).

24.   McMurry, L., Petrucci, R. E. & Levy, S. B. Active efflux of tetracycline encoded by four genetically different tetracycline resistance determinants in Escherichia coli. *Proc. Natl. Acad. Sci. U. S. A.* **77,** 3974–7 (1980).

25.   Nikaido, H. Molecular basis of bacterial outer membrane permeability revisited. *Microbiol. Mol. Biol. Rev.* **67,** 593–656 (2003).

26.   Pagès, J.-M., James, C. E. & Winterhalter, M. The porin and the permeating antibiotic: a selective diffusion barrier in Gram-negative bacteria. *Nat. Rev. Microbiol.* **6,** 893–903 (2008).

27.   Harder, K. J., Nikaido, H. & Matsuhashi, M. Mutants of Escherichia coli that are resistant to certain beta-lactam compounds lack the ompF porin. *Antimicrob. Agents Chemother.* **20,** 549–52 (1981).

28.   *Bacterial and Eukaryotic Porins*. (Wiley-VCH Verlag GmbH & Co. KGaA, 2004). doi:10.1002/3527603875

29.   Charrel, R. N., Pagès, J. M., De Micco, P. & Mallea, M. Prevalence of outer membrane porin alteration in beta-lactam-antibiotic-resistant Enterobacter aerogenes. *Antimicrob. Agents Chemother.* **40,** 2854–8 (1996).

30. Medeiros, A. A., O'Brien, T. F., Rosenberg, E. Y. & Nikaido, H. Loss of OmpC porin in a strain of Salmonella typhimurium causes increased resistance to cephalosporins during therapy. *J. Infect. Dis.* **156,** 751–7 (1987).

31. Doumith, M., Ellington, M. J., Livermore, D. M. & Woodford, N. Molecular mechanisms disrupting porin expression in ertapenem-resistant Klebsiella and Enterobacter spp. clinical isolates from the UK. *J. Antimicrob. Chemother.* **63,** 659–667 (2009).

32. Baquero, F. Low-level antibacterial resistance: a gateway to clinical resistance. *Drug Resist. Updat.* **4,** 93–105 (2001).

33. Dé, E. *et al.* A new mechanism of antibiotic resistance in Enterobacteriaceae induced by a structural modification of the major porin. *Mol. Microbiol.* **41,** 189–98 (2001).

34. Olesky, M., Hobbs, M. & Nicholas, R. A. Identification and analysis of amino acid mutations in porin IB that mediate intermediate-level resistance to penicillin and tetracycline in Neisseria gonorrhoeae. *Antimicrob. Agents Chemother.* **46,** 2811–20 (2002).

35. Arbing, M. A., Hanrahan, J. W. & Coulton, J. W. Altered channel properties of porins from Haemophilus influenzae: isolates from cystic fibrosis patients. *J. Membr. Biol.* **189,** 131–41 (2002).

36. Cowan, S. W. *et al.* Crystal structures explain functional properties of two E. coli porins. *Nature* **358,** 727–33 (1992).

37. Lou, H. *et al.* Altered antibiotic transport in OmpC mutants isolated from a series of clinical strains of multi-drug resistant E. coli. *PLoS One* **6,** e25825 (2011).

38. Nestorovich, E. M., Danelon, C., Winterhalter, M. & Bezrukov, S. M. Designed to penetrate: time-resolved interaction of single antibiotic molecules with bacterial pores. *Proc. Natl. Acad. Sci. U. S. A.* **99,** 9789–94 (2002).

39. Danelon, C., Nestorovich, E. M., Winterhalter, M., Ceccarelli, M. & Bezrukov, S. M. Interaction of zwitterionic penicillins with the OmpF channel facilitates their translocation. *Biophys. J.* **90,** 1617–27 (2006).

40. Raj Singh, P., Ceccarelli, M., Lovelle, M., Winterhalter, M. & Mahendran, K. R. Antibiotic permeation across the OmpF channel: Modulation of the affinity site in the presence of magnesium. *J. Phys. Chem. B* **116,** 4433–4438 (2012).

Part 2

Role of porins in antibiotic resistance

Chapter 1: Antibiotic uptake through porins of *Providencia stuartii*

Previously in 2010 (Tran Q.-T et. al. J. Biol. Chem. 2010, 285), two porins OmpPst1 and OmpPst2 of *P. stuartii* were characterized. The study suggested a prominent role of OmpPst1 porin in the antibiotic uptake of *P. stuartii*. The bacterium showed susceptibility to majority of clinically relevant antibiotics like meropenem a carbapenem antibiotic except for imipenem. This became the motivation, to investigate the relation between antibiotic permeability through porin and its resistance in bacteria (Part P2.1.1). This investigation is the outcome of a close collaboration between our group in Bremen and the group of Prof. Dr. Jean-Marie Pagès (Clinical Microbiology).

Additionally the crystal structure of both the porins were revealed (manuscript under review) by Dr. Jacques-Philippe Colletier. The biophysical characterization of the porins revealed that OmpPst2 showed channel gating at voltages as low as 20mV. Part P2.1.2 gives the molecular interpretation of gating observed in experiments.

P2.1.1: Role of OmpPst1 in carbapenem resistance

Reprinted with permission from America Chemical Society

Bajaj, H., Tran, Q.-T., Mahendran, K. R., Nasrallah, C., Colletier, J.-P., Davin-Regli, A., Bolla, J.-M., Pagès, J.-M., and Winterhalter, M. (2012) Antibiotic uptake through membrane channels: role of Providencia stuartii OmpPst1 porin in carbapenem resistance. Biochemistry 51, 10244–9

Individual Contribution

My main contribution in this manuscript is to perform experiments and analysis of data from single channel electrophysiology and liposome swelling assays. I participated in the composition of manuscript.

This work was performed and published during my Master's study.

The manuscript is attached in the annex at the end of the thesis.

P2.1.2: Voltage Gating of *Providencia stuartii* Porins at Atomic Level

Song W, Bajaj H, Nasrallah C, Jiang H, Winterhalter M, Colletier J-P, et al. (2015) Understanding Voltage Gating of Providencia stuartii *Porins at Atomic Level. PLoS Comput Biol 11(5): e1004255. doi:10.1371/journal.pcbi.1004255*

Individual Contribution

My main contribution in this manuscript is: performing experiments and analysis of data from single channel electrophysiology. I participated in the composition of manuscript.

The manuscript is attached in the annex at the end of the thesis.

Chapter 2: Permeation of carbapenems through OmpC porin

In this work, we study a series of OmpC porin mutants obtained from resistant *E. coli* isolates from a patient during serial antibiotic treatment (Low A. S. et. al. Mol. Microbiol. 2001, 42). Subsequently in 2011(Lou H. et. al. PLoS One 2011, 6) the group from Prof. Dr. James Naismith (in the IMI consortium) reported crystal structures of all the four OmpC mutants and surprisingly did not observe any major changes in the pore size. In the current work we investigated the permeability properties of different antibiotics through these four mutants and understand its correlation to resistance. The molecular explanation for difference in permeability is provided using MD simulations by group of Prof. Dr. Matteo Ceccarelli. The work of this chapter is performed under the IMI-Translocation project.

P2.2.1: Selective penetration of small molecules through Gram-negative outer cell wall channels at molecular level: Quantification of the rate limiting interaction of carbapenem with OmpC.

Manuscript to be submitted

Individual Contribution

My main contribution in this manuscript is to design the study, to perform experiments and analysis of data from single channel electrophysiology and liposome swelling assays. I participated in the composition of manuscript.

Molecular Basis of Filtering Carbapenems by Porins from β-Lactam-resistant Clinical Strains of *Escherichia coli*

Harsha Bajaj [a], Mariano A. Scorciapino [b], Lucile Moynie [c], Malcolm G. P. Page [d], James H. Naismith [c], Matteo Ceccarelli [b], and Mathias Winterhalter [a]

[a]School of Engineering and Sciences, Jacobs University Bremen, Campus Ring 1, 28759, Bremen, Germany

[b]Department of Physics, University of Cagliari, S.P. Monserrato-Sestu km 0.700, I-09042 Monserrato, CA, Italy

[c]Biomedical Sciences Research Complex, University of St. Andrews, St. Andrews, Fife, UK

[d]Basilea Pharmaceutica International Ltd, Grenzacherstr. 487, CH-4058 Basel, Switzerland

Running title: *Transport properties of clinically relevant porin mutants*

To whom correspondence should be addressed: Prof. Mathias Winterhalter, School of Engineering and Sciences, Jacobs University Bremen, Campus Ring 1, 28759, Bremen, Germany, Telephone/FAX: +49 421 200 3248; E-mail: m.winterhalter@jacobs-university.de and Prof. Matteo Ceccarelli, Department of Physics, University of Cagliari, S.P. Monserrato-Sestu km 0.700, I-09042 Monserrato, CA, Italy, Telephone: +39 070 675 4933; FAX: +39 070 675 3191;Email:matteo.ceccarelli@dsf.unica.it

Background: Gram-negative bacteria frequently acquire resistance to antibiotics through porin mutations.

Results: Mutations inside the OmpC porin channel decrease carbapenem uptake by trapping the antibiotic in an unfavorable orientation.

Conclusion: Antibiotic dipole alignment along the channel's electric field, compensating entropic factors and overcoming steric barriers, accelerates translocation.

Significance: A general strategy to screen antibiotics for enhanced uptake has been identified.

ABSTRACT

Integral membrane proteins known as porins are the major pathway by which hydrophilic antibiotics cross the outer membrane of Gram-negative bacteria. Single point-mutations in porins can decrease the permeability of an antibiotic, either by reduction of channel size or modification of electrostatics in the channel, and thereby confer clinical resistance. Here, we investigate four mutant OmpC

proteins from four different clinical isolates of *Escherichia coli* obtained sequentially from a single patient during a course of antimicrobial chemotherapy. OmpC porin from the first isolate (OmpC20) undergoes three consecutive and additive substitutions giving rise to OmpC26, OmpC28 and finally OmpC33. The permeability of two zwitterionic carbapenem molecules, imipenem and meropenem measured using liposome permeation assays and single channel electrophysiology, differ significantly between OmpC20 and OmpC33. Molecular dynamic simulations show that the antibiotics must pass through the constriction zone of porins with a specific orientation, where the antibiotic dipole is aligned along the electric field inside the porin. We identify that changes in the vector of the electric field in the mutated porin, OmpC33, create an additional barrier by "trapping" the antibiotic in an unfavourable orientation in the constriction zone that suffers steric hindrance for the reorientation needed for its onward translocation. Identification and understanding the underlying molecular details of such a barrier to translocation will aid in the design of new antibiotics with improved permeation properties in Gram-negative bacteria.

Bacteria that are resistant to multiple antibiotics, the so-called superbugs, are one of the most challenging problems faced by modern medicine (1, 2). An important parameter for antibiotic efficacy is the accumulation of sufficient antibiotic in the correct location to cause metabolically significant inhibition (1). Target-based approaches to identifying novel, potent inhibitors have frequently failed, in part due to lack of permeability of the compounds particularly for Gram-negative bacteria (3, 4). Porins are known to be responsible for the uptake of several classes of hydrophilic antibiotics, e.g. β-lactams (5–9). Consequently, bacterial resistance to such antibiotics is frequently observed to include reduced influx through porins as one of the main mechanisms. Mutational changes in porins have been linked to stepwise increases in clinical and *in vivo* antibiotic resistance of Gram-negative pathogens (6, 9–11). Dé *et. al.* (12) described a clinical *Enterobacter aerogenes* isolate exhibiting increased resistance to cephalosporins where they observed mutations in the major porin that resulted in drastic reduction of the channel diameter (13). This modification was strongly associated with restricted translocation of antibiotics through the porins and hence conferred resistance to the *E. aerogenes* isolates (12). In another study, seven *E. coli* strains, isolated during two years of treatment of a patient suffering from Caroli syndrome, showed progressively greater antibiotic resistance to the antibiotics used for treatment, including imipenem, meropenem, cefotaxime, ceftazidime and ciprofloxacin (14). There was significant increase in the minimum inhibitory concentrations (MICs) of meropenem (MEM) and imipenem (IPM), for which the MICs increased 32-fold between the third (MEM 0.125 mg/L; IPM 0.5 mg/L) and the seventh (last) isolate (MEM 4 mg/L; IPM 8 mg/L) (10, 14–16). Lou *et. al.* (17) reported crystal structures of four OmpC mutants from the above study: OmpC20 from the first isolate (present in 1st, 2nd and 3rd isolate), OmpC26 with a D18E substitution (present in 4th isolate), OmpC28 with D18E and S271 F

substitutions (found in 5th isolate) and OmpC33 with all D18E, S271F and R124H substitutions (found in 6th and 7th isolates) (14). These mutations did not result in major changes in channel size or ion conductivity (17). The authors suggested that, in contrast to the obvious exclusion due to reduced channel size, effects such as changes in the electric field at the constriction zone might have an impact on the channel permeability (17). Recent computational and experimental studies also suggested that the electrostatic profile inside the channel might play a major role in transit of polar molecules (18, 19). Subsequently, the internal electrostatics of the mutant porins (OmpC20 and OmpC33) were analyzed using water as a probe to sense the internal electric field (20).

In this report we investigate the effect of point mutations on the predicted internal electric field and investigate how these changes correlate with the changes observed in antibiotic uptake among the porin variants. Permeation assays in proteoliposomes and single channel electrophysiology performed with purified mutant porins confirm decreasing permeability among the variants and correlate with the lower antibiotic susceptibility observed *in vivo*. Molecular dynamics suggests a molecular mechanism for this behavior and thus provides a rationale for the design of new antibiotics with improved translocation rates.

EXPERIMENTAL METHODS

Bacterial Strains and Plasmids- Mutant *E. coli* strains lacking porins (22) transformed with vectors containing respective *ompC* genes were used for protein expression and purification as described previously (17).

Solvent-free Lipid Bilayer Measurements- Reconstitution experiments and noise analysis were performed as described previously in detail (23). The Montal and Muller technique was used to form phospholipid bilayer using 1,2-diphytanoyl-*sn*-glycero-3-phosphocholine (Avanti polar lipids) (24). A Teflon film comprising an aperture of approximately 30-60 μm diameters was placed between the two chambers of the Teflon cuvette. The aperture was prepainted with 1% hexadecane in hexane for stable bilayer formation. 1 M KCl (or 200 mM KCl), 20 mM MES, pH 6 was used as the electrolyte solution and added to both sides of the chamber. Ion currents were detected using standard silver-silver chloride electrodes from WPI (World Precision Instruments) that were placed in each side of the cuvette. Single channel measurements were performed by adding the protein to the *cis* side of the chamber (side connected to the ground electrode). Spontaneous channel insertion was typically obtained while stirring under an applied voltage (ranging from 100- 200mV). After successful single channel reconstitution, the *cis* side of the chamber was carefully perfused to remove any remaining porins to prevent further channel insertions. Conductance measurements were performed using an Axopatch 200B amplifier (Molecular Devices) in the voltage clamp mode. Signals were filtered by an on-board, low-pass Bessel filter at 10 kHz and with a sampling frequency set to 50 kHz. Amplitude, probability, and noise analyses were performed using Origin pro 8 (OriginLab) and Clampfit software (Molecular devices). Single-channel analysis was used to determine the antibiotic binding kinetics. In a single-channel measurement, the typical measured parameters were the duration

of blocked levels/residence time (τ_c) and the frequency of blockage events (v). The association rate constant, k_{on}, was derived using the number of blockage events, $k_{on} = $ v/3[c], where c is the concentration of antibiotic. The dissociation rate constant, k_{off}, was determined by averaging the $1/\tau_c$ values recorded over the entire concentration range.

Liposome Swelling Assays- Swelling assays were performed as described previously with slight modification (25, 26). In brief, 2 mg of *E. coli* total lipid extract (Avanti polar lipids) were used to form a lipid film that was dried for several hours. The film was resuspended in 20 mM MES pH 6 (200 µL) (control) or buffer (200 µL) including 1 µg of protein to be reconstituted into the liposome and a thin film was made in a water bath at 45 °C. The lipid-protein mixture was dried under vacuum for several hours and the film was resuspended in 20 mM MES pH 6 (600 µL) containing 5% dextran (Applichem; MW 40,000) by slowly adding the later to the side of the test-tube and gently rotating the tube to wet the film. The tubes were left at room temperature for 60 min, shaken by hand and left for another 60 min. The concentrations of test solute were adjusted so that diluents were apparently isotonic with control liposomes. Stachyose (Fluka) and raffinose (Fluka) were also tested with proteoliposomes to confirm the isotonicity of the multilamellar liposomes. All the test solutions were made to isotonic concentrations using an Osmomat 30 osmolarimeter (Gonotec, Berlin, Germany). Liposome or proteoliposome solution (30 µL) was diluted into 630 µL of an isotonic test/solute solution made in 20 mM MES pH 6 buffer in a 1 mL cuvette and mixed manually. The change in absorbance at 500 nm was monitored using a Cary-Varian UV−vis spectrophotometer in the kinetic measurement mode. The swelling rates were calculated as the change in absorbance min^{-1} which reflects swelling of liposomes. The rates are taken as averages from at least five different sets of experiments, as described previously (27) .

Molecular Dynamics Simulations- The trimeric OmpC20 (PDB ID: 2XE2) and OmpC33 (*vide infra*) were embedded in a pre-equilibrated planar phospholipid bilayer constituted by 260 1-palmitoyl-2-oleoyl-*sn*-glycero-3-phosphocholine (POPC) molecules. Since only poor resolution data are available for OmpC33, the X-ray coordinates of OmpC28 (PDB ID: 2XE3) were used, after introducing the substitution R124H. Then, a cubic simulation box was set up by adding water molecules and the proper number of ions needed to counterbalance the protein net charge. The system was oriented in order to position the center of mass of the protein at the origin of the coordinate system and to align the channels with respect to the z-axis (positive z: extracellular side; negative z: periplasmic side). After 1 ps of energy minimization, a slow heating from 10 to 300 K was carried out for 1.5 ns in the isothermal-isobaric (NPT) ensemble of the program NAMD (28). During this stage, positional restraints were applied on the protein alpha-carbons (all three dimensions) as well as on the phosphorus atoms of the lipids (z only, during the first 0.5 ns). Then, an equilibration stage follows for 6 ns in the NPT ensemble at 1.0 bar and 300 K without any restraint. Finally, 400 ns MD simulations were performed in the NVT ensemble using the ACEMD code (29) designed for GPUs.

The NPT equilibration was performed with 1.0 fs time-steps   and treating long-range

electrostatics with the Soft Particle Mesh Ewald (SPME) method (64 grid points and order 4 with direct cutoff at 1.0 nm and 1.0 Å grid-size). Pressure control was applied using the Nose-Hoover method (extended Lagrangian) with isotropic cell, integrated with the Langevin Dynamics (200 fs and 100 fs of piston period and decay, respectively). The latter was also applied for temperature control with 200 fs thermostat damping time. The ACEMD code for the NVT ensemble allowed to rescale hydrogen mass to 4 amu and to increase the time-step to 4.0 fs (30). The Langevin thermostat was used with a 1 ps damping coefficient. SPME was used to treat electrostatics as done during the equilibration stage. Molecular dynamics simulations were performed employing the Amber99SB-ILDN force field (31) for the protein and lipids, and the TIP3P (32) for waters.

General AMBER force field (GAFF) parameters (33) were used to describe imipenem and meropenem. Partial atomic charges were evaluated according to the Restrained Electrostatic Potential (RESP) approach (34): the molecule was first optimized at the HF/6-31G(d) level up to a convergence in energy of 10^{-5} au, using the Gaussian03 package (35). Atomic RESP charges were derived from the electrostatic potential using the antechamber module of the AMBER package (36).

The antibiotic was placed inside the lumen of the first monomer of the final configuration of the porin simulation. The difference between the z-coordinate of the center of mass of the antibiotic two-ring system and the z-coordinate of the center of mass of the protein monomer was +12.5 Å. A thousand steps of energy minimization were performed. The equilibration stage followed for 1 ns in the NVT ensemble at 300 K as before. Well-tempered metadynamics (37, 38) simulation (100-400 ns) was performed with the ACEMD code, until the first effective translocation through the porin constriction region was observed. Then, four configurations were randomly selected, two with the antibiotic located in the extracellular vestibule and two with it in the periplasmic vestibule. Correspondingly, four multiple-walkers (39) were set to extend the metadynamics reconstruction of the free-energy surface (FES). To achieve this, two biased, collective variables were used, namely, the antibiotic position and orientation inside the porin. In practice, the 'position' Δz was defined as the difference between the z-coordinate of the center of mass of the antibiotic two-ring system and that of the porin monomer. A change in this quantity might be straightforwardly related to the antibiotic reorientations by which its main axis of inertia is rotating. The 'orientation' was defined on the basis of the orientation of the rigid two-ring system, as the difference of the z-coordinate between the lactam carbonyl carbon and the sulfur bonded carbon. 4x400 ns were run, arriving to a total simulation time of 1.7-2.0 μs for each of the investigated cases. During the metadynamics, energy biases were added every 2.0 ps to each collective variable (height 0.2 kcal/mol; σ 0.3 and 0.05 Å for position and orientation, respectively). Well-tempered ΔT was 3000 K. The conformers of each of labeled region in FES were selected through a statistical analysis performed on all the conformers corresponding to the selected FES region, as

the conformer with the lowest average root mean square deviation from all the other.

RESULTS

In the current study we have investigated the transport properties of series of OmpC clinical porin mutants. The trimeric porin variant from the first isolate (OmpC20) embedded in a lipid bilayer is shown in Fig. 1a (front view) and 1b (top view). The substitutions acquired in the subsequent isolates are presented in Fig. 1c, that depicts the monomer from the last porin variant, OmpC33. The translocation rate and mechanism of the carbapenems imipenem and meropenem, whose electrostatic potentials are represented in Fig. 1d and 1e, was studied through the two porin variants OmpC20 and OmpC33.

Liposome Permeation Assay - The rate of diffusion of antibiotics through OmpC mutant porins was determined by measuring the change in optical density of multilamellar liposomes in the presence of an isotonic concentration of antibiotics. To normalize the flux, we used raffinose (MW 504.4 g/mol) and stachyose (MW 666.5 g/mol), both sugars that are too large to diffuse through these porins, and arabinose (MW 150 g/mol), a small sugar that diffuses very rapidly through the channel. The swelling rates of all test solutes were normalized to the diffusion rate of arabinose (100%). Approximately 1 μg of OmpC20 or OmpC33 was reconstituted in the liposomes. For the liposomes reconstituted with OmpC20, imipenem had a relative diffusion rate of 41%, noticeably higher than the relative diffusion rate (24%) into liposomes reconstituted with OmpC33 porin (Fig. 2). The relative diffusion rate of meropenem into liposomes reconstituted with OmpC20 (46%) was similar to that of imipenem, whereas meropenem exhibited poor or no permeation into the liposomes reconstituted with OmpC33 (Fig. 2).

Single Channel Electrophysiology - The planar lipid bilayer technique was used to study the interaction of antibiotics with OmpC20, OmpC26, OmpC28 and OmpC33 at a single molecule level. The conductance values obtained for all four porins were around 2.6 ± 0.3 nS, as reported previously (17). All the porin mutants had slightly asymmetric conductance values, with slightly higher conductance at positive voltage. In the absence of antibiotics, there were negligible fluctuations in the ion currents of single OmpC20 and OmpC33 channels (Fig. 3a, 3d). Ion current fluctuations caused by antibiotic addition to either the *cis* side (extracellular side), or *trans* side (periplasmic side) of the four OmpC mutants, are quantified in Table 1. Addition of 2.5 mM imipenem to *cis* side of OmpC20, caused rapid, unresolved ion current flickering (Fig. 3b). In contrast, addition of imipenem to OmpC33 caused well-resolved full blockages with a lower frequency of fluctuation compared to OmpC20 upon *cis* addition (Fig. 3e). We observed that the binding of imipenem to OmpC20 in the presence of 200mM KCl had asymmetric kinetics (Table 1), with the association rate for addition at the *cis* side being an order of magnitude higher than that for addition on the *trans* side. In contrast, imipenem binding to OmpC33 had symmetric association rates (Table 1). The residence time of the antibiotic was at the resolution limit (about 40 μs) for both the channels. Single channel

measurements were also performed in the presence of 1M KCl, to obtain a better signal-to- noise ratio. At this concentration, the trend was broadly similar to that observed at 200mM KCl, with the association rate being higher in OmpC20 compared to OmpC33 (Table 2). At high salt concentration, the association rate for *cis* side addition of imipenem to OmpC20 was reduced by a factor of 3 compared to low salt concentration (Table 2), whereas in OmpC33, the imipenem association rate was similar to that observed in 200mM KCl. The dissociation rate constants did not differ significantly from those observed in 200mM KCl (Table 2). The expected flux of antibiotic was estimated based on the *cis* side association rate using a simplified model (40). A sharp decrease in association rate of imipenem (by almost a factor of 9) between OmpC26 and OmpC28 was observed in electrophysiology (Table 2). This is an interesting point since imipenem was introduced into the regime prior to the isolation of strain 5, expressing OmpC28. The host strain shows a significantly higher MIC (IPM   2 mg/L) compared to isolate 4 expressing OmpC26 (IPM MIC 0.25 mg/L) (14). In the case of imipenem, the flux decreased in the order OmpC20 > OmpC26 >> OmpC28 ≈ OmpC33, with   a factor of 35 from OmpC20 to OmpC33 in 200mM KCl (Table 1) and a factor of 15 in 1M KCl.

In the case of meropenem, well-resolved partial monomer blockages with both OmpC20 and OmpC33 were observed (Fig. 3c and 3f). However, no significant differences between the association rates of meropenem with OmpC20 or OmpC33 were observed at 200mM KCl and 1M KCl (Table 1 and Table 2). Asymmetric kinetics were obtained when meropenem was added in asymmetric manner to both the porins (Table 1). The association rate was higher by 2 orders of magnitude on *cis* addition compared to *trans* addition. In this case, the flux did not vary significantly between all the four mutants measured (Table 1). The k_{on} of meropenem slightly decreased in presence of 200mM KCl compared to 1M KCl for both the porins and the k_{off} values were similar in the presence of both salts (Table 2).

Molecular Dynamics Simulations- The free energy surface (FES) and molecular pathway of imipenem and meropenem diffusion through the OmpC20 and OmpC33 channels were studied (Fig. 4). The highest free energy values were observed at the constriction region (-5 Å < Δz < +5 Å) in all cases, in agreement with previous reports (17, 41). Different minima along the minimum energy path were analyzed in detail to identify the rate-limiting interactions and are labeled with consecutive numbers in Fig. 4. The barriers that were analyzed are marked with asterisks. Imipenem and meropenem were found to be most likely to cross the constriction region with their positively charged nitrogen pointing downwards (represented as positive values on the x-axis of the FES) in both porins. However, while the minimum energy path of both carbapenems is rather straight in OmpC33 (following the path from 1 to 5), a marked reorientation was found just above the constriction region in OmpC20.

Interestingly, the antibiotic reorientations observed along the minimum energy path inside the channel were found to follow the ordering of water molecules described recently (20). This was particularly remarkable in the constriction region, where

the intrinsic electric field is strongest, suggesting that the minimum energy path is characterized by the translocation occurring with the antibiotic dipole aligned with the channel electric field. For example, the water choreography reported previously for OmpC20 is shown in Fig. 4e (20). The vectors along the channel z axis (from 30 Å to -30 Å) represent the normalized electric net dipole of the water molecules in different sections of the channel. Fig. 4f shows meropenem in the FES minimum 3 (i.e. at the constriction region), with its electric dipole clearly aligned with the net dipole of the water molecules at the same depth inside OmpC20.

According to the ordering of water inside these channels, both OmpC20 and OmpC33 are characterized by an abrupt change of the internal charge distribution (20). Such a change can be clearly observed in Fig. 4e by looking at the vectors n.5 and n.6 that have opposite orientations. This position inside the lumen is particularly critical, corresponding to the transit from the extracellular vestibule to the more restricted region of the channel (20).

Fig. 5 shows the representative conformer of meropenem in each of the FES regions (Fig. 4b, d) analyzed along the minimum energy path. By taking the main molecular axis of the antibiotic as a reference for its reorientations inside the channel, these movements can be conveniently described as longitudinal or transversal with respect to the direction of translocation (porin z axis). Longitudinal reorientations in the constriction region of both OmpC20 and OmpC33 are prevented by steric hindrance. Meropenem maintains its long axis almost parallel to the direction of translocation, adjusting its position by transverse reorientations only in order to align

its electric dipole to the channel electrostatics as well as to find partners to form H-bonding interactions (see below).

The most remarkable difference between the two porins pertains to the transit from the extracellular vestibule down to the constriction region. A large longitudinal reorientation was observed only in OmpC20. In both porins, meropenem is 'pre-oriented' in the extracellular vestibule, with the electric dipole pointing in the opposite direction to that adopted in the constriction region. In OmpC20 (Fig. 5a) such adverse orientation is 'corrected' before entering the constriction region through a marked longitudinal reorientation. In OmpC33, (Fig. 5b) the antibiotic approaches the critical zone in an unfavorable orientation and undergoes a major transverse reorientation at the mouth of constriction region.

Fig. 6 shows the representative conformer of imipenem in each of the FES regions (Fig. 4a, c) analyzed along the minimum energy path. The same general scenario as described for meropenem was observed. The antibiotic points towards the overall negatively charged constriction region with its positively charged group. It is adversely pre-oriented by the channel electrostatics in the extracellular vestibule and needs to reorient its dipole to favorably enter the constriction region. Marked longitudinal reorientations are only observed in OmpC20. In OmpC33 imipenem starts reorienting its dipole at the mouth of the constriction region through a severe transverse reorientation. When in the constriction region, longitudinal reorientations are hindered and the antibiotic adjusts its position mostly through transverse reorientations. For the sake of completeness, antibiotic-specific features

also have taken into consideration: imipenem is smaller than meropenem and its side chain is more flexible. Thus, imipenem exhibits a higher plasticity in the constriction region than the more rigid and straight meropenem.

Finally, it is interesting to note the presence of the minimum labeled by the arrow in the FES of both imipenem and meropenem in OmpC33 (Fig. 4c, d). This specific minimum is fairly accessible in OmpC33 and corresponds to the antibiotic entering the constriction region with a wrong orientation, such that translocation would require a marked reorientation inside the constriction area with a rather high energy barrier.

Each of the labeled minima and barriers in Fig. 4a to 4d was also characterized in terms of the H-bonds formed between the antibiotic and the porin residues (Table 3). All the conformers corresponding to the selected FES region were extracted from the MD trajectories and the H-bond occurrence calculated (Table 3). Generally speaking, a clear difference emerged between minima located inside or outside the constriction region. The latter are characterized by very few H-bonds with a scarce occurrence, usually well below 50%. This indicates a rather weak antibiotic-porin interaction, with the antibiotic being usually found to be highly mobile. On the other hand, minima at the constriction region are characterized by H-bonds with occurrence significantly exceeding 50%. The interaction of meropenem with OmpC33 was the only exception. Additionally, irrespective of the antibiotic tested, OmpC33 has a lower number of H-bonds, especially at the porin constriction zone. The carboxyl oxygens were the best H-bond acceptors in both carbapenems. The H-bonds formed with the

side chain of the arginine residues of the basic ladder at the constriction region were predominant over the other H-bonds observed, although several important interactions of other groups in the antibiotics with the negative residues of the loop L3 were found. Correspondingly, a significant decrease of mobility was observed for the antibiotic upon approaching the constriction region.

Further, each of the labeled FES regions was also characterized in terms of the porin cross-sectional area profile along the channel axis, and compared to the results obtained in the absence of antibiotic, as shown in Fig. 7. The states compatible with current blockages observed in electrophysiology correspond to near or slightly above the constriction region or to the main energy barriers. With imipenem we observed full monomer blockages in both the porins (Fig. 3b/e and Fig. 8a), and with meropenem, we observe fully resolved partial blockages (Fig. 3c/f and Fig. 8b).

DISCUSSION

Molecular Interpretation for Antibiotic Permeability - In clinical settings, resistance is often multifactorial: porin deletion, enzymatic degradation and efflux pump up-regulation have all been implicated in carbapenem resistance. To measure *in vivo* permeation exclusively through porins remains technically challenging, thus denying insights into whether changes in transport rates may be a significant contributor to resistance. We investigated the permeability of carbapenems through OmpC20 and OmpC33 in *in-vitro* systems and found correlations at macroscopic and microscopic levels.

Liposome permeation assays showed reduced permeability through OmpC33 when

compared to OmpC20 for both antibiotics (Fig. 2). This correlates with the decreased susceptibility observed in clinical strains (14). Although single channel electrophysiology is not a direct measure of penetration, is still informative in estimating the affinity of antibiotic for the channel. Simulations have shown (Fig. 4) that in general antibiotic accessibility is clearly asymmetric, with a higher free energy average level for entry from the extracellular side than the periplasmic one, especially for meropenem. The interaction of imipenem with OmpC33 is the exception, where the barriers are symmetric. In general, the asymmetry correlates well with the observed electrophysiology data, with imipenem-OmpC33 representing the only symmetric case (Table 1, Table 2). The FES reported in Fig. 4, indicates that when an antibiotic (either imipenem or meropenem) enters from the periplasmic side it stays in the deep minima and does not cross or reach the constriction region. It therefore would not be predicted to give rise to current blockages. This is in fact what we observe in single molecule experiments.

Meropenem is less basic than imipenem, as its amino group is shielded by the bulky dimethylcarbamoyl substituent on the pyrrolidinyl ring (Fig. 1e). Its behavior is unaffected by salt concentration in electrophysiology whereas imipenem was shown to very sensitive. This is consistent with the observations from MD simulations, where the NH_2^+ group of imipenem was a better H-bond donor in both the porins compared to the NH_2^+ group of meropenem. In particular, in the case of OmpC33, we observed the lowest number of H-bonds at the constriction region when compared to the other cases examined (Table 3).

Molecular dynamic simulations show that in OmpC33 the antibiotics (both cases) approach the constriction region with an adverse orientation more frequently than occurs in OmpC20. Our data suggest this is the result of two important differences in the internal electric field of the two channels, acting synergistically (20). Firstly, 'pre-orientation' is stronger in OmpC33, making it more difficult for the antibiotic to change its overall orientation while approaching the constriction region from the extracellular vestibule. Secondly, the electric field at the mouth of, and inside, the constriction region of OmpC33 is less ordered and less intense (20) resulting in a lower driving force for antibiotic reorientation upon transit from the extracellular vestibule. In summary, in OmpC33 the antibiotic more frequently approaches and engages the constriction region in an orientation incompatible with translocation. In this case the drug must either move back to the extracellular vestibule to change orientation, or pay the high energetic cost for reorientation inside the constriction zone indeed explaining the swelling assay data. We concur with an earlier hypothesis (20) that fine tuning of the electric field at the constriction zone might be a strategy to reduce the uptake of antibiotics by the bacteria. Such subtle mutations can produce dramatic alteration of the translocation dynamics that "trap" the antibiotic in the constriction region with the wrong orientation has not been identified previously.

Rules Governing Translocation

The diffusion barrier for antibiotics is mainly due to the entropic penalty imposed by adopting a specific orientation to transit the constriction zone. In compensation, favorable enthalpic antibiotic-protein interactions (42, 43) ease the passage of the polar molecule. Further, the release of protein (and antibiotic) hydration waters, upon formation of antibiotic-protein H-bonds, is accompanied by a favorable entropy increase (44, 45). A very recent investigation showed how small changes to the 'lateral chains' of these two carbapenems can modulate the penetration through specific channels in *Pseudomonas aeruginosa* (46). In the present report, we have shown that antibiotics appear to continuously respond to the channel electrostatics by properly orienting their electric dipole, in agreement with the water ordering along the channel (20).

A new model for translocation can be put forward, where the translocation rate is ultimately controlled by the ability of the antibiotic to fulfill a set of conditions inside the constriction region. The antibiotic fit the constriction with a restricted number of conformations, corresponding to an electric dipole matching the channel electrostatics and to the correct orientation of the H-bonding groups, will be favored. While the antibiotic crosses the constriction region, the molecules with best permeation performance should be the ones with enough flexibility to change the electric dipole direction with low-cost dihedral torsions of specific groups without the need for free-energy expensive molecular reorientations. Taking the above parameters into consideration will shape the design of novel antibiotics by providing a basis for an *in-silico* screen to identify molecules with enhanced permeation properties.

Conflict of interest: The authors declare that they have no conflicts of interest with the contents of this article.

Author Contributions: HB and MAS contributed equally to this work. HB, MGPP, MC and MW designed and conceived the study. HB and MW performed single channel experiments and liposome permeation assay. LM and JHN provided the protein. MAS and MC performed the simulations. The manuscript was written through contributions of HB, MAS, MGPP, JHN, MC, MW. All authors have given approval to the final version of the manuscript.

References

1.   Wright, G. D. (2007) The antibiotic resistome: the nexus of chemical and genetic diversity. *Nat. Rev. Microbiol.* **5**, 175–86

2.   Levy, S. B., and Marshall, B. (2004) Antibacterial resistance worldwide: causes, challenges and responses. *Nat. Med.* **10**, S122–9

3.   Payne, D. J., Gwynn, M. N., Holmes, D. J., and Pompliano, D. L. (2007) Drugs for bad bugs: confronting the challenges of antibacterial discovery. *Nat. Rev. Drug Discov.* **6**, 29–40

4.   Stavenger, R. A., Leader, T., Unit, D. P., and Winterhalter, M. (2014) TRANSLOCATION Project : How to Get Good Drugs into Bad Bugs. **6**, 228ed7

5.   Nakae, T. (1976) Outer membrane of Salmonella. Isolation of protein complex that produces transmembrane channels. *J. Biol. Chem.* **251**, 2176–2178

6.   Benz, R. (ed.) (2004) *Bacterial and Eukaryotic Porins*, Wiley-VCH Verlag GmbH & Co. KGaA, Weinheim, FRG

7.   Nikaido, H. (2003) Molecular basis of bacterial outer membrane permeability revisited. *Microbiol. Mol. Biol. Rev.* **67**, 593–656

8.   Yoshimura, F., and Nikaido, H. (1985) Diffusion of β-Lactam Antibiotics Through the Porin Channels of Escherichia coli K-12. **27**, 84–92.

9.   Pagès, J.-M., James, C. E., and Winterhalter, M. (2008) The porin and the permeating antibiotic: a selective diffusion barrier in Gram-negative bacteria. *Nat. Rev. Microbiol.* **6**, 893–903

10. Fernández, L., and Hancock, R. E. W. (2012) Adaptive and mutational resistance: role of porins and efflux pumps in drug resistance. *Clin. Microbiol. Rev.* **25**, 661–81

11. Blair, J. M. A., Webber, M. A., Baylay, A. J., Ogbolu, D. O., and Piddock, L. J. V. (2014) Molecular mechanisms of antibiotic resistance. *Nat. Rev. Microbiol.* **13**, 42–51

12. Dé, E., Baslé, A., Jaquinod, M., Saint, N., Malléa, M., Molle, G., and Pagès, J. M. (2001) A new mechanism of antibiotic resistance in Enterobacteriaceae induced by a structural modification of the major porin. *Mol. Microbiol.* **41**, 189–98

13. Jeanteur, D., Schirmer, T., Fourel, D., Simonet, V., Rummel, G., Widmer, C., Rosenbusch, J. P., Pattus, F., and Pagès, J. M. (1994) Structural and functional alterations of a colicin-resistant mutant of OmpF porin from Escherichia coli. *Proc. Natl. Acad. Sci. U. S. A.* **91**, 10675–10679

14. Low, A. S., MacKenzie, F. M., Gould, I. M., and Booth, I. R. (2001) Protected environments allow parallel evolution of a bacterial pathogen in a patient subjected to long-term antibiotic therapy. *Mol. Microbiol.* **42**, 619–630

15. Fernández, L., Breidenstein, E. B. M., and Hancock, R. E. W. (2011) Creeping baselines and adaptive resistance to antibiotics. *Drug Resist. Updat.* **14**, 1–21

16. Baquero, F. (2001) Low-level antibacterial resistance: a gateway to clinical resistance. *Drug Resist. Updat.* **4**, 93–105

17. Lou, H., Chen, M., Black, S. S., Bushell, S. R., Ceccarelli, M., Mach, T., Beis, K., Low, A. S., Bamford, V. A., Booth, I. R., Bayley, H., and Naismith, J. H. (2011) Altered antibiotic transport in OmpC mutants isolated from a series of clinical strains of multi-drug resistant E. coli. *PLoS One* **6**, e25825

18. Kojima, S., and Nikaido, H. (2014) High salt concentrations increase permeability through OmpC channels of Escherichia coli. *J. Biol. Chem.* **289**, 26464–73

19. Raj Singh, P., Ceccarelli, M., Lovelle, M., Winterhalter, M., and Mahendran, K. R. (2012) Antibiotic permeation across the OmpF channel: Modulation of the affinity site in the presence of magnesium. *J. Phys. Chem. B* **116**, 4433–4438

20. Acosta-Gutierrez, S., Scorciapino, M. A., Bodrenko, I., and Ceccarelli, M. (2015) Filtering with Electric Field: The Case of E. coli Porins. *J. Phys. Chem. Lett.*, 1807–1812

21. Prilipov, A., Phale, P. S., Van Gelder, P., Rosenbusch, J. P., and Koebnik, R. (1998) Coupling site-directed mutagenesis with high-level expression: large scale production of mutant porins from E. coli. *FEMS Microbiol. Lett.* **163**, 65–72

22. Sugawara, E., and Nikaido, H. (1992) Pore-forming activity of OmpA protein of Escherichia coli. *J. Biol. Chem.* **267**, 2507–11

23. Singh, P. R., Ceccarelli, M., Lovelle, M., Winterhalter, M., and Mahendran, K. R. (2012) Antibiotic permeation across the OmpF channel: modulation of the affinity site in the presence of magnesium. *J. Phys. Chem. B* **116**, 4433–8

24. Montal, M., and Mueller, P. (1972) Formation of bimolecular membranes from lipid monolayers and a study of their electrical properties. *Proc. Natl. Acad. Sci. U. S. A.* **69**, 3561–3566

25. Trias, J., Dufresne, J., Levesque, R. C., and Nikaido, H. (1989) Decreased outer membrane permeability in imipenem-resistant mutants of Pseudomonas aeruginosa. *Antimicrob. Agents Chemother.* **33**, 1202–6

26. Bajaj, H., Tran, Q.-T., Mahendran, K. R., Nasrallah, C., Colletier, J.-P., Davin-Regli, A., Bolla, J.-M., Pagès, J.-M., and Winterhalter, M. (2012) Antibiotic uptake through membrane channels: role of Providencia stuartii OmpPst1 porin in carbapenem resistance. *Biochemistry* **51**, 10244–9.

27. Yoshimura, F., and Nikaido, H. (1985) Diffusion of beta-lactam antibiotics through the porin channels of Escherichia coli K-12. *Antimicrob. Agents Chemother.* **27**, 84–92

28. Phillips, J. C., Braun, R., Wang, W., Gumbart, J., Tajkhorshid, E., Villa, E., Chipot, C., Skeel, R. D., Kalé, L., and Schulten, K. (2005) Scalable molecular dynamics with NAMD. *J. Comput. Chem.* **26**, 1781–802

29. Harvey, M. J., Giupponi, G., and Fabritiis, G. De (2009) ACEMD: Accelerating Biomolecular Dynamics in the Microsecond Time Scale. *J. Chem. Theory Comput.* **5**, 1632–1639

30. Buch, I., Giorgino, T., and De Fabritiis, G. (2011) Complete reconstruction of an enzyme-inhibitor binding process by molecular dynamics simulations. *Proc. Natl. Acad. Sci. U. S. A.* **108**, 10184–9

31. Lindorff-Larsen, K., Piana, S., Palmo, K., Maragakis, P., Klepeis, J. L., Dror, R. O., and Shaw, D. E. (2010) Improved side-chain torsion potentials for the Amber ff99SB protein force field. *Proteins* **78**, 1950–8

32. Jorgensen, W. L., Chandrasekhar, J., Madura, J. D., Impey, R. W., and Klein, M. L. (1983) Comparison of simple potential functions for simulating liquid water. *J. Chem. Phys.* **79**, 926

33. Wang, J., Wolf, R. M., Caldwell, J. W., Kollman, P. A., and Case, D. A. (2004) Development and testing of a general amber force field. *J. Comput. Chem.* **25**, 1157–74

34. Bayly, C. I., Cieplak, P., Cornell, W., and Kollman, P. A. (1993) A well-behaved electrostatic potential based method using charge restraints for deriving atomic charges: the RESP model. *J. Phys. Chem.* **97**, 10269–10280

35. M. J. Frisch, G. W. Trucks, H. B. Schlegel, G. E. Scuseria, M. A. Robb, J. R. Cheeseman, J. A. Montgomery Jr., T. Vreven, K. N. Kudin, J. C. Burant, J.M.Millam, S. S. Iyengar, J. Tomasi, V. Barone, B. Mennucci, M. Cossi, G. Scalmani, N. Rega, G. A. Peters, C. G. and J. A. P. (2004) GAUSSIAN 03 (Revision B.02). *Gaussian, Inc., Wallingford CT*

36. Case, D.A., Darde, T.A., Cheatham III, T.E., Simmerling, C.L., Wang, J., Duke, R.E., Luo, R., Merz, K.M., Pearlman, D.A., Crowley, M., Walker, R.C., Zhang, W., Wang, B., Hayik, S., Roitberg, A., Seabra, G., Wong, K.F., Paesani, F., Wu, X., Brozell, S., Ts, M., and D.H., Schafmeister, C., Ross, W.S., Kollman, P. A. (2006) Amber 9. *Univ. California, San Fr.*

37. Barducci, A., Bussi, G., and Parrinello, M. (2008) Well-tempered metadynamics: a smoothly converging and tunable free-energy method. *Phys. Rev. Lett.* **100**, 020603

38. Laio, A., and Parrinello, M. (2002) Escaping free-energy minima. *Proc. Natl. Acad. Sci. U. S. A.* **99**, 12562–6

39. Raiteri, P., Laio, A., Gervasio, F. L., Micheletti, C., and Parrinello, M. (2006) Efficient reconstruction of complex free energy landscapes by multiple walkers metadynamics. *J. Phys. Chem. B* **110**, 3533–9

40. Benz, R., Schmid, A., and Vos-Scheperkeuter, G. H. (1987) Mechanism of sugar transport through the sugar-specific LamB channel of Escherichia coli outer membrane. *J. Membr. Biol.* **100**, 21–9

41. Mahendran, K. R., Hajjar, E., Mach, T., Lovelle, M., Kumar, A., Sousa, I., Spiga, E., Weingart, H., Gameiro, P., Winterhalter, M., and Ceccarelli, M. (2010) Molecular basis of enrofloxacin translocation through OmpF, an outer membrane channel of Escherichia coli--when binding does not imply translocation. *J. Phys. Chem. B* **114**, 5170–9

42. Kumar, A., Hajjar, E., Ruggerone, P., and Ceccarelli, M. (2010) Molecular simulations reveal the mechanism and the determinants for ampicillin translocation through OmpF. *J. Phys. Chem. B* **114**, 9608–16

43. Hajjar, E., Bessonov, A., Molitor, A., Kumar, A., Mahendran, K. R., Winterhalter, M., Pagès, J.-M., Ruggerone, P., and Ceccarelli, M. (2010) Toward screening for antibiotics with enhanced permeation properties through bacterial porins. *Biochemistry* **49**, 6928–35

44. Tran, Q.-T., Williams, S., Farid, R., Erdemli, G., and Pearlstein, R. (2013) The translocation kinetics of antibiotics through porin OmpC: insights from structure-based solvation mapping using WaterMap. *Proteins* **81**, 291–9

45. Tran, Q.-T., Pearlstein, R. A., Williams, S., Reilly, J., Krucker, T., and Erdemli, G. (2014) Structure-kinetic relationship of carbapenem antibacterials permeating through E. coli OmpC porin. *Proteins* **82**, 2998–3012

46. Isabella, V. M., Campbell, A. J., Manchester, J., Sylvester, M., Nayar, A. S., Ferguson, K. E., Tommasi, R., and Miller, A. A. (2015) Toward the Rational Design of Carbapenem Uptake in Pseudomonas aeruginosa. *Chem. Biol.* **22**, 535–47

FIGURE LEGENDS

FIGURE 1: The typical arrangement and structure of a trimeric OmpC20 porin, embedded in the lipid bilayer, is shown from the (a) side and (b) top view. In (c) one monomer is shown where the positively charged residues comprising the basic ladder at the constriction region are highlighted in blue, the negatively charged residues of the loop L3 in red, and the three residues mutated in the clinical series from OmpC20 to OmpC33 in green. The chemical structures of (d) imipenem and (e) meropenem are also shown, together with the colour-coded electrostatic potentials corresponding to the atomic partial charges.

FIGURE 2: Liposome permeation assay- relative diffusion rates of the reference sugars arabinose and raffinose and the antibiotics, imipenem and meropenem into liposomes reconstituted with OmpC20 and OmpC33 are shown.

FIGURE 3: Ion current traces of single channels of- OmpC20 in 1M KCl (a) without any antibiotic (b) with 2.5 mM imipenem on *cis* side (c) OmpC20 with 2.5 mM meropenem *cis* side ; OmpC33 (d) without any antibiotic (e) with 2.5 mM imipenem on *cis* side (f) with 2.5 mM meropenem *cis* side. Electrolyte conditions: 1 M KCl, 20 mM MES pH 6 at room temperature and -100 mV.

FIGURE 4: Free Energy Surface of carbapenem translocation, imipenem (a,c) and meropenem (b,d) in the OmpC20 (a,b) and OmpC33 (c,d) porin are shown. The antibiotic orientation is defined as the difference of the z-coordinate between the lactam carbonyl carbon and the sulfur bonded carbon of the antibiotic two-ring core. The difference of the z-coordinate between the center of mass of the antibiotic two-ring core and that of the porin's monomer (Δz) represents the antibiotic depth inside the porin lumen ($\Delta z=0$ corresponds to the constriction region). Each iso contour corresponds to a free energy increase of 2 kcal mol^{-1}. Free energy values were rescaled in order to have the absolute minimum equal to zero. Different labels are used to indicate specific regions analyzed and discussed in the text. Water ordering inside (e) the first monomer of OmpC20 is shown together with the net electric dipole of the water molecules calculated at different depth inside the lumen(the vector n.5 and n.6 are labeled respectively), according to a recent theoretical investigation (20). The loop L3 is highlighted to provide a reference. Meropenem is shown at the constriction region, i.e. the representative conformer for the free energy minimum 3 in Figure 4b. In (f) the system is rotated to show the xy-projection. The electric dipole of the antibiotic is shown together with the net dipole of water molecules at the same level inside the channel.

FIGURE 5: Meropenem translocation through OmpC20 (a) and OmpC33 (b). The representative conformers of the different free energy states, labeled in Fig. 4 b and d, are reported in different colors: red, orange, blue and purple for the minimum 1, 2, 3 and 4, respectively. The position of the positively charged nitrogen is highlighted by a sphere, in order to provide a reference for antibiotic orientation inside the channel. Protein backbone is gray but the loop L3, which has been colored green as a reference.

FIGURE 6: Imipenem translocation through OmpC20 (a: front view; b: top view) and OmpC33 (c). The representative conformers of the different FES regions, labeled in Figure 4 a and c, are reported in different colors: red, orange, blue and purple for the minimum 1, 2, 3 and 4, respectively. Yellow is used for the representative conformer of the main energy barrier. The position of the positively charged nitrogen of the antibiotic is highlighted by a sphere, in order to provide a reference for its orientation inside the channel. Protein backbone is gray but the loop L3, which has been colored green.

FIGURE 7: Porin cross-sectional area profile along the channel axis is reported as the radius of the equivalent circle. The profiles due to the presence of the representative conformers of the different free energy states, labeled in figure 4, are reported with different colored solid lines. The results pertaining to the porin in the absence of antibiotic are reported with the black dashed line as reference

FIGURE 8: Ion current trace of single channel of OmpC20 @ 5 °C (a) 2.5 mM Imipenem on *cis* side at -100 mV, (b) 2.5 mM Meropenem cis side at -100 mV. Electrolyte conditions: 1 M KCl, 20 mM MES pH 6.

TABLES

Table 1: Antibiotic association (k_{on}) and dissociation (k_{off}) rate constants at low salt concentration: From single channel measurements for OmpC20 and OmpC33, conditions: 200 mM KCl, 20 mM MES pH 6, k_{on}= ({No. of events/ sec}/ 3 * [c]), k_{off}= (1/residence time), the flux J = $(k_{on}$ /2) * Δc with Δc=2.5 mM.
$k_{on}{}^{cis}$ is calculated from -100 mV (for *cis* addition) and $k_{on}{}^{trans}$ is calculated from +100 mV (for *trans* addition)
[1] *Calculated from -100 mV*

Antibiotics	Porin	$k_{on}{}^{cis}$ (M^{-1} s^{-1}) (10^3)	$k_{on}{}^{trans}$ (M^{-1} s^{-1}) (10^3)	k_{off} (s^{-1})	J (molecules/sec)
Imipenem	OmpC20	96 ± 16	6[1]	23,000	120 ± 20
	OmpC33	2.8 ± 0.2	7	16,000	3.5
Meropenem	OmpC20	35 ± 0.6	No effect	20,000	43
	OmpC33	29 ± 3	No effect	20,000	36

Table 2: Antibiotic association (k_{on}) and dissociation (k_{off}) rate constants at high salt concentration: From single channel measurements for OmpC20/C26/C28 and C33, conditions: 1 M KCl, 20 mM MES pH 6, k_{on} = ({No. of events/ sec}/ 3 * [c]), k_{off} = (1/residence time), J = $(k_{on}$ /2) * Δc ; Δc=2.5 mM, k_{on}^{cis} is calculated from -100 mV (for cis addition) and k_{on}^{trans} is calculated from +100 mV (for trans addition)

[1] *Calculated from -100 mV*

Antibiotics	Porin	k_{on}^{cis} (M^{-1} s^{-1}) (10^3)	k_{on}^{trans} (M^{-1} s^{-1}) (10^3)	k_{off} (s^{-1})	J (molecules/sec)
Imipenem	OmpC20	34 ± 3	0.3[1]	25000	42 ± 3
	OmpC26	24 ± 4	0.16	25000	30 ± 3
	OmpC28	2.7 ± 0.4	2.3 ± 0.2	25000	3
	OmpC33	2.0 ± 0.06	2.4	25000	2.5
Meropenem	OmpC20	54 ± 1.3	0.4	12,000	67 ± 1
	OmpC26	53 ± 7	0.3	20,000	66 ± 8
	OmpC28	53.7 ± 4	0.3	16,700	67 ± 5
	OmpC33	63 ± 3	0.3[1]	12,000	78 ± 4

Table 3: Predicted occurrence [%] of hydrogen-bonds formed between the antibiotic donor/acceptor groups (in parenthesis) and the porin residues. The latter are reported in decreasing z-coordinate order. Only the H-bonds with an occurrence $\geq 20\%$ are reported. FES regions located at the porin constriction zone are shaded. Antibiotic's donor/acceptor groups are labeled as follows: 'CO_2' carboxyl oxygens; 'LO' β-lactam carbonyl oxygen; 'NH_2^+' imipenem's terminal amino group; 'NH_2^+' meropenem's charged amino group; 'OH' side chain hydroxyl group.
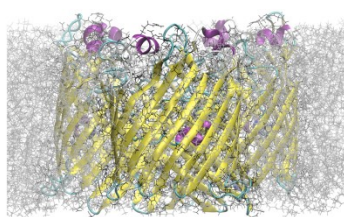
Imipenem / OmpC20

residue	FES region 1	2	3	*	4	5
E752	58 (NH_2)					
E64	51 (OH)	20 (NH_2)				
N63	25 (CO_2)					
K33	40 (CO_2)	36 (CO_2)				
Q123				24 (LO)		
R124			79 (CO_2)	46 (CO_2)		
R74				53 (CO_2)	82 (CO_2)	
E109			31 (OH)			
R37				25 (CO_2)		
D105				48 (NH_2)		
D105				30 (OH)	52 (OH)	
T300						32 (OH)

Meropenem / OmpC20

residue	FES region 1	*	2	3	4	5
G245	28 (LO)					
N330	24 (CO_2)					
R243	28 (OH)					
K29	36 (CO_2)	22 (CO_2)				
E752			27 (NH_2^+)			
K33		24 (CO_2)				
R124				67 (CO_2)		
E109				24 (OH)		
R74				100 (CO_2)	100 (CO_2)	
D105				24 (NH_2^+)		
L107					70 (OH)	
R37				23 (OH)	32 (CO_2)	56 (CO_2)

Imipenem / OmpC33

residue	FES region 1	2	*	3	*	4	5
R243	32 (OH)						
N63		23 (OH)					
K33		22 (CO_2)					
E109				58 (OH)	42 (OH)		
R37				77 (CO_2)	62 (CO_2)	21 (LO)	
E18			23 (NH_2)	50 (NH_2)	27 (NH_2)		
D105			23 (NH_2)			71 (OH)	
R269							27 (CO_2)

Meropenem / OmpC33

residue	FES region 1	*	2	3	4
E752		25 (OH)			
K33		42 (CO_2)			
E109		38 (NH_2^+)			
R37			23 (CO_2)	48 (CO_2)	49 (CO_2)
D105			20 (OH)	34 (NH_2^+)	48 (NH_2^+)
K16			25 (CO_2)	21 (CO_2)	32 (CO_2)

Figure 1

(a)
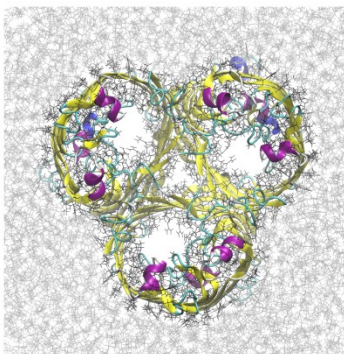
(b)
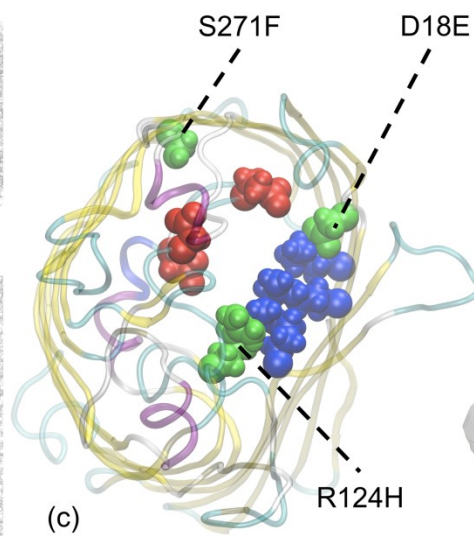
(c)
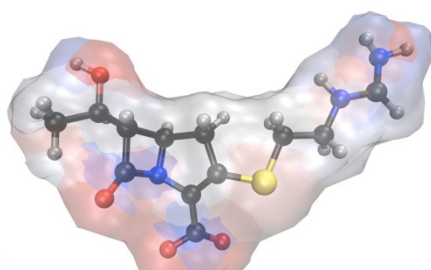
S271F

D18E

R124H

(d) Imipenem

(e) Meropenem

46

Figure 2

Figure 3

(a)
OmpC20 Blank

(b)
2.5mM Imipenem cis side

(c)
2.5mM Meropenem cis side

5ms

5ms

-50pA

-50pA

-50pA

50ms

50ms

50ms

(d)
OmpC33 Blank

(e)
2.5mM Imipenem cis side

(f)
2.5mM Meropenem cis side

5ms

5ms

-50pA

-50pA

-50pA

50ms

50ms

50ms

48

Figure 4

Figure 5

(a)

(b)

50

Figure 6

extracellular side

(a)

(b)

(c)

periplasmic side

Figure 7

Figure 8

Single OmpC20 channel @ 5 °C

a. 2.5 mM imipenem cis side

b. 2.5 mM meropenem cis side

-25pA

50 ms

-25pA

50 ms
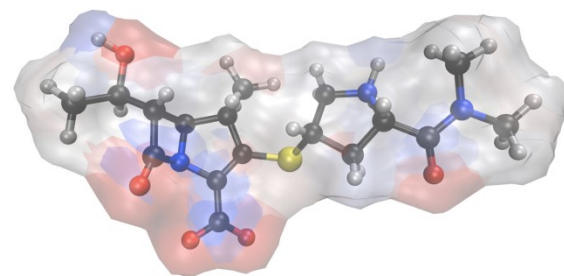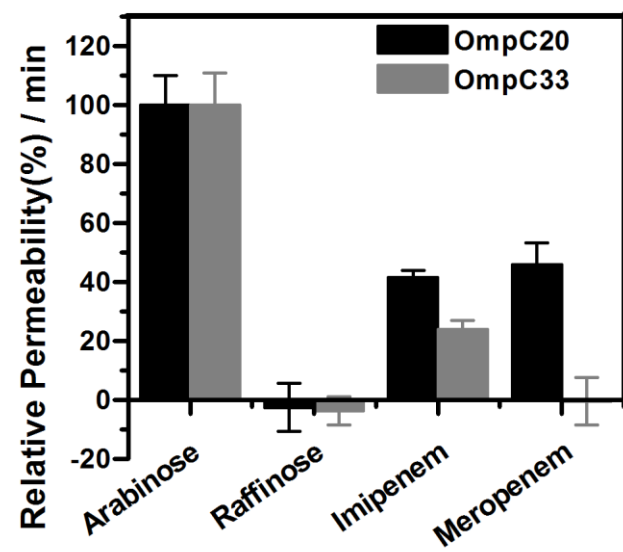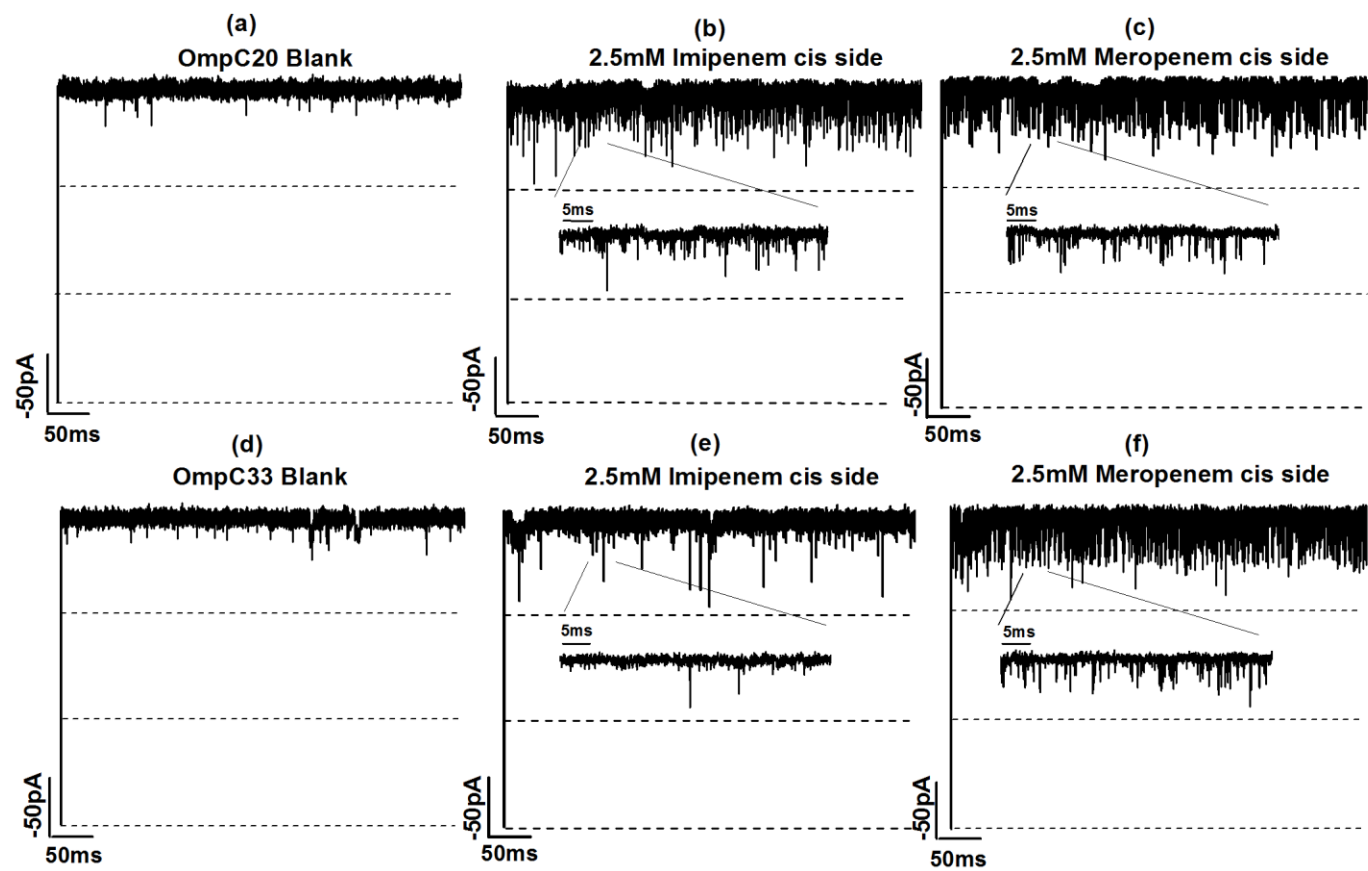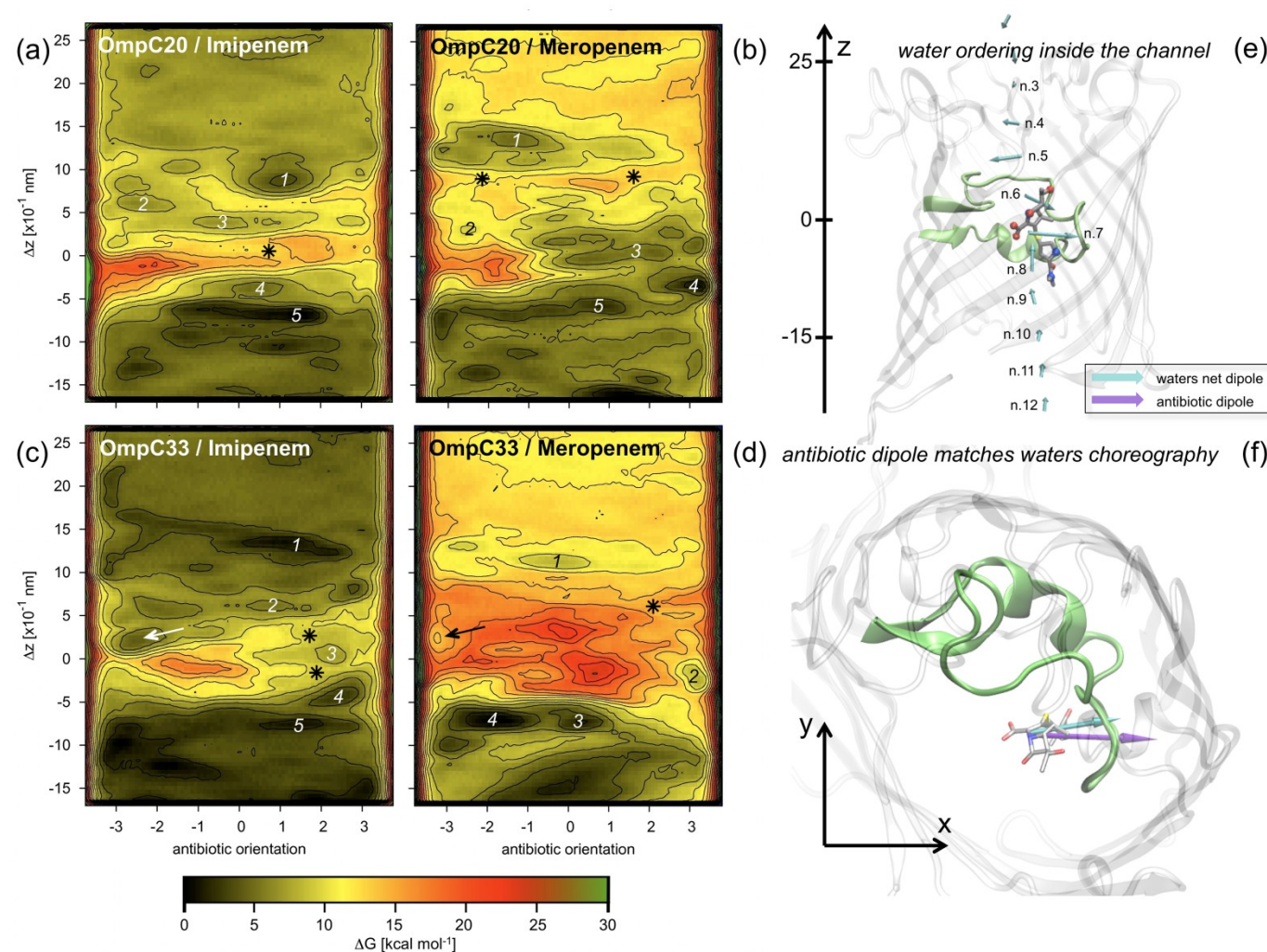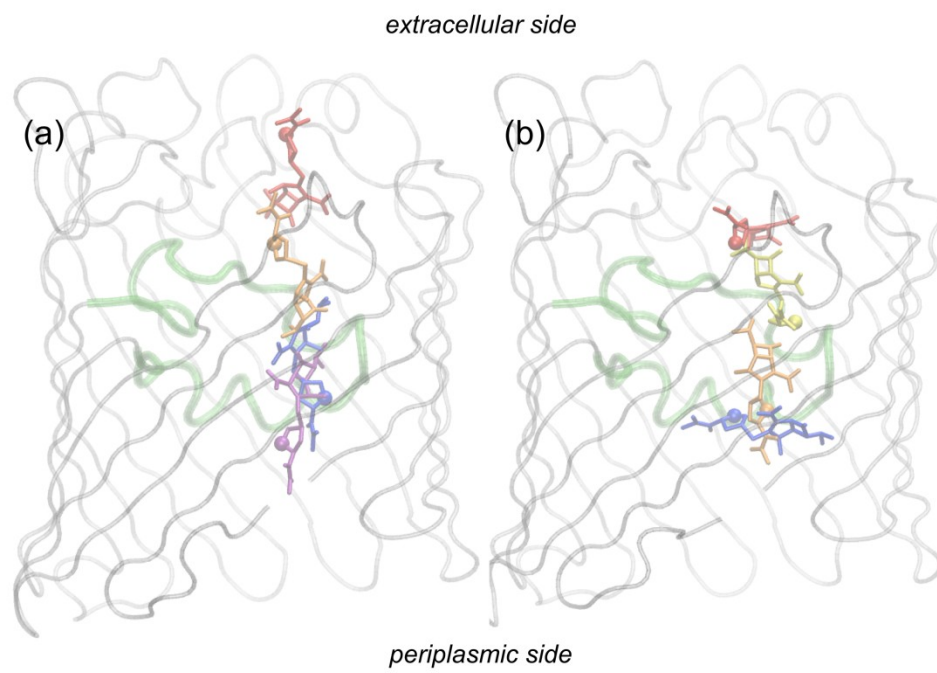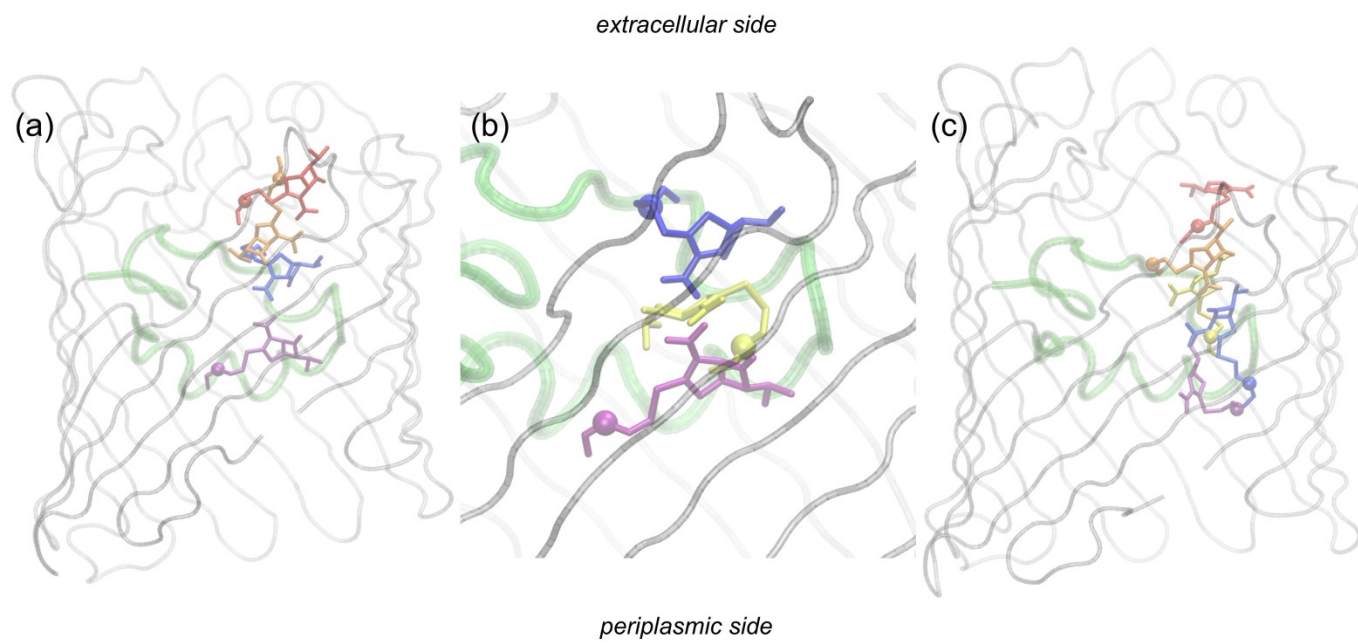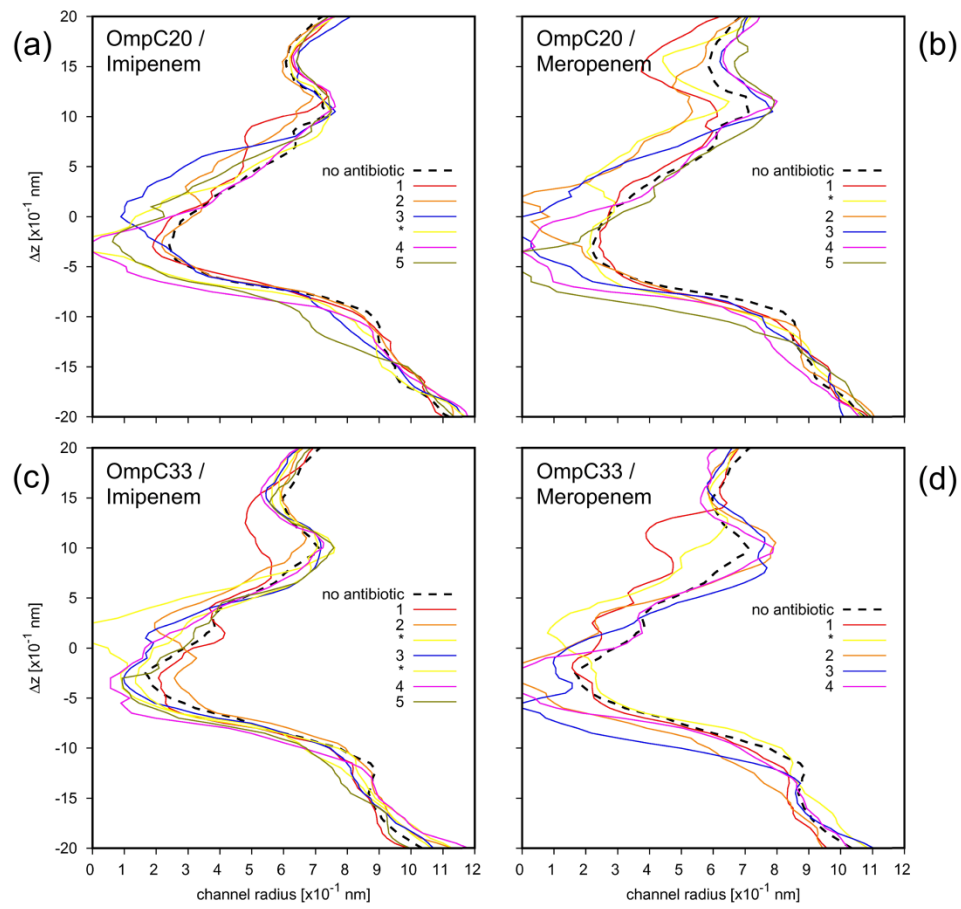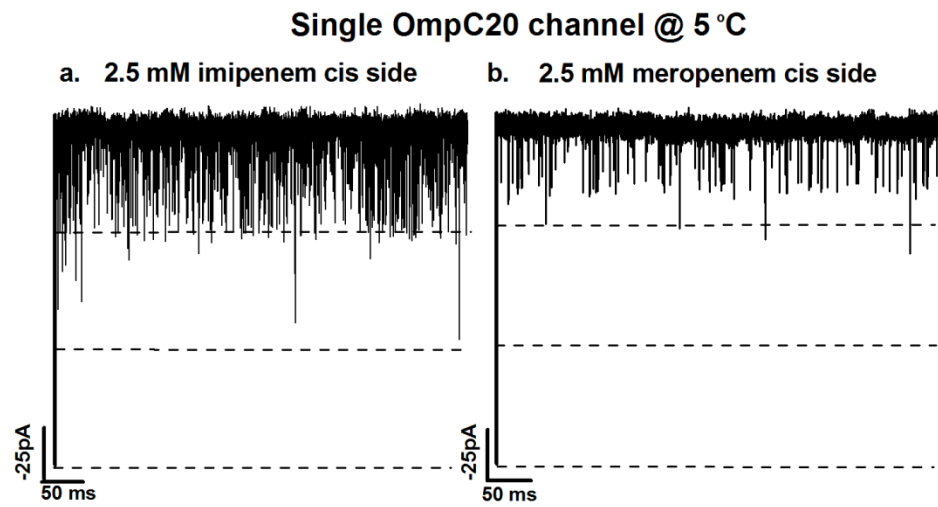
Part 3

Translocation of antibiotics through porins

Chapter 3: New insights on antibiotic permeation across porins

In this study we present novel insights on the uptake of antibiotics through porins from Gram-negative bacteria like *E. coli*. In P3.3.1 we introduce a complementary technique in collaboration with Prof. Dr. Ulrich Keyser. A label-free detection of intrinsic antibiotic fluorescence is used to measure influx of fluoroquinolones in vesicles through porins.

In P3.3.2 we elucidate the kinetic parameters of β-lactams and fluoroquinolones by varying external parameters like pH and voltage. We try to decipher the contribution of different parameters like electrostatic, electro-osmotic and the electric field inside the pore and correlate with the voltage effects observed in electrophysiology to obtain a translocation mechanism through the pore.

P3.3.1: Norfloxacin uptake through OmpF porins using fluorescence based detection in vesicles

Manuscript to be submitted

Individual Contribution

My main contribution in this manuscript is to design the study, to perform experiments and analysis of data from single channel electrophysiology; perform experiments of fluorescence detection in microfluidic-chip. I participated in manuscript composition.

Quantification of fluoroquinolone uptake through the outer membrane channel OmpF of *Escherichia coli*

Jehangir Cama[a], Harsha Bajaj[b], Stefano Pagliara[a,c], Theresa Maier[a], Yvonne Braun[b], Mathias Winterhalter[b] and Ulrich F. Keyser[a],*

Affiliations: a. Biological and Soft Systems, Cavendish Laboratory, Department of Physics, University of Cambridge, JJ Thomson Avenue, Cambridge CB3 0HE, United Kingdom.

b. Jacobs University Bremen, Campus Ring 1, D-28759, Bremen, Germany.

c. Department of Biosciences, College of Life and Environmental Sciences, University of Exeter, Exeter, United Kingdom.

Correspondence: Ulrich F. Keyser, ufk20@cam.ac.uk, +44 (0) 1223 337007.

Decreased drug accumulation is a common cause of antibiotic resistance in microorganisms. However, there are few reliable general techniques capable of quantifying drug uptake through bacterial membranes. We present a semi-quantitative optofluidic assay for studying the uptake of autofluorescent drug molecules in single liposomes. We studied the effect of the *Escherichia coli* outer membrane channel OmpF on the accumulation of the fluoroquinolone antibiotic, norfloxacin, in proteoliposomes. Measurements were performed at pH 5 and pH 7, corresponding to two different charge states of norfloxacin that bacteria are likely to encounter in the human gastrointestinal tract. The optofluidic assay estimates a flux of about 10 norfloxacin molecules per second per OmpF trimer in the presence of a 1 mM concentration gradient of norfloxacin. We also performed single channel electrophysiology measurements and found that the application of transmembrane voltages causes an electric field driven uptake in addition to concentration driven diffusion. We use our results to propose a physical mechanism for the pH mediated change in bacterial susceptibility to fluoroquinolone antibiotics.

Introduction

Antimicrobial resistance is a daunting challenge, threatening to undermine the very fabric of modern medicine today[1-4]. The inexorable emergence of resistant organisms, coupled with a decline in the discovery of new antimicrobials, has led to a global public health crisis. The recent breakthrough discovery of a new antibiotic, teixobactin[5], is extremely good news. However, its relative inactivity against Gram-negative pathogens shows that the battle against antimicrobial resistance will be extremely challenging.

Gram-negative bacteria have a hydrophobic double-membrane cell envelope that presents a barrier for hydrophilic molecules trying to enter the cell. The outer membrane (OM) is even more hydrophobic than a typical phospholipid membrane due to the presence of lipopolysaccharides (LPS), whose strong lateral interactions inhibit the passage of a variety of compounds through the OM[6]. Translocation across the OM is thus mainly governed by the

presence of outer membrane protein "porins" that form water-filled channels allowing the diffusion of compounds through the OM.

Consequently, the down-regulation of these porins enables bacteria to escape the deleterious effects of antibiotics[6-9]. For example, a reduction in the expression of Outer membrane protein F (OmpF), a major porin found in *Escherichia coli,* has been associated with a decrease in the accumulation of fluoroquinolone antibiotics; this eventually gives rise to drug resistance[7,10-12]. Furthermore, antibiotic therapy results in a switch in porin expression from OmpF to the narrower OmpC; this is thought to be due to the high osmolarity conditions existing in patients under drug treatment[7]. This leads to a significant decrease in antibiotic accumulation within the cell, and hence a decrease in antibiotic susceptibility[7]. It is thus clear that understanding antibiotic accumulation in cells is crucial, and methods to better quantify antibiotic permeation are urgently required[13].

Fluoroquinolones are broad-spectrum antibiotics that inhibit bacterial type II topoisomerases. These topoisomerases are essential enzymes, involved in key cellular processes such as DNA replication[14]. Since their targets are intracellular, fluoroquinolones must pass through the outer and inner bacterial membrane to be effective[10]. The OM thus presents the initial diffusion barrier for drug uptake, and the accumulation of fluoroquinolone molecules in the periplasm ultimately determines their flux into the cytoplasm. Changes in bacterial susceptibility to fluoroquinolones due to changes in pH have been reported previously[15,16]. An increase in external pH from acidic to basic was shown to correspond to a reduction in the minimum inhibitory concentration (MIC) of norfloxacin[17]. Further, it was proposed that this pH mediated change in susceptibility is related to changes in the uptake of fluoroquinolones due to alterations of the electric charge of the antibiotic molecule[18,19]; norfloxacin, for example, is positively charged at pH 5 and neutral (zwitterionic, but a significant proportion are also uncharged) at pH 7[18,19]. It thus seems reasonable to assume that the fluoroquinolone susceptibility of bacteria in response to pH changes is a complicated process, which might involve both changes in porin expression[20] and changes in drug transport through porins in the OM as well as through the phospholipid inner membrane.

At acidic pH values, fluoroquinolone molecules carry charge[18] and thus transport across the OM should be strongly influenced by even relatively small potentials across the OM. Donnan potentials are known to exist across the OM due to the presence of anchored, anionic membrane-derived oligosaccharides (MDOs) in the *E. coli* periplasm[21,22]. The magnitude of these potentials depends strongly on the ionic concentration of the surrounding medium. At physiological ion concentrations, the Donnan potential is of the order of 20-30 mV, but variations of 5-100 mV have been reported by changing external cation concentrations[21]. One would expect such changes to have a significant effect on the transport of charged molecules through OM porins.

For autofluorescent antibiotics like quinolones, the determination of antibiotic uptake via a cell ensemble recording has previously been suggested. However, the technique suffers from difficulties in distinguishing between antibiotic molecules that were accumulated inside versus those bound to the cell membrane[23]. More recently, fluorescence based single cell imaging enabled the comparison of fleroxacin uptake in resistant versus susceptible bacteria[24]. However, barring these few exceptions, a quantitative analysis of fluoroquinolone transport through porins and lipids has proven technologically challenging.

In this study we describe an optofluidic assay that measures the permeability of antibiotics through porins exclusively in a proteoliposome system. OmpF porins are reconstituted into giant unilamellar vesicles and norfloxacin uptake into these proteoliposomes is tracked directly in a label-free manner using the UV autofluorescence of the drug. Patching the proteoliposomes reveals an estimate of the porin density, and combining the two measurements enables the calculation of norfloxacin translocation rates through OmpF channels in the proteoliposomes. Furthermore, proteoliposomes are cell-free systems, and thus active or passive uptake processes can be independently examined in highly controlled environments. We compare our measurements with single channel electrophysiology, and explore the combined effect of pH and transmembrane voltage on norfloxacin transport through OmpF.

Results

Optofluidic Permeability Assay
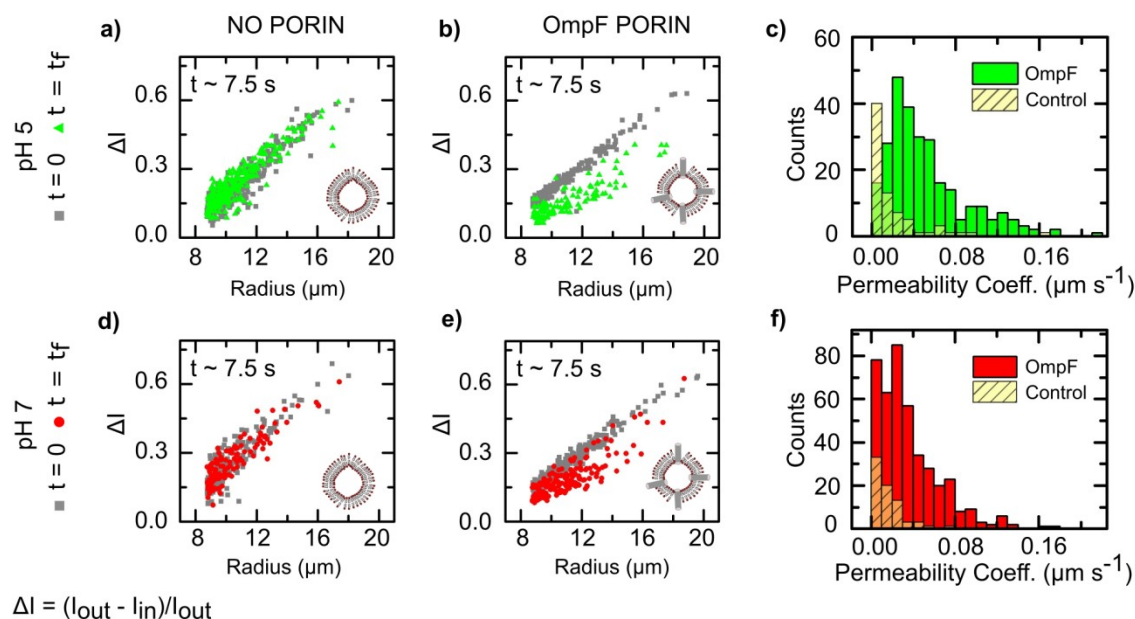
Figure 1. Optofluidic permeability assay (depicted schematically in Figure 3) shows the rapid uptake of norfloxacin in OmpF embedded proteoliposomes. Comparison of the uptake measurements in liposomes and proteoliposomes at pH 5 (a and b) and pH 7 (d and e). Each point references an uptake measurement at the single vesicle level, the grey points being t = 0 and the green (pH 5) and red (pH 7) being the final detection point t = t_f. On average it took individual vesicles about 7.5 s to move from the initial to the final detection point. In the absence of porins (a,d), there is no shift in ΔI values observed at the later time point at either pH. The presence of porins (b,e) leads to a marked downward shift in ΔI for the majority of the proteoliposomes at the later detection point, both at pH 5 and pH 7. The downward shift in ΔI corresponds to an increase in the norfloxacin autofluorescence intensity within the proteoliposome (I_{in}), and is thus a direct measure of norfloxacin uptake. Scatter plots of other porin experiments are presented in the Supplementary Information. The histograms (c,f) are a record of permeability coefficients (P) measured for individual porin-embedded proteoliposomes, and summarise the data from 3 separate experiments at each pH. Histograms from the control measurements with liposomes (no porins) are overlaid to show the shift in P due to the presence of porins in the membrane. Total liposomes/proteoliposomes detected were N = 268 (pH 5, with porins), N = 74 (pH 5, no porins), N = 420 (pH 7, with porins) and N = 74 (pH 7, no porins).

In the optofluidic permeability assay, OmpF embedded proteoliposomes (see Methods) are exposed to norfloxacin by controlled mixing in a T junction microfluidic chip. The vesicles (liposomes/proteoliposomes) are imaged under UV irradiation at two points, first immediately post mixing with the drug and then again after time *t*, a short distance further downstream. A comparison of the drug UV autofluorescence intensities within the vesicles at both points enables the direct visualisation of drug uptake and the calculation of the permeability coefficient (*P*) and flux (*J*) of the drug through the vesicle membrane. This assay also allows the comparison of

norfloxacin flux values through OmpF at different pH conditions in the absence of an applied transmembrane voltage.

The results of the optofluidic permeability assay are summarised in Figure 1 – more results can be viewed in the Supplementary Information Figure S1. The graphs (Figures 1 a,b,d,e) show a normalised intensity difference ($\Delta I = \{(I_{out} - I_{in})/I_{out}\}$) between the background autofluorescence intensity (I_{out}) and the autofluorescence intensity inside the vesicle (I_{in}), versus vesicle radius (R). Each point represents a single vesicle measurement. The grey squares represent vesicles at the initial viewpoint immediately post mixing with the norfloxacin (which for convenience we set to $t = 0$). The green triangles (pH 5) and red circles (pH 7) represent vesicles once they have travelled along the channel to the next detection position. The Permeability Coefficient (P) is given by[25]:

$$P = -\left(\frac{R}{3t}\right) \times \ln\left(\Delta I(t) - \Delta I(0) + 1\right)$$

where t is the time taken for the vesicle to move from the initial detection point to the final detection point (on average this was about 7.5 s). The norfloxacin concentration present in the channel after mixing is about 1 mM; at $t = 0$, there is no norfloxacin inside the vesicles, whereas outside the vesicles the concentration is 1 mM.

The experiments were performed at pH 5 and pH 7. In both cases the presence of OmpF causes a marked change in ΔI indicating the rapid accumulation of the drug inside the proteoliposomes.

Control measurements in the absence of OmpF revealed a substantially slower uptake, indicating that OmpF porins significantly enhance the permeability of the membranes to norfloxacin. We can calculate the contributions to the flux from the porins and lipids separately; details are given in the Supplementary Information. In contrast to permeation in the absence of OmpF[25], the presence of the porins leads to similar permeability coefficients at both pH 5 and pH 7. The relative pH independence suggests that the charge of the molecule does not play a significant role in influencing its transport through the porin in the absence of a transmembrane potential.

The spread in the permeability coefficient histograms (Figure 1 c,f) is caused by the inevitable variability of OmpF insertions into individual vesicles prepared for the optofluidics experiments. This can be seen in the scatter plots as well – it is clear that, at both pH conditions, a handful of vesicles do not show significant transport. It is known, however, that electroformation produces some multilamellar vesicles[26], and in these the porins cannot insert across all membranes; this accounts for the few negative observations.

Norfloxacin Flux Calculation in the Proteoliposomes

To obtain an estimate of the flux per porin from the optofluidics assay, vesicles incubated with OmpF were patched and characterised electrically using a Port-a-Patch system (Nanion Technologies GmbH, Germany) (Supplementary Figure S2). Since the patched area is well-

known (patch diameter = 1 μm) and the number of porin insertions counted (using the ionic current characteristics, details in Methods), this calibration measurement established a [porin]:[lipid surface area] ratio for the vesicles. Our results yield an estimate of ~1800 porins per □m^2 for the proteoliposomes used in the optofluidics assay. It is interesting to compare this result to the estimated number of general diffusion porins found in a typical bacterial cell; these porins are found in excess of 10^5 copies per cell[6]. This translates into an approximately 6-7× higher [porin]:[lipid surface area] ratio than for our experiments.

The flux of norfloxacin through the vesicle membrane is given by $J = P \times 4\pi R^2 \times \Delta c$. Combining this with the Port-a-Patch measurements, we can calculate the flux per porin on a single proteoliposome basis (full details of the calculation are provided in the Supplementary Information). An average over all the proteoliposomes detected gives a norfloxacin flux value per porin of 10 ± 8 molecules/s (N=420) at pH 7 and 15 ± 10 molecules/s (N=268) at pH 5 (errors are Standard Deviations). The errors are a direct consequence of the variability in OmpF insertion, as seen in the Supplementary Information Figure S2. If we include a correction (details in Supplementary Information) to account for the contribution of flux across the pure lipids[25], the change in the final result is negligible, as expected considering the timescales of the measurement.

Antibiotic interaction with OmpF using Single channel electrophysiology

In this assay, electrophysiology was used to study the interaction of norfloxacin with OmpF channels reconstituted in planar lipid bilayers. Traditionally, a lipid bilayer is formed across an aperture in a Teflon film that separates two reservoirs in a cuvette. The reservoirs are filled with an electrolyte solution and a potential difference is applied across the lipid membrane via electrodes in the reservoirs. Porins are reconstituted in the lipid bilayer and their conductance properties studied by measuring the ionic current flowing through the membrane. The addition of antibiotics leads to blockages in the ionic current, since the antibiotic molecules displace ions flowing through the porin. A detailed description of the technique is provided in the Methods section.

We varied the transmembrane voltages (25 mV and 50 mV) to determine whether the charge on the norfloxacin molecule at pH 5 influenced its transport through the channel under an applied electric field comparable to the OM potentials in natural systems. In the absence of antibiotics, fluctuations in the ionic current through a single OmpF channel were negligible, both at pH 7 and pH 5 (Figures 2a and 2c). The addition of 250 μM norfloxacin to the extracellular (*cis*) side of the protein at pH 7 led to well resolved blockages of ionic current as shown in Figure 2b.
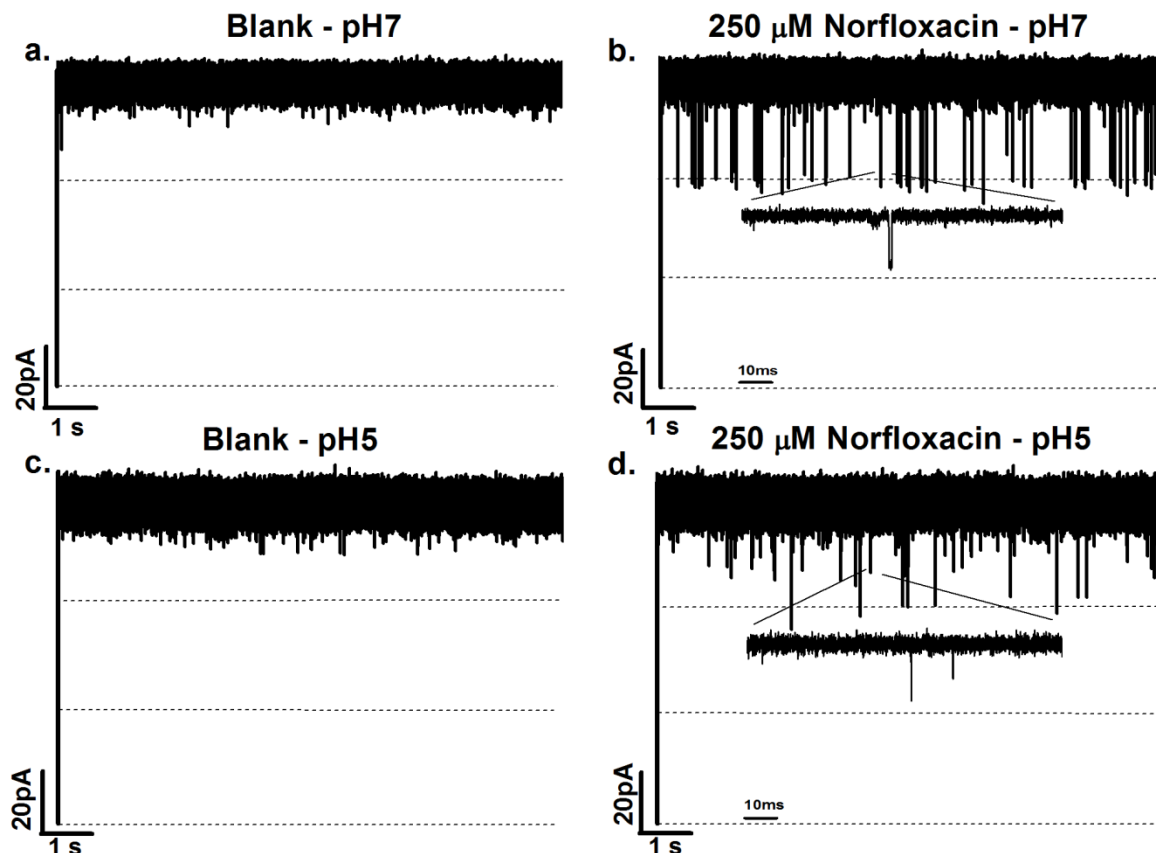
Figure 2. Ionic current traces of a single trimeric OmpF porin: (a) in the absence of antibiotics at pH 7, (b) with 250 μM norfloxacin cis side at pH 7, (c) in the absence of antibiotics at pH 5 and (d) with 250 μM norfloxacin cis side at pH 5. Electrolyte conditions: 1 M KCl, 5 mM acetate (pH 5) or 5 mM PO$_4$ (pH 7). The applied voltage was -25 mV. The dotted lines specify the ionic current levels through single monomers of the OmpF trimer. The addition of norfloxacin at pH 7 (b) leads to well resolved blockages of the ionic current through a monomer, whereas at pH 5 (d) the antibiotic molecules lead to flickering in the ionic current through a monomer – full blockages are not always observed. This is due to the low residence time of the antibiotic in the channel at pH 5, as discussed in the text.

At pH 5, the addition of 250 μM norfloxacin gave rise to partial unresolved flickering in the ionic current (Figure 2d); the ionic current through a monomer was not completely blocked due to the presence of the antibiotic. This was due to the low residence times of the norfloxacin molecules in the channel at pH 5, as discussed below.

The kinetic rate constants (association and dissociation rates) characterising the interaction of norfloxacin molecules with the OmpF channel were calculated as described previously[27]; these are quantified in Table 1. Interestingly, the dissociation rate of the antibiotic varied by an order of magnitude at the different pH conditions. At pH 7 the residence time in the channel was about 900 μs (-25 mV experiments). However at pH 5, when the molecule is positively charged, this

63

reduced to 40 μs (Table 1). This imbalance in the pH 7 and pH 5 residence times was observed at the higher transmembrane voltage of -50 mV as well (650 μs and 40 μs respectively).

The flux (J molecules/s) of norfloxacin through the channel was calculated based on a flux model valid for both symmetric and asymmetric transport through a channel[27-30]. When a transmembrane voltage of -25 mV was applied across the bilayer, the flux was found to be slightly higher at pH 5 (~ 2 molecules/s) than at pH 7 (~ 1 molecule/s). When the transmembrane voltage was increased to -50 mV, the norfloxacin flux value at pH 5 increased to 5 ± 1 molecules/s while the flux at pH 7 remained unchanged (1 molecule/s). An obvious explanation suggests that the positive charge on the norfloxacin molecules at pH 5 results in them being driven through the porin under an applied transmembrane voltage. At pH 7 the overall charge on the molecule is neutral and thus the effect of the transmembrane voltage on the flux appears less important; free diffusion is the primary driving agent. However, there might still be some small voltage dependent effects since a significant proportion of the molecules are zwitterionic at pH 7 – this requires further investigation.

Note that the flux was calculated using $\Delta c = 1$ mM, to compare with the optofluidic permeability assay results described above. This is justified since it was observed that the number of antibiotic events in the ionic current recordings increased linearly with an increasing concentration of the antibiotic, and hence the rate constants measured with a concentration difference of 250 μM were equally applicable at a concentration difference of 1 mM.

Discussion

In this study, we used a label-free optofluidic permeability assay alongside single channel electrophysiology to explore the pH and voltage dependence of norfloxacin transport through OmpF porins. The optofluidic assay directly proves that the uptake of norfloxacin is enhanced by OmpF reconstituted in the proteoliposomes.

An interesting pattern emerges: in the absence of any transmembrane potential, the optofluidics assay shows that the flux per porin is essentially the same (within error) at both pH 5 and pH 7. However, as the transmembrane voltage is increased (electrophysiology), the flux at pH 5 starts to increase over the flux at pH 7. At a transmembrane voltage close to typical physiological OM Donnan potentials[21] of -25 mV, the flux at pH 5 is twice as large as the flux at pH 7. On increasing the transmembrane voltage to -50 mV, the flux at pH 5 increases to five times that at pH 7. This confirms that the positive charge on norfloxacin at pH 5 contributes significantly to its transport across porins in the presence of transmembrane voltages.

It has been reported that a change in the pH from acidic to basic reduced the minimum inhibitory concentration (MIC) of norfloxacin[17]; furthermore, the antibiotic showed maximum cytoplasmic accumulation at pH 7.5[18]. This agrees well with the data obtained in our study. As mentioned above, our experiments suggest that norfloxacin will accumulate in the periplasm (across the porin) of an *E. coli* bacterium at a 2× faster rate at pH 5 compared to pH 7. However, the drug

molecules now encounter the phospholipid inner membrane (IM). Our previous work showed that the direct diffusion of norfloxacin through a pure vesicle lipid bilayer is more effective (by a factor of approximately 6×) at pH 7 than at pH 5[25]. Furthermore, the periplasmic pH is expected to be the same as the external pH[31]. Considering the relative rates of norfloxacin transport across the two membranes at pH 5 and pH 7 thus explains the higher cytoplasmic accumulation at neutral/slightly basic pH values[17,18]. This suggests that diffusion through the inner membrane might present the rate limiting step. However, it should also be noted that medium acidification leads to the preferential expression of the narrower OmpC porins over OmpF[20] in *E. coli*, which might further reduce norfloxacin accumulation at acidic pH values.

Our analysis of norfloxacin transport through porins and lipids has thus clarified some of the mechanisms by which drug transport is affected under changing external conditions. The optofluidics assay also presents a direct visualisation of norfloxacin uptake across a proteoliposome membrane in a microfluidic, label-free system, not previously possible. The results unambiguously confirm the importance of these porins in facilitating the transport of fluoroquinolone antibiotics across the OM. In addition, our optofluidic technique enables the measurement of contributions to diffusion from pure lipids[25] and through porins, which cannot be done in a quantitative manner using the established liposome swelling assays[7,32,33]. Furthermore, our microfluidic based approach has the potential to explore a wide range of porins. Proteoliposomes could be devised containing a combination of passive diffusion porins and active transporters, to study competition between these processes. New vesicle preparation techniques[34] have shown considerable promise for integration into lab-on-a-chip devices, which should translate into better control over porin insertions and proteoliposome modification. A combination of traditional and advanced single vesicle techniques can thus be used to investigate a variety of drug transport phenomena, an urgent need in medicine today.

Methods

Optofluidic Permeability Assay

a) CONTROL EXPERIMENTS

Norfloxacin

Outlet

Vesicles

$T = t_f$

$T = t_i$

Pure Lipid Bilayer

Vesicle Membrane

b) PORIN EXPERIMENTS

Norfloxacin

Outlet

Proteoliposomes

$T = t_f$

$T = t_i$

OmpF Trimer

Proteoliposome Membrane

$\Delta T = (t_f - t_i) \sim 7.5$ s
Channel Width = 40 μm

Figure 3. Schematic of the optofluidic permeability assay. Control experiments (no porin) are represented in a) and proteoliposome experiments (containing OmpF) in b). Vesicles (liposomes/proteoliposomes) are mixed with norfloxacin in a T junction microfluidic chip by applying suction at the outlet reservoir with a syringe pump; norfloxacin autofluorescence is stimulated with a UV epifluorescence microscope. The vesicles are detected at an initial time t_i immediately post mixing and at a later time t_f, a distance of 7.4 mm further downstream. Vesicles took, on average, about 7.5 s to travel the intervening distance. Both time points are observed in the same field of view. Detection of the autofluorescence intensities within the vesicles at both points enables the calculation of the drug permeability coefficient for each vesicle.

The optofluidic permeability assay builds on our previous work studying the Permeability Coefficient of norfloxacin across lipid membranes[25]. It was designed to explore properties of porin mediated transport not accessible to electrophysiology and other traditional techniques. It enables the study of drug transport through porins without the application of a transmembrane voltage. Furthermore, even though electrophysiology has been the method of choice for characterising antibiotic-porin interactions at the single molecule level[35-38], it suffers from an inability to distinguish molecules that translocate through the porin from molecules that simply bind transiently[27]. The optofluidic permeability assay visualises drug transport directly, by observing the drug molecules themselves via their autofluorescence; it is thus label-free. Liposome swelling assays[32,33] were previously used as an alternative to electrophysiology.

66

However, these measure antibiotic flux relative to the flux of a permeable sugar (generally arabinose) and hence cannot measure drug permeability directly. Furthermore, the diffusion of charged compounds in these assays is influenced by the build-up of Donnan potentials inside the liposomes, which can lead to unexpected osmotic behaviour[32]. Our assay overcomes many of these intrinsic limitations and provides a new technique for studies of drug transport with porins.

As described in Figure 3, the optofluidic permeability assay involves a T junction microfluidic chip where the vesicles (liposomes/proteoliposomes) and the drug molecules are mixed in a channel (via the application of suction at the outlet). The T junction geometry of the chip leads to an equal mixing of vesicle and drug solutions. The inlet norfloxacin concentration is 2 mM (prepared in the same buffer solution as the vesicles) and hence the vesicles are exposed to a final norfloxacin concentration of 1 mM. The vesicles are imaged immediately post mixing with the norfloxacin and at a distance 7.4 mm further along the channel; the chip was designed such that both points were observed in the same field of view (Figure 3). The chip design was based on preliminary experiments which showed that a distance of about 7-8 mm between the two points was optimal for the detection of proteoliposomes showing increased uptake of the drug.

The norfloxacin molecules were tracked by stimulating their autofluorescence in the UV[25]. We performed all the optofluidics experiments described in this paper on a commercial Olympus IX73 microscope, using a DAPI filter set (Chroma) and a Mercury arc lamp (Prior Lumen 200). A 60× air objective was used (Olympus LUCPlanFLN, NA 0.70). Images were recorded using a scientific CMOS camera (optiMOS, QImaging) which enabled recording at 100 fps (10 ms exposure, bin 4). The microfluidic flows were controlled using a neMESYS syringe pump with a 250 μl Duran Borosilicate glass syringe (ILS, Germany) connected to the outlet. At the beginning of the experiments, a flow of 30-40 μl/hr was applied until the autofluorescence intensity in the microfluidic channel reached its peak, ensuring an appropriate drug concentration in the channel. Once this level was reached, the flow was slowed to 3 μl/hr enabling the detection of individual vesicles for multiple frames as desired[25].

The images were recorded using Micromanager 1.4[39] and analysed in MATLAB (scripts available on request) to obtain information about the autofluorescence intensities within the vesicles, in addition to the background intensity, vesicle shape and velocity[25]. Upchurch 1520 G tubing (inner diameter 0.03 inch) was used to connect the outlet of the chip to the syringe. Full details of the mathematical model and permeability coefficient calculations can be found in the earlier paper[25]. Calculations of the flux are presented in the Supplementary Information document.

Microfluidic Chip Fabrication

The microfabrication of the fluidic chip relies on photolithography and replica molding. For the fabrication of the mold, a Silicon substrate was covered with a thin layer of adhesion promoter

(Omnicoat, Microchem, spin coating: 2,000 r.p.m., 30 sec). A layer of SU-8 2025 (Microchem) was then deposited (2,000 r.p.m., 30 s), pre-baked (2 min at 65 °C, 5 min at 95 °C) and selectively exposed to ultraviolet light (12 s, 365-405 nm, 20 mWcm^{-2}) through a bespoke pellicle mask (Photodata Ltd, CAD file available on request). The sample was post-baked (1 min at 65 °C, 3 min at 95 °C), developed for 3 min, dried with a gentle stream of Nitrogen and hard baked for 5 min at 95 °C.

Sylgard 184 polydimethylsiloxane (PDMS) was used to create a negative replica from the Silicon mold using standard soft lithography techniques[40] with an elastomer:curing agent ratio of 9:1 (Dow Corning). The PDMS mixture was poured onto the Silicon mold and baked at 60 °C for 55 minutes. The PDMS chip was then peeled off the mold and inlet/outlet columns created using a 1.5 mm biopsy punch (Miltex). The chip was plasma bonded to a glass coverslip (Type I, Assistent, Germany) using an air plasma (10 W, 25 sccm, 10 s exposure, Diener Electronic GmbH & Co. KG, Germany). Post plasma bonding, the chip was left in an oven at 60 °C for 5-10 minutes to enhance the adhesion of PDMS to glass.

Vesicle formation and OmpF incubation

Giant Unilamellar Vesicles (GUVs) of 1,2-diphytanoyl-*sn-glycero*-3-phosphocholine (DPhPC) lipids (Avanti Polar Lipids) were prepared via electroformation using a Nanion Vesicle Prep Pro (Nanion Technologies GmbH, Germany) setup as described previously[25]. The GUVs were prepared in 200 mM Sucrose with 5 mM Phosphate Buffer (pH 7) or 5 mM Acetic Acid (pH 5).

The OmpF incubation followed previously established protocols[41]. Purified stock OmpF (5.5 mg/ml) in a detergent, a 1% solution of n-Octylpolyoxyethylene (octyl-POE, Bachem) prepared in Milipore water, was diluted 1:1 in the same detergent and vortexed; 1 μl of this freshly diluted OmpF solution was added to 199 μl of the vesicle stock solution and incubated at room temperature for an hour. Biobeads® SM-2 (Bio-Rad) were added to remove the detergent and the mixture was incubated at room temperature for 45-60 minutes followed by storage at 4 °C overnight. The next day, the OmpF embedded proteoliposome solution was separated from the Biobeads with a pipette and the sample used directly in experiments. For the control (liposome) experiments, 1 μl of 1% octyl-POE (instead of the OmpF solution) was added to 199 μl of the vesicles; the rest of the incubation protocol remained unchanged.

Single OmpF porin ionic current measurements in a solvent-free lipid bilayer

Reconstitution experiments and noise analyses were performed as described in detail previously[42]. The Montal and Mueller technique[43] was used to form a phospholipid bilayer using DPhPC (Avanti polar lipids). A Teflon film comprising an aperture of approximately 30-60 μm in diameter was placed between the two chambers of a cuvette. The aperture was pre-painted with 1% hexadecane in hexane for stable bilayer formation. 1 M KCl in 5 mM potassium acetate (pH 5) or 5 mM phosphate (pH 7) was used as the electrolyte solution and added to both sides of the chamber. Ionic currents were detected using standard silver-silver chloride electrodes from

WPI (World Precision Instruments) that were inserted in both sides of the cuvette. Single channel measurements were performed by adding the protein to the *cis* side of the chamber (the side connected to the ground electrode). Spontaneous channel insertion was typically obtained while stirring the solution in the cuvette under an applied transmembrane voltage. After a successful single channel reconstitution, the *cis* side of the chamber was carefully perfused to remove any remaining porins, thus preventing further channel insertions. Conductance measurements were performed using an Axopatch 200B amplifier (Molecular Devices) in voltage clamp mode. Signals were filtered by an on-board low pass Bessel filter at 10 kHz with a sampling frequency of 50 kHz. Amplitude, probability and noise analyses were performed using OriginPro 8 (OriginLab) and Clampfit software (Molecular Devices). Single channel analysis was used to determine the antibiotic binding kinetics. In a single channel measurement, the quantities measured were the duration of blocked levels/residence times (τ_c) and the frequency of blockage events (ν). The association rate constant k_{on} was derived using the number of blockage events, $k_{on} = \nu/3[c]$, where [c] is the concentration of the antibiotic. The dissociation rate constant (k_{off}) was determined by averaging the $1/\tau_c$ values recorded over the entire concentration range[38].

Port-a-Patch calibration for estimating the OmpF porin concentration in proteoliposomes

The Port-a-Patch calibration measurement involves patching OmpF embedded proteoliposomes and counting the number of OmpF porins in a patch using electrophysiology. This measurement reveals the number of OmpF porins per unit area on the surface of the proteoliposomes.

Planar lipid bilayers were obtained from proteoliposomes prepared using the same protocols described earlier. Purified stock OmpF (5.5 mg/ml) porins in 1% octyl-POE were diluted in the detergent and reconstituted into GUVs by incubating the porins as described previously; however, the final porin concentrations used in the Port-a-Patch calibration experiments were a factor of 500×, 250× and 100× more dilute than the final concentration used in the optofluidics assay to enable the counting of single porin insertions in the ionic current traces. After incubation, the detergent was removed using Biobeads® SM-2 (Bio-Rad) as described previously. The Biobeads were discarded after centrifugation and the protein containing GUVs (proteoliposomes) used immediately.

For the formation of a planar lipid bilayer containing the proteins, 5 μl of the proteoliposome solution was pipetted into 5 μl of the electrolyte solution (200 mM KCl, 5 mM acetic acid for pH 5 or 5 mM phosphate for pH 7). The resulting solution was placed on a microstructured glass chip (grounded side) containing an aperture approximately 1 μm in diameter. The vesicles burst once they touch the glass surface of the chip thus forming a planar lipid bilayer; additional suction was applied to patch proteoliposomes across the aperture. Ionic current measurements were performed using the same equipment and software as for the black lipid membrane measurements described above. The number of OmpF porins in a patch were directly evaluated from the ionic currents measured (Supplementary Figure S2).

Acknowledgements

Author Contributions

JC and HB contributed equally to this work.

All data accompanying this publication are directly available within the publication.

Financial Interests

The authors declare no competing financial interests.

References

1. Allen, H. K., et al. Call of the wild: antibiotic resistance genes in natural environments. *Nat. Revs. Microbiol.***8**, 251-259 (2010).
2. Cantas, L., et al. A brief multi-disciplinary review on antimicrobial resistance in medicine and its linkage to the global environmental microbiota. *Frontiers in Microbiol.***4**, 1-14 (2013).
3. McKenna, M. The Last Resort. *Nature*, **499**, 394-396 (2013).
4. Davies, J. & Davies, D. Origins and Evolution of Antibiotic Resistance. *Microbiol. and Mol. Biol. Revs.***74**, 417-433 (2010).
5. Ling, L. L., et al. A new antibiotic kills pathogens without detectable resistance. *Nature*, **517**, 455-459 (2015).
6. Delcour, A. H. Outer Membrane Permeability and Antibiotic Resistance. *Biochim. Biophys. Acta*, **1794 (5)**, 808-816 (2009).
7. Pagès, J-M., James, C. E. & Winterhalter, M. The porin and the permeating antibiotic: a selective diffusion barrier in Gram-negative bacteria. *Nat. Revs. Microbiol.*,**6**, 893-903 (2008).

8. Redgrave, L. S., Sutton, S. B., Webber, M. A. & Piddock, L. J. V. Fluoroquinolone resistance: mechanisms, impact on bacteria, and role in evolutionary success. *Trends in Microbiol.*, **22(8)**, 438-445 (2014).

9. Chevalier, J., Malléa, M. & Pagès, J-M. Comparative aspects of the diffusion of norfloxacin, cefepime and spermine through the F porin channel of *Enterobacter cloacae*. *Biochem. J.*, **348**, 223-227 (2000).

10. Hirai, K., et al. Isolation and Characterization of Norfloxacin-Resistant Mutants of *Escherichia coli* K-12. *Antimicrob. Agents Chemother.*, **30**, 248-253 (1986).

11. Cohen, S. P., McMurry, L. M., Hooper, D. C., Wolfson, J. S. & Levy, S. B. Cross-Resistance to Fluoroquinolones in Multiple Antibiotic-Resistant (Mar) *Escherichia coli* Selected by Tetracycline or Chloramphenicol: Decreased Drug Accumulation Associated with Membrane Changes in Addition to OmpF Reduction. *Antimicrob. Agents Chemother.*, **33**, 1318-1325 (1989).

12. Kishii, R. & Takei, M. Relationship between the expression of *ompF* and quinolone resistance in *Escherichia coli*. *J. Infect. Chemother.*, **15**, 361-366 (2009).

13. Stavenger R. A & Winterhalter M. TRANSLOCATION Project: How to Get Good Drugs into Bad Bugs. *Sci. Transl. Med.*, **6**, 228ed7 (2014).

14. Hooper, D. C. Mechanisms of Action of Antimicrobials: Focus on Fluoroquinolones. *Clin. Infect. Dis.*, **32 (Suppl. 1)**, S9-S15 (2001).

15. Zeiler, H. J. Evaluation of the in vitro bactericidal action of ciprofloxacin on cells of Escherichia coli in the logarithmic and stationary phases of growth. *Antimicrob. Agents Chemother.*, **28**, 524–527(1985).

16. Hooper, D. C., Wolfson, J. S., Souza, K. S., Ng, E. Y., McHugh, G. L. & Swartz, M. N. Mechanisms of quinolone resistance in Escherichia coli: characterization of nfxB and cfxB, two mutant resistance loci decreasing norfloxacin accumulation. *Antimicrob. Agents Chemother.* **33**, 283–290(1989).

17. Smith, J. T. & Ratcliffe, N. T. Effect of pH value and magnesium on the antibacterial activity of quinolone preparations. *Infection*, **14 Suppl 1**, S31–35 (1986).

18. Nikaido, H. & Thanassi, D. G. Penetration of Lipophilic Agents with Multiple Protonation Sites into Bacterial Cells: Tetracyclines and Fluoroquinolones as Examples. *Antimicrob. Agents Chemother.*, **37**, 1393-1399 (1993).

19. Piddock, L. J. V., Jin, Y.-F., Ricci, V. & Asuquo, A. E. Quinolone accumulation by *Pseudomonas aeruginosa*, *Staphylococcus aureus* and *Escherichia coli*. *J. Antimicrob. Chemother.*, **43**, 61-70 (1999).

20. Thomas, A. D. & Booth, I. R. The regulation of expression of the porin gene *ompC* by acid pH. *J. Gen. Microbiol.*, **138**, 1829-1835 (1992).

21. Sen, K., Hellman, J. & Nikaido, H. Porin Channels in Intact Cells of *Escherichia coli* Are Not Affected by Donnan Potentials Across the Outer Membrane. *J. Biol. Chem.*, **263 (3)**, 1182-1187 (1988).

22. Kennedy, E. P. Osmotic regulation and the biosynthesis of membrane-derived oligosaccharides in *Escherichia coli*. *Proc. Nat. Acad. Sci. USA*, **79**, 1092-1095 (1982).

23. Mortimer P. G. & Piddock, L. J. A comparison of methods used for measuring the accumulation of quinolones by *Enterobacteriaceae*, *Pseudomonas aeruginosa* and *Staphylococcus aureus*. *J. Antimicrob. Chemother.* **38,** 639-653 (1991).

24. Kaščáková, S., Maigre, L., Chevalier, J., Réfrégiers, M. & Pagès, J. M. Antibiotic transport in resistant bacteria: Synchrotron UV fluorescence microscopy to determine antibiotic accumulation with single cell resolution. PLOS ONE **7**, e38624 (2012).

25. Cama, J., Chimerel, C., Pagliara, S., Javer, A. & Keyser, U. F. A label-free microfluidic assay to quantitatively study antibiotic diffusion through lipid membranes. *Lab Chip*, **14**, 2303-2308 (2014).

26. Angelova, M. I. & Dimitrov, D. S. Liposome Electroformation. *Faraday Discuss. Chem. Soc.*, **81**, 303-311 (1986).

27. Mahendran, K. R., et al. Molecular Basis of Enrofloxacin Translocation through OmpF, an Outer Membrane Channel of *Escherichia coli* – When Binding Does Not Imply Translocation. *J. Phys. Chem. B*,**114**, 5170–5179 (2010).

28. Benz, R., Schmid, A. & Vos-Scheperkeuter, G. H. Mechanism of sugar transport through the sugar-specific LamB channel of Escherichia coli outer membrane. *J. Membr. Biol.***100(1)**, 21–29(1987).

29. Schwarz, G., Danelon, C. & Winterhalter, M. On Translocation Through a Membrane Channel via an Internal Binding Site: Kinetics and Voltage Dependence. *Biophys. J.*, **84**, 2990-2998 (2003).

30. Bezrukov, S. M., Berezhkovskii, A. M. & Szabo, A. Diffusion model of solute dynamics in a membrane channel: Mapping onto the two-site model and optimizing the flux. *J. Chem. Phys.*, **127**, 115101 (2007).

31. Wilks, J. C. & Slonczewski, J. L. pH of the cytoplasm and periplasm of Escherichia coli: rapid measurement by green fluorescent protein fluorimetry. *J. Bacteriol.***189**, 5601–5607 (2007).

32. Nikaido, H. & Rosenberg, E. Y. Porin channels in Escherichia coli: studies with liposomes reconstituted from purified proteins. *J. Bacteriol.***153**, 241–252 (1983).

33. Yoshimura, F. & Nikaido, H. Diffusion of beta-lactam antibiotics through the porin channels of Escherichia coli K-12. *Antimicrob. Agents Chemother.***27**, 84–92(1985).

34. Karamdad, K., Law, R. V., Seddon, J. M., Brooks, N. J. & Ces, O. Preparation and mechanical characterisation of giant unilamellar vesicles by a microfluidic method. *Lab Chip*, **15**, 557-562 (2015).

35. Delcour, A. H. Function and modulation of bacterial porins: insights from electrophysiology. *FEMS Microbiol. Lett.*,**151**, 115-123 (1997).

36. Delcour, A. H., Martinac, B., Adler, J. & Kung, C. Modified reconstitution method used in patch-clamp studies of *Escherichia coli* ion channels. *Biophys. J.*, **56**, 632-636 (1989).

37. Buechner, M., Delcour, A. H., Martinac, B., Adler, J. & Kung, C. Ion channel activities in the *Escherichia coli* outer membrane. *Biochim. Biophys. Acta*, **1024**, 111-121 (1990).

38. Nestorovich, E. M., Danelon, C., Winterhalter, M. & Bezrukov, S. M. Designed to penetrate: Time-resolved interaction of single antibiotic molecules with bacterial pores. *Proc. Nat. Acad. Sci. USA*, **99**, 9789-9794 (2002).

39. Stuurman, N., Amdodaj, N. & Vale, R. □Manager: Open Source Software for Light Microscope Imaging. *Microscopy Today*, **15**, 42-43 (2007).

40. Qin, D., Xia, Y. & Whitesides, G. M. Soft lithography for micro- and nanoscale patterning. *Nat. Protocols*, **5**, 491-502 (2010).

41. Kreir, M., Farre, C., Beckler, M., George, M. & Fertig, N. Rapid screening of membrane protein activity: electrophysiological analysis of OmpF reconstituted in proteoliposomes. *Lab Chip*, **8**, 587-595 (2008).

42. Singh, P. R., Ceccarelli, M., Lovelle, M., Winterhalter, M. & Mahendran, K. R. Antibiotic Permeation across the OmpF Channel: Modulation of the Affinity Site in the Presence of Magnesium. *J. Phys. Chem. B*, **116**, 4433-4438 (2012).

43. Montal, M. & Mueller, P. Formation of Bimolecular Membranes from Lipid Monolayers and a Study of their Electrical Properties. *Proc. Nat. Acad. Sci. USA*, **69**, 3561-3566 (1972).

Table 3: Antibiotic association (k_{on}) and dissociation (k_{off}) rate constants obtained by single channel measurements for OmpF at pH 5 and pH 7. Electrolyte conditions: 1 M KCl, 5 mM PO_4 (pH 7)/acetate (pH 5).
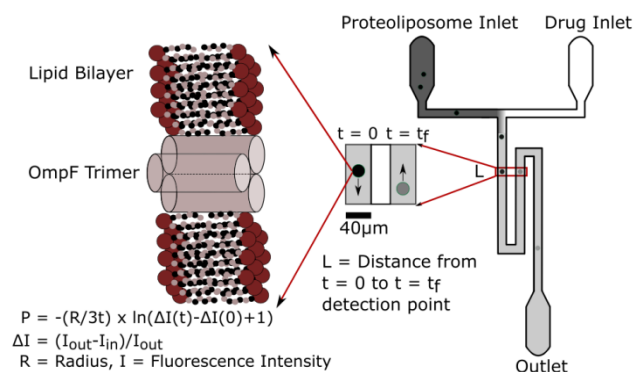
k_{on}= ({No. of events/sec}/ 3*[c]), k_{off}= (1/residence time)

$$J= \frac{k_{on}^{cis} \cdot c_{cis} \cdot k_{on}^{trans}}{(k_{on}^{cis} + k_{on}^{trans})}; \Delta c=1 \text{ mM: valid under } k_{off} >>> k_{on} \cdot c$$

Antibiotics	k_{on}^{cis} (10^3) {1/(s*M)}	k_{on}^{trans} (10^3) {1/(s*M)}	k_{off}^{total} 1/(s)	J (molecules/s)
Norfloxacin	**-50mV**	**+50mV**		Δc=1 mM
pH 7	13 ± 5	1.3	1561 ± 120	1
pH 5	11 ± 3	10	25000	5 ± 1
	-25mV	**+25mV**		
pH 7	9 ± 2.5	1	1150 ± 60	0.9
pH 5	3 ± 1	5 ± 2	27000	1.8 ± 0.7
	0 mV (Optofluidics)			
pH 7				10 ± 7
pH 5				14 ± 9

Errors are standard deviations.

Table of Contents Graphic

Lipid Bilayer

OmpF Trimer

$P = -(R/3t) \times \ln(\Delta I(t) - \Delta I(0) + 1)$
$\Delta I = (I_{out} - I_{in})/I_{out}$
R = Radius, I = Fluorescence Intensity

Proteoliposome Inlet   Drug Inlet

$t = 0$ $t = t_f$

40µm

L = Distance from
$t = 0$ to $t = t_f$
detection point

Outlet

Quantification of fluoroquinolone uptake through the outer membrane channel OmpF of *Escherichia coli*

Jehangir Cama, Harsha Bajaj, Stefano Pagliara, Theresa Maier, Yvonne Braun, Mathias Winterhalter and Ulrich F. Keyser

SUPPLEMENTARY MATERIAL

Optofluidics Assay Porin Measurements:

$$\Delta I = (I_{out} - I_{in})/I_{out}$$
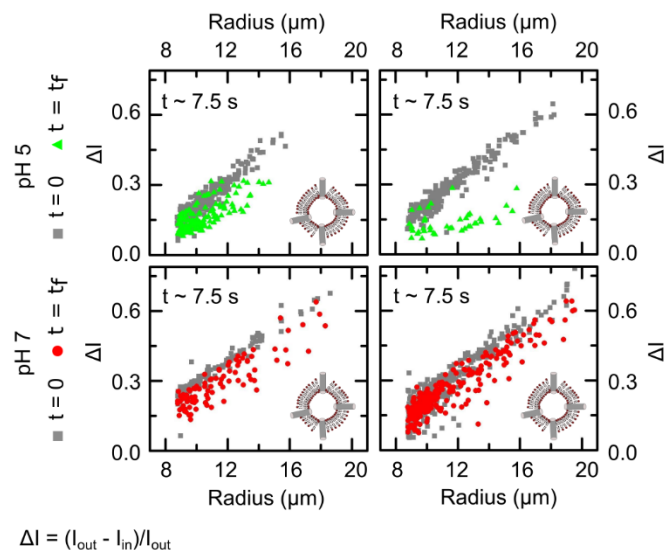
Figure S1. Repeat norfloxacin uptake measurements of OmpF-embedded proteoliposomes in the optofluidic assay. Each scatter plot represents an individual experiment, with a different batch of proteoliposomes. Differences in the nature of the spread can be attributed to differences in the vesicle batch quality and porin insertion efficiency. However, in all plots enhanced uptake is observed for a significant proportion of the proteoliposomes.

Enhanced norfloxacin uptake is observed due to the presence of OmpF in the proteoliposome membranes as seen in Figure 2 (main text) and Figure S1 above. Different vesicle batches led to slightly different spreads in the scatter plots; this is attributable to differences in vesicle quality across different electroformation preparations, which affects the porin insertion efficiency as seen in Figure S2 below.

The porin insertion efficiency was similar (within error) at both pH 5 and pH 7. As mentioned in the main text, the OmpF concentrations measured were 500×, 250× and 100× lower in the Nanion Port-a-Patch vesicle incubations as compared with the vesicles used for the microfluidics. Higher concentrations could not be measured since the patches formed were not stable.

The diameter of the patched vesicle membrane was 1 μm. From the calibration curve (Fig. S2), we calculate an estimate of approximately 1800 porins per μm^2 membrane surface area for the vesicles in the optofluidic assay. Since we measure the vesicle radius in the optofluidic assay, it is straightforward to calculate the surface area of each vesicle and use the Port-a-Patch calibration measurement to estimate the number of porins per vesicle. The permeability coefficient of the vesicle contains information about the total flux of drug molecules into the vesicle, and hence an estimate of the flux per porin can be calculated (as detailed below).
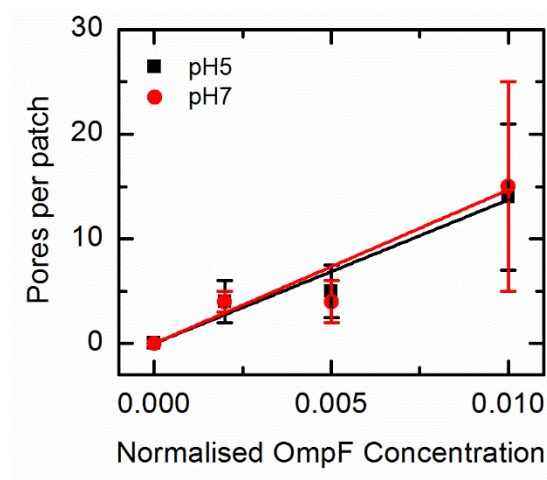
Figure S2. OmpF insertion efficiency calibration. To estimate the number of OmpF porins in the vesicles used in the optofluidics assay, a range of OmpF concentrations were measured in vesicles in a Port-a-Patch setup as described in the text. The number of OmpF porins per membrane patch (d = 1 μm) were counted and used to plot a calibration curve. The OmpF concentrations displayed are normalised with respect to the concentrations used in the optofluidics assay. Within error, we observe a linear increase in the number of porins measured per patch. Extrapolating to the concentrations used in the optofluidics assay, we estimate 1750 ± 114 porins per μm^2 in the vesicles at pH 5 and 1871 ± 137 porins per μm^2 at pH 7. For each OmpF concentration, four batches of proteoliposomes were prepared at both pH 5 and pH 7. The number of proteoliposome patches measured for each OmpF concentration (at each pH) was, in order of increasing OmpF concentration, N = 17, N = 6 and N = 11.

If we neglect the contribution of diffusion through the lipids, an average over all events gives a flux value of 10 ± 8 norfloxacin molecules/s per porin at pH 7 and 15 ± 10 molecules/s per porin at pH 5 (mean ± s.d). The reported flux per porin is an average over the value obtained from all the proteoliposomes (N = 420 at pH 7 and N = 268 at pH 5) over 3 individual experiments at each pH.

Subtracting the contribution due to the diffusion through pure lipids leaves the flux values unchanged. This is expected, since there is little diffusion of the drug across pure lipid membranes within the timescales studied[1].

Flux Calculations:

The flux (J) through a proteoliposome can be calculated from its Permeability Coefficient (P) as follows[1]:

$$P = -\left(\frac{R}{3t}\right) \times \ln\left(\Delta I(t) - \Delta I(0) + 1\right) \qquad (1)$$

$$J = 4\pi R^2 \times P \times \left(\Delta I(t) - \Delta I(0) + 1\right) \times c_{out} \qquad (2)$$

where c_{out} is 1 mM.

The main contribution to J is the flux through the OmpF porins in the proteoliposomes. There is a small contribution that arises due to norfloxacin diffusion through the pure lipid bilayer. This can be quantified using known values of the permeability coefficient of norfloxacin across DPhPC vesicle membranes, as measured previously[1]. The control measurements show that in the absence of porins, $\Delta I(t) \sim \Delta I(0)$ on the probed timescales. Therefore, the (maximum) contribution of the diffusion through lipids, J_{lipids}, to the total flux measured is given by:

$$J_{lipids} = 4\pi R^2 \times P_{lipids} \times c_{out} \qquad (3)$$

where c_{out} is 1 mM, as usual. P_{lipids} = 0.006 µm/s at pH 7; $P_{lipids} \sim$ 0.001 µm/s at pH 5[1].

The actual flux through **all** the porins in a proteoliposome, J_{porin}, is thus:

$$J_{porin} = J - J_{lipids} \qquad (4)$$

Dividing J_{porin} by the number of porins in the proteoliposome gives us the flux per porin for that proteoliposome, corrected for the contribution of the flux through the lipids.

To summarise the flux calculation:

1. We measure the permeability coefficient of individual proteoliposomes using equation (1) above, as described previously[1]. The spread in the permeability coefficients for individual vesicles is shown in the histograms in Figure 1 (c,f) of the main text.
2. Using equation (2) above, we calculate the flux through the entire proteoliposome membrane for each proteoliposome. Thus the permeability coefficient of a proteoliposome is used to calculate the flux of norfloxacin through the membrane of that proteoliposome.
3. From equations (3) and (4) above, we subtract the contribution of norfloxacin flux through pure lipids for the individual proteoliposome. We thus have, for each proteoliposome studied, the total flux of norfloxacin molecules through the active/open OmpF porins in its membrane.
4. The calibration measurement (Figure S2) provides the number of functional OmpF porins per unit surface area of the proteoliposomes.

5. For each individual proteoliposome, we measure the radius, and hence calculate its surface area. Using the surface area and the calibration measurement, we calculate the number of functional OmpF porins in the protoeliposome.
6. Dividing the total porin-mediated flux by the number of porins in the proteoliposome thus provides the flux per porin for that particular proteoliposome.
7. We thus calculate the flux per porin for each proteoliposome studied. The value reported is an average over all the proteoliposomes detected at each pH.

Data Analysis:

In the data analysis of the optofluidic assay, four selection criteria were applied to separate genuine vesicle detection events from lipid aggregates. Firstly, the MATLAB analysis code detects the shape of the vesicle and measures its major and minor axis. A circularity criterion, defined as the ratio of Minor axis: Major axis, is calculated and only events with a circularity greater than 0.7 are considered for analysis.

Only those vesicles with radii between 20 and 45 pixels (i.e., approximately 8.8 µm to 19.7 µm) were chosen for analysis; vesicles with radii below 20 pixels were difficult to distinguish from lipid aggregates, and were hence discarded. Since the microfluidic channel width is 40 µm, vesicles with radii greater than 20 µm were subject to shear by the channel walls, which can affect drug uptake. Therefore these events were discarded as well.

Vesicles with velocities only between 0.4 – 1.5 mm/s were chosen for analysis. Events with velocities above 1.5 mm/s were generally false positives; events below 0.4 mm/s were either false positives or cases where vesicles were moving along the channel walls and were hence subject to shear.

Finally, it was observed that ΔI values below 0.05 were associated with lipid aggregates and false positives. Therefore all events with $\Delta I < 0.05$ were discarded.

The main purpose of the selection criteria is to speed up the analysis process. However, the frames corresponding to vesicle events are saved separately during image analysis in MATLAB, and hence each point in the scatter plots can be checked visually as well if desired.

For the calculation of the permeability coefficient (P), a fit of ΔI vs R for the $t = 0$ points is made, and the difference in ΔI between the $t = t_f$ and $t = 0$ points is evaluated based on this fit (full details are available in ref. 1). This difference is used to calculate P. Therefore, owing to the nature of the calculation technique, a few $t = t_f$ points that overlapped with the $t = 0$ points in the scatter plots (representing vesicles that were multilamellar or had improper porin insertions, hence no drug uptake) resulted in negative P values, which are obviously unphysical. These points were not included in the histograms in Figure 2 of the main text, and were excluded from the flux calculations. In the histograms from the control experiments, this fraction of negative P values was naturally higher; these were also discarded.

Port-a-Patch confirmation of functional channels:
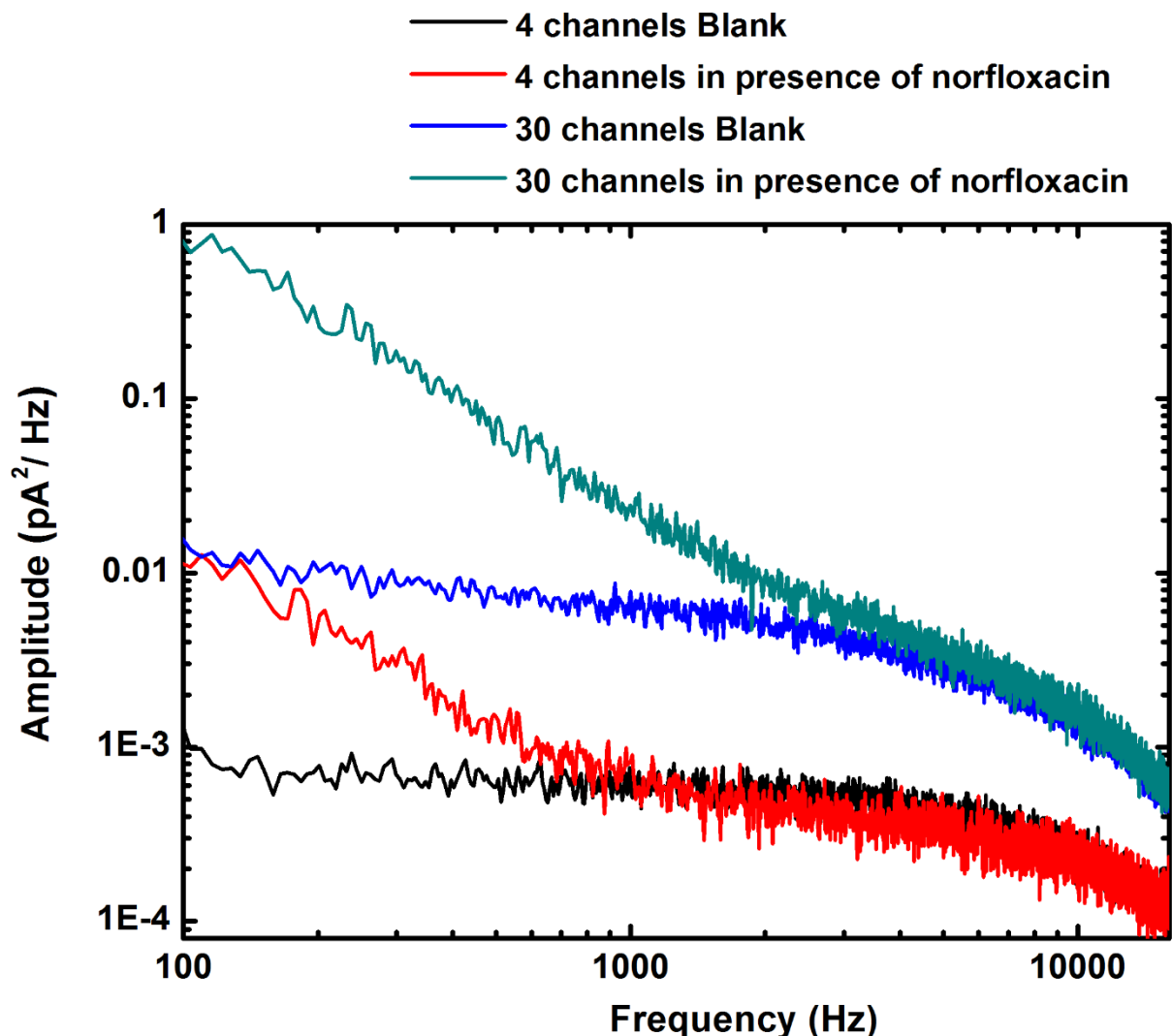
Figure S3. Port-a-Patch Power Spectrum. The black line shows the noise in the presence of 4 OmpF channels and the bright blue line represents the noise in the presence of 30 channels. We study the interaction of norfloxacin with these channels. If the membrane patch with a current was simply a leak, there would be no interaction (i.e, no increased noise) in the presence of norfloxacin. The red and the blue-grey lines show that the noise increases, for both patches, in the presence of norfloxacin, proving that these are indeed patches formed of functional OmpF channels. This interaction is similar to what was observed in our single channel planar lipid bilayer experiments.

To confirm that the membrane patches observed in the Port-a-Patch system contained functional OmpF channels, we present power spectra of ionic current measurements in the Port-a-Patch system in Figure S3. The power spectra for patches containing 4 and 30 OmpF channels respectively are presented. The increased noise in the presence of norfloxacin indicates that the patches are not simply leaks, but contain functional OmpF channels.

References

44. Cama, J., Chimerel, C., Pagliara, S., Javer, A. & Keyser, U. F. A label-free microfluidic assay to quantitatively study antibiotic diffusion through lipid membranes. *Lab Chip*, **14**, 2303-2308 (2014).

P3.3.2: Revealing single antibiotic molecule translocation through porins

Manuscript in preparation

Individual Contribution

My main contribution in this manuscript is to design the study, to perform experiments and analysis of data from single channel electrophysiology. I participated in the composition of manuscript.

Revealing single antibiotic molecule translocation through biological nanopores

Harsha Bajaj[a], Matteo Ceccarelli[b], Mathias Winterhalter[a]

[a]School of Engineering and Science, Jacobs University Bremen, Bremen, Germany [b]Department of Physics, University of Cagliari, Cagliari, Italy

Abstract

Single channel electrophysiology is used to the study interaction of β-lactam antibiotics with porins from *Escherichia coli* at a single molecule level. Varying external parameters like pH changes the charge state of the antibiotic norfloxacin, which modulates drastically the interaction with the pore from milliseconds to microseconds range. Applied external voltages act as driving force for the antibiotic and the association rate increases exponentially. The residence time of the antibiotic in the pore, on the other hand decreases with increasing applied voltage. We try to elucidate the contribution of different parameters like electrostatic, electro-osmotic and the electric field inside the pore on the translocation of antibiotics through OmpF by varying the type of salt and salt concentration.

Introduction

The complex membrane in Gram-negative bacteria ensures its survival by allowing a selective passage of nutrients and waste into and from the cell cytoplasm. Influx is largely controlled by porins[1], which are water-filled open channels that span the outer membrane of Gram-negative bacteria and allow the passive penetration of hydrophilic molecules. Apart from various nutrient molecules many classes of antibiotics like β-lactams are also known to use outer membrane channels to the reach target site[1,2]. Electrophysiology is an appropriate method to analyze the physico-chemical properties of these porins, like conductance, selectivity and voltage gating[2]. Interactions between antibiotics and a single outer membrane channel have been characterized previously[3]. Based on single channel study and 3D structure of the porin [4], authors postulated that ampicillin, a zwitterionic antibiotic "binds" to the positively and negatively charged residues at the constriction zone of the OmpF monomer[3]. Later in 2010 Hajjar *et. al.* [5], revealed the molecular mechanism of antibiotic translocation through porin using combination of techniques at different time scales, like liposome swelling assays, temperature-dependent ion current

fluctuation and MD simulations. This study demonstrated the importance of local molecular interactions of antibiotic in diffusion through porin. Another step forward made in a study by Mahendran *et. al.*[6,7], where they distinguished between binding of antibiotic to the channel and effective translocation. Therefore, single channel recording experiments, together with the results from MD simulations and liposome swelling assays suggest that binding at the constriction zone might facilitate efficient antibiotic transfer across OmpF porin[5,8,9]. However, a recent study[10] determined the X-ray crystal structure of OmpF with antibiotics, highlighting the "binding sites" of β-lactam antibiotics with the porin and showed that in bacteria there is an increased antibiotic uptake with expression of OmpF mutants that disrupt its binding interactions with antibiotics. Hence the study suggested that in fact binding of antibiotic to the channel reduces the uptake of antibiotics. In spite of significant research efforts in this area, it still remains unclear on how specific interactions of different antibiotics play a role in their translocation rates. Aspects like voltage effects (applied in electrophysiology) on small molecules like antibiotics were not addressed earlier. Previous studies have suggested that antibiotic molecules do have effect due to polarity of voltage but have not clearly reported it[11,12].

In this study we employ single channel electrophysiology to elucidate the rate limiting interaction of antibiotics like fluoroquinolones and β- lactams with porins from *E. coli.* We also investigated the interaction of carbapenem and cephalosporin through OmpF and OmpC porin. The asymmetry in the kinetics due to the polarity of voltage and asymmetric addition of antibiotic are reported. Additionally, we studied the translocation of norfloxacin through OmpF in a pH dependent and voltage dependent manner. The molecular explanation of observed voltage dependence is further investigated by varying the salt concentration and type of salt to elucidate the underlying electrostatic and electro-osmotic contributions.

Results and Discussion

Interaction of β-lactam antibiotics with OmpF and OmpC- We studied the interaction of β-lactam antibiotics presented in *Figure 1*(a- f). The corresponding molecular weights of antibiotics and charge state at physiologic pH conditions are presented *Figure 1*. The calculated dipole moment of antibiotics is also presented in *Figure 1*. We studied in particular the interaction of carbapenem class and cephalosporin with both the porins.
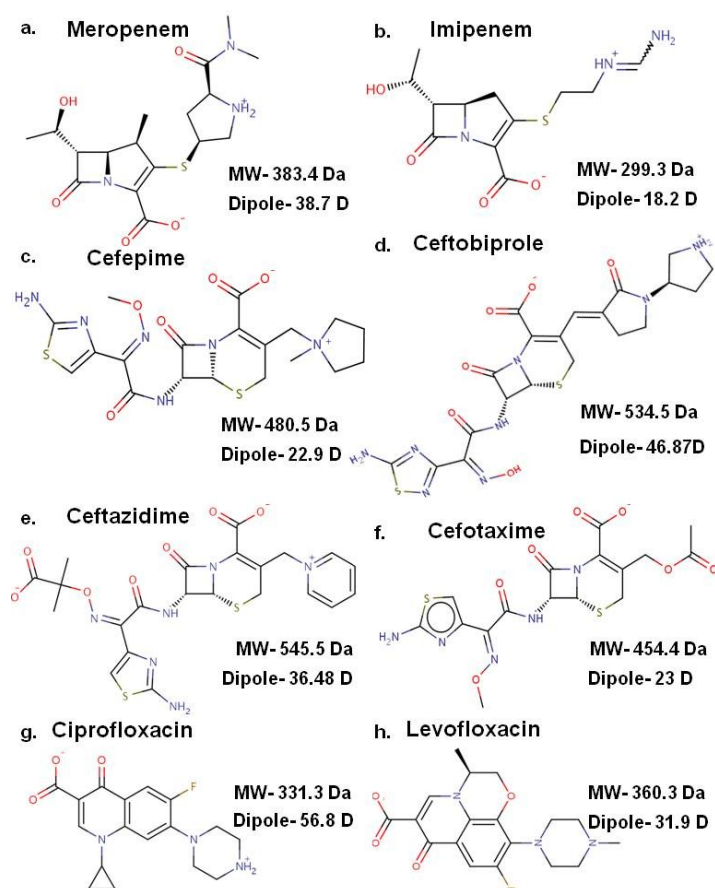
Figure 1: Chemical structures of antibiotics (a) meropenem, (b) imipenem, (c) cefepime (d) ceftobiprole (e) ceftazidime (f) cefotaxime (g) ciprofloxacin and (h) levofloxacin are shown. Charge states of the above antibiotics at physiological pH (7.5), the respective molecular weight (MW) and the dipole values calculated in water are presented here. The structure and the dipole values are taken from http://www.dsf.unica.it/translocation/db/

Both the porins have slight asymmetric conductance values with the polarity of the voltage which is used as a probe for the orientation of porin (slightly higher conductance at positive voltage for both OmpF and OmpC; at negative voltage short flickering is observed for OmpF *Figure 2*a). In the absence of antibiotics, negligible fluctuation in the ion current was detected in single OmpF/OmpC channel (*Figure 2*a and *Figure 3*a). Ion current fluctuations through single porin channel caused by antibiotic addition either to *cis*/ground side (corresponds to extracellular side of porin facing *cis* side, when porin is added to the same side) or *trans* side (corresponds to the periplasmic side of porin facing *trans* side), was quantified (Table 1 and Table 2).
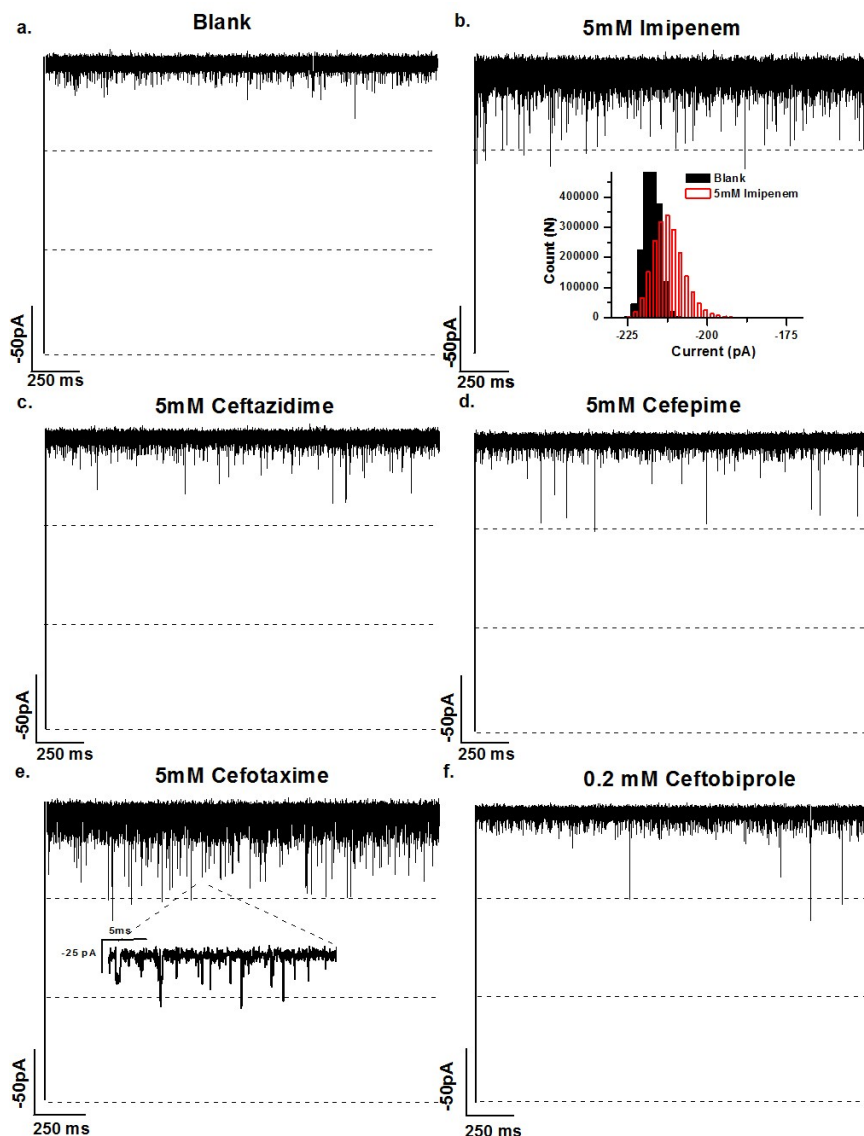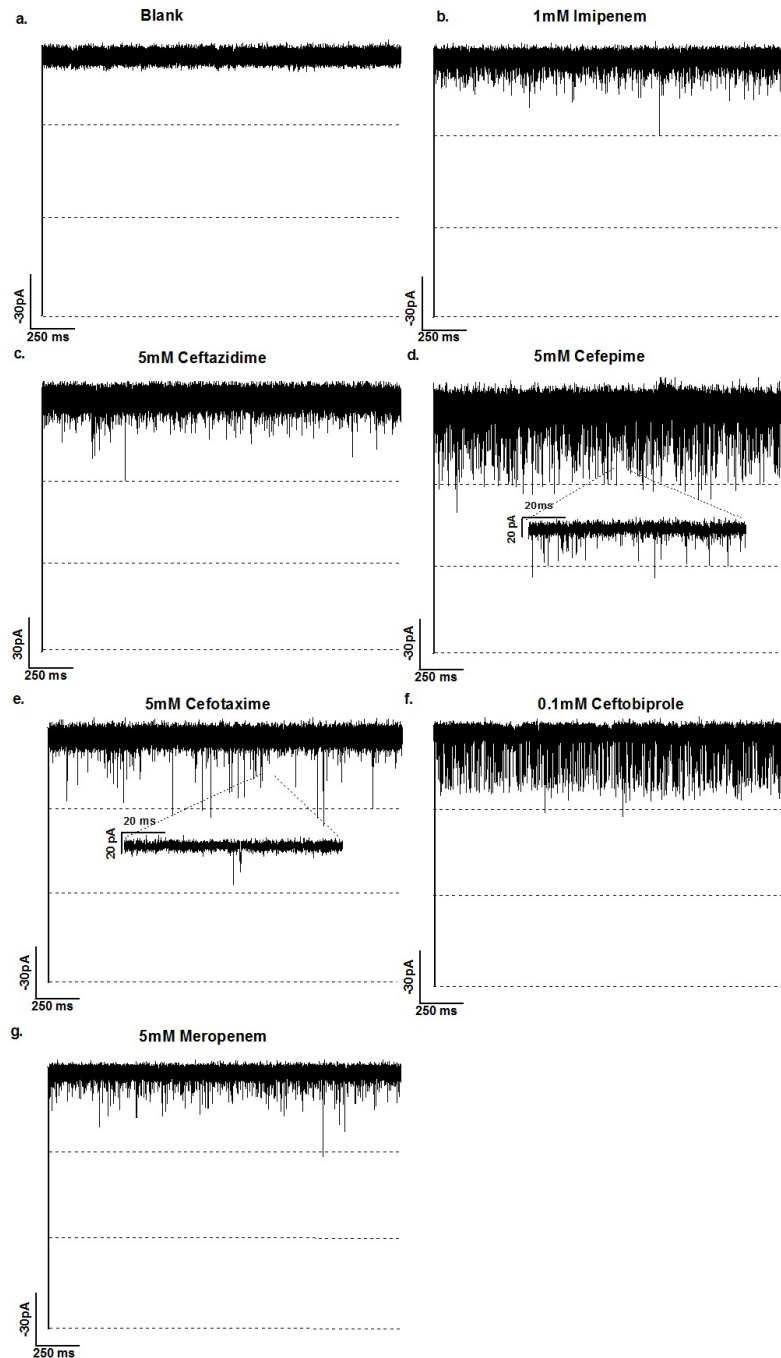
Figure 2: Ion current trace of single channel of OmpF- (a) without any antibiotic (b) 5 mM imipenem on cis side (c) 5 mM ceftazidime cis side (d) 5 mM cefepime cis side (e) 5 mM cefotaxime cis side (f) 0.2 mM ceftobiprole cis side. Electrolyte conditions: 1 M, 20 mM MES pH 6 at -50mV.

Addition of 5mM imipenem to cis side of OmpF channel cause well resolved monomer blockages as shown in *Figure 2*b. Apart from the well resolved monomer blockages which can be quantified using single channel event analysis (outlined in materials and methods) Table 1, we also observed a shift in the average current (or associated noise) shown in the inset of *Figure 2*a. The ion-current histogram does not have second peak due to the blockages of antibiotics but it has a tail shown in the inset (red colored) of *Figure 2*a. The associated noise/reduction in

conductance is also observed when imipenem is added to *trans* side in combination with well resolved events quantified in Table 1. The analysis of such a component is dealt in detail in the next section using meropenem-OmpF as an example.

Figure 3: Ion current trace of single channel of OmpC- (a) without any antibiotic (b) 1 mM imipenem on cis side (c) 5 mM ceftazidime cis side (d) 5 mM cefepime cis side (e) 5 mM cefotaxime cis side (f) 0.1 mM

ceftobiprole cis side and (g)5mM meropenem. Electrolyte conditions: 1 M, 20 mM MES pH 6 at -50mV; except for ceftazidime which is at +50mV.

Apart from carbapenem, we studied the interaction of 3rd (cefotaxime, ceftazidime), 4th (cefepime) and 5th (ceftobiprole) generation cephalosporins with OmpF. Addition of ceftazidime to the *cis* side of OmpF resulted in partial ion current flickering. In contrast addition of 5mM cefepime caused well resolved monomer blockages. Asymmetric addition of ceftazidime caused slight asymmetries in the kinetics from *cis* side and *trans* side addition, whereas cefepime showed huge asymmetry in kinetics when added to *trans* side as shown in Table 1. Addition of cefepime to the *trans* produced well resolved blockages (quantified in Table 1) and is associated with an increased noise (the origin of which is not very clear yet). Addition of cefotaxime in a single OmpF channel causes well resolved partial monomer and full monomer blockages as shown in *Figure 2*e (zoomed in part). Cefotaxime showed asymmetric kinetics when added to *trans* side the association rate being slightly higher at *cis* side compared to *trans* side. Ceftobiprole on the other hand caused huge asymmetry in kinetics when added from *cis* and *trans* sides. Addition of 0.2 mM of ceftobiprole on *cis* side caused well resolved full monomer blockages. The residence time for all the β-lactam antibiotics were about ≤ 100 μs.

Interactions of the β-lactams were investigated with single OmpC channel. Addition of imipenem and meropenem to the *cis* side of the channel caused very short unresolved events as shown *Figure 3*b and *Figure 3*g. Stronger interaction is observed in case of imipenem as compared to meropenem with OmpC Table 2. Both the antibiotics are more accessible to the channel from the *cis* side as compared to *trans* side. The residence time of the carbapenem tested here are about 100 μs (near the resolution limit of the instrument).

Addition of cephalosporins to the channel caused ion current interruptions as depicted in *Figure 3*. Cefotaxime and ceftazidime showed weaker interaction as compared to cefepime and ceftobiprole Table 2. Ceftazidime addition to *cis* side of the channel gave rise to short ion current fluctuation *Figure 3*c and ceftazidime seems to be more accessible from the *cis* side of the channel compared to *trans* side Table 2. On other hand cefotaxime showed higher kinetics with *trans* addition as compared to *cis* side. Addition of cefotaxime to *cis* side showed fully resolved short events and monomer blockages *Figure 3*e. *Figure 3*d presents the interaction of cefepime when added to cis side of the channel. We observe well resolved full monomer blockages and it

seems to be highly asymmetric where almost no interaction is observed from the *trans* side of the chamber Table 2. On the contrary, addition of ceftobiprole to the single OmpC channel lead to partial monomer well resolved ion current blockages shown in *Figure 3*f. Ceftobiprole seems to be exceptional candidate with the highest association rates on the *cis* side among all the measured antibiotics with OmpC Table 2. It shows higher accessibility from the *cis* side as compare to the *trans* side of the bilayer. The residence times of the cephalosporin antibiotics within OmpC porin is ≤ 100 μs.

Asymmetric kinetics with the polarity of the voltage

In this study we analyzed in detail the β-lactam antibiotic interaction with a single OmpF and OmpC channel as presented in Table 1 and Table 2. We report the effect of polarity of voltage and asymmetric addition of antibiotics to single channel. As a general trend we observe that, all the antibiotics seems to have a prominent effect at negative potentials as compared to positive potential when added on the *cis* side of the channel (Table 1 and Table 2). And when added to *trans* side of the chamber, higher interaction is observed at positive potentials. The difference of magnitude in kinetic rates at different polarity of voltage varies by a factor from $2 - 10$ times depending on the antibiotic and the porin. This trend is observed irrespective of charge, size of antibiotic or the porin being investigate.

A simplified explanation for this could be to:

1. Orientation of antibiotic: The antibiotic might orient in presence of an applied transmembrane voltage due to presence of a dipole moment shown in *Figure 1*. Since both the channels are cation selective[13–15] (in the present conditions measured in electrophysiology i.e. in KCl), it might prefer antibiotic with its positive orientation entering the channel. This correlates at least qualitatively with the electrophysiology data i.e. when antibiotic is added to *cis* side (grounded side) prominent effect is observed at negative voltage (which might orient the antibiotic dipole) where as when added to *trans* side (side of applied voltage) a prominent effect is observed at positive potentials (where the antibiotic might be oriented with its positive group entering the channel).

2. Electro-osmotic effect driving the molecule: Another possible mechanism could be based on electro-osmosis driving the molecule into the channel. At an applied negative potential

at the *trans* side, there would be a higher cation flow from *cis* to *trans* direction compared to anion flow from *trans* to *cis*. When the antibiotic molecule is in the *cis* compartment, the movement of molecule would be in same direction as electro osmotic flow (water flow) at an applied negative potential (giving rise to higher kinetics at negative potential in electrophysiology). Vice versa is obtained when molecule is added to *trans* side and the electro osmotic flow at positive potentials is from *trans* to *cis* side.

Interaction of fluoroquinolones

We also investigated the effect of fluoroquinolones on OmpF and OmpC. In particular we studied interaction of levofloxacin with OmpF. Asymmetric kinetics is observed with asymmetric addition of antibiotic to the channel Table 1.

Voltage dependent translocation of norfloxacin

In this study we report for the first time voltage dependent translocation of an antibiotic molecule. Norfloxacin interaction with OmpF in a voltage dependent and pH dependent manner is characterized. We observed a exponential increase in association rate with decreasing voltage (from positive to negative) when norfloxacin is added to the cis side of the channel at pH 7 *Figure 4*a. A similar trend is observed at pH 5 with norfloxacin but association rate becomes almost 3 orders of magnitude higher *Figure 4*a. On the other hand, the dissociation rates at pH 7 and pH 5 are significantly different. At pH 5, the dissociation rate is almost constant with decreasing voltage, where as at pH 7 it increases with decreasing transmembrane voltage, suggesting translocation of molecule as shown in *Figure 4*b.

Based on the above result we propose a mechanism of norfloxacin translocation which could be a combination of several effects like orientation of antibiotic and/or electro-osmotic effects. Antibiotic senses a external applied voltage which likely orients the molecule in channel/solution (seen in association rate with polarity of voltage). Since the zwitterionic form of antibiotic has a high dipole (*Figure 4*c) as compared to positively charged state of norfloxacin (*Figure 4*d), this fits along electric field/dipole inside the pore and dissociation rates are much less compared to pH 5 at lower voltages (*Figure 4*b).
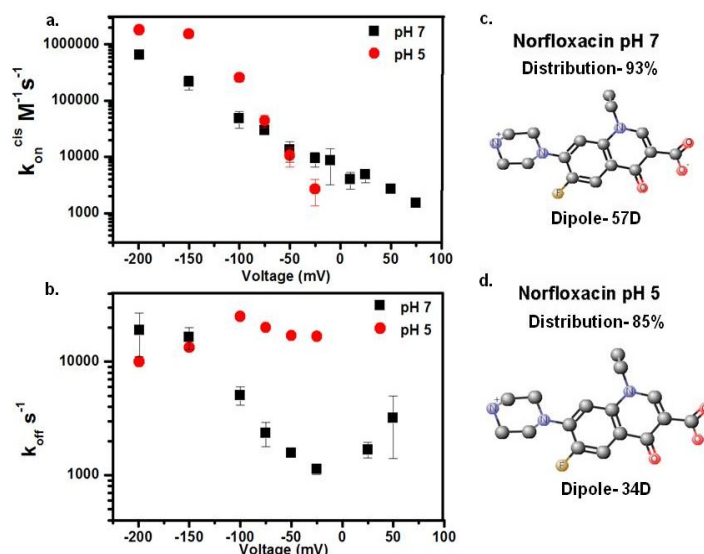
Figure 4: Voltage dependence of kinetic rate constants of norfloxacin at pH 7 and pH 5 through single OmpF channel- (a) association rate(when antibiotic added to cis side) (b) dissociation rate; Charge state of norfloxacin and corresponding dipole values at (c) pH 7 (d) pH 5. Electrolyte conditions: 1 M KCl, 5mM PO₄ (pH 7) /acetate (pH 5).

At pH 7, depending on the magnitude of external –ve voltage the antibiotic might be able to reorient itself inside the pore and hence translocate. Another way to explain this might be since we observe a continuous increase in the dissociation rate a continuous change in the free energy of antibiotic-porin interaction might be involved. The phenomenon of electro-osmotic flows, known to cause such continuous changes in the binding of neutral molecules like cyclodextrin to pores, has been investigated previously[16,17]. In this case, voltage driven electro-osmotic flows coupled to the changes in orientation of the antibiotic due to its dipole might be playing a role in the translocation of the molecule through OmpF. Although in order to know the electrostatic and electro-osmotic contributions additional experiments at low salt concentration and different types of salts are being performed. Further to get a more quantitative description, theoretical calculations and molecular dynamics simulations need to be performed.

Materials and Methods

Single channel electrophysiology

Reconstitution experiments and noise analysis have been performed as described in detail previously[3,7]. The Montal and Muller technique was used to form phospholipid bilayer using DPhPC (Avanti polar lipids)[18] . A Teflon cell comprising an aperture of approximately 30-60 μm diameters was placed between the two chambers of the cuvette. The aperture was prepainted with 1% hexadecane in hexane for stable bilayer formation. 1 M KCl (or 200 mM KCl), 20 mM MES, pH 6 was used as the electrolyte solution and added to both sides of the chamber. Ion current was detected using standard silver-silver chloride electrodes from WPI (World Precision Instruments) that were placed in each side of the cuvette. Single channel measurements were performed by adding the protein to the *cis* side of the chamber (side connected to the ground electrode). Spontaneous channel insertion was typically obtained while stirring under applied voltage. After successful single channel reconstitution, the *cis* side of the chamber was carefully perfused to remove any remaining porins to prevent further channel insertions. Conductance measurements were performed using an Axopatch 200B amplifier (Molecular Devices) in the voltage clamp mode. Signals were filtered by an on board low pass Bessel filter at 10 kHz and with a sampling frequency set to 50 kHz. Amplitude, probability, and noise analyses were performed using Origin pro 8 (OriginLab) and Clampfit software (Molecular devices). Single channel analysis was used to determine the antibiotics binding kinetics. In a single channel measurement the typical measured quantities were the duration of blocked levels/residence time (τ_c) and the frequency of blockage events (ν). The association rate constant k_{on} was derived using the number of blockage events, $k_{on} = \nu/3[c]$, where c is the concentration of antibiotic. The dissociation rate constant (k_{off}) was determined by averaging the $1/\tau_c$ values recorded over the entire concentration range.

Table 1: Antibiotic association (k_{on}) and dissociation (k_{off}) rate constants obtained by measurements from single OmpF channel. Electrolyte conditions: 1 M KCl, 20 mM MES pH 6; except for norfloxacin.

Antibiotics	k_{on}^{cis} (10^3) {1/(s*M)}		k_{on}^{trans} (10^3) {1/(s*M)}		k_{off} (1/s) (@ -50 mV)
	-50mV	+50mV	-50mV	+50mV	
Imipenem	1.1± 0.1	0.1	0.26	0.6	16,700
Cefotaxime	40 ± 3	3.3 ± 0.3	3.2	17	12,500
Cefepime	0.3	-	0.4	9.6 ± 0.2	20,000
Ceftazidime	1.5	0.4	0.2	0.2	25,000
Ceftobiprole	5± 3	-	23± 7	63 ± 10	10,000
Levofloxacin	11.7± 0.7	0.9 ± 0.3	-	0.3	20,000
Norfloxacin pH 5	11 ± 3	-	4	10	25000
Norfloxacin pH 7	13 ± 5	2.6	-	1.3	1561 ± 120

Table 2: Antibiotic association (k_{on}) and dissociation (k_{off}) rate constants obtained by measurements from single OmpC channel. Electrolyte conditions: 1 M KCl, 20 mM MES pH 6; except for norfloxacin.

Antibiotics	k_{on}^{cis} (10^3) {1/(s*M)}		k_{on}^{trans} (10^3) {1/(s*M)}		k_{off} (1/s) (@ -50 mV)
	-50mV	+50mV	-50mV	+50mV	
Imipenem	60 ± 3.3	-	-	0.6	28,570

Meropenem	5 ± 0.3	0.3	-	-	28,000
Cefotaxime	1.8 ± 0.3	1.2 ± 0.7	2.1	8.5 ± 0.5	8300
Cefepime	10 ± 2	2.4 ± 0.3	-	-	16,000
Ceftazidime	-	3 ± 0.3	0.2 ± 0.06	-	25,000
Ceftobiprole	650 ± 33	323 ± 10	-	3	20,000

References

(1)   Nikaido, H. *Microbiol. Mol. Biol. Rev.* **2003**, *67*, 593.

(2)   Pagès, J.-M.; James, C. E.; Winterhalter, M. *Nat. Rev. Microbiol.* **2008**, *6*, 893.

(3)   Nestorovich, E. M.; Danelon, C.; Winterhalter, M.; Bezrukov, S. M. *Proc. Natl. Acad. Sci. U. S. A.* **2002**, *99*, 9789.

(4)   Cowan, S. W.; Schirmer, T.; Rummel, G.; Steiert, M.; Ghosh, R.; Pauptit, R. A.; Jansonius, J. N.; Rosenbusch, J. P. *Nature* **1992**, *358*, 727.

(5)   Hajjar, E.; Mahendran, K. R.; Kumar, A.; Bessonov, A.; Petrescu, M.; Weingart, H.; Ruggerone, P.; Winterhalter, M.; Ceccarelli, M. *Biophys. J.* **2010**, *98*, 569.

(6)   Mahendran, K. R.; Hajjar, E.; Mach, T.; Lovelle, M.; Kumar, A.; Sousa, I.; Spiga, E.; Weingart, H.; Gameiro, P.; Winterhalter, M.; Ceccarelli, M. *J. Phys. Chem. B* **2010**, *114*, 5170.

(7)   Raj Singh, P.; Ceccarelli, M.; Lovelle, M.; Winterhalter, M.; Mahendran, K. R. *J. Phys. Chem. B* **2012**, *116*, 4433.

(8)   Ceccarelli, M.; Vargiu, A. V; Ruggerone, P. *J. Phys. Condens. Matter* **2012**, *24*, 104012.

(9)   Yoshimura, F.; Nikaido, H. *Antimicrob. Agents Chemother.* **1985**, *27*, 84.

(10)   Ziervogel, B. K.; Roux, B. *Structure* **2013**, *21*, 76.

(11) Tran, Q.-T.; Pearlstein, R. A.; Williams, S.; Reilly, J.; Krucker, T.; Erdemli, G. *Proteins* **2014**, *82*, 2998.

(12) Mahendran, K. R.; Kreir, M.; Weingart, H.; Fertig, N.; Winterhalter, M. *J. Biomol. Screen. Off. J. Soc. Biomol. Screen.* **2010**, *15*, 302.

(13) Benz, R.; Janko, K.; Läuger, P. *Biochim. Biophys. Acta* **1979**, *551*, 238.

(14) López, M. L.; García-Giménez, E.; Aguilella, V. M.; Alcaraz, A. *J. Phys. Condens. Matter* **2010**, *22*, 454106.

(15) Alcaraz, A.; Nestorovich, E. M.; Aguilella-Arzo, M.; Aguilella, V. M.; Bezrukov, S. M. *Biophys. J.* **2004**, *87*, 943.

(16) Gu, L.-Q.; Cheley, S.; Bayley, H. *Proc. Natl. Acad. Sci. U. S. A.* **2003**, *100*, 15498.

(17) Gu, L. Q.; Bayley, H. *Biophys. J.* **2000**, *79*, 1967.

(18) Montal, M.; Mueller, P. *Proc. Natl. Acad. Sci. U. S. A.* **1972**, *69*, 3561.

Chapter 4: Detecting antibiotic translocation events at high resolution

In this chapter we deal with time resolution aspect of antibiotic interaction with porin in electrophysiology. In an attempt to improve the resolution of the current system, we introduce an adapted power spectrum method to analyse very fast antibiotic events in P3.4.1, in collaboration with Matteo Ceccarelli. In P3.4.2, we compare the noise and resolution of different bilayer platforms currently available together with Nanion Technologies, a consortium partner.

P3.4.1: Analysis of fast channel blockage: revealing substrate binding in the microsecond range

Individual Contribution

My main contribution in this manuscript is to perform experiments of single channel electrophysiology. I participated in the composition of manuscript.

Analysis of fast channel blockage: revealing substrate binding in the microsecond range†

Igor Bodrenko,[a] Harsha Bajaj,[b] Paolo Ruggerone,[a] Mathias Winterhalter[b] and Matteo Ceccarelli*[a]

For an antibiotic to be effective, it needs to cross the outer membrane barrier and reach the target inside the cell. Hydrophilic antibiotics, *e.g.* β-lactams, use porin channels to cross the outer membrane and accumulate in the periplasm. Experimental determination of antibiotic interactions with porin is performed by using electrophysiology on a single channel level by noise analysis or single event analysis methods. We report a novel framework for analyzing the ion-current noise, taking into account the corrections due to the analogous filter and the sampling procedure, with the goal of extending the time resolution to a range previously inaccessible by event analysis or by conventional noise analysis. The new method allows one to analyse fast binding events and/or the case when the single channel is not completely blocked by the substrate. We demonstrate the power of this approach by using as an example the interactions of meropenem, an antibiotic of the carbapenem family, with the OmpF porin that is considered to be one of the main pathways for antibiotics to enter *Escherichia coli*. The presence of meropenem in OmpF is detected by ion current blockages, and the *on* and *off* rates are estimated from the concentration dependence of the average ion current and of its power spectral density. The obtained average residence time of the antibiotic inside the channel is in the range of a few microseconds, *i.e.* more than 50 times smaller than the inverse cut-off frequency of the analogous filter.

1. Introduction

The complex membrane of Gram-negative bacteria controls the selective passage of nutrients and waste into and from the cell cytoplasm. Influx of solute is largely restricted by porins, which are water-filled open channels that span the outer membrane of Gram-negative bacteria and allow the passive penetration of hydrophilic molecules.[1,2] Apart from various nutrient molecules, many classes of antibiotics like β-lactams are also known to use outer membrane channels to reach their target inside the cell.[2] Consequently, bacterial adaptation to reduce influx through porins is an increasing problem worldwide that contributes, together with efflux and/or enzymatic systems, to the emergence and dissemination of antibiotic resistance.[1,3,4] This highlights the need to measure the antibiotic translocation rate through porin in a quantitative manner in order to rationalize the permeation mechanism through porins and identify new potential antibacterials.

An appropriate method to analyze the physico-chemical properties of these porins, such as conductance, selectivity and voltage gating, is reconstitution of porins in a planar lipid bilayer and measuring an ion current through the lipid bilayer.[5,6] Interaction between substrates (sugars, antibiotic, and peptides) and outer membrane channels has been characterized using the planar lipid technique in a quantitative manner.[5,7–9] For example, the binding constant of sugars through a LamB channel (sugar specific channel), explained by a simple two-barrier one-binding-site model, has been probed using pore conductance.[5,10] An analysis of the conductance with respect to the sugar concentration yields information about the affinity constant K of the sugar to the channel lumen.[5]

To address the transport of sugars through maltoporin, Benz and his colleagues had initiated noise analysis of ion currents through reconstituted maltoporin channels.[11] In contrast to the binding constants, which are determined from the effect of sugar addition on the average current, the noise analysis gives the absolute rates of the sugar binding reaction. Results of a spectral analysis of sugar-induced noise in the current were well fitted by Lorentzian power spectral densities.[11,12] Lorentzian spectra are usually associated with two-state Markovian processes; therefore the binding process can be approximated by such a process, where one state is a pore

[a]Department of Physics, University of Cagliari, S.P. Monserrato-Sestu km 0.700, I-09042 Monserrato, CA, Italy. E-mail: matteo.ceccarelli@dsf.unica.it; Fax: +39-070-6753191; Tel: +39-070-6754933

[b]Jacobs University, Campus Ring 1, 28759 Bremen, Germany

occupied by a sugar molecule and the other state corresponds to an empty pore. The corner frequency values, obtained by fitting the experimental ion-current power spectra to Lorentzian at different sugar concentrations, were used to calculate the k_{on} (association) and k_{off} (dissociation) rates of the maltose sugars (maltotriose to maltoheptaose) in the LamB channel.[11]

Experimental studies of sugar–LamB interactions were attempted at the single channel level, where the authors observed time resolved ion current fluctuations[13] in the presence of sugars, unlike a reduction in conductance observed in a multichannel system.[12] One of the advantages of working with a single channel is that individual kinetic rate constants can be obtained directly by single event analysis of ion current inhibitions caused by substrate residing in the channel.[7] For example, OmpF, the outer membrane protein F from *Escherichia coli* that is involved in the uptake of antibiotics, was characterized in the presence of several β-lactams at the single channel level in a planar lipid bilayer.[14] Transient downward current steps with the amplitude of one-third (monomer) of the total initial current through the channel correspond to time-resolved events of antibiotic binding to channel.[7,14] These events are reversible and each of them is caused by a single antibiotic molecule entering the aqueous pore of one subunit of the OmpF trimer. The average time between successive blockages is observed to decrease with increasing antibiotic concentration and provides the association rate constant.[7] The dissociation rate, on the other hand, is the inverse of residence time of the antibiotic in the channel, which is determined experimentally from the dwell time histogram analysis of events.[7] Inspection of ion current fluctuation through the porin at a single channel level in the presence of antibiotics provides comparable thermodynamic and kinetic parameters both in the single event method/the noise analysis method.[7,14,15]

These methods suffer from the time resolution problem: blockage faster than 50 μs cannot be well resolved.[16] Several experimental techniques were proposed to study the fast blockages. Thus, the kinetics can be slowed down by decreasing the temperature[17] or by adding ionic liquid.[18] In this context, we should also mention a different technique, the so-called liposome swelling method,[19] which provides complementary information on the permeation.

In the present paper, we demonstrate how to improve the time resolution by using an advanced noise analysis. In particular, we investigated the interaction of meropenem, a β-lactam antibiotic, with a single trimeric OmpF channel in a planar lipid bilayer. Addition of meropenem to the solution causes an increase in the ion-current noise and a subsequent decrease in the average conductance of the pore in planar lipid bilayer experiments. However, single events are too fast to be resolved using the conventional noise analysis. We calculated the auto-correlation function of the ion current trace and then, after Fourier transformation, we obtained the power spectral density. The power spectrum was fitted with a Lorentzian function taking into account the sampling and the filter correction factors. As expected, the power spectral density and the average ion current depend on the antibiotic concentration

and, thus, allow one to obtain the kinetic parameters from the concentration dependence. The equilibrium constant ($K = k_{on}/k_{off}$) calculated from the rates obtained in our analysis including the correction factors agreed well with that obtained by the equilibrium titration using the averaged ion conductance.

The analysis of the data for meropenem supports the idea that accounting for correction factors has the potential to reveal the fast events, thus increasing the power of the single channel technique as a tool for a more reliable characterization of substrates' translocation through porins. The information extracted from the experiments and analyzed according to the procedure described here might be converted into data related to the interaction of compounds with porins and, thus, might provide insights possibly useful to rationalize drug design.

2. Theory

The effect of a substrate on the ion current through a membrane channel results in a shift of the average current (reduction of the conductance) and in an increase of the current fluctuations (see Fig. 1).
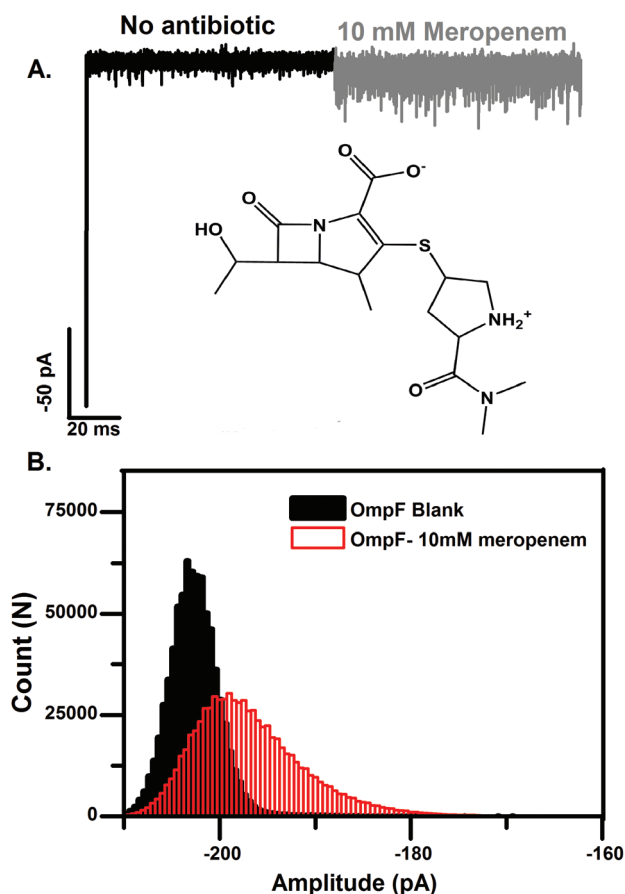
Fig. 1 A. Ion current trace of a single OmpF channel in the presence and absence of 10 mM meropenem (chemical structure is shown in the panel). B. Corresponding histogram of ion current (10 seconds of trace) through OmpF in the absence (black) and presence of 10 mM meropenem (red). Conditions: 1 M KCl, 20 mM MES, pH 6, at −50 mV.

If the average current through a single open monomer channel is j_0 and that through the monomer channel occupied by a substrate is j_1, then, within the two-state Markov model, the average current through the multimer pore reads

$$j_{av}(c) = N_c[j_1 P(c) + j_0(1 - P(c))], \qquad (1)$$

where N_c is the number of monomer channels in the multimer pore and $P(c)$ is the equilibrium probability of finding a monomer channel occupied by a substrate at a concentration c of the latter. At zero concentration, the probability to find a substrate molecule in a channel is zero, and one has $j_{av}(0) = j_0 N_c$. Then, by expressing the occupation probability, $P(c)$, in terms of the transition rates,[11,20] one obtains the shift of the average current through the channel due to the presence of the antibiotic,

$$\langle \Delta j \rangle = |j_{av}(c) - j_{av}(0)| = \frac{N_c \Delta j c k_{on}}{k_{off} + c k_{on}}, \qquad (2)$$

where $\Delta j = |j_1 - j_0|$ is the absolute difference of the average current in the open monomer channel and that in the blocked one at the given applied potential; k_{off} and k_{on} are the dissociation and the association rates, respectively. If the channel is completely blocked by the substrate, then $\Delta j = |j_{av}(0)|/N_c = |j_0|$.[11,20] If the ion current through the channel occupied by a substrate molecule is not completely blocked, then $\Delta j < |j_0|$.

The power spectral density (PSD) of the ion current fluctuations due to the blockages by the antibiotic molecules in the two-state Markov model reads[7]

$$G(f) = \frac{a}{1 + (2\pi f \tau_c)^2}; \qquad (3)$$

$$a = 4N_c(\Delta j)^2 c k_{on} k_{off} \tau_c^3; \qquad (4)$$

$$\tau_c = \frac{1}{k_{off} + c k_{on}}. \qquad (5)$$

Here, τ_c indicates the correlation time of the blockage process.

In case $k_{off} \gg c k_{on}$, the average current shift, $\langle \Delta j \rangle$, as well as the Lorentzian factor, a, of the PSD may be expanded up to the second order in concentration as

$$\langle \Delta j \rangle(c) = N_c \Delta j \frac{c k_{on}}{k_{off}} \left(1 - \frac{c k_{on}}{k_{off}}\right) + o\left(\left(\frac{c k_{on}}{k_{off}}\right)^2\right); \qquad (6)$$

$$a(c) = \frac{4N_c(\Delta j)^2}{k_{off}} \frac{c k_{on}}{k_{off}} \left(1 - 3\frac{c k_{on}}{k_{off}}\right) + o\left(\left(\frac{c k_{on}}{k_{off}}\right)^2\right). \qquad (7)$$

In the electrophysiology experiments, the ion-current signal is filtered by an analogous low-pass linear filter and then sampled at a specific rate, $f_s = 1/\Delta t$. The sampling procedure consists of the averaging of a signal for the period Δt and, thus, corresponds to the application of a linear filter after the first analogous one. The average value of the ion-current signal, j_{av}, is not affected by a linear filter whereas the dispersion, the auto-correlation function, and the PSD are modified by both filters. If the transfer function of the analogous filter is $H_a(\omega)$ and that of the sampling filter is $H_s(\omega)$, then

the relationship between the PSD of the original ion current, eqn (3), and that of the signal after successive application of the two filters is the following:[21]

$$G_m(f) = \frac{a}{1 + (2\pi f \tau_c)^2} |H_a(2\pi f)|^2 |H_s(2\pi f)|^2. \qquad (8)$$

At small frequencies, $f \approx 0$, the transfer functions are close to 1 and do not modify the PSD. At large frequencies, $f \gg f_c$ (f_c is the filter cut-off frequency) or $f \gg 1/\Delta t$, the original PSD is suppressed by the filters. Thus, if the correlation time, τ_c, of the ion-current signal which determines the width of the PSD [see, e.g., eqn (3)] is close to or smaller than the sampling interval Δt or f_c^{-1}, then filter corrections are very important for the PSD analysis.

By fitting the filter-corrected Lorentzian model [eqn (8)] to the PSD of the observed signal, one can obtain a and τ_c at different concentrations of the substrate. The computational procedure and the data analysis protocol are described in detail in the ESI.†

Once the model parameter a is determined, then depending on the availability of τ_c and of $\langle \Delta j \rangle$, one may use the alternative approaches outlined below to extract the kinetic parameters, k_{off} and k_{on}, characterizing the substrate–channel interaction.

Method 1

If the correlation time, τ_c, and the Lorentzian factor, a, are determined by fitting form (8) to the experimental PSD, and Δj is known, e.g. from the ion-current frequency histogram, then the kinetic parameters can be calculated from eqn (4) and (5) (assuming that $k_{off} > c k_{on}$),

$$k_{off} = \frac{1}{2\tau_c} \left(1 + \sqrt{1 - \frac{a}{N_c \tau_c (\Delta j)^2}}\right); \qquad (9)$$

$$k_{on} = \frac{1}{2\tau_c c} \left(1 - \sqrt{1 - \frac{a}{N_c \tau_c (\Delta j)^2}}\right). \qquad (10)$$

Method 2

If Δj is unknown a priori, one can still determine k_{off} and k_{on} from the concentration dependence of the correlation time by using eqn (5). Then, Δj may be also calculated from eqn (4) as follows:

$$\Delta j = \sqrt{\frac{a}{4N_c c k_{on} k_{off} \tau_c^3}}. \qquad (11)$$

Method 3

If the correlation time is very small and it is not possible to determine it by fitting eqn (8) to the experimental PSD, one may utilize the antibiotic concentration dependence measurements and fit the Lorentzian factor, a, and the average current shift, $\langle \Delta j \rangle$, by using the following equations, respectively:

$$a(c) = b_a c(1 - 3rc); \qquad (12)$$

$$\langle \Delta j \rangle(c) = b_j c(1 - rc), \qquad (13)$$

where the fitting parameter $r = K = k_{on}/k_{off}$ is equal to the equilibrium (or stability) constant of the antibiotic–channel interaction. Then, by using eqn (6) and (7), one obtains

$$k_{on} = \frac{4b_j^2}{N_c b_a}; \qquad (14)$$

$$k_{off} = \frac{k_{on}}{r}; \qquad (15)$$

$$\Delta j = \frac{b_j}{N_c r}. \qquad (16)$$

Method 4

If the correlation time is very small and its dependence on antibiotic concentration is not accessible but an *a priori* knowledge of Δj is possible, then one can determine the kinetic parameters from the concentration dependence of the PSD Lorentzian factor, $a(c)$, and of the average current shift, $\langle \Delta j \rangle$. In this case, one fits first the function

$$\langle \Delta j \rangle (c) = N_c \Delta j (1 - rc) rc \qquad (17)$$

to the experimental average current shift and determines the equilibrium constant $K = r$. This step is similar to the conductance probe method[5] except for the fact that we use the second-order expansion in the latter equation instead of the exact formula given by eqn (2) used in ref. 5 In the second step, by fitting eqn (12) to the concentration dependence of the Lorentzian factor keeping r fixed, one determines parameter b_a and then obtains

$$k_{off} = \frac{4N_c(\Delta j)^2 r}{b_a}; \qquad (18)$$

$$k_{on} = r k_{off}. \qquad (19)$$

3. Experiment – single channel electrophysiology

To form a planar lipid bilayer with the lipid monolayer opposition technique,[22] we used a 5 mg mL^{-1} solution of 1,2-diphytanoyl-*sn*-glycero-3-phosphocholine (Avanti Polar Lipids, Inc., Alabaster, AL) in pentane. A bilayer is formed across a 50–100 μm diameter aperture in a 25 μm thick Teflon partition. Silver chloride electrodes from WPI (World Precision Instruments), one connected to the live side of the amplifier (referred to as the *trans* side; where the voltage is applied) and the other connected to the ground side (referred to as the *cis* side), were used. A small amount (up to 0.1 μL) of wild-type OmpF from a diluted stock solution of 60 ng mL^{-1} in 1% (v/v) of genapol is added to the *cis* side of the chamber. Spontaneous insertion of a single OmpF channel usually happens within minutes after protein addition to the aqueous phase with a volume of 250 μL (1 M KCl, 20 mM MES, pH 6). Both the small-ion conductance and the gating properties were used as an indication of directional channel insertion (likely with

Table 1 Specification of the independent measurements for OmpF/meropenem. Columns from left to right: the number of the data set, the used concentrations of the substrate, and the used sampling rates

Set	c (mM)	f_s (kHz)
1	0, 2.5, 5, 7.5, 9	50
2	0, 2.5, 5, 7.5, 10	50
3	0, 5, 10, 12.5, 15, 20, 23	50, 250
4	0, 5, 10, 12.5, 15, 20, 24	50, 250
5	0, 5, 10, 12.5, 15, 20, 24	50, 250

the *cis* side of the lipid bilayer corresponding to the extracellular side of the porin 80% of the time). Our convention is that the plus sign (positive voltage) means that the *trans* side of the membrane cell compartment is more positive. Conductance measurements were performed using an Axopatch 200B amplifier (Axon Instruments, Inc., Foster City, CA) in the voltage clamp mode. Data were filtered by a low-pass 4-pole Bessel filter at 10 kHz with a sampling frequency of 50 kHz or 250 kHz and recorded simultaneously into the computer memory. Meropenem (Sequoia research products) stock solutions were prepared up to 40 mM in 1 M KCl, 20 mM MES, pH 6, and added in a concentration dependent manner to the *cis* side of the chamber and diluted at the end of measurements for blank pore/control measurements. The chemical structure of meropenem ($M_W = 383$ g mol^{-1}) is shown in Fig. 1A; the molecule is zwitterionic under the conditions of measurements. Due to the heating of the amplifier, many times we observed an increase of temperature (up to 2–3 °C increase from room temperature) in the cuvette of small volumes (250 μL). For this reason the measurements were finished within 2–3 hours to minimize (although not completely eliminate; an increase to 1–1.5 °C is observed) conductance/transport properties fluctuation due to temperature changes.

We performed several independent electrophysiology measurements. The specifications of the measurements are collected in Table 1.

4. Results

In the present investigation, we studied the meropenem interaction with OmpF. Addition of meropenem to a single trimeric OmpF channel caused unresolved short flickering and a subsequent reduction in ion current (Fig. 1A).

According to the proposed data analysis protocol described in ESI,† for each measurement specified in Table 1 (at each concentration of the substrate), we selected 3 independent data records, denoted I, II and III. The duration T of the records equals 5 seconds for the data sampled at 50 kHz rate (2.5×10^5 events) and 4 seconds for the data sampled at 250 kHz rate (10^6 events).

The ion-current event frequency histograms do not have the secondary peak but exhibit a strong asymmetry (Fig. 1B). Thus, it is impossible to determine Δj directly. There is no evidence of spontaneous channel gating under the present conditions.

The auto-correlation function, $R(\tau)$, is calculated for τ up to τ_{max} = 20 ms for the data sampled at 50 kHz rate and up to τ_{max} = 4 ms for the data sampled at 250 kHz rate. As an example, the auto-correlation functions of the ion current sampled at 50 kHz and that sampled at 250 kHz are shown in Fig. 2 for a small range of τ to show the significant details.

For all data sets, the signal PSD, $G_s(f)$, calculated according to eqn (20) of the ESI† by subtracting the background PSD, is well fitted by the filter-corrected Lorentzian, eqn (8). However, the fitting procedure allows one to determine only the upper bound of the correlation time, $i.e.$, it could be only stated that $\tau_c < 0.01$ ms in the case of the 50 kHz sampling and $\tau_c < 0.005$ ms for the 250 kHz sampling. The signal PSD of the ion current sampled at 50 kHz and that sampled at 250 kHz are shown in Fig. 3 (panels A and B, respectively) for the three data records (the ion-current data are taken from set 3, see Table 1, for c = 10 mM; the PSDs for data record I correspond to the auto-correlation functions of Fig. 2).

The best fits of the filter-corrected Lorentzian model, eqn (8), to the signal PSD of a record I for each sampling rate are also presented in Fig. 3. The fitting range was chosen to be $f \in [1, 25]$ kHz. The PSD values below 1 kHz strongly fluctuate and are different in the data records, I, II, III; thus, they are neglected in the fitting procedure (see section 5). Only the upper bound of the correlation time may be determined as was indicated above; τ_c was set to zero for the plots in Fig. 3. The Lorentzian factor, a, obtained by the fitting has the values of 2.6 pA^2 kHz^{-1} and 2.7 pA^2 kHz^{-1} for the data sampled at 50 kHz and 250 kHz rate, respectively. The same order of dispersion in a is observed between the different data records (I, II, III) within the same sampling rate measurements. To demonstrate the effect of the sampling correction, we also plot $G_m(f)$ without the $|H_s(2\pi f)|^2$ factor (dashed lines in Fig. 3, panels A and B). The fit of the pure Lorentzian, filter-uncorrected PSD profile to the signal PSD is presented in Fig. 3(B); the parameters are a = 3.5 pA^2 kHz^{-1} and τ_c = 0.03 ms.

Fig. 3 The signal PSD of the ion current fluctuations sampled at 50 kHz rate (A) and 250 kHz rate (B). The thick solid line is the fit by the filters-corrected Lorentzian model, eqn (8); the dashed line is the same Lorentzian model but corrected for the Bessel filter only, $i.e.$, without the sampling correction. The dotted line in (B) is the fit by the pure Lorentzian filters-uncorrected model, eqn (3). More traditional double-logarithmic scale PSD plots are shown in ESI.†

Then, we averaged a over the data records (I, II, III) and estimated the error as the maximum between the fitting errors and the averaging error. The concentration dependence of the obtained Lorentzian factor, a, is quite smooth (see Fig. 4A for an example).

The average ion current shift, $\langle \Delta j \rangle$, averaged also over the data records (I, II, III), is also fairly smooth $vs.$ concentration (see Fig. 4B for an example), permitting the use of $Method\ 3$ outlined in section 2 for the determination of the parameters. The fitting parameters, corresponding to the data in Fig. 4, are presented in Table 2. The related parameters of blockage kinetics are collected in Table 3. The kinetic parameters of the meropenem-induced channel blockage determined by $Method\ 3$ for all the sets of data are presented in Table 4.

Sets 1 and 2 do not allow to determine the parameters by $Method\ 3$, being the uncertainty of the fitting parameters nearly 100%. However, from the sets 3 to 5 one can conclude that the Δj value is equal (within the uncertainty error) to 1/3 of the ion current through the open trimer channel. The latter
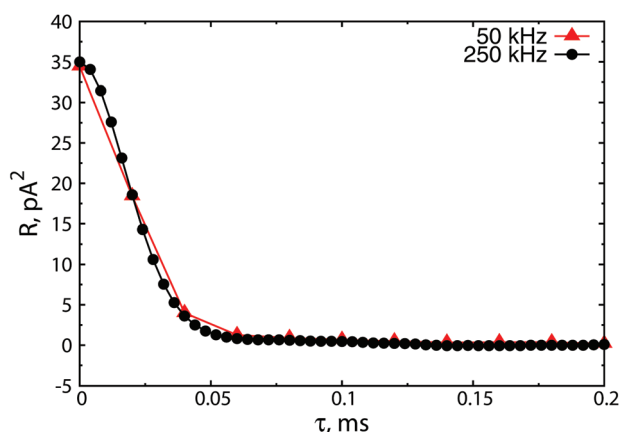

Fig. 2 Auto-correlation function of the ion current fluctuations sampled at 50 kHz rate (red triangles) and at 250 kHz rate (black circles). Data set 3, see Table 1, c = 10 mM.
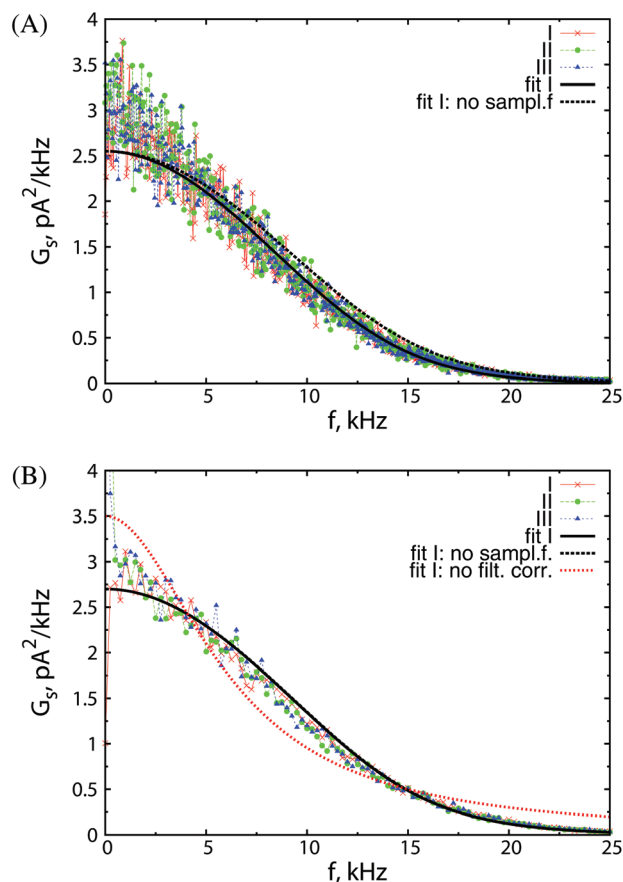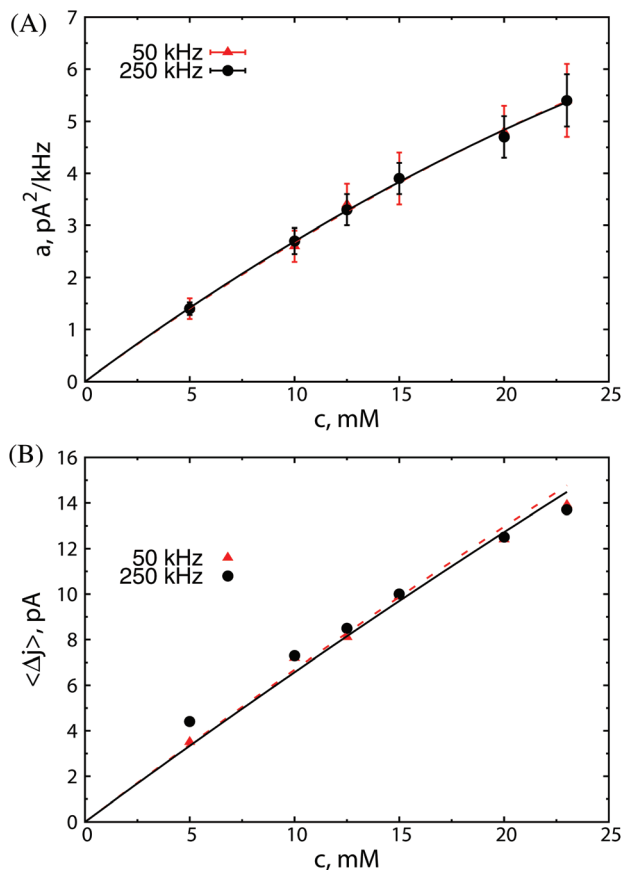
Fig. 4 The meropenem concentration dependence (data set 3, see Table 1) of (A) the Lorentzian factor, a, and (B) the average ion current shift, $\langle \Delta j \rangle$. The curves are the fits with the parameters presented in Table 2. The red triangles and dashed curves correspond to the 50 kHz sampled data; the black circles and solid lines correspond to 250 kHz sample data.

Table 2 The fitting parameters for ion-current fluctuations (data set 3) due to channel blockages, determined by using *Method 3* (see section 2, for details). The absolute error estimates are given in round brackets

f_s (kHz)	b_a	r	b_j
50	0.293 (0.019)	0.0029 (0.0011)	0.688 (0.015)
250	0.297 (0.013)	0.0031 (0.0008)	0.678 (0.020)

Table 3 Kinetic parameters of ion-current fluctuations (data set 3) due to channel blockages, determined by using *Method 3* (see section 2, for details). The absolute error estimates are given in round brackets

f_s (kHz)	Δj (pA)	k_{off} (ms^{-1})	k_{on} (ms^{-1} M^{-1})
50	80 (30)	700 (250)	2030 (140)
250	72 (16)	660 (150)	2060 (140)

suggests that the monomer channel is completely blocked by an antibiotic molecule. Using the above assumption, we applied *Method 4* to re-analyze all the data sets. The results are presented in Table 5. In addition, we calculated the equilibrium binding constant according to the definition, $K = k_{on}/$

Table 4 OpmF/meropenem kinetic parameters of ion-current fluctuations due to channel blockages, determined by using *Method 3* (see section 2, for details). The data sampled at 50 kHz were used. The absolute error estimates are given in round brackets

Set	Δj (pA)	k_{off} (ms^{-1})	k_{on} (ms^{-1} M^{-1})
1	NA	NA	800 (500)
2	NA	NA	800 (400)
3	80 (30)	700 (250)	2030 (140)
4	140 (70)	1200 (600)	1500 (100)
5	80 (20)	750 (200)	2030 (140)

Table 5 OpmF/meropenem kinetic parameters of ion-current fluctuations due to channel blockages, determined by using *Method 4* (see section 2, for details). The data sampled at 50 kHz were used. The absolute error estimates are given in round brackets. The equilibrium binding constants calculated within the presented method and those obtained by using the conductance probe method[5] are presented in columns 5 and 6, respectively

Set	Δj (pA)	k_{off} (ms^{-1})	k_{on} (ms^{-1} M^{-1})	K (M^{-1})	K_{cp} (M^{-1})
1	73 (2)	370 (100)	800 (400)	2.2	NA
2	70 (2)	340 (80)	800 (400)	2.3	NA
3	66 (2)	600 (40)	2030 (120)	3.4	3.6
4	66 (2)	540 (40)	1430 (110)	2.6	2.1
5	68 (2)	580 (50)	2000 (200)	3.4	3.3

k_{off}, by using the obtained rate constants (column 5 of Table 5) as well as by using the conductance probe method,[5] K_{cp} (column 6 of Table 5). The available values of K_{cp} are in good accordance with those obtained by our approach.

5. Discussion

For the fast channel-blocking events, the correlation time of the original ion-current fluctuations, τ_c, is less than the inverse cut-off frequency of the subsequent low-pass filter. The observable signal does not permit time resolved blockage events to be detected,[16] as in the case of the meropenem interaction with OmpF seen in Fig. 1A. Hence, the kinetic parameters of the channel blocking cannot be deduced by the standard way.[7] The ion-current event histogram does not have a clear secondary peak due to the blockages but instead it has a tail as seen in Fig. 1B, and therefore the current change Δj in the blocked monomer channel also cannot be determined directly. Fingerprints of the channel blockages due to the interaction with the antibiotic are observed in the strong asymmetry of the ion-current event histogram as well as in the antibiotic concentration dependence of the average current and of the current fluctuations. The latter two properties are used to quantify the channel blockage kinetics of meropenem in OmpF in the present study.

The observed auto-correlation function, $R(\tau)$, of the ion-current signal presented in Fig. 2 looks confusing at first sight. First, it has a clear non-exponential form (this is particularly evident for the data sampled at 250 kHz rate) and, thus, is not

reproducible by the one-binding-site Markovian model of channel blocking. Second, the correlation time estimated as the width of $R(\tau)$ is about 30 μs, *i.e.*, the blockage events would be observable directly, but they are not. Actually, the shape of this auto-correlation function is mainly determined by the low-pass Bessel filter while the magnitude does depend on the antibiotic induced blockages.

Instead of computing the filters' correction to $R(\tau)$, we turn to the equivalent Fourier representation and consider the correction to the power spectral density of the signal, which is fairly simple, given by eqn (8). By fitting the filter-corrected model PSD to the observed data, we find that the correlation time of the blockage process is less than 5 μs. Thus, the shape of the PSD presented in Fig. 3 is determined by the transfer functions of the filters in the examined frequency range. The Lorentzian factor, a, determines the magnitude of the PSD.

For the low-pass 4-pole Bessel filter with 10 kHz cut-off frequency used in the current experiment, the sampling correction to the PSD is important for the 50 kHz sampling (Fig. 3A), while for the 250 kHz sampling the effect of the correction is negligible (Fig. 3B). The Lorentzian factor and the bounds of the correlation time determined by fitting the filter-corrected Lorentzian to the signal PSD are the same within the fitting errors. Thus, by using the current low-pass analogous filter, one may record the current at 50 kHz rate and analyze it with the sampling correction taken into account. Alternatively, one may collect the current at 250 kHz rate; in this case the sampling correction is not necessary.

To appreciate the power of our approach, we fitted the signal PSD with a pure uncorrected Lorentzian (see Fig. 3B). It becomes clear that the shape of the Lorentzian is not compatible with the signal PSD, especially for the high frequency tail which decays as $1/f^2$ for the Lorentzian compared to $1/f^8$ for the Bessel filter, as is discussed in ESI.† While the Lorentzian factor a obtained in such a fitting may be quite close (within 30%) to that obtained by using the filter corrections, the correlation time $\tau_c = 0.03$ ms is completely incorrect. It is close to the width of the auto-correlation function discussed above and characterizes the filter rather than the channel blockages due to the antibiotic.

At a lower frequency range, the signal PSD exhibits strong fluctuations between the data records (see Fig. 3). These very slow current fluctuations may come from the infrequent partial channel gating or uncontrollable changes under the external conditions (*e.g.*, temperature). We excluded the range $f \in [0:1]$ kHz from the fitting procedure and, thus, got rid of slow uncontrollable processes. This is a clear advantage of using the Fourier space analysis instead of the real space analysis (auto-correlation function, event counting), for which it is difficult to separate these slow processes from the signal.

In *Method 3* discussed in section 2, one fits the antibiotic concentration dependence of the Lorentzian factor, $a(c)$, and of the average current shift, $\langle \Delta j \rangle (c)$, with quadratic functions. This provides 3 fitting parameters, b_a, b_j, r from which one may extract the blockage kinetic parameters, k_{on}, k_{off}, and also Δj. The $\langle \Delta j \rangle$ values, however, are very sensitive to the slow

changes of the external conditions (like temperature). For example, from the data presented in Fig. 4b, the second-order coefficient, r, may not be extracted due to large fitting errors. In contrast, from the $a(c)$ data of Fig. 4a, b_a and r values can be extracted and, by using $\langle \Delta j \rangle(c)$, b_j is estimated. Still, the uncertainty in r is quite large, about 30% (see Table 2), but the kinetic parameters and the $\langle \Delta j \rangle$ value can be determined (Table 3). The parameters extracted from the analysis of the ion current sampled at 50 kHz and that sampled at 250 kHz coincide within the estimated error. The corresponding residence time, $\tau_{res} = 1/k_{off} = 0.0015 \pm 0.0004$ ms, is in accordance with the correlation-time upper limits determined directly by fitting the PSD to a filter-corrected Lorentzian.

The obtained reduction of the average ion current through a single blocked state, Δj, should be compared to its maximal possible value (complete blocking of the current) determined as 1/3 of the average current without antibiotic, $j_0 = 66 \pm 1$ pA. Therefore, a monomer channel is completely blocked by the antibiotic.

The results of the analysis by *Method 3* of all the available data sets (Table 4) indicate that only in two cases (data sets 3 and 5) the kinetic parameters are obtained with a reasonable accuracy. In one case (data set 4) the accuracy of k_{off} and Δj is roughly 50%. In the remaining two cases, only k_{on} can be estimated with an accuracy worse than 50%. In the more recent experiments 3–5, we took special care of the temperature control (see section 3) and have considered a wider range of meropenem concentrations (Table 1). In the earlier measurements 1–2, the control of the external conditions was not so good and fewer antibiotic concentrations were considered, and this is the reason for the failure of *Method 3* in those cases.

From data sets 3 and 5, where the uncertainty of the extracted parameters is small, one concludes that meropenem completely blocks ion current once it is in the monomer channel, *i.e.*, Δj may be estimated as 1/3 of the average current without antibiotic. By using the latter assumption, we re-analyzed all the data sets with *Method 4*. The obtained kinetic parameters (Table 5) coincide within the uncertainty range with those derived by *Method 3*. The uncertainty for the parameters obtained by *Method 4* is much smaller, and also the values for all the measurements are available.

Table 5 also reveals two groups of data. The first one (sets 1–2) gives $k_{on} \sim 800$ ms^{-1} M^{-1} and $k_{off} \sim 350$ ms^{-1}. The second one (sets 3–5) gives $k_{on} \sim 2000$ ms^{-1} M^{-1} and $k_{off} \sim 550$ ms^{-1}. The reason for this grouping is not quite clear. It may be due to pore-to-pore variation, changes in external conditions like temperature (this could likely be eliminated by looking at the conductance which is almost the same over different pores) or due to any other experimental uncertainty. Further analysis is ongoing.

The range of antibiotic concentrations the method may be applied to is limited from the above by the condition that at most one substrate molecule can occupy the channel at a time, *i.e.*, $ck_{on}/k_{off} \ll 1$. On the other hand, the ion-current shift, $\langle \Delta j \rangle$, due to the channel blockages by the antibiotic should be measurable, *i.e.* be larger than some instrumental accuracy δj. As $\langle \Delta j \rangle$ is proportional to c at small concentrations, from eqn (6), one may write down the lower-bound conditions for the concentrations,

$N_c \Delta jck_{on}/k_{off} > \delta j$. Finally, the practical range of antibiotic concentrations to be used in the measurements reads

$$\frac{\delta j}{N_c \Delta j}\frac{1}{K} < c \ll \frac{1}{K}, \qquad (20)$$

where K is the equilibrium constant for the antibiotic–channel interaction. Thus, the suitable range of concentrations depends both on the channel–substrate interaction properties and on the instrumental accuracy.

6. Conclusion

The work reported here shows that a careful analysis by the modified power spectral density method, taking into account the sampling and filter effects, is able to resolve the residence times of 1 µs, and this is a factor of 100 below the inverse cut-off frequency of the experimental setup. We use interactions of meropenem with OmpF as an example to obtain the kinetic parameters by using the PSD method developed here.

Gaining the ability to extract the kinetic parameters by using the corrected analysis method, which are otherwise off limits using the conventional methods, becomes necessary. This is particularly important for molecules like antibiotics translocating through general channels, where we expect weak interactions due to the lack of specificity. Apart from meropenem, there are other examples where an increased noise in the ion current trace does not provide well resolved events. In such cases, the rate constants cannot be obtained because of limited temporal resolution; hence the analysis method developed here could be used successfully.

In addition, a future application of the method will be in combination with kinetic Monte Carlo simulations[23] to scout possible free energy profiles attributable to events extracted from electrophysiology experiments by the analysis protocols described here.

Acknowledgements

References

1 H. Nikaido, *Microbiol. Mol. Biol. Rev.*, 2003, **67**, 593–656.

2 J.-M. Pagès, C. E. James and M. Winterhalter, *Nat. Rev. Microbiol.*, 2008, **6**, 893–903.

3 L. Fernández and R. E. W. Hancock, *Clin. Microbiol. Rev.*, 2012, **25**, 661–681.

4 H. Nikaido, *Science*, 1994, **264**, 382–388.

5 R. Benz, A. Schmid and G. H. Vos-Scheperkeuter, *J. Membr. Biol.*, 1987, **100**, 21–29.

6 A. H. Delcour, *Annu. Rev. Microbiol.*, 2013, **67**, 179–197.

7 E. M. Nestorovich, C. Danelon, M. Winterhalter and S. M. Bezrukov, *Proc. Natl. Acad. Sci. U. S. A.*, 2002, **99**, 9789–9794.

8 P. R. Singh, I. Bárcena-Uribarri, N. Modi, U. Kleinekathöfer, R. Benz, M. Winterhalter and K. R. Mahendran, *ACS Nano*, 2012, **6**, 10699–10707.

9 H. Bajaj, Q.-T. Tran, K. R. Mahendran, C. Nasrallah, J.-P. Colletier, A. Davin-Regli, J.-M. Bolla, J.-M. Pagès and M. Winterhalter, *Biochemistry*, 2012, **51**, 10244–10249.

10 R. Benz, A. Schmid, T. Nakae and G. H. Vos-Scheperkeuter, *J. Bacteriol.*, 1986, **165**, 978–986.

11 S. Nekolla, C. Andersen and R. Benz, *Biophys. J.*, 1994, **66**, 1388–1397.

12 C. Hilty and M. Winterhalter, *Phys. Rev. Lett.*, 2001, **86**, 5624–5627.

13 L. Kullman, M. Winterhalter and S. M. Bezrukov, *Biophys. J.*, 2002, **82**, 803–812.

14 C. Danelon, E. M. Nestorovich, M. Winterhalter, M. Ceccarelli and S. M. Bezrukov, *Biophys. J.*, 2006, **90**, 1617–1627.

15 A. Brauser, I. Schroeder, T. Gutsmann, C. Cosentino, A. Moroni, U.-P. Hansen and M. Winterhalter, *J. Gen. Physiol.*, 2012, **140**, 69–82.

16 E. Hajjar, K. R. Mahendran, A. Kumar, A. Bessonov, M. Petrescu, H. Weingart, P. Ruggerone, M. Winterhalter and M. Ceccarelli, *Biophys. J.*, 2010, **98**, 569–575.

17 K. R. Mahendran, C. Chimerel, T. Mach and M. Winterhalter, *Eur. Biophys. J.*, 2009, **38**, 1141–1145.

18 N. Modi, P. R. Singh, K. R. Mahendran, R. Schulz, M. Winterhalter and U. Kleinekathofer, *J. Phys. Chem. Lett.*, 2011, **2**, 2331–2336.

19 E. Hajjar, A. Bessonov, A. Molitor, A. Kumar, K. R. Mahendran, M. Winterhalter, J.-M. Pagès, P. Ruggerone and M. Ceccarelli, *Biochemistry*, 2010, **49**, 6928–6935.

20 G. Schwarz, C. Danelon and M. Winterhalter, *Biophys. J.*, 2003, **84**, 2990–2998.

21 S. Orfanidis, *Introduction to Signal Processing*, Prentice Hall Inc., 96th edn, 1995.

22 M. Montal and P. Mueller, *Proc. Natl. Acad. Sci. U. S. A.*, 1972, **69**, 3561–3566.

23 M. Ceccarelli, A. V. Vargiu and P. Ruggerone, *J. Phys.: Condens. Matter*, 2012, **24**, 104012.

Computational procedure
and data analysis protocol†

February 10, 2015

1   Characteristics of ion-current fluctuation

If the observed ion current, j_k, is sampled at rate $f_s = 1/\Delta t$ (Δt is the sampling period) the average current for a data record taped for a period $T = N_T \Delta t$ reads

$$j_{\text{av}}(T) \;=\; \frac{1}{N_T} \sum_{k=1}^{N_T} j_k \quad . \tag{1}$$

We also define the partial average for the record by using only the data that start from time $\tau = M_\tau \Delta t$, where $M_\tau = 0, 1, \ldots, N_T - 1$,

$$j_{\text{av}}(\tau, T) \;=\; \frac{1}{N_T - M_\tau} \sum_{k=1}^{N_T - M_\tau} j_{k+M_\tau} \quad . \tag{2}$$

Clearly, $j_{\text{av}}(T) = j_{\text{av}}(0, T)$.

The auto-correlation function calculated for the data record is defined as follows,

$$R(\tau, T) \;=\; \frac{1}{N_T - M_\tau} \sum_{k=1}^{N_T - M_\tau} \Big[j_k - j_{\text{av}}(T) \Big]\Big[j_{k+M_\tau} - j_{\text{av}}(\tau, T) \Big] \quad . \tag{3}$$

---

^{0†} This is the Electronic Supplementary Information (ESI) for *I. Bodrenko, H. Bajaj, P. Ruggerone, M.Winterhalter, and M. Ceccarelli, 'Analysis of fast channel gating: revealing substrate binding in the microsecond range'*

1

With the above definition, the squared standard deviation of the ion current, σ_j^2, is equal to the auto-correlation function at zero time shift,

$$\sigma_j^2 \;\; = \;\; R(0, T) \quad . \tag{4}$$

The power spectral density (PSD) of a signal is formally defined as the Fourier transform of its auto-correlation function, $R(\tau) \equiv R(\tau, T \to \infty)$,

$$g(\omega) \;\; = \;\; \frac{1}{\pi} \int_0^{+\infty} R(\tau) \cos(\omega\tau) d\tau \quad . \tag{5}$$

Below, we will also use an alternative definition of the power spectral density by using the temporal frequency $f = \omega/2\pi$ instead of the angular frequency ω,

$$G(f) \;\; \equiv \;\; 4\pi g(2\pi f) \quad . \tag{6}$$

Then, we define the finite-interval power spectral density as follows

$$g(\omega, \tau_{\max}, T) \;\; = \;\; \frac{1}{\pi} \int_0^{\tau_{\max}} R(\tau, T) \cos(\omega\tau) d\tau \quad , \tag{7}$$

so that

$$\lim_{\tau_{\max} \to \infty} \left[\lim_{T \to \infty} g(\omega, \tau_{\max}, T) \right] \;\; = \;\; g(\omega), \tag{8}$$

assuming that integrals and limits exist. If the correlation function decays sufficiently fast by increasing τ and if the correlation time of the process is smaller than $\tau_{\max} \ll T$, then one may expect that $g(\omega, \tau_{\max}, T) \approx g(\omega)$.

The auto-correlation function of the ion-current record, (3), is defined at discrete time shifts, $\tau_l = l\Delta t$, $l = 0, 1, \ldots, M_\tau$, as

$$R_k^T \;\; \equiv \;\; R(\tau_k, T) \quad . \tag{9}$$

If a linear interpolation between the time points is assumed, then the auto-correlation function may be continuously represented over the interval $\tau \in [0, \tau_{\max}]$, where $\tau_{\max} = M_\tau \Delta t$, as

$$R(\tau, T) \;\; \approx \;\; \sum_{l=0}^{M_\tau - 1} \left[\left(R_{l+1}^T - R_l^T \right) \frac{\tau - \tau_l}{\Delta t} + R_l^T \right] \mathrm{rect}\left(\frac{\tau - \tau_l}{\Delta t} \right) \quad , \tag{10}$$

2

where $\text{rect}(x) = \theta(x) - \theta(x-1)$ is the rectangular function on interval $[0, 1]$ and $\theta(x)$ the Heaviside step function. Then, the PSD at the characteristic frequencies may be approximately calculated as follows

$$
g(\omega_l, \tau_{\max}, T) \approx \frac{\Delta t}{\pi}\text{sinc}\left(\frac{\omega_l \Delta t}{2}\right)\sum_{k=0}^{M_\tau - 1}\frac{R_{k+1}^T + R_k^T}{2}\cos\left[\omega_l\left(\tau_k + \frac{\Delta t}{2}\right)\right] +
$$
$$
+ \frac{\Delta t}{\pi}\text{sinc}^{(1)}\left(\frac{\omega_l \Delta t}{2}\right)\sum_{k=0}^{M_\tau - 1}\frac{R_{k+1}^T - R_k^T}{2}\sin\left[\omega_l\left(\tau_k + \frac{\Delta t}{2}\right)\right]
$$
$$(11)$$

$$
\omega_l = \frac{2\pi}{\Delta t}l \; ; \; l = 0, 1, \ldots, M_\tau \tag{12}
$$

Here, $\text{sinc}\,(x) = \sin(x)/x$ and $\text{sinc}^{(1)}\,(x) = [x\cos(x) - \sin(x)]/x^2$.

2   Filter and sampling corrections

In the electrophysiology experiments, the ion-current signal is filtered by an analogous low-pass linear filter and then sampled at a specific rate, $f_s = 1/\Delta t$. The sampling procedure consists of averaging a signal for the period Δt and, thus, is also a linear filter applied after the first analogous one. The average value of the ion-current signal, j_{av}, is not affected by a linear filter whereas the dispersion, the auto-correlation function, and the PSD are modified by both filters. If the transfer function (its Fourier transform) of the analogous filter is $H_{\text{a}}(\omega)$ and that of the sampling filter $H_{\text{s}}(\omega)$, then the relation between the PSD of the original ion current, $g_{\text{o}}(\omega)$, and the one of the signal after successive application of the two filters reads,

$$
g(\omega) = g_{\text{o}}(\omega)|H_{\text{a}}(\omega)|^2|H_{\text{s}}(\omega)|^2 \quad . \tag{13}
$$

A 4-order (4-pole) low-pass Bessel filter is used in the current measurements. The transfer function of the Bessel filter of order n is designed as follows,

$$
H_n(\omega) = \frac{\theta_n(0)}{\theta_n(\iota\omega/\omega_0)}, \tag{14}
$$

where $\theta_n(x)$ is the reverse Bessel polynomial of order n; ω_0 is a frequency chosen to give the desired cut-off frequency. For the 4-order low-pass Bessel

3

filter, $\theta_n(x) = x^4 + 10x^3 + 45x^2 + 105x + 105$, and the absolute square of the transfer function reads,

$$|H_\mathrm{a}(\omega)|^2 \;\; = \;\; \frac{11025}{\left(\frac{\omega}{\omega_0}\right)^8 + 10\left(\frac{\omega}{\omega_0}\right)^6 + 135\left(\frac{\omega}{\omega_0}\right)^4 + 1575\left(\frac{\omega}{\omega_0}\right)^2 + 11025} \tag{.15}$$

Here, $\omega_0 = 2\pi f_c/x_c$, where f_c is the cutoff frequency, $x_c \approx 2.114$ the scaling factor determined by the following condition, $|H_\mathrm{a}(2\pi f_c)|^2 = 1/2$.

The absolute square of the PSD of the sampling filter is

$$|H_\mathrm{s}(\omega)|^2 \;\; = \;\; \left(\frac{\sin\left(\frac{\omega\Delta t}{2}\right)}{\frac{\omega\Delta t}{2}}\right)^2 \;\; , \tag{16}$$

where Δt is the sampling interval.

Note that formally at small frequencies, $\omega \approx 0$, the transfer functions are close to 1 and do not modify the PSD,

$$g(\omega)|_{\omega\approx 0} \;\; \approx \;\; g_\mathrm{o}(\omega) \;\; . \tag{17}$$

At large frequencies, $\omega > \omega_0$; $\omega > 1/\Delta t$, the original PSD is strongly reduced by a factor ω^{10},

$$g(\omega)|_{\omega\to\infty} \;\; \sim \;\; g_\mathrm{o}(\omega)\frac{1}{\omega^{10}} \;\; . \tag{18}$$

Thus, if the correlation time τ of the ion-current signal, which determines the width of the PSD, is close to or smaller than the sampling interval Δt or the inverse filter cutoff frequency f_c, then corrections associated with the filters are very important for the PSD analysis.

3 Data analysis protocol

Selection of ion-current data records. For each concentration of a substrate one selects 3-5 independent ion-current records, lasting each T seconds. T must be much larger than the typical correlation time τ_c of the blockages due to substrate; if the latter is less than few milliseconds the former may be 5-10 sec. One has to make sure that the selected records are free from an apparent external noise, like symmetric spikes, etc.

4

Average current. At every substrate concentration, c, one calculates the average current j_{av} for each data record by using Eq. (1). Then, the mean value and the error estimate of the average current are computed for every concentration, $j_{\mathrm{av}}(c)$. Thus, the shift of the average ion current at concentration c is given by

$$\langle \Delta j \rangle (c) \;\; = \;\; j_{\mathrm{av}}(c) - j_{\mathrm{av}}(0) \quad . \tag{19}$$

Ion-current frequency histogram. At every substrate concentration, one calculates the ion-current frequency histogram. At zero substrate concentration, the histogram usually contains a single peak corresponding to the ion current through open channel. If the channel closes spontaneously, a secondary peak (or peaks) may appear. By comparing the histogram with and without a substrate the secondary peak due to the channel blockages by the substrate molecule (different from the one due to channel gating) might be located. Once the secondary peak is identified, the shift of its position with respect to the position of the main peak provides an estimate to the Δj value, i.e., the absolute difference of the average current in the open monomer channel and that in the blocked one at the given applied potential (we assume that the concentration is small enough, so that the probability of simultaneous blockages of two monomer channels in the trimer is negligible). If Δj is determined, *Methods 1* or *4* are applicable to extract the kinetic parameters of the channel blocking. However, if the blockage events are fast enough the secondary peak may disappear, and only the asymmetry of the histogram is evident. In the latter case, Δj is not measurable directly, and *Method 2* or *3* should be used to determine it together with the kinetic parameters of the channel blocking.

Auto-correlation function and PSD. At every substrate concentration, c, one calculates the autocorrelation function, $R(\tau, T)$, and the PSD $G(f, \tau_{\mathrm{max}}, T)$, for each data record by using Eqs. (3), (11), (6). τ_{max} must be much larger than the typical correlation time τ_c of the blockages due to substrate but smaller than T; if τ_c is smaller than few milliseconds, τ_{max} may be equal to 20-100 ms.

Background and PSD of the blocking signal. The ion-current fluctuations for the open channel without a substrate represent the background. One computes the PSD of the background, $G_{\mathrm{b}}(f)$, by averaging the PSDs

5

for the data records at $c = 0$. Successively, the PSD of the blocking signal is calculated for every substrate concentration and for each data record by subtracting the PSD of the background,

$$G_{\mathrm{s}}(f, c) \quad = \quad G(f, c) - G_{\mathrm{b}}(f) \quad . \tag{20}$$

The latter relation requires the non-trivial assumption that the ion-current fluctuations in an open channel do not correlate with the current fluctuations due to channel blocking by substrate molecules.

Frequency range. By comparing the signal PSDs, $G_{\mathrm{s}}(f)$, for the same substrate concentration but different data records one notes that at small frequencies (below a certain $f_{\min}$) they differ significantly while at $f \geq f_{\min}$ they well coincide within the statistical errors. This low-frequency difference may come from slow incontrollable changes of the external conditions (e.g., temperature) but also from infrequent spontaneous channel gating. The upper frequency, $f_{\max}$, is selected so that for $f > f_{\max}$ the absolute value of the PSD is close to or smaller than the statistical errors. The choice of the frequency range, $f \in [f_{\min}, f_{\max}]$, therefore, identifies statistically significant values of the PSD and gets rid of the slow incontrollable processes.

PSD fitting. At every substrate concentration, c, and for each data record one fits the model (filters-corrected) PSD,

$$G_{\mathrm{m}}(f) \quad = \quad \frac{a}{1 + (2\pi f \tau_c)^2} |H_{\mathrm{a}}(2\pi f)|^2 |H_{\mathrm{s}}(2\pi f)|^2, \tag{21}$$

to the signal PSD, $G_{\mathrm{s}}(f)$, in the frequency range $f \in [f_{\min}, f_{\max}]$, and obtains the Lorenzian factor a and the correlation time τ_c as well as the estimates of their uncertainties. Successively, the parameters are averaged over the data records for the same concentration of the substrate.

The weighted least squares method is used for the fitting. One minimizes the following scoring function,

$$S \quad = \quad \sum_{f_l \in [f_{\min}, f_{\max}]} \frac{[G_{\mathrm{m}}(f_l) - G_s(f_l)]^2}{\sigma^2(f_l)}, \tag{22}$$

$$f_l \quad = \quad \frac{1}{\Delta t} l \; ; \; l = 0, 1, \ldots \quad ; \tag{23}$$

6

where the frequency dependence of the weight function, $\sigma^2(f) = G_{\mathrm{m}}(f)$, is selected to make more or less uniform the contribution of each f_l point to the sum of Eq. (22). We found that the choice $\sigma^2(f) = G_{\mathrm{m}}(f)$ is better than $\sigma^2(f) = 1$ and than $\sigma^2(f) = G_{\mathrm{m}}^2(f)$, as the former overweights the smaller-frequency region while the latter overestimates the higher frequency domain.

To estimate the fitting error (uncertainty) of the parameters, δa and $\delta \tau_c$ are determined so that

$$\min_{\tau'} S(a \pm \delta a, \tau') \;=\; 2S_{\min} \quad , \tag{24}$$

$$\min_{a'} S(a', \tau_c \pm \delta \tau_c) \;=\; 2S_{\min} \quad . \tag{25}$$

Here, $S_{\min} = \min_{a',\tau'} S(a', \tau') = S(a, \tau_c)$ is the minimum value of the scoring function calculated at the optimal values of a and τ_c.

Kinetic parameters. Finally, one uses one or, independently, several of the methods discussed in Section *Theory* to determine the kinetic parameters of the ion current blocking due to substrate molecules.

4 Double-logarithmic scale PSD plots

7
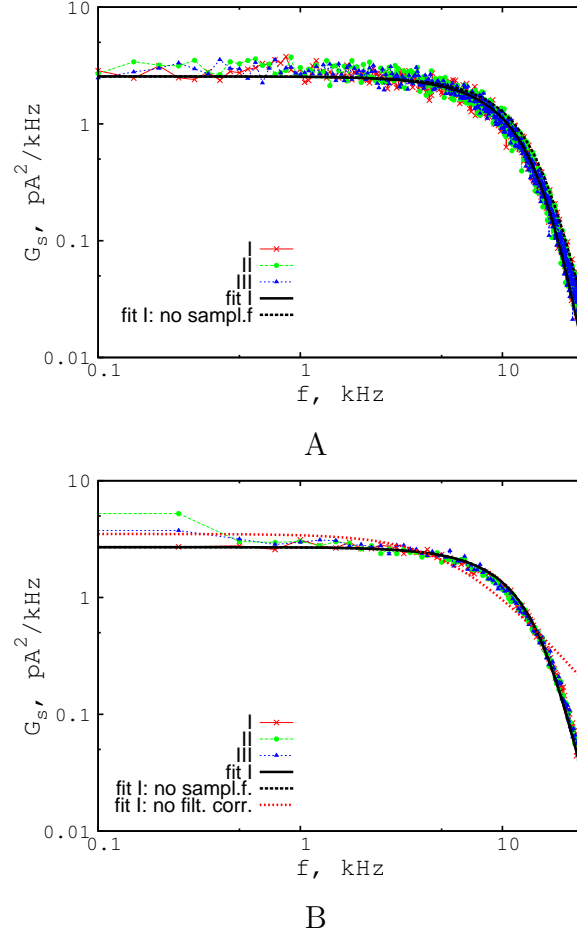
Figure 1: The signal PSD of the ion current fluctuations sampled at 50 kHz rate (A) and at 250 kHz rate (B). The thick solid line is the fit by the filters-corrected Lorenzian model; the dased line is the same Lorenzian model but corrected for the Bessel filter only, i.e., without the sampling correction. The dotted line in (B) is the fit by the pure Lorentzian filters-incorrected model. These data are plotted in linear scale in Figure 3.

8

113

P3.4.2: Interaction of Antibiotic with porins studied in planar lipid bilayers using parallelized platforms

*Weichbrodt, C., **Bajaj, H**., Baaken, G., Wang, J., Guinot, S., Kreir, M., Behrends, J., Winterhalter, M., and Fertig, N. (2015) Antibiotic translocation through porins studied in planar lipid bilayers using parallel platforms. Analyst. http://pubs.rsc.org/en/content/articlelanding/2015/an/c4an02335h.*

<u>Reproduced by permission of The Royal Society of Chemistry</u>

<u>Individual Contribution</u>

My main contribution in this manuscript is to perform experiments and analysis of data from single channel electrophysiology (black lipid/solvent free membrane). I participated in the composition of manuscript.

Antibiotic translocation through porins studied in planar lipid bilayers using parallel platforms

Conrad Weichbrodt[1], Harsha Bajaj[2], Gerhard Baaken[3], Jiajun Wang[1,2], Serap Guinot[1], Mohamed Kreir[1], Jan C. Behrends[3,4], Mathias Winterhalter[2], Niels Fertig[1]

[1] Nanion Technologies GmbH, Gabrielenstr. 9, 80 636 München, Germany
[2] Jacobs University Bremen, Campusring 1, 28 759 Bremen, Germany
[3] Ionera Technologies GmbH, Hermann-Herder-Str.7, 79104 Freiburg, Germany
[4] Laboratory for Membrane Physiology and –Technology, Department of Physiology, University of Freiburg, Hermann-Herder-Str.7, 79104 Freiburg, Germany

A comparative study of the three different techniques Orbit16, Port-a-Patch and BLM applied for the investigation of antibiotic translocation

Abstract

In general, the method of choice to characterize the conductance properties of channel-forming bacterial porins is electrophysiology. Here, the classical method is to reconstitute single porins into planar lipid bilayers to derive functional information from the observed channel conductance. In addition to an estimated pore size, ion selectivity or transport properties in general are of importance. For the latter question measuring the ion current fluctuation can provide some information about the mode of transport of charged molecules penetrating the proteins. For instance, increasing the external voltage modifies the residence time in the channel: charged molecules with the ability to permeate through channels will travel faster whereas non-permeating molecules get pushed to the constriction zone with enhanced residence time. Here, we are interested in the ability of antibiotics to permeate channels and compare different techniques to reveal fast events.

Keywords: single molecule, nanopore, planar lipid bilayer, antibiotic

Introduction

Emergence of bacterial resistance to common antibiotics has become a worldwide problem. The existing antibiotics face more and more resistant strains while there is a dramatic reduction of new antibiotic classes introduced[1,2]. In Gram-negative bacteria, resistance is often correlated with modification of the porin composition in the outer membrane[3–5]. The European Union recognized the problem and launched a private-public platform called 'New Drugs for Bad Bugs'. The subproject "Translocation" is devoted to the elucidation of the molecular origin of the observed low permeability of antibiotics across the cell wall of Gram-negative bacteria. Understanding the permeability across porins might open new routes for the design of tailor-made molecules with optimized permeation rates. Unfortunately, to date there is no direct assay to quantify permeation across single porins. Previously, we have used the ion-current fluctuation in the absence and presence of antibiotics to elucidate on and off rates[6,7]. Inspection of the ion current fluctuation

allows conclusion on the interaction of sugars, peptides or antibiotics with the channel[8–10]. However, as outlined previously, the temporal resolution of the translocation experiments is rather limited and there is a need for improvement[11,12]. In that regard, characterizing the kinetic rates by studying translocation of antibiotics through porins using different techniques can give useful information for developing new antibacterial molecules. A further step towards automated screening would then be to upscale the validated procedures to a parallel platform with higher throughput.

Previously, we have shown that the kinetic rates of interactions between the constriction zone inside a channel and different antibiotics can be obtained through an analysis of the ion-current fluctuation in the presence of antibiotics[6]. One particular bottleneck for this type of analysis is the limited time resolution, which does not cover the entire range of possible fast diffusion events. To elucidate the optimal setup, we herein provide a comparative study of the different techniques used in a quantitative manner. In particular, we study the interaction of three beta-lactam antibiotics (cefepime, ceftazidime and imipenem) with the bacterial outer membrane protein OmpF and compare the rate constants obtained for three different types of experimental techniques. We were able to show that the translocation experiments performed were comparable in terms of noise and rates obtained among all the three techniques. We also discuss the potentials and draw backs of each technique to measure antibiotic/porin interaction quantitatively.

Material and Methods

In all experiments, 1,2-Diphytanoyl-*sn*-Glycero-3-Phosphocholine (DPhPC) from Avanti polar lipids, Inc. (Alabaster, AL), was used. Cholesterol, Sorbitol, KCl, chloroform, HEPES and KOH were obtained from Roth (Carl Roth GmbH, Karlsruhe, Germany) and *n*-Octylpolyoxyethylene (OPOE) was obtained from Bachem, Bubendorf, Switzerland. Bio-Beads were obtained from Bio-Rad (Bio-Rad Laboratories GmbH, Munich, Germany). All antibiotics were obtained from SeqChem (Sequoia Research Products) except for Ceftazidime (Sigma-Aldrich).

Experiments on a single channel level were carried out using artificial planar lipid bilayer techniques. Lipid membrane bilayers can be made in a variety of ways, such as painting an aperture with dissolved lipids in an organic solvent[13] (black lipid membrane, BLM), or by slowly rising the buffer level of each half chamber after a lipid monolayer has been formed at the water/air interface (folded bilayer technique). The monolayers were made either from an organic solvent-based mixture of phospholipids[14], or by self-assembly from solvent-free lipid vesicles[15]. These techniques require extra equipment necessary for the high resolution recordings, such as a Faraday cage, an anti-vibration table or an acoustic chamber. An alternative method involves the formation of lipid bilayers on a glass substrate with a μm sized aperture[16]. Stable lipid bilayers are formed by the spreading of giant unilamellar vesicles (GUVs) or proteo-GUVs on the glass surface which form a free-standing portion of lipid bilayer with protein already reconstituted above the hole[16–18]. The latter method was found to be a robust platform which provides a first step towards screening, the next step towards a rapid automated screening would then be to significantly increase the throughput of these experiments. In a recent study, a chip-based microarray (MECA) offered the possibility to perform parallel high-resolution single-molecule analysis[19,20]. This could lead to a potential method to screen antibiotic interactions with the porin and this information eventually could be used for development of new antibiotics.

In this report, we describe the reconstitution of the outer-membrane channel-forming protein OmpF from Escherichia coli into planar lipid bilayers made by classic folded bilayer technique across a a ≈50 µm aperture (planar lipid bilayer technique) or by bursting GUV's on a glass chip with an about 1µm sized aperture (Port-a-Patch).We were also able to show that specific translocation experiments can easily be upscaled using the micro electrode array (MECA) chips up to sixteen-fold (Orbit 16).

Planar lipid bilayer (BLM) assays

In the so-called solvent-free method suggested by Montal-Mueller[14], the lipids are spread with an organic solvent on top of an aqueous buffer. The lipid bilayer is generated from two monolayers over a Teflon hole with a diameter of 50-100 µm. The Teflon hole is pre-painted with an organic solvent which typically is hexadecane. The advantage of this technique is that the content of each lipid monolayer can be controlled. This gives the possibility to form an asymmetric membrane by spreading a second lipid layer on the other compartment and raising both water levels after spreading of the lipids. After lipid membrane formation, reconstitution is usually initiated by adding very small amounts of protein from stock solutions, which contain a detergent at a concentration that is higher than the critical micelle concentration (CMC). Single channel reconstitution is reproducibly obtained by optimizing the concentration of the protein in a stock solution. Obviously, the larger the lipid membrane area is, the higher is the probability that a protein will be incorporated. OmpF was reconstituted by adding 0.1 µl of purified protein into the *cis* chamber containing 250 µL electrolyte solution (1M KCl, 20 mM MES pH 6) at a final concentration of 60 ng/ml. There is a strong indication that when the protein is added to the *cis* side the OmpF porin inserts with periplasmic loop first, i.e the extracellular loops face the *cis* side (reference/grounded side) and the periplasmic loops face the trans side of the chamber (live side; potential applied on this electrode). The orientation is determined based on asymmetry of the channel conductance at positive and negative voltages.

Microelectrode cavity array, MECA16 chips

MECA16 chips were prepared following the protocol described in Baaken et al. [20,21]. Briefly, to define the metal structures (gold contact pads, strip lines and electrodes) an image reversal photoresist (AZ 5214E, Microchemicals GmbH, Ulm, Germany) was lithographically patterned on a glass substrate, followed by deposition of a 20 nm chromium adhesion layer and a gold-layer of 200 nm using electron-beam evaporation. Subsequently a standard lift-off process was performed to remove excess metal. SU-8 3025 (MicroChem, Newton, MA, USA) was spun onto the substrate to a thickness of 20 µm and lithographically structured to form cavities at the position of the electrodes and insulate all other gold layers except the contact pads. Unless stated otherwise cavities had a diameter of 50 µm. Ag was electrochemically deposited on the electrodes from an $AgNO_3$ solution. A layer of AgCl was formed by anodizing in 150 mM KCl.

Bilayer formation was performed as described in Del Rio et al.[19]. Briefly, 150µl of electrolyte solution (1 M KCl, 20 mM MES, pH6) was added to the measurement chamber of the Orbit 16 System (Nanion Technologies GmbH, Munich, Germany). For the automated formation of bilayers in parallel on the 16 cavities, a small amount (approx. 0.1 µl of DPhPC at 5 mg/ml in octane) was applied beside the micro cavities to the chip surface. Subsequently, the counter magnet was turned repeatedly (up to 10 times) at a speed of 45-180°/s to evenly spread the lipid-solvent mixture over the surface, leading to an increasing fraction of the cavities being electrically sealed. Using the MECA chips the

Analyst Accepted Manuscript

orientation can be controlled in the same way as the BLM technique. When using the MECA chip, one or two microliter of OmpF porin micelle suspension from 2 ng/ml with 0.5% octyl-POE is added on top of the chip (the grounded side) and the incorporation is achieved by applying a transmembrane voltage of ±200 mV.

Free standing bilayers on microstructured borosilicate glass chip

Planar lipid bilayers were obtained from Giant Unilamellar Vesicles (GUVs) prepared by using the electroformation method[17] in an indium-tin oxide (ITO) coated glass chamber connected to the Nanion Vesicle Prep Pro setup (Nanion Technologies GmbH, Munich, Germany). The purified OmpF (150 µg/ml) in 1% Octyl-POE was then reconstituted into GUVs as described previously[11,17]. Briefly, the GUVs prepared by electroformation were incubated with the porins solubilized in detergent at a concentration of 1 to 5 µg/ml. After incubation the detergent Octyl-POE was removed using Biobeads® SM-2 (Bio-Rad) at 40 mg/ml. The Bio-Beads were discarded after centrifugation and the protein containing GUVs could be used immediately.

For formation of a planar lipid bilayer containing proteins, 5 µL of the proteoliposomes solution (1-5 µg/ml) was pipetted in 5 µL of electrolyte solution containing 1M KCL, 20 mM MES pH 6 onto the microstructured glass chip (grounded side) with an aperture of approximately 1 µm in diameter. The vesicles burst when they touch the glass surface of the chip forming a planar lipid bilayer and additional suction was applied to patch GUV's in this aperture. The orientation of OmpF in lipid bilayer in this case is not very clear since the proteo-GUV's bursting on the aperture could contain OmpF in both orientations.

Data recording and analysis

Kinetic parameters can be derived from ion current fluctuation as described previously[6,22] . Briefly, at low concentration (c), $c \ll k_{off}/k_{on}$, the characteristic time is close to the average residence time of the drug τ thus allowing us to use the following equations: $\tau \approx \tau_r = k_{off}^{-1}$, k_{off} being the dissociation rate constant and the inverse of the dwell time τ_r and $k_{on} = v/(3[c])$, k_{on} being the association rate constant where v is the number of binding events and $[c]$ is the antibiotic concentration. As the data were filtered with a Bessel filter at a cut-off frequency (-3 dB attenuation) of f_c = 10 kHz and hence a filter rise time of $\tau_{rise} = 0.33 f_c^{-1}$ = 33 µs[23], only events displaying a dwell time of τ = 30-50 µs or more were taken into consideration for further evaluation. (this cut off is based on the type of events observed, analysis parameters are chosen where there is no underestimation of amplitude of events observed)

Here k_{on}^{cis} is the association rate for antibiotic being added to the *cis* side (extracellular side of protein) and the k_{on}^{trans} is the association rate obtained for antibiotic being added to the *trans* side of the protein.

Planar lipid bilayer assays (BLM)

Ion current was recorded using an Axopatch 200B (Axon instruments) amplifier and the signal was filtered by a low-pass 4-pole Bessel filter at 10 kHz and sampled at a frequency of 50 kHz. The analysis was done by counting single events using the Clampfit 10 software as described above. The

Analyst Accepted Manuscript

experiments were performed in 1 M KCl, 20 mM MES pH 6 solution for all the antibiotics unless otherwise specified. Antibiotic stock solutions were made up to 30 mM in 1 M KCl, 20 mM MES pH 6 and diluted into chamber in a concentration dependent manner.

Port-a-Patch

Patch clamp experiments were performed with the Port-a-Patch automated patch clamp system (Nanion Technologies GmbH, Munich, Germany), using borosilicate glass chips. Experiments were done in symmetric solutions of 1 M KCl, 20 mM MES pH 6. Application of all solutions was achieved using an automated external and internal perfusion system. Currents were recorded with an Axopatch 200B (Axon instruments) amplifier and the signal was filtered by a low-pass 4-pole Bessel filter at 10 kHz and sampled at a frequency of 50 kHz. The analysis was done by counting of single events using the Clampfit 10 software as described above.

MECA:

A single channel amplifier (Axopatch 200B, Molecular Devices, Sunnyvale, CA, USA) was connected to the multiplexer electronics port of the Orbit 16 system. The 16 bilayers on the MECA chip were scanned for insertions of porins. Bilayers which showed a successful reconstituted single protein were then recorded at a sampling rate of 50 kHz and filtered at 10 kHz using a 4-pole Bessel filter integrated in the amplifier. Data were analysed using Clampfit (Molecular Devices, Sunnyvale, CA, USA).

Results

To elucidate the information content of each platform with respect to antibiotic translocation we selected OmpF, the most abundant porin in *E. coli*'s outer membrane. This channel is well investigated and exhibits a slight conductance asymmetry allowing to conclude on the probability for an oriented insertion. We chose commonly used antibiotics: imipenem, a member of the carbapenem class of antibiotics, cefazidime and cefepime, members of the third and the fourth generation antibiotics cephalosporins respectively to study their interaction with the porin and further compare all three techniques.

Planar lipid bilayers were formed following optimized respective protocols as described in materials and methods section. To ensure the comparability of the data recorded, all experiments were carried out using the same conditions (as specified in materials and methods) in each platform.

The best signal to noise ratio is obtained on single channel recordings and thus allows the best comparison. In a first series of measurements we determined the conductance of OmpF in 1 M KCl to be G_{OmpF} = 4 nS which decreases at transmembrane potentials exceeding V_m = ±150 mV in a stepwise manner corresponding to successive monomer closures. The characteristic of OmpF, conductance (4 ± 0.2 nS), critical voltage gating (150 -199 mV) , subconductances (at –ve voltage very short flickering were observed as observed in figure 2, did not change significantly in "virtual" solvent free (BLM), solvent free (microstructured glass chip) and solvent containing bilayers (MECA chip) as described previously [24].

A detailed look on respective techniques reveals an overall root-mean-square (RMS) noise (calculated from standard deviation of mean of the ion current) level of the open pore at a

transmembrane voltage of U_m=50 mV of 2.6 pA (figure 2a) for BLM technique compared to the microstructured glass chip (Port-a-Patch), which was calculated to be 1.6 pA at 10 kHz Bessel filter (figure 2b). The RMS noise in the parallel automated bilayers using the MECA chips, was calculated to be 2.3 pA at 10 kHz Bessel filter (figure 2c).

In a second series of measurements we were interested in the kinetics of antibiotic penetration. Application of a transmembrane voltage establishes an ion current through the channel and, in the absence of antibiotics, no visible current blockages are detected (figure 2). Addition of antibiotics causes fluctuation in the ion current reflecting the possible channel-drug interactions. Addition of Imipenem, a zwitterionic carbapenem antibiotic, caused rapid blockages of the ionic current through the monomer (figure 3). The number of blockages increased with increasing concentration of the antibiotic. The three platforms showed similar kinetics for imipenem in the OmpF pore (within the statistical error) calculated and reported in the Table 1. Apart from observing ion current flickering we also observed a huge increase in noise in presence of imipenem (figure 4B). The noise level was calculated to be 5.4, 5.8 and 5.7 pA for the BLM technique, the microstructured glass chip and the MECA chip containing 16 bilayers in parallel, respectively. Figure 4A shows a single event caused by imipenem blocking the channel at zoomed in time scale for BLM and the corresponding dwell time histogram for the determination of the dwell time t (inset). Both Orbit 16 and Port- a-Patch displayed similar noise levels and parameters of interaction in presence of imipenem with OmpF channel as seen in power spectrum from both systems compared to BLM (Supplementary figure 1)

Interactions of OmpF with cefepime, a zwitterionic cephalosporin (s. Fig. 5 a), were also detected, but the blockage events were shorter and less frequent than those caused by imipenem when antibiotic was added to the *cis* side (electrical ground). Table 1 shows the kinetics calculated for cefepime in OmpF for all three platforms. In contrast, the addition of cefepime to the *trans* side lead to an increase of k_{on} of about a factor of 30 (s.Fig. 5b) compared to the addition to the *cis* side. This asymmetry in the kinetics was used in further experiments as an indicator for the orientation of the porin in the lipid membrane. As a result, in 80% of the cases (n=6) in the BLM experiments the pore was inserted in the lipid membrane with an orientation leading to rather low k_{on} rates. In comparison, this orientation was observed in 50% of the experiments with the MECAs and in 60% of the cases with the Port-a-Patch, indicating a slightly different distribution of porin orientation in between the BLM and the two other systems. Subsequent addition of cefepime to the same channel on the *trans* side caused well resolved ion current fluctuations with all bilayer forming methods. For MECA chips the kinetics where calculated for the cases of ion channel orientation exhibiting high current fluctuation in presence of cefepime.

Addition of ceftazidime to a single OmpF channel causes partial ion current blockages in all the three platforms (Figure 6). Figure 6 shows a scatter plot of the amplitudes of all the single blocking events counted over the dwell time derived from measurements with the three systems. BLM and Port-a-Patch show similar characteristics where both full monomer blockages about 60 pA amplitude events and short events around 30 pA amplitude events are observed in contrast to Orbit 16 where only these short events were observed. In this case as well, the rate constants obtained in all three platforms were comparable. Within all the experiments reported here the minimum residence time of the antibiotic in the porin which could be measured was τ=30 µs, due to the limited availability of diverse filter settings in the range from >10 kHz to <100 kHz of the single channel amplifiers used. Table 1 summarizes the kinetics for 3 antibiotics (cefepime, ceftazidime and imipenem).

Discussion

Electrophysiology is a technique to quantify antibiotic-pore interaction at the single molecule level by measuring fluctuations in the ion current caused by antibiotic molecules residing within a single pore[6,11,25]. In this study we use OmpF, an outer membrane protein of *E. coli*, as a model porin to investigate the interactions of beta-lactam antibiotics and compare the kinetics obtained from three experimental platforms and methods of bilayer formation respectively: Solvent free lipid bilayer technique (BLM), Port-a-Patch and Orbit 16. We obtained kinetic parameters of cefepime, ceftazidime and imipenem with the OmpF channel. Here we observed that experiments conducted on the three different platforms gave rise to comparable data sets (Table 1). Addition of imipenem to a single OmpF channel causes an increase of ion current noise and well resolved monomer blockages (figure 3 and 4B). The latter suggests that at least 50% of the events correspond to translocation events, which correlates well to a report by Yoshimura *et al.* in which high diffusion rates of imipenem through OmpF in permeation assays were observed[26]. In contrast, in a recent study with OmpPst1 porin, a homologue of *E. coli* OmpF porin from *Providencia stuartii*, no well-resolved events were observed[9], although the addition of imipinem resulted in a similar increase in noise and reduction of average conductance found with OmpF and imipenem . A liposome permeation assay was employed in case of OmpPst1, which suggested binding/poor permeation of imipenem through this porin. This indicates strongly that the increased noise in the ion current and the reduction of conductance observed with OmpF after addition of imipinem are a result of an interaction of imipenem with the protein. As yet, this cannot be correlated with the effectivity of permeation or translocation of imipinem through the porins. For future experiments, the origin of the noise increase is an interesting problem to solve, which might require a better method for quantitative analysis, apart from single event analysis employed here. However, the main purpose of this study was to compare the kinetics/interaction of imipenem with OmpF pore in different systems to see whether an improved signal to noise ratio (e. g. as obtained with the Port-a-Patch) would give rise to different kinetics, but as it can be seen from table 1 this was not the case.

In case of cefepime, we observed asymmetric kinetics where a prominent effect was observed with *trans* addition compared to *cis* addition (figure 5). BLM membrane technique is taken as a reference for the orientation of the porin (as described in results section) and asymmetric kinetics observed by asymmetric cefepime addition due to accessibility of antibiotic addition on both sides of the membrane. On the Port-a-Patch, although providing accessibility to both sides of the membrane, the orientation of the porin seems to be random which is also observed for MECA chips. In this context, the orientation of the porin seems to play an important role in concluding on the kinetics which is probably physiologically relevant (k_{on}^{cis}; as described in methods section) and not misinterpreted because of a different orientation in lipid bilayer. Another parameter which could change the absolute rate constants are the parameters used in Clampfit for single event analysis e.g. a significant change in kinetics can be obtained due to different dead time/ignore duration used. Table 1 has been calculated by using same parameters in all the three platforms (details in materials and methods) for single event counting, changing the ignore duration/ dead time (from 30 µs to 50 µs) led to different kinetic parameters especially the association rates by factor of 3 irrespective of the system/platform (supplementary table 1). This highlights at least in case of cefepime that many events below 50 µs of residence time were observed and were missed in calculation in supplementary Table 1 and 30 µs dead time seems to be more optimum in this case. Although we

present the kinetics mainly at an ignore time of 30 µs since this can vary mainly to count the un-attenuated events that mostly reach the full amplitudes [23].

Apart from cefepime and imipenem measured with OmpF, we investigated and compared the effect of ceftazidime on OmpF in all three systems. For ceftazidime, since we observed partial ion current blockages (Figure 6), probably using Port-a-Patch, we could get a better signal to noise ratio and hence a slightly better resolution due to small sized aperture about 1 µm compared to ≥50 µm apertures in BLM. As seen in table 1, the kinetics obtained using single event analysis for all the three systems are identical in the error range, leaving the scope for an instrument needed with a much higher resolution to catch all these fast events. As seen in Figure 6, we observe a scatter of events with amplitude about 30 pA to 60 pA in Port-a-Patch as well as BLM, unlike Orbit 16 where the distribution does not have these full monomer blockages. This might be a result of a slightly higher temperature in the Orbit device (27°C) leading to faster kinetics and, thus, shorter dwell times. One way to catch the fast events could be measuring antibiotic kinetics at lower temperature, BLM[27] and Port-a-Patch offer such a possibility (Table 2). Port-a-Patch/Orbit 16 in this sense also provide a more stable platform in terms of high stability in lipid bilayers formed compared to BLM (Table 2).

Another issue we address in this study is the possibility to increase the throughput of the experiments to enable screening of antibiotics to suggest a trend on efficiency of translocation through porins. Micro-electrode array (MECA) chips offer such a prospect to upscale the system sixteen-fold with a throughput on average up to n=7-8 bilayers with single pore, making it a medium throughput platform compared to BLM or Port-a-Patch, which are low throughput platforms (Table 2). Another requirement for successful screening of several compounds is the usage of very little of material, in this respect Port-a-Patch provides promising platform compared to BLM (Table 2). Another aspect for drug screening is the portability of instrument , where Port-a-Patch /Orbit 16 do not require other accessories such as a Faraday cage to record high resolution traces The BLM apparatus requires tedious building of a Faraday cage on an anti-vibration table , acoustic isolation and proper grounding of the instrument (figure 1).

Conclusion

A single porin reconstituted into a planar lipid bilayer embedded into an electrophysiological setup can be used to study the interactions between the protein and single antibiotic molecules. Three different methods are frequently used for the formation of such a lipid bilayer: painting from lipid solution, the Montal-Mueller technique and vesicle fusion to a hydrophilic surface. In this study, three experimental setups: a black lipid membrane workstation, the Port-a-Patch and the Orbit16 (both from Nanion Technologies), each of them using one particular method of bilayer formation, are compared in regard of the quantitative information yield derived from antibiotic – porin experiments. From studies investigating interaction of 3 beta-lactam antibiotics imipenem, cefepime and ceftazidime with the model pore OmpF using BLM, Port-a-Patch and Orbit 16 (figure 1), we observe that the RMS noise values of the open pore ion currents are comparable: BLM: 2.6 pA; Port-a-Patch: 1.6 pA and Orbit 16: 2.3 pA. The rate constants obtained from the three different platforms are similar, revealing an equivalent time and current resolution of all the setups at a filter cut off frequency of 10 kHz. An increase of the bandwidth could possibly resolve the current fluctuations obtained with ceftazidime more precisely. A drastic reduction of the bilayer size (Ø 1µm, Port-a-Patch) compared to larger bilayers (Ø50µm, Orbit 16 and BLM) does not improve significantly the

signal to noise ratio and the resolution of the blocking events at the filter frequencies used here. However smaller diameters most probably will play a significant role in future experiments at higher bandwidths which could also facilitate further investigations regarding the increased noise in the ion current of OmpF in presence of Imipenem. However it is more likely that an alternate analysis method to quantify this phenomenon is needed. Aspects like orientation of protein in relation to the side of addition of the antibiotics play an important role in obtaining relevant kinetics (antibiotic flux from extracellular to periplasmic side); a point which is highlighted in case of cefepime.

We conclude that BLM and Port-a-Patch are viable platforms for the quantification of antibiotic-pore interactions at lower experimental throughput. The Orbit 16 is suitable for medium experimental throughput and has the potential for further upscaling towards a higher throughput screening device.

References

1. M. N. Gwynn, A. Portnoy, S. F. Rittenhouse, and D. J. Payne, *Ann. N. Y. Acad. Sci.*, 2010, **1213**, 5–19.

2. D. J. Payne, M. N. Gwynn, D. J. Holmes, and D. L. Pompliano, *Nat. Rev. Drug Discov.*, 2007, **6**, 29–40.

3. C. Bornet, A. Davin-Regli, C. Bosi, J. M. Pages, and C. Bollet, *J. Clin. Microbiol.*, 2000, **38**, 1048–1052.

4. J. P. Lavigne, A. Sotto, M. H. Nicolas-Chanoine, N. Bouziges, G. Bourg, A. Davin-Regli, and J. M. Pagès, *Clin. Microbiol. Infect.*, 2012, **18**, 539–545.

5. J.-M. Pagès, C. E. James, and M. Winterhalter, *Nat. Rev. Microbiol.*, 2008, **6**, 893–903.

6. E. M. Nestorovich, C. Danelon, M. Winterhalter, and S. M. Bezrukov, *Proc. Natl. Acad. Sci. U. S. A.*, 2002, **99**, 9789–94.

7. K. R. Mahendran, E. Hajjar, T. Mach, M. Lovelle, A. Kumar, I. Sousa, E. Spiga, H. Weingart, P. Gameiro, M. Winterhalter, and M. Ceccarelli, *J. Phys. Chem. B*, 2010, **114**, 5170–9.

8. P. R. Singh, I. Bárcena-Uribarri, N. Modi, U. Kleinekathöfer, R. Benz, M. Winterhalter, and K. R. Mahendran, *ACS Nano*, 2012, **6**, 10699–707.

9. H. Bajaj, Q.-T. Tran, K. R. Mahendran, C. Nasrallah, J.-P. Colletier, A. Davin-Regli, J.-M. Bolla, J.-M. Pagès, and M. Winterhalter, *Biochemistry*, 2012, **51**, 10244–9.

10. L. Kullman, M. Winterhalter, and S. M. Bezrukov, *Biophys. J.*, 2002, **82**, 803–12.

11. K. R. Mahendran, M. Kreir, H. Weingart, N. Fertig, and M. Winterhalter, *J. Biomol. Screen. Off. J. Soc. Biomol. Screen.*, 2010, **15**, 302–307.

12. J. L. Gornall, K. R. Mahendran, O. J. Pambos, L. J. Steinbock, O. Otto, C. Chimerel, M. Winterhalter, and U. F. Keyser, *Nano Lett.*, 2011, **11**, 3334–3340.

13. P. Mueller, D. O. Rudin, H. T. Tien, and W. C. Wescott, *Nature*, 1962, **194**, 979–80.

14. M. Montal and P. Mueller, *Proc. Natl. Acad. Sci. U. S. A.*, 1972, **69**, 3561–3566.

15. H. Schindler, *FEBS Lett.*, 1980, **122**, 77–9.

16. C. Schmidt, M. Mayer, and H. Vogel, *Angew. Chem. Int. Ed. Engl.*, 2000, **39**, 3137–3140.

17. M. Kreir, C. Farre, M. Beckler, M. George, and N. Fertig, *Lab Chip*, 2008, **8**, 587–95.

18. M. Sondermann, M. George, N. Fertig, and J. C. Behrends, *Biochim. Biophys. Acta*, 2006, **1758**, 545–51.

19. J. M. Del Rio Martinez, E. Zaitseva, S. Petersen, G. Baaken, and J. C. Behrends, *Small*, 2014.

20. G. Baaken, N. Ankri, A.-K. Schuler, J. Rühe, and J. C. Behrends, *ACS Nano*, 2011, **5**, 8080–8.

21. G. Baaken, M. Sondermann, C. Schlemmer, J. Rühe, and J. C. Behrends, *Lab Chip*, 2008, **8**, 938–44.

22. P. R. Singh, M. Ceccarelli, M. Lovelle, M. Winterhalter, and K. R. Mahendran, *J. Phys. Chem. B*, 2012, **116**, 4433–8.

23. D. Colquhoun and F. L. Sigworth, in *In Single Channel Recording*, eds. B. Sakmann and E. Neher, New York: Plenum Press., 1983, pp. 483–587.

24. C. Danelon, E. M. Nestorovich, M. Winterhalter, M. Ceccarelli, and S. M. Bezrukov, *Biophys. J.*, 2006, **90**, 1617–27.

25. C. Danelon, E. M. Nestorovich, M. Winterhalter, M. Ceccarelli, and S. M. Bezrukov, *Biophys. J.*, 2006, **90**, 1617–27.

26. F. Yoshimura and H. Nikaido, *Antimicrob. Agents Chemother.*, 1985, **27**, 84–92.

27. K. R. Mahendran, C. Chimerel, T. Mach, and M. Winterhalter, *Eur. Biophys. J.*, 2009, **38**, 1141–1145.

Analyst

Tables

Table 1: Kinetic properties found for the interaction of a single OmpF protein and three different antibiotics. (Analysis performed with dead time/ignore duration as 30 µs: conditions: 1M KCl, 20mM MES pH 6, at -50 mV for cis addition and +50mV for trans addition) 1 Calculated from -50 mV (no much effect at +50mV)

Antibiotic	Method	k_{on}^{cis} [M^{-1} s^{-1}]	k_{on}^{trans} [M^{-1} s^{-1}]	k_{off} [s^{-1}]
Cefepime	BLM	300	9.600 ± 200	20.000
	Orbit 16	100*	6.400 ± 600	13.000
	Port-a-Patch	1.200 ± 400	9.500 ± 700	15.300
Ceftazidime	BLM	1.500 ± 300	200	25.000
	Orbit 16	1.800 ± 600	220 ± 100	20.000
	Port-a-Patch	2100 ± 300	350 ± 100	17.000
Imipenem	BLM	1.100 ± 100	600 ± 60	16.700
	Orbit 16	1.600 ± 200	300 ± 100	22.000
	Port-a-Patch	2.800 ± 600	700 ± 200	19.000

Table 2: Comparison of the systems

System	RMS noise (open pore)	Through put	Resolution	Volume	Accessibility	Membrane stability	Portability	Temperature control
BLM	2.6	N=1	Filter @ 10 KHz; rise time 33 µs	250 µL or 2.5 mL	both sides of protein (extracellular and periplasmic side)	200 – 250 mV	low	Yes
Port a patch	1.7	N=1	Filter @ 10 KHz; rise time 33 µs	5 µL	Both sides of protein	More than 300 mV	high	Yes
Orbit 16	2.3[a]/2.1[b]	N=16	Filter @ 10 KHz; rise time 33 µs	150 µL	Only one side of the protein	More than 300 mV	medium	No

[a] MECA-chips with 50µm cavity diameter. [b] MECA-chips with 16µm cavity diameter

Figure legends

Figure 1: The 3 different planar lipid bilayer techniques a) BLM b) Port-a-Patch c) Orbit16

Figure 2: Ion current trace of single OmpF channel without antibiotic in a) BLM planar lipid bilayer (open pore current: 210 ± 12 pA) b) Port a patch (open pore current: 208 ± 7 pA) c) Orbit 16 (open pore current: 202 pA ± 12 pA). Conditions: 1M KCl, 20mM MES pH 6, at -50 mV.

Figure 3: Steady state frequency of translocation events of Imipenem (c = 5 mM) through a single OmpF channel observed at a transmembrane potential of Um = -50 mV on a) BLM planar lipid bilayer b) the Port-a-Patch® c) Orbit16. Conditions: 1M KCl, 20mM MES pH 6, at -50 mV

Figure 4: Detail of the current trace shown in Fig. 3. A. At high magnification single translocation events can clearly be identified. (Inset) the dwell time of these events τ is then used for the calculation of kinetic rate constants B. Power spectrum of single OmpF pore in presence and absence of 5mM Imipenem. Conditions: 1M KCl, 20mM MES pH 6, at -50 mV

Figure 5: Ion current trace of single trimeric OmpF recorded in BLM with Cefepime added to *cis* side (- 50 mV) and *trans* (+ 50 mV) side. Conditions: 1M KCl, 20 mM MES pH 6, at ±50 mV.

Figure 6. Scatter plot of events in presence of Ceftazidime through a single trimeric OmpF channel measured through BLM (black squares), Port a patch (blue triangle) and Orbit 16 (red circles). Conditions: 1M KCl, 20mM MES pH 6, at -50 mV.

Figure 1

Figure 2

A. BLM

B. Port-a-Patch

C. Orbit16

127

Figure 3

A. BLM   B. Port-a-Patch   C. Orbit16

Figure 4

Figure 5

5 mM Cefepime cis side

5 mM Cefepime trans side

Figure 6

Antibiotic translocation through porins studied in planar lipid bilayers using parallel platforms

Conrad Weichbrodt[1], Harsha Bajaj[2], Gerhard Baaken[3], Jiajun Wang[1,2], Serap Guinot[1], Mohamed Kreir[1], Jan C. Behrends[3, 4], Mathias Winterhalter[2], Niels Fertig[1]

[1] Nanion Technologies GmbH, Gabrielenstr. 9, 80 636 Münichen, Germany

[2] Jacobs University Bremen, Campusring 1, 28 759 Bremen, Germany

[3] Ionera Technologies GmbH, Hermann-Herder-Str.7, 79104 Freiburg, Germany

[4] Laboratory for Membrane Physiology and –Technology, Department of Physiology, University of Freiburg, Hermann-Herder-Str.7, 79104 Freiburg, Germany

Supporting Information

Supplementary Table 1: Kinetic properties found for the interaction of a single OmpF protein and three different antibiotics. (Analysis performed with dead time/ignore duration as 50 µs: conditions: 1M KCl, 20mM MES pH 6, at ±50 mV)

Antibiotic	Method	k_{on} [M^{-1} s^{-1}]	k_{off} [s^{-1}]
Cefepime (*trans* side addition)	BLM	3.200 ± 200	11.100
	Orbit 16	2.000 ± 700	16.100
	Port-a-Patch	3.800 ± 700	9.100
Ceftazidime (*cis* addition)	BLM	600 ± 100	12.000
	Orbit 16	900 ± 300	16.400
	Port-a-Patch	700 ± 400	11.400
Imipenem (*cis* side addition)	BLM	1.100 ± 100	14.000
	Orbit 16	1.600 ± 200	19.000
	Port-a-Patch	2.800 ± 600	14.000
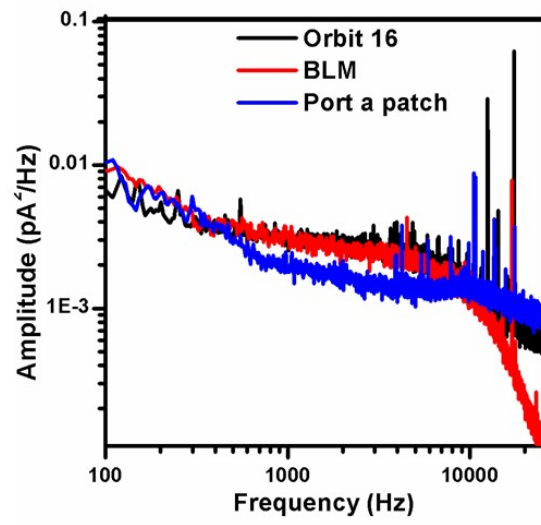
Supplementary Figure 1: Power spectrum from both systems compared to BLM.

Chapter 5: Transport across porin from *Nocardia farcinica*

In this chapter, we mainly investigate the uptake of solutes and antibiotics through porin from Gram-positive Mycolata *N. farcinica.* The porin was first identified and characterized in 1998 by group of Prof. Dr. Roland Benz. In 2011 the same group suggested the porin to be hetero-oligomeric channel consisting of two subunits (*NfpA/NfpB*) and highly similar to that of the homo-octameric MspA channel from *Mycobacterium smegmatis*. This formed motivation of our subsequent studies in collaboration with Prof. Dr. Roland Benz.

P3.4.1: Transport across the outer membrane porin of mycolic acid containing actinomycetales: *Nocardia farcinica*

Individual Contribution:
My main contribution in this manuscript is to perform cloning (mutagenesis experiments), protein expression and purification experiments. I also performed and analyzed the data from liposome swelling assay experiments.

Transport across the outer membrane porin of mycolic acid containing actinomycetales: *Nocardia farcinica*

Pratik Raj Singh, Harsha Bajaj, Roland Benz, Mathias Winterhalter, Kozhinjampara R. Mahendran *

School of Engineering and Science, Jacobs University Bremen, Campus Ring 1, D-28759 Bremen, Germany

ABSTRACT

The role of the outer-membrane channel from a mycolic acid containing Gram-positive bacteria *Nocardia farcinica*, which forms a hydrophilic pathway across the cell wall, was characterized. Single channel electrophysiology measurements and liposome swelling assays revealed the permeation of hydrophilic solutes including sugars, amino acids and antibiotics. The cation selective *N. farcinica* channel exhibited strong interaction with the positively charged antibiotics; amikacin and kanamycin, and surprisingly also with the negatively charged ertapenem. Voltage dependent kinetics of amikacin and kanamycin interactions were studied to distinguish binding from translocation. Moreover, the importance of charged residues inside the channel was investigated using mutational studies that revealed rate limiting interactions during the permeation.

© 2014 Elsevier B.V. All rights reserved.

1. Introduction

With the increasing awareness of antibiotic resistance against bacteria, recent findings have revealed a strong correlation of resistance with permeability changes of the cell wall [1–3]. The outer membrane of Gram-negative bacteria contributes to the intrinsic resistance by decreasing the flow of antimicrobial agents into the cell [4–6]. In contrast, Gram-positive bacteria lacking an outer membrane in their cell wall are in general, more sensitive to antibiotics [7]. A further group of Gram-positive bacteria belonging to the actinomycetales taxon, also called mycolata, has a high intrinsic resistance to a wide range of antibiotics due to the presence of an additional mycolic acid layer [7–10]. The mycolic acid layer is mainly composed of long chain mycolic acids and free lipids. It resembles the function of an outer membrane of Gram-negative bacteria [11–13].

Surprisingly, the cell envelope of mycolata also contains water-filled protein channels called porins, which facilitate the diffusion of hydrophilic molecules into the cell [14]. Porins spanning the outer membrane have been identified in the cell wall of some members of the mycolata, such as *Mycobacterium chelonea* [14,15], *Corynebacterium glutamicum* [16], *Mycobacterium smegmatis* [17] and *Nocardia farcinica* [18]. For example MspA, a porin from *M. smegmatis*, forms pores which allow the uptake of various sugars and hydrophilic antibiotics [19,20]. In recent years the importance of the role of porins in the uptake of antibiotics has been recognized in Gram-negative bacteria [21]. Additionally, Gram-positive mycolata group of bacterium comprises microorganisms such as *Mycobacterium tuberculosis* (TBC), *Mycobacterium leprae* (leprae), *N. farcinica* (nocardiosis) and *Corynebacterium diphtheriae* (diphtheria) that exhibit a pronounced and broad natural resistance to various antimicrobial drugs and contribute towards various dangerous infections worldwide [22,23]. Hence, there is a strong interest in understanding the rate limiting steps of antibiotic transport through the channels. In this study, we focus on understanding the pathway of various hydrophilic antibiotics as well as solutes through the outer-membrane porin from the Gram-positive mycolata, *N. farcinica.*

The outer membrane porin from *N. farcinica* was first identified in 1998 [18], which was later resolved as a hetero-oligomeric channel composed of two different subunits; *NfpA* and *NfpB* [24]. The crystal structure of the protein is unknown but the sequence analysis suggests that it has a high homology to the MspA channel [24]. Previously, we have studied the translocation of polypeptides through the *N. farcinica* channel reconstituted into lipid bilayers [25]. In the present study, we focused on the functionality of the *N. farcinica* channel using planar lipid bilayer electrophysiology and liposome swelling assay. Liposome swelling assay was employed to study the translocation of various uncharged/zwitterionic hydrophilic nutrient molecules such as sugars and amino acids. Using single channel electrophysiology, we studied ion current fluctuations of the channel in the presence of clinically relevant antibiotic molecules; positively charged amikacin and kanamycin, and negatively charged ertapenem [18]. Additionally, we selectively neutralized the negatively charged amino acid residues at the pore

* Corresponding author at: Department of Chemistry, University of Oxford, Oxford OX1 3TA, United Kingdom. Tel.: +49 4212003588.
E-mail addresses: p.singh@jacobs-university.de (P.R. Singh),
mahendran.kozhinjampararadhakrishnan@chem.ox.ac.uk (K.R. Mahendran).

lumen to elucidate the effect of charge on antibiotic–solute interaction within the channel.

2. Materials and methods

2.1. Bacterial strains and growth conditions

Escherichia coli cells containing the pARAJS2 vector with *NfpA* and *NfpB* genes were used in each experiment. For plasmid purification *E. coli* DH5Alpha cells were grown in LB medium at 37 °C with ampicillin antibiotic used for selection. *E. coli* BL21 (DE3) Omp8 was utilized for expression experiments. 100 μg/mL ampicillin and 40 μg/mL kanamycin were used for selection.

2.2. Site directed mutagenesis of genes NfpA and NfpB

Cultures of *E. coli* DH5Alpha grown at 37 °C, containing the pARAJS2 plasmids harboring wild-type (WT) genes, are used for extraction of the plasmid. *In vitro* site-directed mutagenesis was employed to obtain the desired mutations. The mutations were generated using two approaches; quick change site directed mutagenesis and the megaprimer method using PCR. The primers used to introduce substitution-mutations were listed in Supplementary Table 1. The PCR conditions used for quick change mutagenesis were: initial denaturing at 95 °C for 1 min, 30 cycles at 95 °C for 30 s, 55 °C for 1 min, 68 °C for 7 min and final extension at 68 °C for 10 min. Forward primer *NfpA* and reverse primer *NfpA* D141N D142N led to complete copy of pARAJS2 plasmid containing desired mutations. The megaprimer required two steps of PCR, first step led to megaprimers with typical lengths of 250–300 bp and in the second step these megaprimers were used as primers for second PCR. The conditions used were: first step 95 °C for 1 min, 30 cycles at 95 °C for 30 s, 55 °C for 1 min, 68 °C for 45 s and final extension at 68 °C for 5 min. The second step consisted of 95 °C for 10 min, 30 cycles at 95 °C for 1 min, 72 °C for 7 min and final extension at 72 °C for 30 min. *DpnI* digestion was carried out on the PCR product and then run on 1% agarose gel.

2.3. Protein expression and purification

The purification of the two subunits *NfpA* and *NfpB* expressed in *E. coli* BL21 (DE3) Omp8 was performed as described previously with slight modifications [24,25]. Briefly, pARAJS2_*nfpA* (mutant)/*nfpB* (mutant) transformed in the porin-deficient *E. coli* BL21(DE3)Omp8 cells was grown in LB media at 37 °C to an OD600 of 0.5–0.9. The cells were then induced with 0.02% of arabinose for over-expression of proteins and were grown at 16 °C for 16 h. The cells are collected by centrifugation at 5000 ×*g* for 20 min at 4 °C, and the resulting pellet was re-suspended in 10 mM Tris pH 8. The re-suspended pellet was broken down by French press, and the cell debris was separated by centrifugation at 5000 ×*g* for 10 min at 4 °C. The supernatant was ultra-centrifuged at 48,000 ×*g* for 1 h at 4 °C to separate the cytosolic proteins present in supernatant and the pellet containing membrane proteins. The protein of interest was further purified from the supernatant fraction to avoid contamination from membrane proteins of *E. coli* present in the pellet fraction. His-tagged protein purification from the supernatant fraction was then performed using Ni-NTA beads under denaturing conditions. The protein of interest was eluted using a gradient of imidazole concentration. The two subunits, purified separately, were refolded together to form a hetero-oligomeric channel by ammonium sulfate precipitation. The two purified subunits are mixed together in a 1:1 ratio and precipitated using saturated ammonium sulfate solution. The solution was incubated overnight at 4 °C and centrifuged at 18,000 ×*g* for 30 min. The precipitated protein pellet was refolded to native state by incubating at 4 °C in 150 mM NaCl, 25 mM Tris–HCl and 1% Genapol.

2.4. Liposome swelling assays

N. farcinica porin was reconstituted into liposomes as described by Nikaido and Rosenberg [26]. *E. coli* total lipid extract was used to form liposomes; 15% Dextran (MW 40,000) was used to entrap the liposomes, and their final size was checked using a Nano-ZS ZEN3600 zetasizer (Malvern Instruments, Malvern, United Kingdom). Control liposomes were prepared in the same manner but without the addition of porin. 0.5–1 μg of protein per 2 mg of lipid was used to make proteoliposomes. The concentrations of test solute were adjusted so that diluents were apparently isotonic with control liposomes. Stachyose was also tested with proteoliposomes to confirm the isotonicity of the multilamellar liposomes. Liposome or proteoliposome solution (30 μL) was diluted into 630 μL of an isotonic test/solute solution made in 10 mM Tris–HCl pH 7.5 buffer in a 1 mL cuvette and mixed manually. The change in absorbance at 500 nm was monitored using a Cary–Varian UV–vis spectrophotometer in the kinetic measurement mode. The swelling rates were taken as averages from at least five different sets of experiments, calculated as described previously [27].

2.5. Solvent free lipid bilayer technique

Reconstitution experiments and noise analysis have been performed as described in detail previously. The Montal and Muller technique was used to form phospholipid bilayer using DPhPC (Avanti polar lipids) [28]. A Teflon cell comprising an aperture of approximately 30–60 μm diameter was placed between the two chambers of the cuvette. The aperture was prepainted with 1% hexadecane in hexane for stable bilayer formation. 1 M KCl (or 150 mM KCl) and 10 mM HEPES, pH 7.4 were used as the electrolyte solution and added to both sides of the chamber. Ion current was detected using standard silver–silver chloride electrodes from WPI (World Precision Instruments) that were placed in each side of the cuvette. Single channel measurements were performed by adding the protein to the *cis*-side of the chamber (side connected to the ground electrode). Spontaneous channel insertion was typically obtained while stirring under applied voltage. Channel insertion was almost always oriented with the extracellular region facing *the cis-side*. After successful single channel reconstitution, the *cis*-side of the chamber was carefully perfused to remove any remaining porins to prevent further channel insertions. Conductance measurements were performed using an Axopatch 200B amplifier (Molecular devices) in the voltage clamp mode. Signals were filtered by an on board low pass Bessel filter at 10 kHz and with a sampling frequency set to 50 kHz. Amplitude, probability, and noise analyses were performed using Origin pro 8 (OriginLab) and Clampfit softwares (Molecular devices). Single channel analysis was used to determine the antibiotic binding kinetics. In a single-channel measurement the typical measured quantities were the duration of closed blocked levels' residence time (τ_c) and the frequency of blockage events (ν). The association rate constants k_{on} were derived using the number of blockage events, $k_{on} = \nu / [c]$, where c is the concentration of antibiotic. The dissociation rate constants (k_{off}) were determined by averaging the $1/\tau_c$ values recorded over the entire concentration range [29]. Similarly, the selectivity measurements were performed using two different salt solutions in the two chambers of the cuvette. The reverse potential required to obtain zero-current was calculated and the ratio of the permeabilities of cation/anion was calculated using the Goldman–Hodgkin–Katz equation [30,31].

3. Results and discussion

3.1. Mutational studies on N. farcinica cell wall channel

Based on the homology modeling of the porin with the known structure of MspA, we selected various negatively charged amino acids; located strategically at the periplasmic side of the channel in the two different subunits, *NfpA* and *NfpB*, and mutated them to neutral

amino acids with a similar length of the side chain. Table 1 shows the selected mutations in both subunits and the corresponding channel conductance of the mutant channels in 1 M KCl solution. In particular, we performed at maximum two mutations (D141N and D142N) in *NfpA* and 4 ones (E123Q, E144Q, D127N, E140Q) in *NfpB*, resulting in a total number of maximum 24 mutations in the pore-forming oligomer. Fig. 1 shows the expected positions of the mutations. Some other mutations led to proteins that had no channel-forming activity. This is presumably the result of the loss of channel function caused by the mutation of residues that were crucial for protein folding and assembly of the oligomers (Table 1). To elucidate the effect of charge residues inside the pore on the interaction with antibiotics, we choose the mutant oligomer with the highest number of negatively charged residues mutated to neutral ones and compared the effect of antibiotics on channel conductance with those on wild-type (WT) porin.

Based on homology modeling we created the surface potential of the porin and compared both the WT and the mutant channel as shown in Supplementary Fig. 1. The mutations rendered its periplasmic side rather neutral compared to the WT channel. To study the interaction of the mutant channel with cationic peptide we performed single-channel measurements to determine the approximate locations of these mutations. As shown in Supplementary Fig. 1A, we observed that hepta-arginine showed a very strong interaction with the WT channel resulting in frequent blockages of ionic current in multiple steps when added to the periplasmic side (*trans*) of the channel [25]. However, when the same experiment was performed with the mutant porins (Supplementary Fig. 1B), we observed reduced interactions of hepta-arginine with the channel. This reduction was due to the absence of negatively charged amino acids in the periplasmic entry of the pore, suggesting that the mutations were located at the correct positions.

3.2. Ion selectivity measurements

Ion selectivity measurements of both the WT and mutant pore were performed using different concentrations of monovalent KCl salt solutions on both sides of DphPC membranes. As expected, the channel was highly cation selective due to the large number of negatively charged residues inside the channel as shown in Table 2. As shown previously, the cation selectivity of the channel is not caused due to a particular binding site inside the channel but by the presence of point negative charges inside the lumen of the channel [18,32]. This changes the cation selectivity of the channel using different concentrations of the electrolyte solution on both sides of the membrane. At high salt concentration (1 M KCl/150 mM KCl), caused by electrostatic effects, the cation selectivity of the channel ($pK^+/pCl^- = 3.8$) was lower compared to the selectivity (7.8) at a lower salt concentration on both sides of the membranes (500 mM KCl/75 mM KCl). Similarly, the ion selectivity of the mutant pore was lower compared to WT pore in both salt concentrations, making it slightly less cation selective because many negatively charged groups became neutral by mutation.

3.3. Functional assays with liposomes

The channel functionality of *NfpA*/*NfpB* WT and mutant oligomers was further confirmed by reconstituting them in liposomes and measuring their permeability for small hydrophilic molecules such as sugars
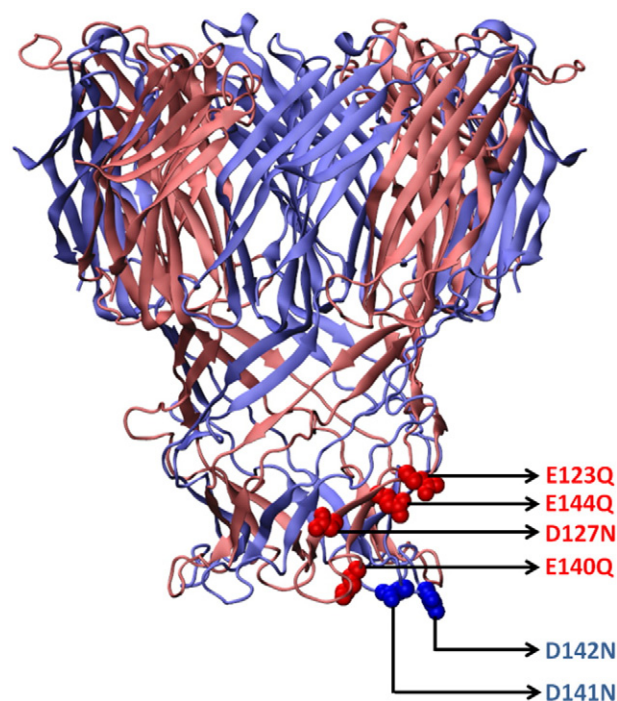
Fig. 1. Homology modeling of hetero-oligomeric *N. farcinica* channel based on the template MspA porin from *M. smegmatis* [25]. Selected mutations are shown for one *NfpA* monomer (blue) and one *NfpB* monomer (red) resulting in total of 24 mutations in the channel-forming oligomer. Note that the bottom side of the oligomer is exposed to the inner side of the mycolic acid layer and the top to the external medium. Reconstitution into lipid bilayer membranes occurs exclusively with the periplasmic side of the oligomer exposed to the *trans*-side of the bilayer.

and amino acids. The rate of diffusion of sugars and amino acids was calculated by measuring the change in optical density of proteoliposomes in the presence of an isotonic concentration of sugars/amino acids [26]. Permeation rates were obtained within the same batch allowing us to normalize the diffusion rates with respect to arabinose [26]. We found that the exclusion limit of the channel was slightly higher than that observed in the case of Gram-negative porins, as shown in Fig. 2 by the considerably higher diffusion rate of large molecules, such as raffinose. This suggested a larger exclusion limit of the channel which may be due to the larger pore size of the channel. Importantly, these results were coherent with previous results for porin from *Mycobacterium chelonae* which has similar properties as the *N. farcinica* channel [14]. The highest diffusion rates were obtained for the two amino acids glycine and L-serine; they were approximately 80% higher than that observed for arabinose. The diffusion rates of other sugars including maltose, sucrose and glucose were approximately 20% lower than arabinose. Liposome swelling assays performed on *N. farcinica* channel indicated passive diffusion of different sugars and amino acids through the channel with the rate of permeation proportional to the size of the substrate. The diffusion rate was found to decrease with the increase of molecular mass of solutes as reported previously [14,26]. There was no significant difference in diffusion rates of sugar and amino acids between the WT and mutant protein. This was expected since all the

Table 1
Mutations performed in both the *NfpA* and *NfpB* subunits of *N. farcinica* porin. This table shows the conductance at 1 M KCl and 20 mM HEPES, pH 7.5 once the mutants have been refolded.

Mutations in *NfpA*	Mutations in *NfpB*	Average conductance (nS) n = 10
Wild-type (WT)	E123Q, E144Q, D127N, E140Q	3.1 ± 0.2
D141N, D142N	E123Q, D127N	2.8 ± 0.3
D141N, D142N	E123Q, E144Q, D127N, E140Q	2.7 ± 0.3 (selected for further studies)
D141N, D142N	E123Q, E144Q, D127R, E140Q	2.2 ± 0.1
E101K, D141N, D142N, D181R	E123Q, E144Q, D127N, E140Q	No channel-forming activity observed

Table 2
Ion selectivity of WT and mutant *N. farcinica* channels using different KCl concentration gradients on both sides of the DphPC membranes.

N. farcinica	Concentration gradient [*cis/trans*]	Reverse potential on the more dilute side [mV]	Pc/Pa (n = 3)
Wild-type (WT)	1 M KCl/150 mM KCl	23 ± 1	3.8 ± 0.2
	500 mM KCl/75 mM KCl	33 ± 1	7.8 ± 0.3
Mutant	1 M KCl/150 mM KCl	21 ± 1	3.2 ± 0.2
NfpA (D141N, D142N)	500 mM KCl/75 mM KCl	27 ± 1	4.8 ± 0.2
NfpB (E123Q, E144Q, D127N, E140Q)			

sugars or amino acids tested were neutral or zwitterionic. Furthermore, we also performed single channel electrophysiology experiment on sugar transport through the *N. farcinica* channel. However, it seemed that the sugar molecules did probably not bind inside the channel. They diffused through the channel which means that our instrumental set-up could not resolve any interaction between sugars and channel in terms of ion current fluctuations.

3.4. Interaction between antibiotics and the N. farcinica channel

One of the main focuses in this study was to investigate the interaction of clinically relevant antibiotics with the *N. farcinica* channel. Identifying the antibiotic affinity site and its position inside the channel helps to understand the rate limiting interaction and sheds light on the pathway of the antibiotic through the channel [33–36]. Based on the selectivity of the *N. farcinica* channel and the presence of negatively charged residues in the channel's mouth, it has been postulated that positively charged antibiotic may utilize this channel as the pathway for permeation [18]. Using this assumption, we selected two positively charged aminoglycosides for our study, kanamycin and amikacin.

The *N. farcinica* channel has a strong asymmetry of the channel gating such that it is highly stable at negative voltages but gates significantly at positive voltages as low as +30 mV (protein addition to the *cis*/ground side) [25]. Thus the majority of the experiments were performed at negative voltages at the *trans*-side. In the absence of antibiotics, no fluctuation in the ion current was detected here and in a previous study [18,25]. This changed completely when amikacin and kanamycin were added in μM concentration to the *cis*-side of the membranes. Ion current fluctuations observed for both amikacin and kanamycin at 150 mM KCl solution are shown in Figs. 3A and 4A, respectively. Addition of antibiotics to the *cis* (ground) side of the channel induced ion current blocks, suggesting possible antibiotic–porin

Fig. 2. Liposome swelling assay performed for both WT and mutant *N. farcinica* porins reveals the qualitative diffusion rate of different sugars and amino acids based on their sizes. Note that the difference of the relative rate of diffusion between the WT channel and its mutant was within the SD of the experimental error.
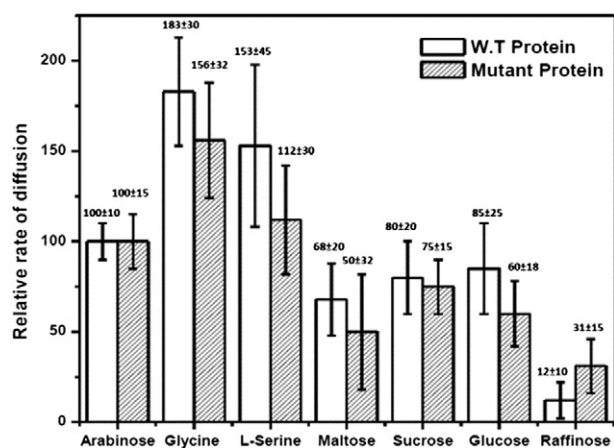
interaction. In contrast to this, we did not observe at applied positive voltages any interactions, which might be caused by the positive voltage repelling the positively charged antibiotic molecules from the channel. As a control we reversed the experiment with respect to voltage. Addition of the antibiotics to the *trans*-side under negative voltages also caused no ion current fluctuations.

The most prominent interactions were observed at *cis* addition and applied negative voltages with a lowered salt solution from 1 M KCl to 150 mM KCl. This suggested that the interaction between the antibiotic and porin had a strong charge–charge interaction component. Similarly, previous experiments that have been performed on peptides and DNA molecules have also reported this enhanced interaction, upon lowering of the salt concentration [37,38].

Amikacin is an aminoglycoside with a net positive charge of 4 at pH 7.4 [39]. Increasing the concentration of amikacin showed increased interaction with both the WT and mutant channels. However, addition of amikacin to the mutant pore with <24 negative amino acid residues showed significantly less interaction than the WT channel, as depicted by the ion current trace in Fig. 3D. The current amplitude histogram shown in Fig. 3B and E provides the decreased current counts of the closed state (blocked state) in the mutant pore compared to those of WT. The scatter plot of amplitude (y-axis) and dwell time (x-axis), Fig. 3C and F, represents the antibiotic–channel interactions. The residence (dwell) time of antibiotic interaction with the porin ranged from 100 μs to 800 μs with an average residence time of 200 μs for the WT channel. In the case of the mutant channel, the average residence time decreased to something like 100 μs close to the time resolution limit of our instrumentation. We also observe a slight decrease in amplitude of amikacin blocking in mutant channel compared to the WT channel, which is due to the decrease in the overall conductance of the mutant channel (Table 1).

Similarly, kanamycin is also an aminoglycoside with a net positive charge of 4 and as expected, kanamycin also showed interaction with the pore. Nevertheless, the interaction of kanamycin was significantly different to that observed for amikacin (Figs. 3A and 4A). Kanamycin exhibited lower frequency of events compared to amikacin. In addition, the interaction of kanamycin with the pore was not uniform as depicted in the plots in Fig. 4B and E. From Fig. 4C, we observed that the dwell times of the kanamycin interaction ranged from 100 μs to 80 ms. This suggested that kanamycin may have more than one binding site within the channel surface. Likewise to amikacin, the number of events and the residence time of kanamycin interaction decreased in the mutant pore as shown in Fig. 4D and F.

Previous reports on antibiotic translocations through porins of Gram-negative bacteria highlight that charged residues within a pore influence the interaction between the antibiotics and pore and hence the rate of translocation [40–45]. Mutation of amino acid D113N of *E. coli* OmpF loop 3 shows an increased rate of permeation of ampicillin [42]. Similarly, a single mutation in the loop 3 region (glycine to aspartate) of *Enterobacter aerogenes* Omp36 porin exhibits a reduced pore conductance and decreased cephalosporin permeation [46]. To elucidate the importance of charge and the presence of affinity site inside the porin, we performed an antibiotic titration experiment with *N. farcinica* mutant pore, where 24 amino-acids were neutralized. In such an experiment (Supplementary Table 2), we observed that both
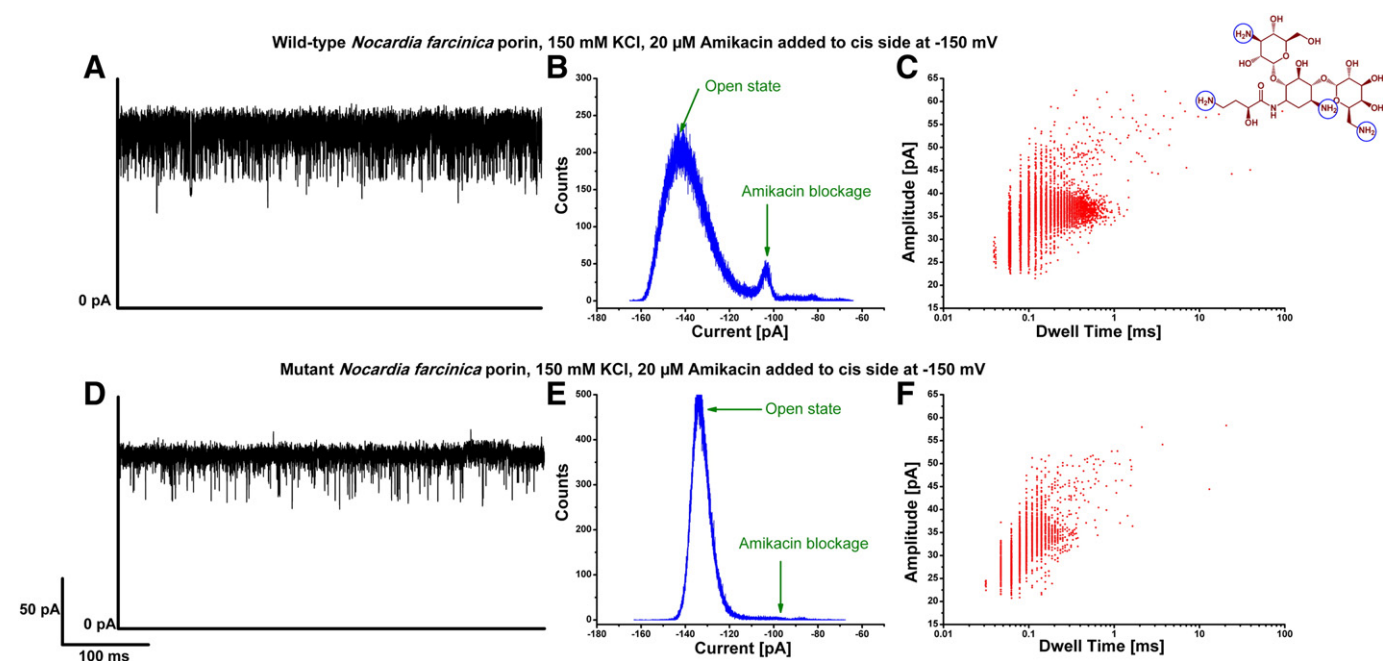
Fig. 3. Interaction of amikacin (chemical structure top right) with WT and mutant *N. farcinica* channel. (A) 20 μM amikacin was added to the *cis*-side of the WT channel at an applied voltage of −150 mV. (B) Event histogram of amikacin with the WT channel. (C) Amplitude-dwell time scatter plot of amikacin events with the WT channel. (D) 20 μM amikacin was added to the *cis*-side of the mutant channel at an applied voltage of −150 mV. (E) Event histogram of amikacin with the mutant channel. (F) Amplitude-dwell time scatter plot of amikacin events with the mutant channel. Experimental conditions were 150 mM KCl and 10 mM HEPES, pH 7.4.

the on-rate as well as the residence time of amikacin and kanamycin were reduced for the mutated pore, emphasizing the importance of affinity sites inside the channel.

In our experiment, both the positively charged antibiotics belong to the antibiotic class of aminoglycoside. Amikacin and kanamycin both possess 4 positive charges at pH 7.4 and the structures of the antibiotics share a similar scaffold. However, we observed a very sharp difference

in the binding kinetics of these two antibiotics with the pore. Amikacin had a significantly higher on-rate as compared to kanamycin (Supplementary Table 2). *In vivo* Minimum Inhibitory Concentration (MIC) assay of different antibiotics performed with *N. farcinica* showed amikacin to be an effective drug compared to kanamycin [47,48]. Could the higher on-rate of amikacin compared to kanamycin be the reason for such difference in effectiveness? However, the presented
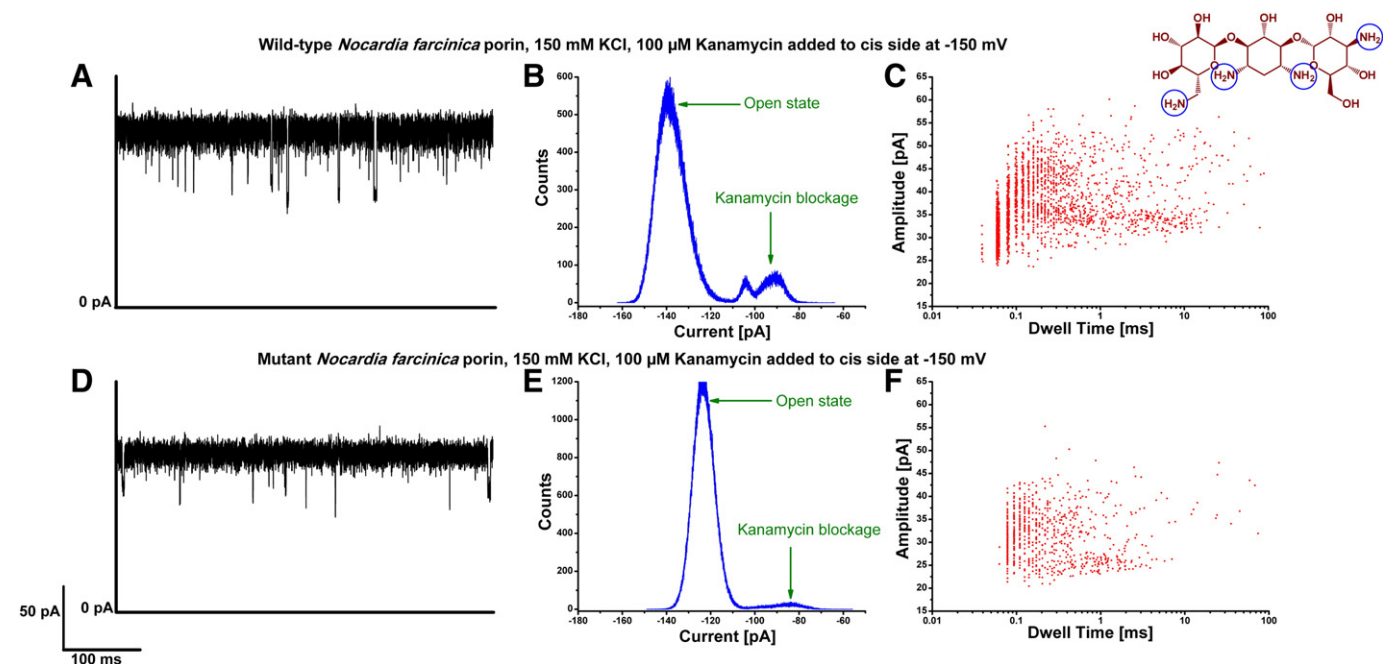
Fig. 4. Interaction of kanamycin (chemical structure top right) with WT and mutant *N. farcinica* channel. (A) 100 μM kanamycin was added to the *cis*-side of the WT channel at an applied voltage of −150 mV. (B) Event histogram of kanamycin with the WT channel. (C) Amplitude-dwell time scatter plot of kanamycin events with the WT channel. (D) 100 μM kanamycin was added to the *cis*-side of the mutant channel at an applied voltage of −150 mV. (E) Event histogram of kanamycin with the mutant channel. (F) Amplitude-dwell time scatter plot of kanamycin events with the mutant channel. Experimental conditions were 150 mM KCl and 10 mM HEPES, pH 7.4.

results of channel blocking cannot be converted directly into translocation, since binding does not always imply translocation. For uncharged solutes, liposome swelling assays can be performed to distinguish if the molecule is indeed permeating through the channel, which is not feasible with charged molecules. For charged molecules, as in our case; we performed a voltage dependent analysis of kinetic off-rate to distinguish binding from translocation as previously reported to distinguish binding from translocation for short peptides [25,49].

Increasing voltages tended to increase the residence time of the kanamycin, whereas the residence time of amikacin decreased as shown in Fig. 5. As mentioned earlier, the average residence time of amikacin was 200 μs at −150 mV. An increase of the external voltage up to −200 mV resulted in an overall decrease of the channel conductance instead of observing single ion fluctuation events. This may be due to significantly fast permeation events. However, in the case of kanamycin, increasing the voltage increased the residence time of the antibiotic. At high voltages (>200 mV), we observed an apparent strong binding which suggested that the molecule is held inside the pore in such a way that the pore remained in its closed state (figure not shown). The abovementioned observation suggested that amikacin is permeating through the channel; whereas kanamycin is not able to penetrate the channel, supporting the susceptibility of N. farcinica for amikacin over kanamycin. The impermeability of kanamycin through the homologous MspA porin using MIC assays has also been reported earlier, which correlated with our results [20,50]. However, in vivo biological systems can be far more complicated and there could be other probable reasons for such discrepancy in susceptibility. Even though we cannot directly compare the in vitro results obtained using single channel electrophysiology to the in vivo data, here we present an important factor of antibiotic permeability (by distinguishing binding and translocation) through the porins that could alter the effectiveness of antibiotics.

Apart from the positively charged antibiotics, we also investigated various chemically and structurally/clinically relevant antibiotics such as fluoroquinolones, penicillins, carbapenems and sulfonamides [47, 48,51]. Most of these antibiotics are either zwitterionic or negatively charged and thus no interaction was observed with the highly negatively charged amino acids inside the pore lumen of the N. farcinica porin. Surprisingly, addition of the carbapenem antibiotic ertapenem showed ion current fluctuation with the single N. farcinica channel (Fig. 6A). Ertapenem, which is a negatively charged antibiotic, is prone to repulsive forces from the negatively charged interior of the channel. This implies that the interaction observed with the antibiotic and the pore could be due to non-ionic interactions. To confirm the role of electrostatic interaction between antibiotic and pore, we performed our experiments in both 1 M and 150 mM KCl solution and found that the interaction was similar (i.e. residence time of ertapenem inside the pore was ~200 μs) in both cases, supporting the assumption of non-ionic interaction (Supplementary Fig. 2). By looking at the structure of ertapenem, we noted that it consists of multiple aromatic rings; which, as we hypothesize, may interact with the hydrophobic amino acids inside the pore lumen.

Ion current blockages were observed for both the WT and mutant porins in the presence of ertapenem and an increased number of events were observed with increased ertapenem concentration as shown in Fig. 6C. The event frequency of ertapenem was similar in both WT and mutant when the antibiotic was added to the cis (extracellular) side; however a significant difference was observed for the event frequency when the antibiotic was added to the trans (periplasmic) side as shown in Fig. 6A and B. The mutant pore exhibited a higher number of ertapenem interactions in comparison to WT pore. During the entry of ertapenem into the channel from the periplasmic side, it faces strong repulsive forces from the surrounding negatively charged amino acids. In contrast, when the negatively charged residues in the periplasmic space were neutralized, the lower repulsive forces in this case seemed to enhance the on-rate of ertapenem with the channel. Previous reports on MspA porin from M. smegmatis that has point negative charges in the mouth of the channel reported a 10-fold lower permeability of mono-anionic beta-lactams compared to zwitterionic cephaloridine [52]. The presence of a negatively charged residue in the mouth of the channel affected the permeation of a negatively charged molecule, which correlates well with our observations.
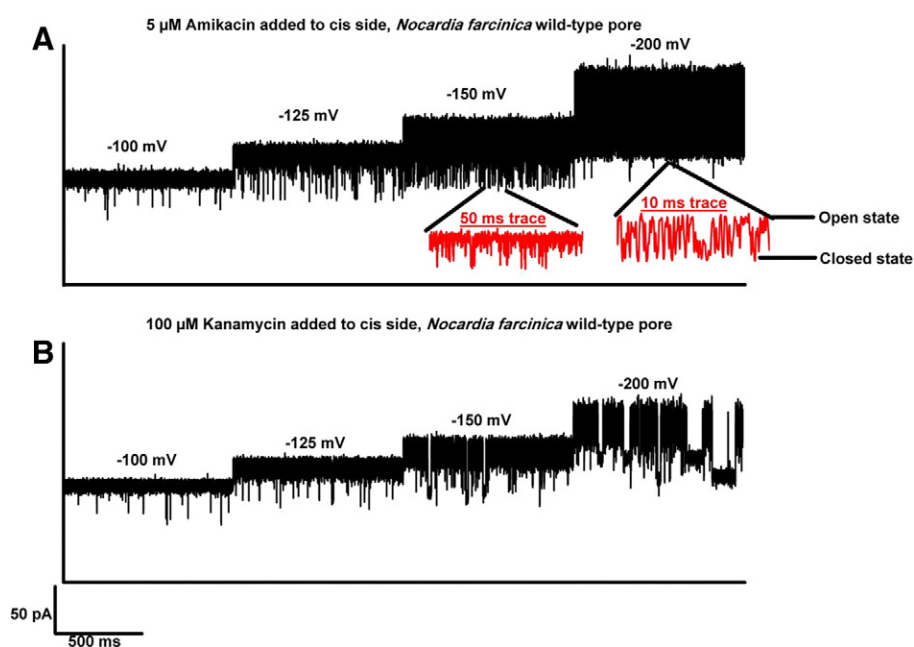

Fig. 5. Distinguishing binding from translocation: Voltage scan of ion current fluctuation of antibiotics through the N. farcinica channel. (A) Increasing the application of external voltage with addition of amikacin to the cis-side of the channel. At higher voltages, the residence time of the channel decreased to the limit of the instrument and could not be resolved. (B) Increasing the application of external voltage with addition of kanamycin to the cis-side of the channel. With increasing voltage, the binding of kanamycin with the channel increases. Experimental conditions were 150 mM KCl and 10 mM HEPES, pH 7.4.
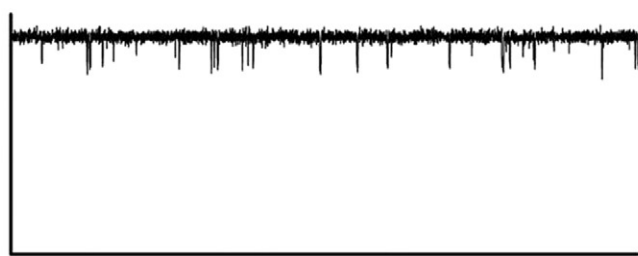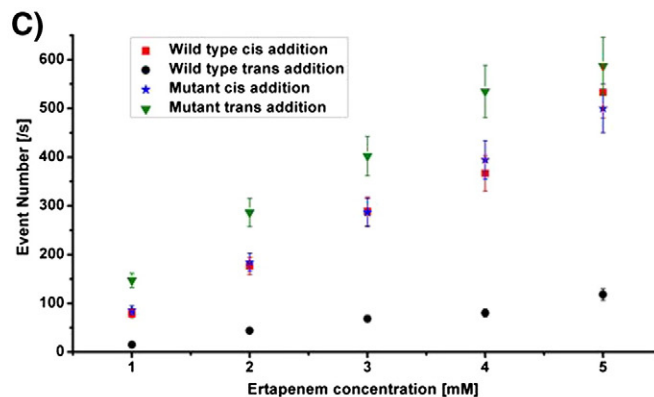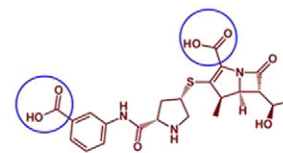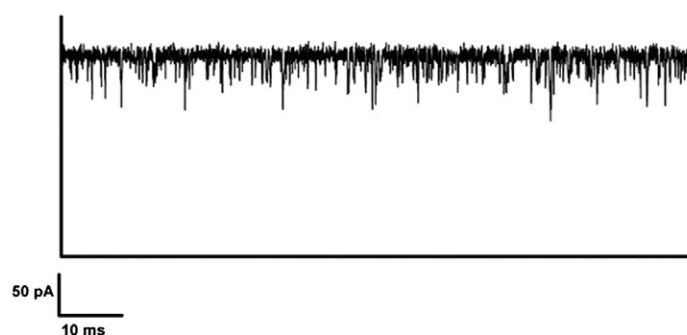
Fig. 6. Interaction of ertapenem (chemical structure top right) with WT and mutant *N. farcinica* channel. Ion current trace obtained when ertapenem was added to the *trans*-side of the channel at an applied voltage of −100 mV for (A) WT porin and (B) mutant porin. (C) Number of event plotted against concentration of ertapenem added to both WT and mutant porin in both extracellular (*cis*) and periplasmic (*trans*) side of the channel. Experimental conditions were 1 M KCl and 10 mM HEPES, pH 7.4.

4. Conclusion

Mycolata have evolved a complex cell wall, comprising peptidoglycan–arabinogalactan polymer covalently bound to mycolic acids of considerable size (up to 90 carbon atoms), a variety of extractable lipids, and pore-forming proteins [11,53,54]. Since the role of the outer-membrane is indispensable in the mycobacterial resistance to antibiotics, it is tempting to reconstitute the porins in a mycolic acid containing bilayer to retain their physiological environment. Reconstitution of MspA from *M. smegmatis* in mycolic acid membrane has been studied before [55], however, our effort to form and reconstitute the *N. farcinica* porin in the mycolic acid containing membrane was unsuccessful. Nonetheless, we were able to successfully reconstitute the protein in phospholipid bilayers and liposomes to perform single channel measurements and liposome swelling assays.

Current investigation represents one of the first detailed studies on solute and antibiotic permeation through porin from bacterium belonging to mycolata. We have confirmed the channel functionality of *N. farcinica* porin using liposome swelling assays and permeation of nutrient molecules including different sized sugars and amino acids. In addition to different solutes, the interaction of clinically relevant antibiotics such as amikacin, kanamycin and ertapenem was also studied at the single molecule level. Well defined ion current fluctuations were observed in the presence of these antibiotics that interact with the pore. We were also able to distinguish between translocation and binding for amikacin and kanamycin using voltage dependent analysis. Our results indicated that kanamycin was unable to translocate while amikacin was able to translocate through the channel. Furthermore, we elucidated the effect of various charged amino acids present inside the channel on the permeation of charged antibiotics and uncharged/zwitterionic molecules.

Appendix A. Supplementary data

Supplementary data to this article can be found online at http://dx.doi.org/10.1016/j.bbamem.2014.11.020.

References

[1] H. Nikaido, Prevention of drug access to bacterial targets: permeability barriers and active efflux, Science 264 (1994) 382–388, http://dx.doi.org/10.1126/science.8153625.
[2] H. Nikaido, Molecular basis of bacterial outer membrane permeability revisited, Microbiol. Mol. Biol. Rev. 67 (2003) 593–656.
[3] A.H. Delcour, Outer membrane permeability and antibiotic resistance, Biochim. Biophys. Acta 1794 (2009) 808–816, http://dx.doi.org/10.1016/j.bbapap.2008.11.005.
[4] J.-M. Pagès, C.E. James, M. Winterhalter, The porin and the permeating antibiotic: a selective diffusion barrier in Gram-negative bacteria, Nat. Rev. Microbiol. 6 (2008) 893–903, http://dx.doi.org/10.1038/nrmicro1994.
[5] K. Poole, Outer membranes and efflux: the path to multidrug resistance in Gram-negative bacteria, Curr. Pharm. Biotechnol. 3 (2002) 77–98.
[6] H. Nikaido, Outer membrane barrier as a mechanism of antimicrobial resistance, Antimicrob. Agents Chemother. 33 (1989) 1831–1836, http://dx.doi.org/10.1128/AAC.33.11.1831.
[7] T.J. Silhavy, D. Kahne, S. Walker, The bacterial cell envelope, Cold Spring Harb. Perspect. Biol. 2 (2010) a000414, http://dx.doi.org/10.1101/cshperspect.a000414.
[8] V. Jarlier, H. Nikaido, Mycobacterial cell wall: structure and role in natural resistance to antibiotics, FEMS Microbiol. Lett. 123 (1994) 11–18.
[9] V. Jarlier, L. Gutmann, H. Nikaido, Interplay of cell wall barrier and beta-lactamase activity determines high resistance to beta-lactam antibiotics in *Mycobacterium chelonae*, Antimicrob. Agents Chemother. 35 (1991) 1937–1939, http://dx.doi.org/10.1128/AAC.35.9.1937.

[10] D.E. Minnikin, S.M. Minnikin, M. Goodfellow, J.L. Stanford, The mycolic acids of *Mycobacterium chelonei*, J. Gen. Microbiol. 128 (1982) 817–822, http://dx.doi.org/10.1099/00221287-131-9-2237.

[11] D.E. Minnikin, Chemical principles in the organization of lipid components in the mycobacterial cell envelope, Res. Microbiol. 142 (1991) 423–427, http://dx.doi.org/10.1016/0923-2508(91)90114-P.

[12] P.J. Brennan, H. Nikaido, The envelope of mycobacteria, Annu. Rev. Biochem. 64 (1995) 29–63, http://dx.doi.org/10.1146/annurev.biochem.64.1.29.

[13] D.E. Minnikin, S.M. Minnikin, J.H. Parlett, M. Goodfellow, M. Magnusson, Mycolic acid patterns of some species of *Mycobacterium*, Arch. Microbiol. 139 (1984) 225–231, http://dx.doi.org/10.1007/BF00402005.

[14] J. Trias, V. Jarlier, R. Benz, Porins in the cell wall of mycobacteria, Science 258 (1992) 1479–1481, http://dx.doi.org/10.1126/science.1279810.

[15] M. Niederweis, Mycobacterial porins — new channel proteins in unique outer membranes, Mol. Microbiol. 49 (2003) 1167–1177, http://dx.doi.org/10.1046/j.1365-2958.2003.03662.x.

[16] T. Lichtinger, A. Burkovski, M. Niederweis, R. Krámer, R. Benz, Biochemical and biophysical characterization of the cell wall porin of *Corynebacterium glutamicum*: the channel is formed by a low molecular mass polypeptide, Biochemistry 37 (1998) 15024–15032, http://dx.doi.org/10.1021/bi980961e.

[17] J. Trias, R. Benz, Permeability of the cell wall of *Mycobacterium smegmatis*, Mol. Microbiol. 14 (1994) 283–290, http://dx.doi.org/10.1111/j.1365-2958.1994.tb01289.x.

[18] F.G. Riess, T. Lichtinger, R. Cseh, A.F. Yassin, K.P. Schaal, R. Benz, The cell wall porin of *Nocardia farcinica*: biochemical identification of the channel-forming protein and biophysical characterization of the channel properties, Mol. Microbiol. 29 (1998) 139–150, http://dx.doi.org/10.1046/j.1365-2958.1998.00914.x.

[19] C.M. Jones, M. Niederweis, Role of porins in iron uptake by *Mycobacterium smegmatis*, J. Bacteriol. 192 (2010) 6411–6417.

[20] O. Danilchanka, M. Pavlenok, M. Niederweis, Role of porins for uptake of antibiotics by *Mycobacterium smegmatis*, Antimicrob. Agents Chemother. 52 (2008) 3127–3134, http://dx.doi.org/10.1128/AAC.00239-08.

[21] R. Benz, Bacterial Cell Wall, Elsevier, 1994., http://dx.doi.org/10.1016/S0167-7306(08)60422-6.

[22] World Health Organization, Global Tuberculosis Control 2011, , 2011, ISBN 978 92 9061 522 4.

[23] B.R. Bloom, Vaccines for the Third World, Nature 342 (1989) 115–120.

[24] C. Kläckta, P. Knörzer, F. Riess, R. Benz, Hetero-oligomeric cell wall channels (porins) of *Nocardia farcinica*, Biochim. Biophys. Acta Biomembr. 1808 (2011) 1601–1610, http://dx.doi.org/10.1016/j.bbamem.2010.11.011.

[25] P.R. Singh, I. Bárcena-Uribarri, N. Modi, U. Kleinekathöfer, R. Benz, M. Winterhalter, et al., Pulling peptides across nanochannels: resolving peptide binding and translocation through the hetero-oligomeric channel from *Nocardia farcinica*, ACS Nano 6 (2012) 10699–10707, http://dx.doi.org/10.1021/nn303900y.

[26] H. Nikaido, E.Y. Rosenberg, Porin channels in *Escherichia coli*: studies with liposomes reconstituted from purified proteins, J. Bacteriol. 153 (1983) 241–252.

[27] F. Yoshimura, H. Nikaido, Diffusion of beta-lactam antibiotics through the porin channels of *Escherichia coli* K-12, Antimicrob. Agents Chemother. 27 (1985) 84–92.

[28] M. Montal, P. Mueller, Formation of bimolecular membranes from lipid monolayers and a study of their electrical properties, Proc. Natl. Acad. Sci. U. S. A. 69 (1972) 3561–3566, http://dx.doi.org/10.1073/pnas.69.12.3561.

[29] E.M. Nestorovich, C. Danelon, M. Winterhalter, S.M. Bezrukov, Designed to penetrate: time-resolved interaction of single antibiotic molecules with bacterial pores, Proc. Natl. Acad. Sci. U. S. A. 99 (2002) 9789–9794, http://dx.doi.org/10.1073/pnas.152206799.

[30] A.L. Hodgkin, B. Katz, The effect of sodium ions on the electrical activity of the giant axon of the squid, J. Physiol. 108 (1949) 37–77.

[31] C. Danelon, A. Suenaga, M. Winterhalter, I. Yamato, Molecular origin of the cation selectivity in OmpF porin: single channel conductances vs. free energy calculation, Biophys. Chem. 104 (2003) 591–603, http://dx.doi.org/10.1016/S0301-4622(03)00062-0.

[32] J. Trias, R. Benz, Characterization of the channel formed by the mycobacterial porin in lipid bilayer membranes. Demonstration of voltage gating and of negative point charges at the channel mouth, J. Biol. Chem. 268 (1993) 6234–6240.

[33] H. Bajaj, Q.T. Tran, K.R. Mahendran, C. Nasrallah, J.P. Colletier, A. Davin-Regli, et al., Antibiotic uptake through membrane channels: role of *Providencia stuartii* omppst1 porin in carbapenem resistance, Biochemistry 51 (2012) 10244–10249, http://dx.doi.org/10.1021/bi301398j.

[34] K.R. Mahendran, M. Kreir, H. Weingart, N. Fertig, M. Winterhalter, Permeation of antibiotics through *Escherichia coli* OmpF and OmpC porins: screening for influx on a single-molecule level, J. Biomol. Screen. 15 (2010) 302–307, http://dx.doi.org/10.1177/1087057109357791.

[35] B.K. Ziervogel, B. Roux, The binding of antibiotics in OmpF porin, Structure 21 (2013) 76–87, http://dx.doi.org/10.1016/j.str.2012.10.014.

[36] P.R. Singh, M. Ceccarelli, M. Lovelle, M. Winterhalter, K.R. Mahendran, Antibiotic permeation across the OmpF channel: modulation of the affinity site in the presence of magnesium, J. Phys. Chem. B 116 (2012) 4433–4438, http://dx.doi.org/10.1021/jp2123136.

[37] D. Fologea, J. Uplinger, B. Thomas, D.S. McNabb, J. Li, Slowing DNA translocation in a solid-state nanopore, Nano Lett. 5 (2005) 1734–1737, http://dx.doi.org/10.1021/nl051063o.

[38] K.R. Mahendran, M. Romero-Ruiz, A. Schlösinger, M. Winterhalter, S. Nussberger, Protein translocation through Tom40: kinetics of peptide release, Biophys. J. 102 (2012) 39–47, http://dx.doi.org/10.1016/j.bpj.2011.11.4003.

[39] R.S. Kane, P.T. Glink, R.G. Chapman, J.C. McDonald, P.K. Jensen, H. Gao, et al., Basicity of the amino groups of the aminoglycoside amikacin using capillary electrophoresis and coupled CE–MS–MS techniques, Anal. Chem. 73 (2001) 4028–4036, http://dx.doi.org/10.1021/ac010173m.

[40] C. Danelon, E.M. Nestorovich, M. Winterhalter, M. Ceccarelli, S.M. Bezrukov, Interaction of zwitterionic penicillins with the OmpF channel facilitates their translocation, Biophys. J. 90 (2006) 1617–1627, http://dx.doi.org/10.1529/biophysj.105.075192.

[41] K.R. Mahendran, E. Hajjar, T. MacH, M. Lovelle, A. Kumar, I. Sousa, et al., Molecular basis of enrofloxacin translocation through OmpF, an outer membrane channel of *Escherichia coli* — when binding does not imply translocation, J. Phys. Chem. B 114 (2010) 5170–5179, http://dx.doi.org/10.1021/jp911485k.

[42] E. Hajjar, K.R. Mahendran, A. Kumar, A. Bessonov, M. Petrescu, H. Weingart, et al., Bridging timescales and length scales: from macroscopic flux to the molecular mechanism of antibiotic diffusion through porins, Biophys. J. 98 (2010) 569–575, http://dx.doi.org/10.1016/j.bpj.2009.10.045.

[43] S. Vidal, J. Bredin, J.M. Pagès, J. Barbe, β-Lactam screening by specific residues of the OmpF eyelet, J. Med. Chem. 48 (2005) 1395–1400, http://dx.doi.org/10.1021/jm049652e.

[44] S.A. Benson, J.L. Occi, B.A. Sampson, Mutations that alter the pore function of the OmpF porin of *Escherichia coli* K12, J. Mol. Biol. 203 (1988) 961–970, http://dx.doi.org/10.1016/0022-2836(88)90121-0.

[45] R. Misra, S.A. Benson, Isolation and characterization of OmpC porin mutants with altered pore properties, J. Bacteriol. 170 (1988) 528–533.

[46] A. Thiolas, C. Bornet, A. Davin-Régli, J.M. Pagès, C. Bollet, Resistance to imipenem, cefepime, and cefpirome associated with mutation in Omp36 osmoporin of *Enterobacter aerogenes*, Biochem. Biophys. Res. Commun. 317 (2004) 851–856, http://dx.doi.org/10.1016/j.bbrc.2004.03.130.

[47] J. Ishikawa, A. Yamashita, Y. Mikami, Y. Hoshino, H. Kurita, K. Hotta, et al., The complete genomic sequence of *Nocardia farcinica* IFM 10152, Proc. Natl. Acad. Sci. U. S. A. 101 (2004) 14925–14930, http://dx.doi.org/10.1073/pnas.0406410101.

[48] E. Cercenado, M. Marín, M. Sánchez-Martínez, O. Cuevas, J. Martínez-Alarcón, E. Bouza, In vitro activities of tigecycline and eight other antimicrobials against different *Nocardia* species identified by molecular methods, Antimicrob. Agents Chemother. 51 (2007) 1102–1104, http://dx.doi.org/10.1128/AAC.01102-06.

[49] L. Movileanu, J.P. Schmittschmitt, J.M. Scholtz, H. Bayley, Interactions of peptides with a protein pore, Biophys. J. 89 (2005) 1030–1045, http://dx.doi.org/10.1529/biophysj.104.057406.

[50] J. Stephan, C. Mailaender, G. Etienne, M. Daffé, M. Niederweis, Multidrug resistance of a porin deletion mutant of *Mycobacterium smegmatis*, Antimicrob. Agents Chemother. 48 (2004) 4163–4170, http://dx.doi.org/10.1128/AAC.48.11.4163-4170.2004.

[51] O.H. Torres, P. Domingo, R. Pericas, P. Boiron, J.A. Montiel, G. Vázquez, Infection Caused by *Nocardia farcinica*: Case Report and Review, 2000., http://dx.doi.org/10.1007/s100960050460.

[52] V. Jarlier, H. Nikaido, Permeability barrier to hydrophilic solutes in *Mycobacterium chelonei*, J. Bacteriol. 172 (1990) 1418–1423.

[53] H. Gebhardt, X. Meniche, M. Tropis, R. Krämer, M. Daffé, S. Morbach, The key role of the mycolic acid content in the functionality of the cell wall permeability barrier in *Corynebacterineae*, Microbiology 153 (2007) 1424–1434, http://dx.doi.org/10.1099/mic.0.2006/003541-0.

[54] C.E. Barry, R.E. Lee, K. Mdluli, A.E. Sampson, B.G. Schroeder, R.A. Slayden, et al., Mycolic acids: structure, biosynthesis and physiological functions, Prog. Lipid Res. 37 (1998) 143–179, http://dx.doi.org/10.1016/S0163-7827(98)00008-3.

[55] K.W. Langford, B. Penkov, I.M. Derrington, J.H. Gundlach, Unsupported planar lipid membranes formed from mycolic acids of *Mycobacterium tuberculosis*, J. Lipid Res. 52 (2011) 272–277, http://dx.doi.org/10.1194/jlr.M012013.
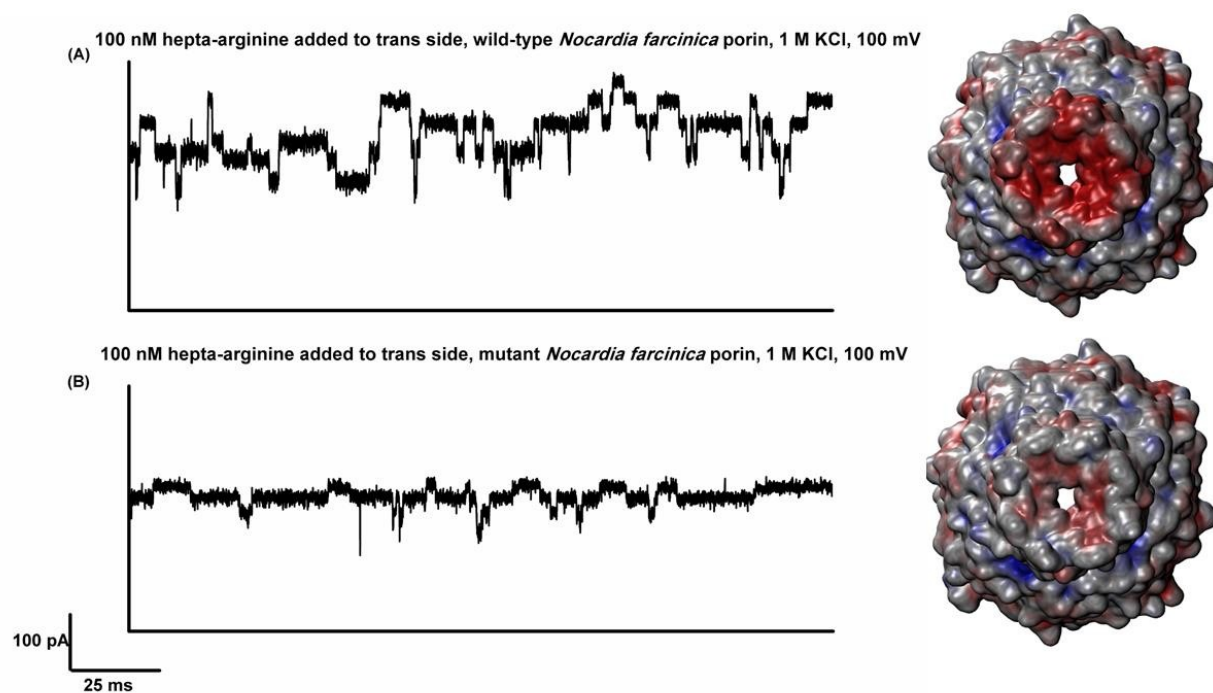
Supplementary Table 1: Primers used in this study to generate mutants, pARAJS2_*nfpA*/*nfpB* was used as template. (The bases to be mutated are highlighted in red with small letters)

Primers	Sequence 5' → 3'
FP *nfpA* D141N D142N	GC CAG GTC AGC ATC GGT aACaACGCC ATC TCG GCC GGC C
RP *nfpA* D141N D142N	G GCC GGC CGA GAT GGC GTtGTtACC GAT GCT GAC CTG GC
FP *nfpB* E123Q D127N	G GGC GGC GTG cAAGGC TCG GCC aAtTGG AGC GGT GAC
FP *nfpB* E140Q and E144Q	GGC GTG GGC GCC cAGTCC GGC GGCcAGCTG ACG CTC GG
RP *nfpB*	A GCC GAG GCT GAA CGG CTG GCC CCA CAG GG
FP pARAJS2	GCA CGG CGT CAC ACT TTG C
RP pARAJS2	GAC CCG TTT AGA CCG CCC

Supplementary Table 2: Amikacin and kanamycin binding kinetics were measured at 150 mM KCl, pH 7.4 at an application of -150 mV voltage. Ertapenem binding kinetics was measured at 1 M KCl, pH 7.4 at -100 mV.

	Wildtype porin			Mutant porin		
	K_{on}^{cis} [M^{-1}s^{-1} *10^4]	K_{on}^{trans} [M^{-1}s^{-1} *10^4]	K_{off} [s^{-1} *10^3]	K_{on}^{cis} [M^{-1}s^{-1} *10^4]	K_{on}^{trans} [M^{-1}s^{-1} *10^4]	K_{off} [s^{-1} *10^3]
Amikacin	2300 ± 200	NA	5 ± 1	750 ± 50	NA	10 ± 1
Kanamycin	27.5 ± 2	NA	NA	17 ± 2	NA	NA
Ertapenem	10.1 ± 1	2.4 ± 0.5	5.5 ± 1	10 ± 1	12 ± 1	5.5 ± 1

NA= Not Applicable

Supplementary Figure 1: Functional activity of the hepta-arginine with the (A) WT and (B) mutant *N. farcinica* channel. The structures on the right panel show the electro-potential surface of both the channels visualized from the periplasmic (*trans*) side.

Wild-type *Nocardia farcinica* porin, 1 mM Ertapenem added to cis side, 150 mM KCl, -100 mV

25 pA

10 ms
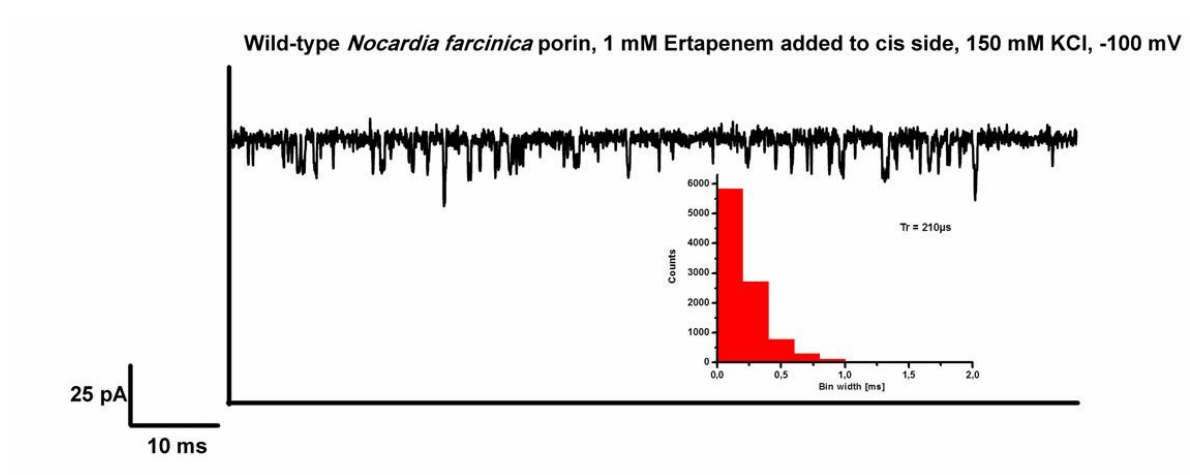
Supplementary Figure 2: Elucidating the electrostatic interaction of ertapenem with the *N. farcinica* cell wall channel. Ion current fluctuation were observed at 150 mM KCl, 10 mM MES, pH 7.4.

Part 4
Conclusion and future outlook

4.1 Conclusion

In this thesis we study the molecular transport of antibiotics across bacterial porins. Notably, we studied two aspects of antibiotic permeation.

In the first part we mainly investigated the **role of porins in antibiotic resistance.**

We conclude that an altered permeation of antibiotics through porins can contribute to decreased susceptibility. We employ a multidisciplinary approach to understand the involvement of porin in uptake of antibiotics (chapter 1 and chapter 2). We show that imipenem and meropenem although being structurally very similar have drastically different permeation rates through OmpPst1 channel. This in fact contributes to the increased MIC value of the antibiotic against the bacteria. Importantly, we also studied OmpC porin mutants from clinics. Permeation of carbapenem antibiotics is modulated through sequential mutants of OmpC which contributes to progressively decreased susceptibility observed in clinical strains. Further we are able to conclude that a single mutation in channel is able to modify the uptake of antibiotics and this might be a "strategy" of bacteria to gain time to accumulate more resistance.

In the second part, we focused on **translocation of antibiotics across bacterial porins and to fine tune various external parameters for efficient influx.** We measure the transport of antibiotics across bacterial porins using single channel electrophysiology and fluorescence based detection in vesicles. We report a microfluidic based technique to measure the transport of a fluoroquinolone through OmpF reconstituted in liposomes, using the auto fluorescence of antibiotic in the UV. We employ single channel electrophysiology to determine the kinetic parameters of antibiotics like fluoroquinolones and β- lactams with porins from *E. coli*. Different facets like voltage dependent translocation of antibiotic through OmpF and OmpC porins is reported. Varying the pH changes the charge state of norfloxacin antibiotic which drastically modulates the interaction with OmpF pore. One particular bottleneck for this type of analysis is the limited time resolution and cases of irresolvable antibiotic events with the channel are observed. We report a modified power spectrum analysis method taking into consideration the sampling and filter correction factor. A comparison between three platforms to reveal the fast events observed with antibiotics showed that all the three bilayer systems are comparable in terms of noise and kinetic rates. In addition to Gram-negative porins, we characterize the transport of antibiotics and solute through *N. farcinica* porin.

4.2 Future outlook

Chemical modification of antibiotic

Previously we have revealed the rate limiting interactions of antibiotics by mutating specific residues in the channel[1,2] or studying the effect of naturally occurring mutations on permeation of antibiotics (in this study; P2.2.1). A relatively unexplored aspect in this regard is to chemically modify existing antibiotics and measure the kinetic rate in single channel. As a general feature observed for β-lactam/ fluoroquinolones interaction with OmpF/C porins, an enhanced effect at negative applied voltage is seen (part P3.3.2). That is higher interaction of antibiotic is observed; either at negative transmembrane potential present on the opposite side of the antibiotic addition in the system or positive potential applied when the antibiotic is added on same side as applied voltage. As hypothesized in the part P3.3.2 this effect might be due to orientation of antibiotic under an applied electric field, which favors positive group entering the channel. In this context chemical modification/protection of the positive (amino) functional group might substantiate the assumption. For example in case of imipenem, the positively charged amino group can be modified to an uncharged charged group to specifically probe the enthalpy/electrostatic contribution by keeping the overall size of the antibiotic same *(Figure 1a)*. Further, thienamycin (a "first" carbapenem)[3] which is structurally quite similar to imipenem; as shown in *Figure 1b* can be tested in electrophysiology and the amino group can be further modified to give an uncharged form.
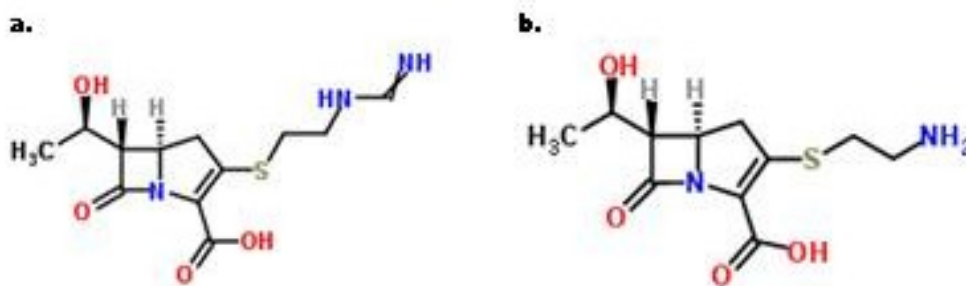

Figure 1: Chemical structure of antibiotics a) imipenem b) thienamycin. Structure obtained from ChemSpider.

In this case we could elucidate the entropic contribution since the size of the antibiotic is slightly changed as compared to imipenem. Similarly, the carboxyl group of imipenem can be modified to reveal the specific interactions caused by the formation of hydrogen bonds of carboxyl

oxygen's with the porin. A similar strategy can be adopted for other antibiotics molecules like ceftobiprole (a fifth generation cephalosporin) which showed exceptional kinetic rates in electrophysiology (P3.3.2). This together with molecular dynamic simulations might improve our understanding on the underlying effects observed in single channel experiments and in long term also help us for rationale drug designing[4].

Effect of donnan potentials on flux

Voltage dependent interaction of antibiotic has been reported in the current thesis. We observed that increasing the voltage exponentially increased the association rate and the dissociation rate of antibiotic-norfloxacin suggesting enhanced translocation under an applied potential. This opens a new question: "if there is any effect of transmembrane potentials in transport across bacterial cells?" Previous studies have shown that so called "donnan" or transmembrane potentials exist across the OM due to the presence of anchored, anionic membrane-derived oligosaccharides (MDOs) in the periplasm[5,6] which varies from 4-117 mV by changing external conditions[6]. However, there was no effect of such potentials on transport of zwitterionic compounds like cephaloridine[6]. Since, in electrophysiology study we observe a strong correlation of the dipole of antibiotic (in case of norfloxacin) and the voltage dependent effect (P3.3.2). It might be interesting to measure the flux in presence of such voltage in cells or cell mimicking environments. Also, previous studies were able to create a donnan potential by encapsulating charged polymers or proteins into liposomes [7]. In this context a future task will be to induce such artificial voltages in giant vesicles and to measure the transport in the fluorescence based detection reported in this thesis (P3.3.1).

References

(1)   Mahendran, K. R.; Hajjar, E.; Mach, T.; Lovelle, M.; Kumar, A.; Sousa, I.; Spiga, E.; Weingart, H.; Gameiro, P.; Winterhalter, M.; Ceccarelli, M. *J. Phys. Chem. B* **2010**, *114*, 5170.

(2)   Hajjar, E.; Mahendran, K. R.; Kumar, A.; Bessonov, A.; Petrescu, M.; Weingart, H.; Ruggerone, P.; Winterhalter, M.; Ceccarelli, M. *Biophys. J.* **2010**, *98*, 569.

(3)   Papp-Wallace, K. M.; Endimiani, A.; Taracila, M. A.; Bonomo, R. A. *Antimicrob. Agents Chemother.* **2011**, *55*, 4943.

(4)   Stavenger, R. A.; Winterhalter, M. *Sci. Transl. Med.* **2014**, *6*, 228ed7.

(5)   Kennedy, E. P. *Proc. Natl. Acad. Sci. U. S. A.* **1982**, *79*, 1092.

(6)   Sen, K.; Hellman, J.; Nikaido, H. *J. Biol. Chem.* **1988**, *263*, 1182.

(7)   Lindemann, M.; Winterhalter, M. *IEE Proc. Nanobiotechnol.* **2006**, *153*, 107.

Part 5

Annex

Antibiotic Uptake through Membrane Channels: Role of *Providencia stuartii* OmpPst1 Porin in Carbapenem Resistance

Harsha Bajaj,[†] Que-Tien Tran,[†,‡] Kozhinjampara R. Mahendran,[†] Chady Nasrallah,[§] Jacques-Phillippe Colletier,[§] Anne Davin-Regli,[‡] Jean-Michel Bolla,[‡] Jean-Marie Pagès,[‡] and Mathias Winterhalter*,[†]

[†]School of Engineering and Science, Jacobs University Bremen, Bremen, Germany
[‡]UMR-MD1, Aix-Marseille Université, IRBA, Marseille, France
[§]Institut de Biologie Structurale UMR5075, CEA-CNRS-UJF, Grenoble, France

S *Supporting Information*

ABSTRACT: The role of major porin OmpPst1 of *Providencia stuartii* in antibiotic susceptibility for two carbapenems is investigated by combining high-resolution conductance measurements, liposome swelling, and microbiological assays. Reconstitution of a single OmpPst1 into a planar lipid bilayer and measuring the ion current, in the presence of imipenem, revealed a concentration-dependent decrease in conductance, whereas meropenem produced well-resolved short ion current blockages. Liposome swelling assays suggested a small flux of imipenem in contrast to a rapid permeation of meropenem. The lower antibiotic susceptibility of *P. stuartii* to imipenem compared to meropenem correlated well with the decreased level of permeation of the former through the OmpPst1 channel.
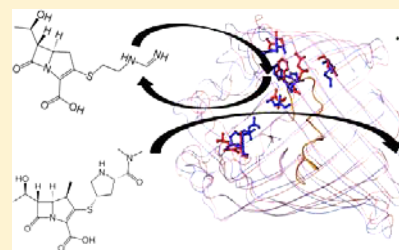
Gram-negative bacteria have a complex cell envelope comprising an outer membrane and an inner membrane that delimit the periplasm. The outer membrane contains various protein channels, called porins, involved in the influx of hydrophilic compounds, including several classes of antibiotics.[1−3] A major requirement for effective antibacterial activity is the rapid delivery to the target site. The occurrence of bacterial resistance requires that we understand the molecular mechanisms. Altered porin permeability might be the limiting factor for intracellular target achievement of hydrophilic antibiotics such as β-lactams.[4−8]

For example, *Providencia stuartii*, belonging to the Proteae in the Enterobacteriaceae family, is one of the most pathogenic bacteria in clinics.[9,10] It causes hospital-acquired infections and is usually found in urinary tract of patients undergoing long-term indwelling catheterization. *P. stuartii* strains show high levels of resistance to a majority of antibiotic classes but were found to remain susceptible to most of the carbapenems.[11] However, carbapenem resistance has occurred in clinical isolates and is frequently related to the alteration of porins, although sometimes in association with an enzymatic mechanism, e.g., carbapenemase.[12−15] Our previous study revealed two major porins in *P. stuartii*: OmpPst1 and OmpPst2. OmpPst1 is known to be involved in the passive diffusion of β-lactams.[16] Ertapenem, a carbapenem molecule, revealed strong antibiotic−channel interaction compared to that of cephalosporins.[16] In the following, we focus on the permeation of two clinically relevant and chemically divergent antibiotics, imipenem and meropenem, through OmpPst1 (Figures 1A and 2A). An appropriate method is their reconstitution into a planar lipid bilayer with subsequent recording of the ion current. As previously shown, the penetration of antibiotic molecules into the channel and subsequent interaction of the drug with the channel may interrupt the ion current.[17] The analysis of ion current fluctuation allows us to obtain permeation rates as previously shown for sugars and ampicillin.[17,18] However, there are limitations of this technique. In particular, because of finite time resolution, the signal of very fast permeation is indistinguishable from no permeation. Thus, a combination of techniques is needed to reach a conclusion about antibiotic translocation.

Here, we first determined the antibiotic susceptibility of *P. stuartii* for two clinically used antibiotics, imipenem and meropenem, by measuring their MIC values.[16] We then reconstituted a single OmpPst1 into an artificial planar lipid bilayer and characterized time-resolved ion current fluctuations in the presence of antibiotics. Single-channel analysis of ion currents through a porin in the presence of antibiotics revealed effective binding constants and subsequently the transport parameters at a single-molecule level. To further confirm translocation events, we performed liposome swelling assays,[19,20] which allowed estimation of the flux of the two antibiotics through OmpPst1 channels.

10244

■ MATERIALS AND METHODS

All chemicals used were purchased from Applichem (Darmstadt, Germany), except *n*-octyl polyoxyethylene (octyl-POE) (Alexis, Läuflingen, Switzerland) and all lipids from Avanti Polar Lipids (Alabaster, AL). Imipenem and meropenem were purchased from Sequoia Research Products (Pangbourne, United Kingdom).

Antibiotic Susceptibility Tests. The MIC values were determined in triplicate by a standard 2-fold broth dilution method according to the CLSI guidelines as previously reported.[16] Approximately 10^6 cells were inoculated into 1 mL of MH broth for 18 h at 37 °C. The results were scored in micrograms per milliliter, and the susceptibility was classified according to the Antibiogram Committee of the French Society for Microbiology (http://www.sfm-microbiologie.org/). The bacterial strains were tested against different antibacterial drugs of different classes, among which imipenem (Tienam) and meropenem (Merrem) were obtained from Merck Sharp & Dohme and AztraZeneca (Paris, France), respectively.

Expression and Purification of *P. stuartii* Porins. Expression and extraction of *Providencia* porins were conducted as previously described with minor modifications.[16,21] Briefly, expression vector pGOmpPst1 harboring the *ompPst1* gene with the signal sequence was electroporated into *Escherichia coli* BL21(DE3) omp8.[16] Cells were grown in LB broth substituted with 100 μg/mL ampicillin and 30 μg/mL kanamycin. At the exponential phase, the cell culture was induced for 6 h with 0.4 mM IPTG. The cell suspension was harvested using Sorval centrifugation at 10000 rpm for 30 min at 4 °C. The cell pellet was then washed with 20 mM phosphate buffer (pH 7.4) and disrupted twice with a French press technique using an EmulsiFlex-C3 high-pressure homogenizer (Avestin Europe, Mannheim, Germany). The membrane pellet was collected by centrifugation at 22000 rpm for 1 h after a 2% sodium dodecyl sulfate stirring treatment at 60 °C. The membrane fraction was washed twice with 0.125% octyl polyoxyethylene (octyl-POE) in 20 mM phosphate buffer followed by ultracentrifugation at 40000 rpm at 4 °C for 1 h. OmpPst1 porin was extracted with 3% octyl-POE in 20 mM phosphate buffer followed by an ultracentrifugation step at 20 °C. The extracted porins were concentrated using Amicon Ultra-15 Centrifugal Filter Units (Millipore) with the molecular cutoff at 30K Da. The buffer was exchanged with 1% octyl-POE in a final porin dilution for bilayer measurements.

Conductance Measurements. Planar lipid bilayers were formed according to the monolayer technique of Montal and Mueller.[22] The bilayer is formed by two monolayers juxtaposed and extended across a hole that is 50−100 μm in diameter in a 25 μm thick polytetrafluoroethylene (PTFE) film. Prior to bilayer membrane formation, the aperture is prepainted with 1 μL of a 1% solution of *n*-hexadecane in *n*-hexane to make it lipophilic. After being dried for 10 min, both chambers are filled with buffer [throughout 1 M KCl and 20 mM MES (pH 6)], and a lipid bilayer is prepared by spreading 1 μL of a 5 mg/mL solution of 1,2-diphytanoyl-*sn*-glycero-3-phosphocholine in a solvent mixture of *n*-pentane in the aperture. Ag/AgCl electrodes are used to detect the ionic currents. The electrode on the *cis* side of the cell is grounded, whereas the other one on the *trans* side is connected to the headstage of an Axopatch 200B amplifier. Purified detergent-solubilized porins (1 ng/mL) are added to the *cis* side of the chamber and inserted into the bilayer membrane by applying a 150−200 mV voltage.

Electrical recordings were made through a pair of Ag/AgCl electrodes (World Precision Instruments, Sarasota, FL), attached to an Axon Instruments 200B amplifier with a capacitive headstage, digitized by an Axon Digidata 1440A digitizer, computer controlled by Clampex 10.0 (all by Axon Instruments, Foster City, CA). The data were filtered by an analogue low-pass four-pole Bessel filter at 10 kHz and digitally sampled at 50 kHz. Data analysis was conducted with Clampfit 10.0.
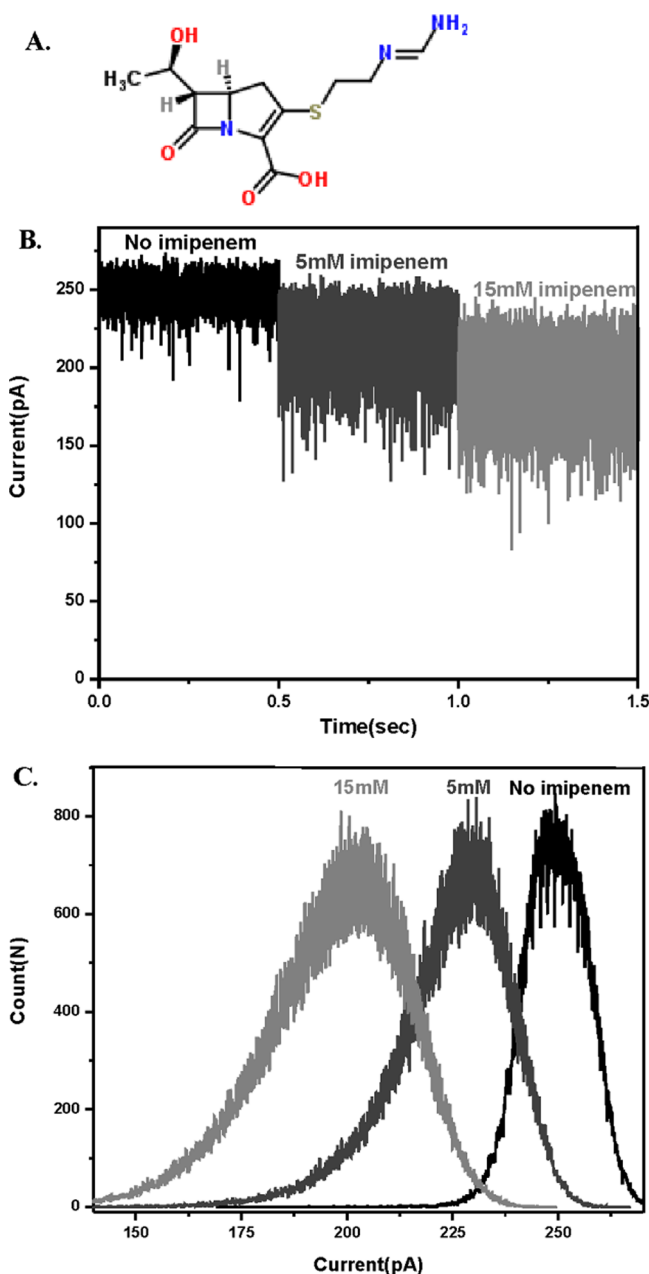
Liposome Swelling Assay. OmpPst1 porin (2 mg/mL) in 1% octyl-POE is reconstituted into liposomes as described by Nikaido and Rosenberg.[20] *E. coli* total lipid extract is used to form liposomes; 15% dextran (MW of 40000) is used to entrap the liposomes, and size is checked using a Nano-ZS ZEN3600 zetasizer (Malvern Instruments, Malvern, United Kingdom). Control liposomes are prepared in the same manner but without the addition of porin. The isotonic concentration is determined by diluting control and proteoliposomes made in 15% dextran in different concentrations of raffinose measured by an Osmomat 30 osmolarimeter (Gonotec, Berlin, Germany). The value obtained for the isotonic concentration of raffinose is used as an approximation to facilitate the adjustment of isotonic concentrations for different solutes. A liposome or proteoliposome solution (30 μL) is diluted into 630 μL of an isotonic test solution in phosphate buffer in a 1 mL cuvette and mixed manually. The change in absorbance at 500 nm is monitored using a Cary-Varian UV−vis spectrophotometer in the kinetic measurement mode. The swelling rates are taken as averages from at least five different sets of experiments, calculated as previously described.[20]

■ RESULTS

Antibiotic Susceptibility Assays. The ability of β-lactams to traverse the outer membrane barrier via the OmpPst1 channel was initially approached using microbiological assays (MIC)[16] that determine the lowest concentration of a particular antibiotic needed to inhibit the growth of bacteria. The MIC results were determined with a biological assay corresponding to the complete mechanism of antibiotic action, including (i) diffusion through the porin channel, (ii) the affinity constant for the binding site of the periplasmic target (PBP), and (iii) the inhibitory constant on the PBP. These data confirmed the involvement of OmpPst1 porin in β-lactam susceptibility.[16] We further measured the activity of carbapenems by exposing *P. stuartii* ATCC 29914 bacterial cells. The MIC test of strain *P. stuartii* ATCC 29914 shows a higher MIC for imipenem and a significantly lower MIC value for meropenem given that the two molecules belong to the same carbapenem class in the β-lactam family. The test indicated a MIC value of 2 μg/mL with imipenem compared to ≤0.06 μg/mL with meropenem. It has been reported that carbapenems, like many other hydrophilic antibiotics, use porin channels as the intracellular influx pathway. Our previous study has confirmed that *P. stuartii* ATCC 29914 does not produce any extended β-lactamases or metallo-β-lactamases that are capable of hydrolyzing carbapenems.[16] To further confirm the role of OmpPst1 in antibiotic permeation, a porin-deficient *E. coli* BL21(DE3) omp8 strain is used to express OmpPst1 porin and the MIC value is determined for carbapenems (Table S1 of the Supporting Information). The data suggested that the lower MIC value of *P. stuartii* for meropenem, as compared to that for imipenem, may be due to a faster rate of influx of meropenem across the membrane channels, thereby accelerating the

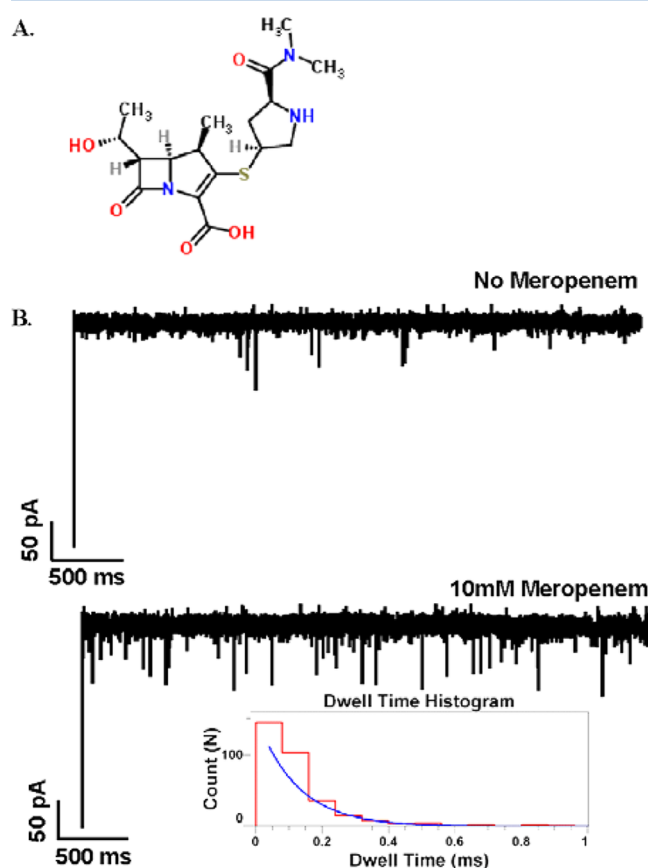intraperiplasmic concentration of the drug and the access to the target.

Conductance Measurements. A single OmpPst1 channel was reconstituted into a planar lipid membrane and showed a single trimer channel conductance of 2.7 ± 0.3 nS in 1 M KCl as shown previously.[16] In the absence of antibiotics, the ion current through the channel was stable without any modification of the flow of ions. Addition of imipenem to one or both sides of the lipid membrane caused a decrease in ionic conductance that is strongly concentration dependent. Figure 1B shows that addition of 5 mM imipenem to both sides of the chamber reduces the single-channel conductance from 2.5 to 2.2 nS. Further increasing the imipenem concentration to

15 mM reduces the conductance to 2 nS at 100 mV in 1 M KCl. A corresponding amplitude histogram is shown in Figure 1C. It must be noted that the direct effect of the antibiotic in solution on the bulk conductance is negligible in the applied concentration range, i.e., up to 15 mM (Table S2 of the Supporting Information). The resolution limit of our technique indeed restricts the detection of events occurring below 100 μs. Previous studies have shown that by lowering the temperature the kinetics of translocation slows and thus allows resolution of the translocation events. In the case of imipenem, lowering the temperature did not allow us to resolve individual translocation events even at a temperature as low as 5 °C (Figure S1 of the Supporting Information). Thus, we hypothesize that imipenem binds to the channel surface, resulting in the reduction of ion current.

In contrast, addition of meropenem to the system caused transient blockage of the ionic current (Figure 2B). At a low

Figure 1. (A) Chemical structure of imipenem. (B) Ion current trace through a single OmpPst1 channel reconstituted into planar lipid membranes in the presence of imipenem. (C) Corresponding amplitude histogram of the OmpPst1 channel in the absence and presence of imipenem.


Figure 2. (A) Chemical structure of meropenem. (B) Ion current recordings through a single OmpPst1 channel in the absence of meropenem and in the presence of 10 mM meropenem added to both sides of the chamber. Conditions: 1 M KCl, 20 mM MES, pH 6, 100 mV applied voltage.

drug concentration, meropenem interacts with the OmpPst1 channel, resulting in monomer blocking. Increasing the antibiotic concentration increases the number of events. The dwell time, τ_c, does not depend on the concentration of the antibiotic used and was calculated to be around 150 μs at 100 mV. Kinetic analysis of the antibiotic binding at different voltages and ionic strengths of the solution demonstrated that the interactions are of electrostatic origin. Previous studies on OmpF have revealed a charge reversal of the negatively

charged aspartic acid in the presence of multivalent cations.[23] To elucidate a similar contribution, we tested the effect of divalent and trivalent cations. The addition of 10 mM $MgCl_2$ in the presence of imipenem resulted in a partial closure of the channel (Figure S2 of the Supporting Information), while addition of 10 mM $LaCl_3$ in the presence of imipenem caused modulation of the ion current and highly resolvable blocking events (Figure 3). This is in contrast with the case for
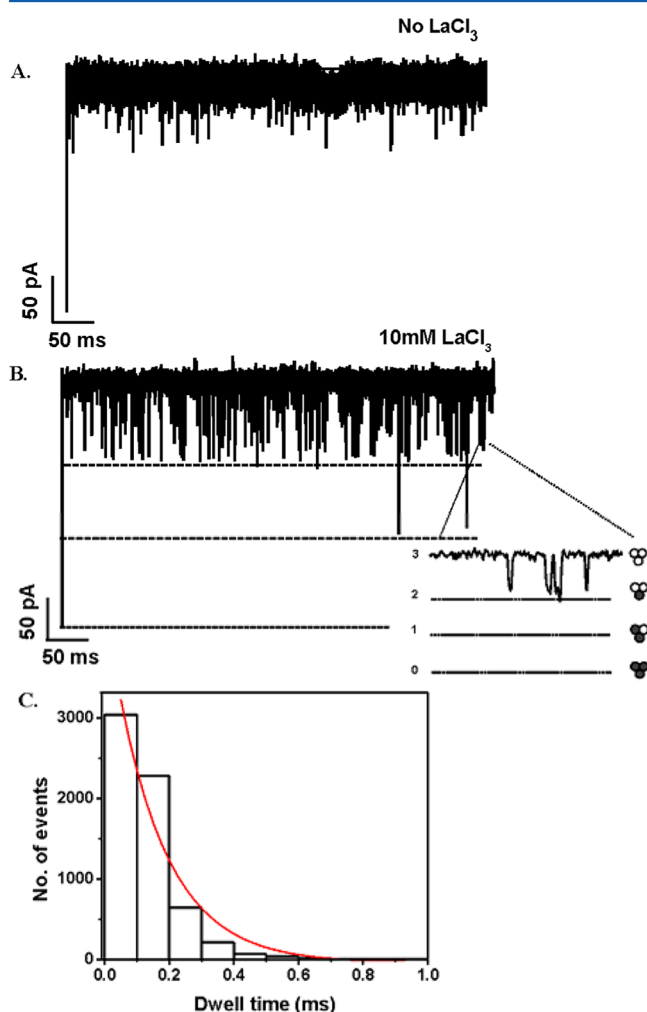
Figure 3. Ion current trace of a single OmpPst1 channel reconstituted into a bilayer in the presence of 10 mM imipenem without La^{3+} (A) and with La^{3+} (B). (C) Dwell time histogram in presence of 10 mM imipenem and $LaCl_3$.

meropenem, for which binding kinetics were not significantly affected in the presence of trivalent cations (Figure S3 of the Supporting Information).

The number of events and the residence time obtained from ion current blockages can be readily inserted into a simplified enzymatic model, where the channel is thought to catalyze antibiotic translocation. The association rate constant, k_{on}, gives the permeation of the antibiotic molecule from the *cis* or *trans* side to the affinity site in the channel calculated from the number of antibiotic binding events per second. The dissociation rate constant, k_{off}, gives the rate at which antibiotic molecules are released from the channel affinity site to the *cis* or *trans* aqueous phase calculated from the average residence time of antibiotic blockage[17,23−25] (Table 1).

Table 1. Rate Constants of Entry and Exit of Carbapenems through OmpPst1

	10 mM imipenem in the presence of $LaCl_3$ at 100 mV	10 mM meropenem in the presence of $LaCl_3$ at 100 mV
$k_{on}{}^a$ ($\times 10^3$ M^{-1} s^{-1})	9 ± 3	0.6 ± 0.2
$k_{off}{}^b$ ($\times 10^3$ s^{-1})	10 ± 3	8 ± 1.7

$^a k_{on}$ = (number of events per second)/(3[c]), where [c] is the antibiotic concentration. $^b k_{off}$ = 1/(average residence time).

Permeation Assays through Liposomes. To support the conclusion about transport from the ion current fluctuation analysis, we performed liposome swelling assays. The rate of diffusion of antibiotics through OmpPst1 is calculated by reconstituting channels in liposomes and by measuring the change in optical density in the presence of an isotonic concentration of antibiotics. A requirement to conduct a liposome swelling assay is that the molecule of interest be zwitterionic, making imipenem and meropenem suitable candidates for such measurement. To scale the flux, we first use raffinose a high-molecular weight sugar too large to diffuse through the porins and then arabinose, a small sugar that permeates through the channel. Permeation rates for different sugars are obtained together within the same batch allowing us to normalize the antibiotic diffusion values with respect to arabinose. The value obtained for arabinose, which is set to 100%, is 20% higher than that obtained for galactose and 80% higher than that for maltopentaose, confirming that the swelling rate decreases as the size of the solute increases (Figure 4).
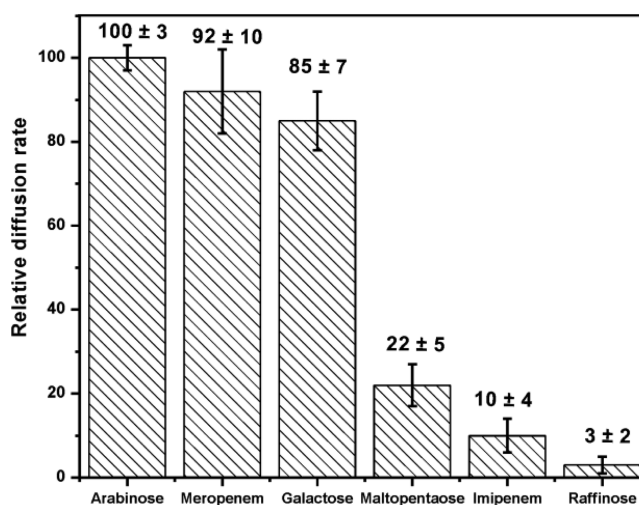
Figure 4. Relative rate of diffusion of imipenem compared to those of various sugars and meropenem through proteoliposomes. The swelling rates, which were averaged over at least three different sets of experiments, were calculated as described previously,[12] normalized by setting the rate of arabinose diffusion to 100%.

However, in the presence of imipenem, there is no significant change observed in the absorbance of proteoliposomes. The swelling rate obtained for imipenem is around 10%, i.e., comparable to that of large sugar molecules like raffinose and maltopentaose that are known to display poor or no permeation through porin channels. From the results described above, we can conclude that imipenem translocates very slowly through the OmpPst1 channel. In contrast, meropenem

showed a very high diffusion rate of around 90%, indicating it is able to translocate at a fast rate through OmpPst1. The results from liposome swelling assays thus complement the microbiological assays and bilayer measurements in suggesting poor permeation of imipenem through OmpPst1, which contrasts with the case of meropenem that translocates efficiently through the channel.

DISCUSSION

Currently, carbapenems are the most recent available β-lactams against Gram-negative bacteria. Because of their broad activity, they have become widely used in clinics; e.g., imipenem is the most used carbapenem in hospital wards. However, carbapenem efficacy is being threatened by the dissemination of bacterial resistance. During the treatment of infected patients, a correlation between the level of antibiotic resistance and the absence of porins was observed.[11] In *P. stuartii*, the major porin OmpPst1 provides the main pathway for the penetration of an antibiotic through the outer membrane.[16] Our focus here is on the mechanism of uptake of an antibiotic through porins and its role in antibiotic resistance. In particular, we investigated the relation between pore properties, the structure of the antibiotic, and the correlation with the uptake of these molecules. Our results indicate that both imipenem and meropenem interact with OmpPst1, albeit with different binding kinetics. From the observation that imipenem reduces the channel conductance without resolvable single blocking events, we hypothesize that either imipenem translocates very fast through the channel where the time resolution of the instrument limits the visualization of well-defined events or imipenem binds to the channel, inhibiting the flow of ions and hence reducing the channel conductance. To reach further conclusions based on the observation described above, we performed temperature measurements as shown previously[26] to catch the fast events, but these measurements were inconclusive. To differentiate binding from translocation, a liposome swelling assay was performed that suggested low flux of imipenem in contrast to rapid permeation of meropenem. Combining single-channel measurements and liposome swelling assays, we could conclude that imipenem binds to the channel, where it may interact with side chains of amino acids present in the channel surface. Thus, imipenem can be envisaged as a plug that reduces the extent of passage of other ions.

Similar studies have shown that enrofloxacin, a fluoroquinolone antibiotic, blocks the OmpF channel.[23] The interactions between the enrofloxacin and the OmpF channel wall are strong enough to close the pore for ~3 ms, revealing a strong affinity of the antibiotic for the channel without efficient translocation.[23] Interestingly, in the presence of magnesium chloride, the affinity of enrofloxacin for the OmpF channel was altered, as well as the orientation of the antibiotic during translocation.[23,27] Similarly, in the case of OmpPst1, the presence of trivalent cations caused a dramatic change in the imipenem binding kinetics (Table 1). The number of imipenem blocking events increased with the increase in the antibiotic concentration, and the average residence time was calculated to be around 150 μs. It is important to note that trivalent cations have no effect on the binding or translocation kinetics of the interaction of meropenem with OmpPst1 (Figure S3 of the Supporting Information). Kinetic constants of on and off rates for binding of imipenem and meropenem to OmpPst1 in the presence of trivalent cations are listed in Table 1.

Previously, we used homology modeling to predict the structure of the OmpPst1 channel, using as a starting model the homologous porin OmpF.[16] Important differences in amino acid residues were predicted for OmpPst1, with regard to OmpF. For example, M38, which in OmpF forms an important hydrophobic pocket above the constriction region, is substituted with an aspartic acid in OmpPst1. We speculate that this specific residue modification is correlated to the reduced rate of uptake of imipenem through OmpPst1 porin. The side chain of D38 could indeed act as a sensor that recognizes and binds the exposed NH^{2+} group in the iminomethylaminoethyl strongly polar side chain of imipenem, thereby stopping its progression in the channel and conferring partial insusceptibility to *P. stuartii*. In this context, our interpretation of the effect of trivalent cations is that they reverse the charge of D38 and thereby allow the uptake of imipenem by OmpPst1. This proposition is supported by the observation that meropenem, whose side chain is a more bulky dimethylcarbomylpyrrolidinyl group, translocates through OmpPst1 and shows efficiency against *P. stuartii*.

Thus, our results highlight the importance of efficient influx through porins for β-lactams to reach their target site and provide useful information for the rational design of drugs exhibiting enhanced bacterial penetration. We show an example in which porins screen antibiotic molecules entering the channel surface and those attractive forces facilitate translocation through the channel. In addition, our study provides clues that could explain some paradoxical susceptibilities to carbapenems in other clinical isolates (Lavigne et al., unpublished results). Thus, not only the affinity of each carbapenem for its PBP target but also the efficiency of its translocation across the outer membrane participates in the regulation of the bacterial susceptibility to this class of antibiotics.

ASSOCIATED CONTENT

Ⓢ Supporting Information

MIC values of carbapenems against porin-deficient strain *E. coli* BL21(DE3) omp8 (Table S1), bulk conductivity of 1 M KCl (pH 6) in the absence and presence of imipenem (Table S2), ion current trace of OmpPst1 in the presence of imipenem at two different temperatures (Figure S1), ion current trace of a single OmpPst1 channel in the presence of divalent cations (Figure S2), single-OmpPst1 channel recording in the presence of meropenem and La^{3+} (Figure S3), and dwell time histogram of 10 mM meropenem in the presence of LaCl$_3$ (Figure S4). This material is available free of charge via the Internet at http://pubs.acs.org.

AUTHOR INFORMATION

Corresponding Author

*School of Engineering and Science, Research II, Jacobs University Bremen, D-28759 Bremen, Germany. E-mail: m.winterhalter@jacobs-university.de. Phone: +494212003248. Fax: +494212003249.

Notes

The authors declare no competing financial interest.

ABBREVIATIONS

PBP, penicillin binding protein; OmpPst1, outer membrane protein Pst1; MIC, minimal inhibitory concentration.

REFERENCES

(1) Nikaido, H. (2003) Molecular basis of bacterial outer membrane permeability revisited. *Microbiol. Mol. Biol. Rev. 67*, 593−656.

(2) Hancock, R. E., and Bell, A. (1988) Antibiotic uptake into Gram-negative bacteria. *Eur. J. Clin. Microbiol. Infect. Dis. 7*, 713−720.

(3) Delcour, A. H. (2009) Outer membrane permeability and antibiotic resistance. *Biochim. Biophys. Acta 1794* (5), 808−816.

(4) James, C. E., Mahendran, K. R., Molitor, A., Bolla, J. M., Bessonov, A. N., Winterhalter, M., and Pagès, J. M. (2009) How β-lactam antibiotics enter bacteria: A dialogue with the porins. *PLoS One 4* (5), e5453.

(5) Simonet, V., Malléa, M., and Pagès, J. M. (2000) Substitutions in the eyelet region disrupt cefepime diffusion through the *Escherichia coli* OmpF channel. *Antimicrob. Agents Chemother. 44* (2), 311−315.

(6) Jeanteur, D., Schirmer, T., Fourel, D., Simonet, V., Rummel, G., Widmer, C., Rosenbusch, J. P., Pattus, F., and Pagès, J. M. (1994) Structural and functional alterations of a colicin-resistant mutant of OmpF porin from *Escherichia coli*. *Proc. Natl. Acad. Sci. U.S.A. 91* (22), 10675−10679.

(7) Poole, K. (2004) Resistance to β-lactam antibiotics. *Cell. Mol. Life Sci. 61*, 2200−2223.

(8) Lou, H., Chen, M., Black, S. S., Bushell, S. R., Ceccarelli, M., Mach, T., Beis, K., Low, A. S., Bamford, V. A., Booth, I. R., Bayley, H., and Naismith, J. H. (2011) Altered antibiotic transport in OmpC mutants isolated from a series of clinical strains of multi-drug resistant *E. coli*. *PLoS One 6* (10), e25825.

(9) Penner, J. L. (2005) Genus XXX. Providencia. In *Bergey's Manual of Systematic Bacteriology* (Brenner, D. J., Kreig, N. R., Staley, J. T., and Garrity, G. M., Eds.) 2nd ed., pp 753−759, Springer, New York.

(10) Stock, I., and Wiedemann, B. J. (1998) Natural antibiotic susceptibility of *Providencia stuartii*, *P. rettgeri*, *P. alcalifaciens* and *P. rustigianii* strains. *J. Med. Microbiol. 47*, 629−642.

(11) Fass, R. J., Barnishan, J., and Ayers, L. W. (1995) Emergence of bacterial resistance to imipenem and ciprofloxacin in a university hospital. *J. Antimicrob. Chemother. 36* (2), 343−353.

(12) Akova, M., Daikos, G. L., Tzouvelekis, L., and Carmeli, Y. (2012) Interventional strategies and current clinical experience with carbapenemase-producing Gram-negative bacteria. *Clin. Microbiol. Infect. 18*, 439−448.

(13) Gupta, N., Limbago, B. M., Patel, J. B., and Kallen, A. J. (2011) Carbapenem-resistant *Enterobacteriaceae*: Epidemiology and prevention. *Clin. Infect. Dis. 53*, 60−67.

(14) Cornaglia, G., Giamarellou, H., and Rossolini, G. M. (2011) Metallo-β-lactamases: A last frontier for β-lactams? *Lancet Infect. Dis. 11*, 381−393.

(15) Nordmann, P., Naas, T., and Poirel, L. (2011) Global spread of carbapenemase-producing *Enterobacteriaceae*. *Emerging Infect. Dis. 17*, 1791−1798.

(16) Tran, Q. T., Mahendran, K. R., Hajjar, E., Ceccarelli, M., Davin-Regli, A., Winterhalter, M., Weingart, H., and Pagès, J. M. (2010) Implication of porins in β-lactam resistance of *Providencia stuartii*. *J. Biol. Chem. 285*, 32273−32281.

(17) Nestorovich, E. M., Danelon, C., Winterhalter, M., and Bezrukov, S. M. (2002) Designed to penetrate: Time-resolved interaction of single antibiotic molecules with bacterial pores. *Proc. Natl. Acad. Sci. U.S.A. 99* (15), 9789−9794.

(18) Benz, R., Schmid, A., Nakae, T., and Vos-Scheperkeuter, G. H. (1986) Pore formation by LamB of *Escherichia coli* in lipid bilayer membranes. *J. Bacteriol. 165* (3), 978−986.

(19) Bangham, A. D., Hill, M. W., and Miller, N. G. A. (1974) Preparation and use of liposomes as models of biological membranes. In *Methods in Membrane Biology* (Korn, N. D., Ed.) pp 1−68, Plenum, New York.

(20) Yoshimura, F., and Nikaido, H. (1985) Diffusion of β-lactam antibiotics through the porin channels of *Escherichia coli* K-12. *Antimicrob. Agents Chemother. 27* (1), 84−92.

(21) Garavito, R. M., and Rosenbusch, J. P. (1986) Isolation and crystallization of bacterial porin. *Methods Enzymol. 125*, 309−328.

(22) Montal, M., and Mueller, P. (1972) Formation of bimolecular membranes from lipid monolayers and a study of their electrical properties. *Proc. Natl. Acad. Sci. U.S.A. 69* (12), 3561−3566.

(23) Singh, P. R., Ceccarelli, M., Lovelle, M., Winterhalter, M., and Mahendran, K. R. (2012) Antibiotic permeation across the OmpF channel: Modulation of the affinity site in the presence of magnesium. *J. Phys. Chem. B 116* (15), 4433−4438.

(24) Movileanu, L., Schmittschmitt, J. P., Scholtz, J. M., and Bayley, H. (2005) Interactions of peptides with a protein pore. *Biophys. J. 89*, 1030−1045.

(25) Berezhkovskii, A. M., and Bezrukov, S. M. (2005) Optimizing transport of metabolites through large channels: Molecular sieves with and without binding. *Biophys. J. 88*, L17−L19.

(26) Mahendran, K. R., Chimerel, C., Mach, T., and Winterhalter, M. (2009) Antibiotic translocation through membrane channels: Temperature-dependent ion current fluctuation for catching the fast events. *Eur. Biophys. J. 38* (8), 1141−1145.

(27) García-Giménez, E., Alcaraz, A., and Aguilella, V. M. (2010) Overcharging below the nanoscale: Multivalent cations reverse the ion selectivity of a biological channel. *Phys. Rev. E: Stat., Nonlinear, Soft Matter Phys. 81* (2), 021912.

Supplementary Material

Table S1: Impact of *Providencia* porins on the carbapenem susceptibility of *E. coli* BL21(DE3)omp8.

|		MIC (mg/L)	
E. coli strain	plasmid	IPM	MERO
BL21(DE3)omp8/pG	-	1	1
BL21(DE3)omp8/pG	pGOmpPst1-ATCC	0.25	0.125

IPM, imipenem ; MERO, meropenem

Table S2: Bulk conductivity of 1M KCl , pH- 6 in absence and in presence of imipenem.

Concentration of imipenem in 1M KCl, pH- 6	Bulk Conductivity (mS/cm)
No imipenem	105.5 ± 3
5 mM Imipenem	104 ± 2
15 mM Imipenem	105 ± 2

Fig. S1. Ion current traces of single OmpPst1 channel in the presence of imipenem at (A) 5.6 C and (B) 20 C.
Conditions: 1 M KCl, 20 mM PO4 pH- 6; 100 mV applied.

At 5.6° C

A.

20 pA

50 ms

At 20° C

B.

20 pA

50ms
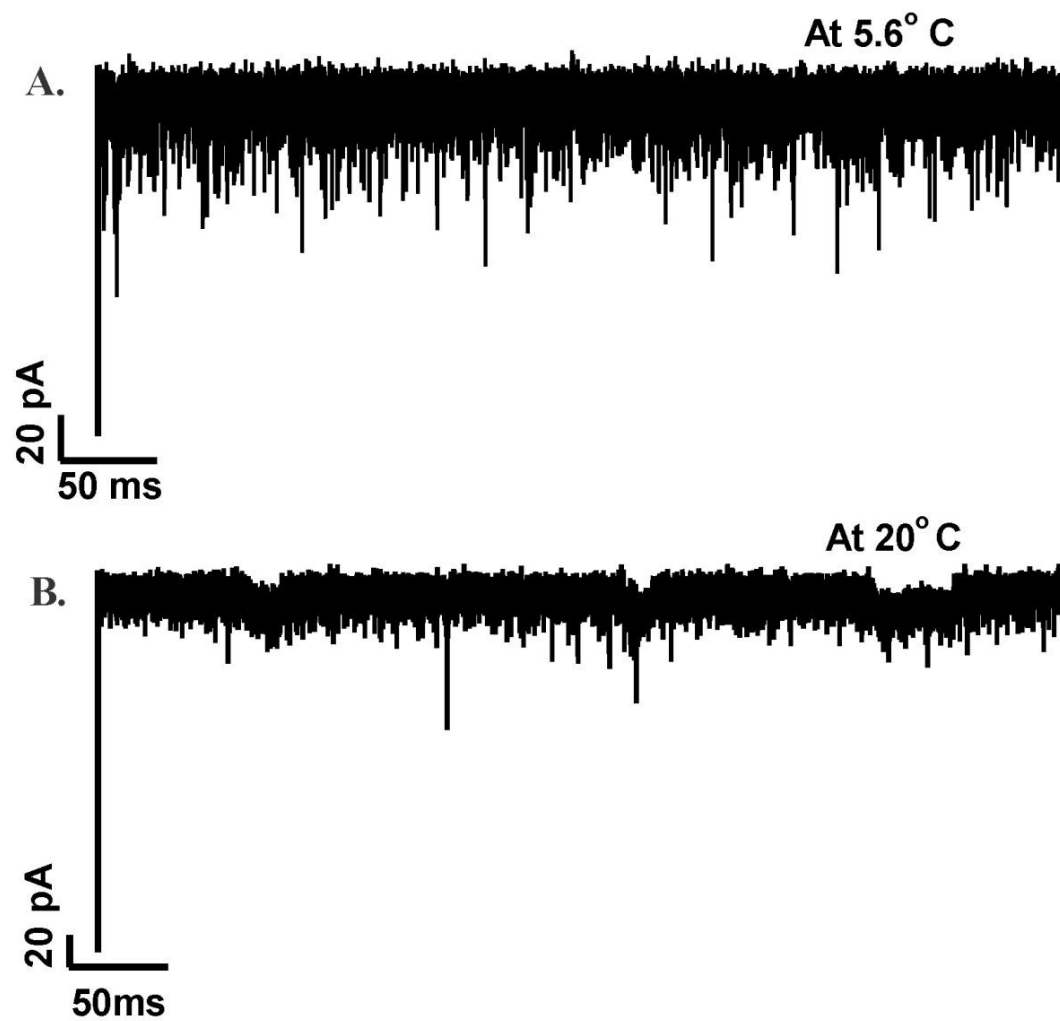
Fig. S2. Ion current traces of single OmpPst1 channel in presence of MgCl2 (A) without imipenem and (B) with 10 mM imipenem.
Conditions: 1 M KCl, 10 mM MgCl2, 20 mM MES pH- 6, 100 mV applied.
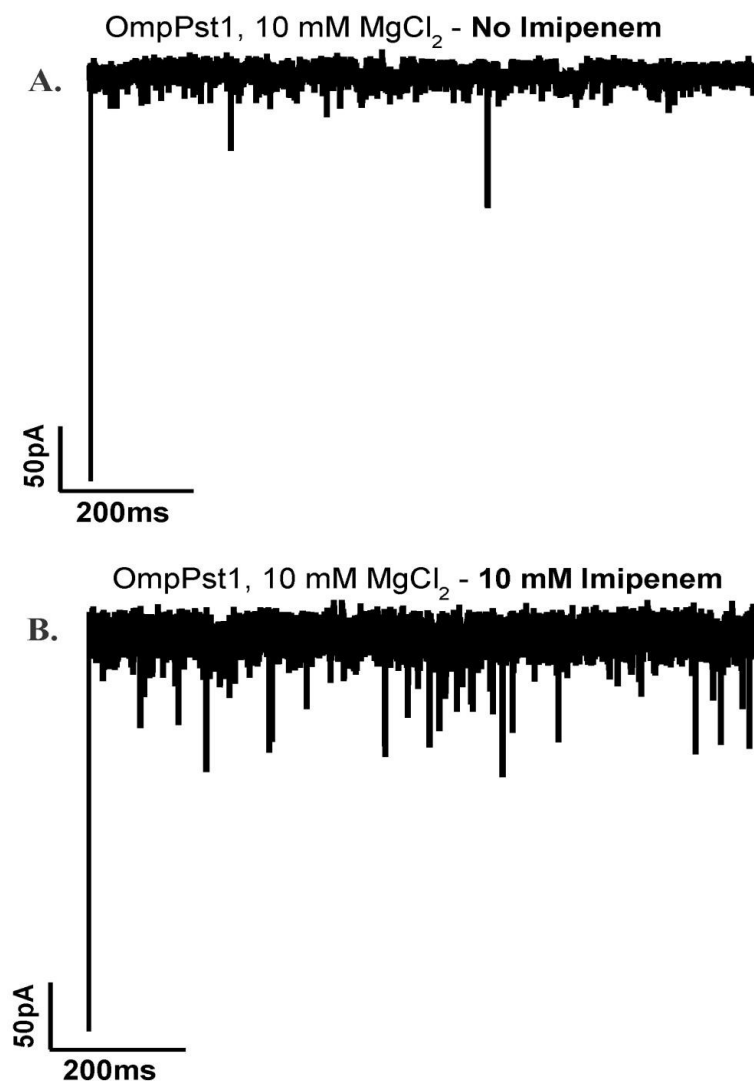
Fig. S3. Ion current trace of single OmpPst1 channel reconstituted into bilayer in 10 mM Meropenem and (A) No LaCl3 (B) 10 mM LaCl3. Corresponding dwell time histograms are provided.
Conditions : 1 M KCl, 20 mM MES pH- 6, 100 mV applied.
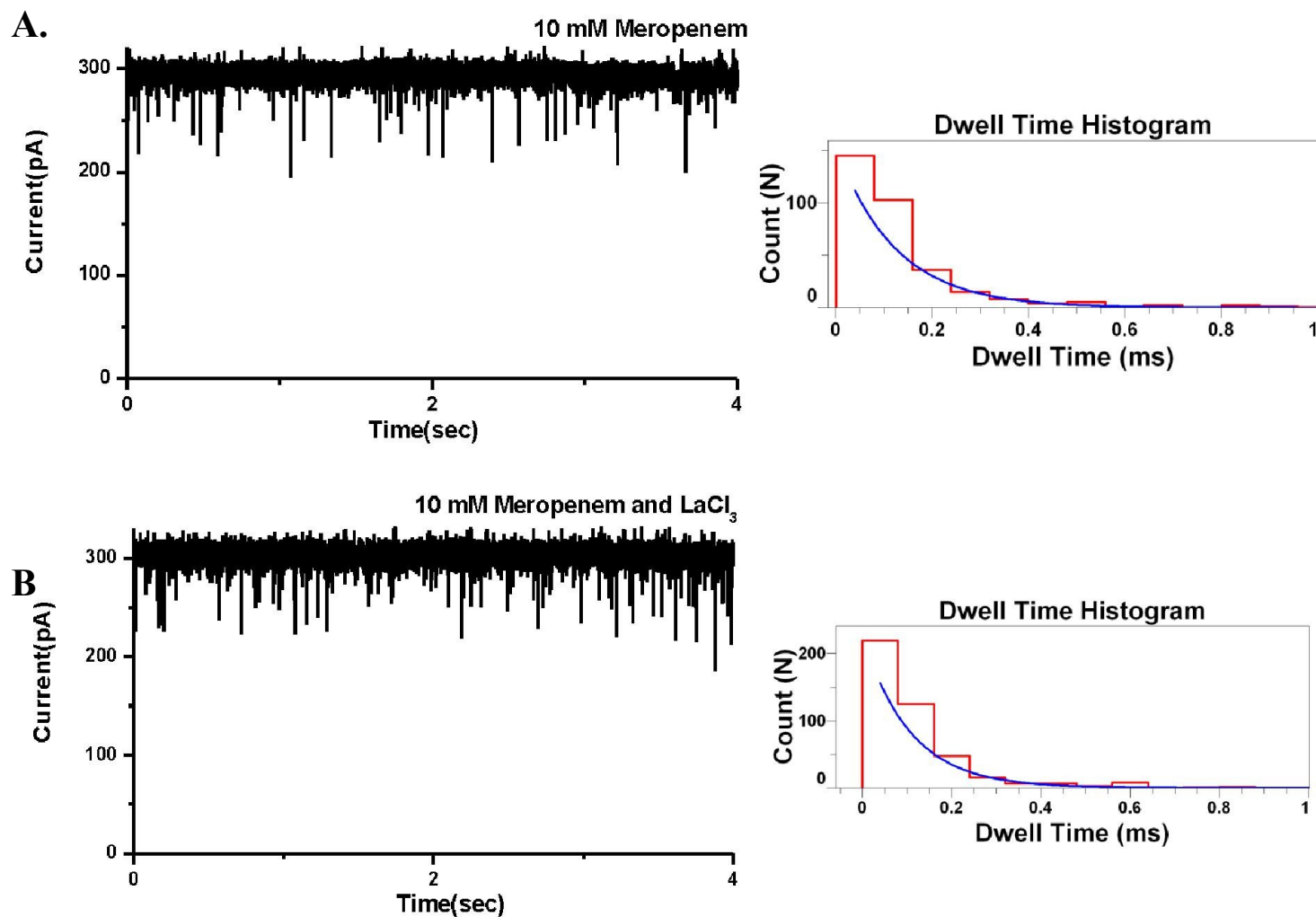
Fig. S4. Dwell time histogram of 10 mMn meropenem in presence of LaCl₃.
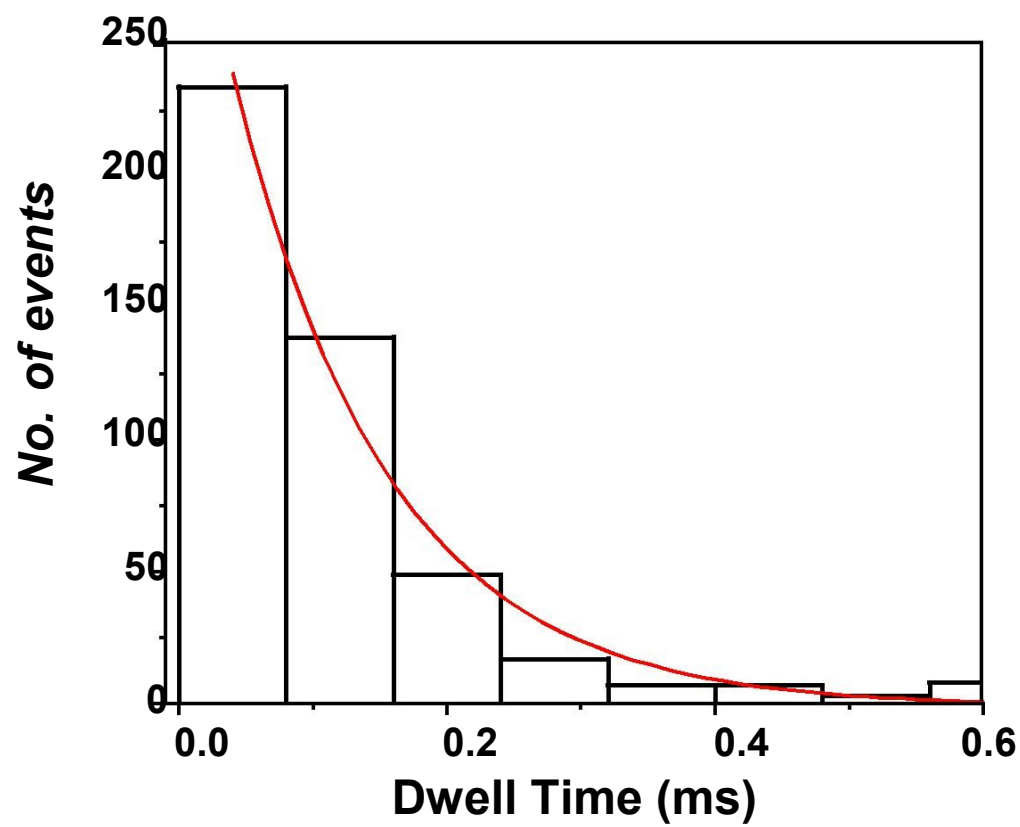
RESEARCH ARTICLE

Understanding Voltage Gating of *Providencia stuartii* Porins at Atomic Level

Wanling Song[1], Harsha Bajaj[2], Chady Nasrallah[3,4,5¤], Hualiang Jiang[1], Mathias Winterhalter[2], Jacques-Philippe Colletier[3,4,5]*, Yechun Xu[1]*

1 CAS Key Laboratory of Receptor Research, Drug Discovery and Design Centre, Shanghai Institute of Materia Medica, Chinese Academy of Sciences (CAS), Shanghai, China, **2** School of Engineering and Sciences, Jacobs University Bremen, Bremen, Germany, **3** University Grenoble Alpes, Institut de Biologie Structurale (IBS), Grenoble, France, **4** CNRS, Institut de Biologie Structurale (IBS), Grenoble, France, **5** CEA, Institut de Biologie Structurale (IBS), Grenoble, France

¤ Current address: Institut de Génomique Fonctionnelle, Montpellier, France
* colletier@ibs.fr (JPC); ycxu@simm.ac.cn (YX)

Abstract

Bacterial porins are water-filled β-barrel channels that allow translocation of solutes across the outer membrane. They feature a constriction zone, contributed by the plunging of extracellular loop 3 (L3) into the channel lumen. Porins are generally in the open state, but undergo gating in response to external voltages. To date the underlying mechanism is unclear. Here we report results from molecular dynamics simulations on the two porins of *Providenica stuartii*, Omp-Pst1 and Omp-Pst2, which display distinct voltage sensitivities. Voltage gating was observed in Omp-Pst2, where the binding of cations in-between L3 and the barrel wall results in exposing a conserved aromatic residue in the channel lumen, thereby halting ion permeation. Comparison of Omp-Pst1 and Omp-Pst2 structures and trajectories suggests that their sensitivity to voltage is encoded in the hydrogen-bonding network anchoring L3 onto the barrel wall, as we observed that it is the strength of this network that governs the probability of cations binding behind L3. That Omp-Pst2 gating is observed only when ions flow against the electrostatic potential gradient of the channel furthermore suggests a possible role for this porin in the regulation of charge distribution across the outer membrane and bacterial homeostasis.

Author Summary

Porins are the main conduits for hydrophilic nutrients and ions uptake into the periplasm of Gram-negative bacteria. Their translocation permeability is determined by the amino-acid distribution on their extracellular loop L3. Bacterial porin channels have long been known to undergo step-wise gating, under the application of a transmembrane potential. Yet the exact molecular mechanism by which gating is achieved and the exact relevance of this evolved characteristic remain elusive. In the present study, we report on electrophysiology experiments and molecular dynamics simulations on the two general-diffusion porins of *Providencia stuartii*, Omp-Pst1 and Omp-Pst2. Our results show that gating in

Omp-Pst2 occurs as the result of L3 displacement, which follows from the binding of cations in acidic niches between L3 and the barrel wall and effects in exposing the side chain of a highly conserved aromatic residue at the tip of L3 in the channel lumen. That Omp-Pst2 displays asymmetric voltage sensitivity and that the likelihood of gating is increased when cations transit from the extracellular to the intracellular side suggests voltage-gating underlies a regulatory role in bacterial homeostasis. Rational antibiotic-design strategies based on the maximization of antibiotic penetration and accumulation at their target sites, should take this role into account.

Introduction

The outer membrane of Gram-negative bacteria is sprinkled of homotrimeric channels comprised of three 16-stranded β-barrels. They are the principal conduits for the passive penetration of hydrophilic molecules into the periplasm, and are often referred to as the general diffusion porins. Classical examples include *Escherichia coli* OmpF [1], OmpC [2] and PhoE [1]. The general diffusion porins display a conserved β-barrel architecture with eight periplasmic turns and eight extracellular loops (L1–L8). Also conserved is the presence of a constriction zone (CZ), at mid height of the channel. The CZ is contributed by the plunging of extracellular loop L3 into the channel lumen, where it adopts a helix-turn-loop fold and interacts with the barrel wall through hydrogen bonding and Van der Waals (VDW) interactions. The amino-acid distributions in L3 and on the barrel wall opposite to it ("anti-L3 region") determine the sieving properties of the porins, *i.e.* their ion specificity and size exclusion limit [3, 4]. The L3 and anti-L3 region generally display opposed charge distribution, with L3 being negatively charged and anti-L3 positively charged.

The general diffusion porins can switch from their open state to gated states when a transmembrane potential is applied [5–10], a phenomenon termed as voltage gating (VG). VG is characterized by step-wise, long-lasting closed states that persist until the transmembrane potential is suppressed. The critical voltage required for voltage gating (Vc) varies among porins, but is generally in the order of hundreds of mV. Vc can be influenced by a variety of environmental cues, including pH and salt concentration [11, 12], membrane constitution [8, 13], polarity of the transmembrane potential [9], or the presence of effectors such as oligosaccharides [13] and polyamines [14]. Accumulated evidences have suggested that voltage sensing in general diffusion porins occurs at the CZ [15–21]. It was shown that replacement of L3 charged residues by uncharged ones invariably results in alteration of voltage sensitivity, channel conductance and/or ion selectivity [15, 21, 22]. In particular, replacement of negatively charged residues from L3 leads to an increase of Vc in cation-selective *E. coli* OmpF, while that of the positively charged residues in anti-L3 regions causes the decrease of Vc in anion-selective *E. coli* PhoE [15]. In addition, mutagenesis studies on OmpF showed that destabilization of L3 by deletion of residues at its tip leads to increased voltage sensitivity (lower Vc) and reduced conductance [18, 19], whereas mutations of residues involved in L3 stabilization result in reduced voltage sensitivity (higher Vc) [19, 20].

More than a decade ago, Tieleman *et al* reported the first molecular dynamics (MD) simulation of *E. coli* OmpF embedded in explicit lipids. Their results revealed instability in L3 due to a breakdown of the hydrogen-bonding network (HBN) anchoring L3 to the barrel wall [23]. Suspecting that the fluctuation in the CZ may have been due to the protonation setting, Im *et al* and Varma *et al* respectively implemented MD simulations using different ionization states to the charged residues on L3 [24–26]. The invariable observation was that L3 is prone to

large fluctuations, suggesting that this loop could intervene in translocation across porin and possibly also in voltage-gating. Owing to constant improvements in MD simulation algorithms [27, 28] and the successful implementation of artificial transmembrane potentials [29], it has become possible to simulate ion mobilizing within the channel and thus to study the channel transport properties at a molecular level. For example, Pezeshki *et al* showed that mutation of one charged residue within CZ leads to visible effects on ion permeation and selectivity in OmpF [4]; Faraudo *et al* found that removal of negative charges in CZ influences the distribution of cations along OmpF channel [30]. However, owing both to limited computational resources and to the low voltage sensitivity (high Vc) of the hitherto simulated porin (OmpF), the molecular mechanism by which the general diffusion porin gating occurs has not yet been reported.

In the following, we report on extensive comparison of sub-microsecond scale MD simulations that provide insights into the molecular basis of voltage gating in general diffusion porins. Simulations were conducted on Omp-Pst1 and Omp-Pst2, two general diffusion porins from *Providencia stuartii* [31]. The sequence identities with OmpF of Omp-Pst1 and Omp-Pst2 are 50% and 46.1% respectively, while the RMS deviation of their Cα atoms (as measured from their respective X-ray structures) are 0.94 Å and 0.89 Å respectively. Omp-Pst1 and Omp-Pst2 show a high level of structural similarity, but owing to a completely different pattern of charge distribution along their channel wall, the two porins display opposite ion selectivities. Furthermore, whereas Omp-Pst1 gates at voltages above 199 mV, Omp-Pst2 undergoes the typical three-step gating at voltages as low as ~20 mV, making it the most voltage sensitive bacterial porin studied to date. Taking advantage of this striking contrast, we constructed parallel simulations between Omp-Pst1 and Omp-Pst2 at positive, negative and none transmembrane potentials (V_{TM}; extracellular to intracellular). In Omp-Pst2, we observed gating at $V_{TM} < 0$ V, but not at $V_{TM} > 0$ V, consistent with asymmetrical gating observed experimentally. At $V_{TM} < 0$ V, the gating stems from stable binding of cations in acidic niches behind L3, which in turn disrupts the HBN anchoring L3 to the barrel wall and thereby allows a local conformational change in conserved W111 at the tip of L3. The repositioning of W111 aromatic side chain in the middle of the CZ effectively halts ionic permeation across the Omp-Pst2 channel. At $V_{TM} > 0$ V, the HBN between L3 and the barrel wall strengthens. The stabilized L3 impedes cation binding, and thus thwarts gating. In Omp-Pst1, gating was not observed, regardless of the V_{TM} applied. Additional hydrogen bonds in HBN contribute to a more resilient L3. Altogether, our results suggest that the voltage sensitivity of Omp-Pst1 and Omp-Pst2 is encoded in the HBN that anchors L3 onto the channel wall, and that conformational changes in the side chain of conserved W111 at tip of L3 leads to channel closing.

Results

Single channel electrophysiology

Reconstitution of a single Omp-Pst1 / Omp-Pst2 channel in a planar lipid bilayer showed a single trimer conductance of 2.7 ± 0.1 / 3.7 ± 0.2 nS respectively at 1M KCl, pH 7. In the ion selectivity measurements performed as described in [32], Omp-Pst2 shows strong cation selectivity whereas Omp-Pst1 shows indistinctive cation selectivity (Table 1). For Omp-Pst1, the critical voltage (Vc) for observing the typical three-step gating was ≥199 mV in all measurements (n = 8). For Omp-Pst2, pore-to-pore variation was observed, and Vc measurements varied between 20 and 90 mV, with a median at 50 mV (n = 20).

Table 1. Conductance, ion selectivity and critical voltage of Omp-Pst1 and Omp-Pst2 measured in single channel.

Porin	Conductance* (nS)	P_K^+/P_{Cl}^-**	Critical voltage (mV)
Omp-Pst1	2.7 ± 0.2	1.3	≥199
Omp-Pst2	3.7 ± 0.1	8.3 ± 1.5	20–90

* Conductance of porins was measured at 1M KCl, 10 mM HEPES at pH 7.

** Selectivity of porins (cations over anions) was measured in presence of 100 mM KCl on *cis* side and 1M KCl on *trans* side at pH7.

doi:10.1371/journal.pcbi.1004255.t001

Simulated ion selectivity and conductance agree with experimental data

The crystallographic structures of Omp-Pst1 and Omp-Pst2 trimers were used as starting model for the simulations. Briefly, each porin was inserted in a lipid bilayer, solvated at pH 7, and the ionic concentration was adjusted to 1 M KCl. After equilibration, the two systems were subjected to either a negative (V_{TM} direction pointing from extracellular to intracellular) or a positive transmembrane potential (V_{TM} direction pointing from intracellular to extracellular) and each simulation was ran for > 500 ns. Additional simulations without a transmembrane potential were also carried out for both porins and each lasted for 100 ns. The β-barrel remains rigid in all voltage conditions, showing RMS fluctuation lower than 1 Å (S1 Fig). Larger fluctuation is observed in extracellular loops, especially in L1, L4, L5 and L6. L1 lies on the interface of the trimer and interacts with the positively charged residues at anti-L3 regions from another monomer. L4, L5 and L6 form secondary structure elements that associate to cover the extracellular entrance of the channels. Applying transmembrane potentials does increase the amplitude of loop fluctuation. However, according to the principal component analysis, their movements are constrained in a radius of ~5 Å, as imposed by a strong network of polar interactions between adjacent loops (S2 Fig).

In simulations with $V_{TM} \neq 0$, anions and cations separate into two pathways at the CZ: cations (K^+) trail along negatively charged L3 (residues Y98 to D123 in Omp-Pst1 and Y95 to D120 in Omp-Pst2, respectively), while anions (Cl^-) duct on the positively charged anti-L3 region (Fig 1A and 1B). In Omp-Pst1, K^+ mainly shuffle between the acidic side chains of L3 residues D109 and D117, while Cl^- interact with the basic side chains of anti-L3 residues K16, R20, R41, R59, K65, R78, K163 and K170. In Omp-Pst2, these residues are D106, D114 and D117, on the one hand, and R20, R38, R56, R75, K160 and K168, on the other.

Steady ionic currents were developed in the voltage-applied systems except for Omp-Pst2 at $V_{TM} < 0$ mV. As we show below, gating occurred in this simulation, thus impacting ion current across the channels (Figs 2A and S3). In the other simulations, ion currents across the channel reached excellent agreement with the experimental measurements after fluctuating for ~200 ns. The current curve suggests that long equilibration time (~100–200 ns) is required when simulating porins at high ionic concentration (1M in our case). That this requirement was not fulfilled in earlier simulations on porins at high ionic concentrations may explain the discrepancy between their simulated and experimentally measured currents [4, 33]. From the stable K^+ and Cl^- permeation after 200 ns or before gating in the case of Omp-Pst2 at $V_{TM} < 0$ mV, we derived the simulated conductance via least-square linear regression of the I/V curve (V_{TM} = [−1, 0, 1] V). The raw conductance for Omp-Pst1 and Omp-Pst2 are 3.64 nS and 4.01 nS respectively, while the corrected values based on ion diffusion coefficients (See Methods) are 3.95 nS and 4.47 nS respectively. The deviation from experimental observables might result from poor data samples in regression fitting.

166
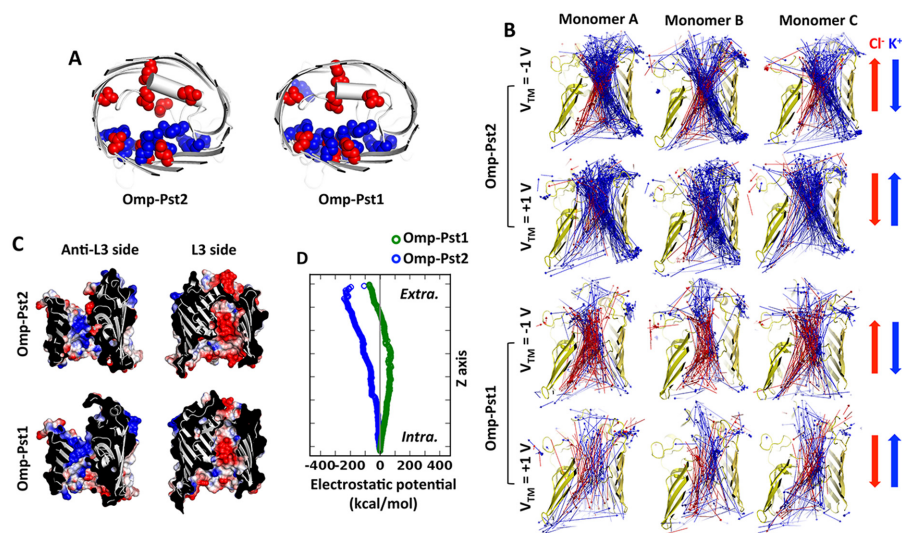
Fig 1. Electrostatic properties of Omp-Pst1 and Omp-Pst2. (A) Charge distribution at constriction zone. The constriction zone is defined as the area within 5 Å of the narrowest point of the channel. The negatively charged residues are shown in red spheres and the positively charged in blue spheres. (B) Mode vectors of cations (blue) and anions (red) for every 1 ns within the first 100 ns in the voltage-applied simulations. (C) Electrostatic surface of anti-L3 side and L3 side. Contour color set as ± 100 kT/e. (D) Electrostatic potentials along the pores calculated by HOLE. The values are normalized to intracellular entrance.

Simulations indicate a strong cation-selectivity for Omp-Pst2 and a mild anion-selectivity for Omp-Pst1 (Fig 2C), in line with experimental electrophysiology data and also with the analysis of their structures. The net charge of Omp-Pst1 is indeed +1 e at the constriction zone (within 5 Å radius of channel's narrowest point) and +5 e along the pore, while that of Omp-Pst2 is -4 e at the constriction zone and -3 e along the pore. In the case of Omp-Pst2, we observed that translocation of cations from the intracellular to the extracellular side is more efficient than the other way around (and conversely for Cl⁻ ions), as grounded by its two times more pronounced cation-selectivity at $V_{TM} > 0$ than at $V_{TM} < 0$ (Fig 2C). This asymmetry in ion selectivity correlates with the asymmetry in charge distribution (and thus with the gradient of electrostatic potential) along Omp-Pst2 channel, which features more acidic residues on the extracellular side than on the intracellular side. In Omp-Pst1, where the distribution of charged residues is even along the pore (Fig 1C), ion selectivity and translocation rate are less affected by the direction of the transmembrane potential (Fig 2C). Our simulations thus suggest that the ion selectivity of porins is not only determined by the charge distribution at their constriction zone [30, 34, 35], but also by the profile of charge distribution along the channel.

Voltage gating in Omp-Pst2 at V_{TM} < 0 V

After 100 ns, a decline in ion fluxes was observed in the simulation of Omp-Pst2 at $V_{TM} < 0$. Examination of ion fluxes on a monomer basis reveals that the decline mainly stems from one monomer in the trimer (monomer B) undergoing gating. At $V_{TM} < 0$, K⁺ ions are forced to translocate from the extracellular to the intracellular side, and inversely for Cl⁻ ions. This direction of transit is unfavourable for cations, as suggested by the electrostatic potential developed along Omp-Pst2 channel and established by the two times slower uptake of cations in comparison to the other direction. As this unfavourable flux gets heavier across the channel of monomer B, it effects in disorganizing the HBN within L3 (S4 Fig). A main-chain flip consequently
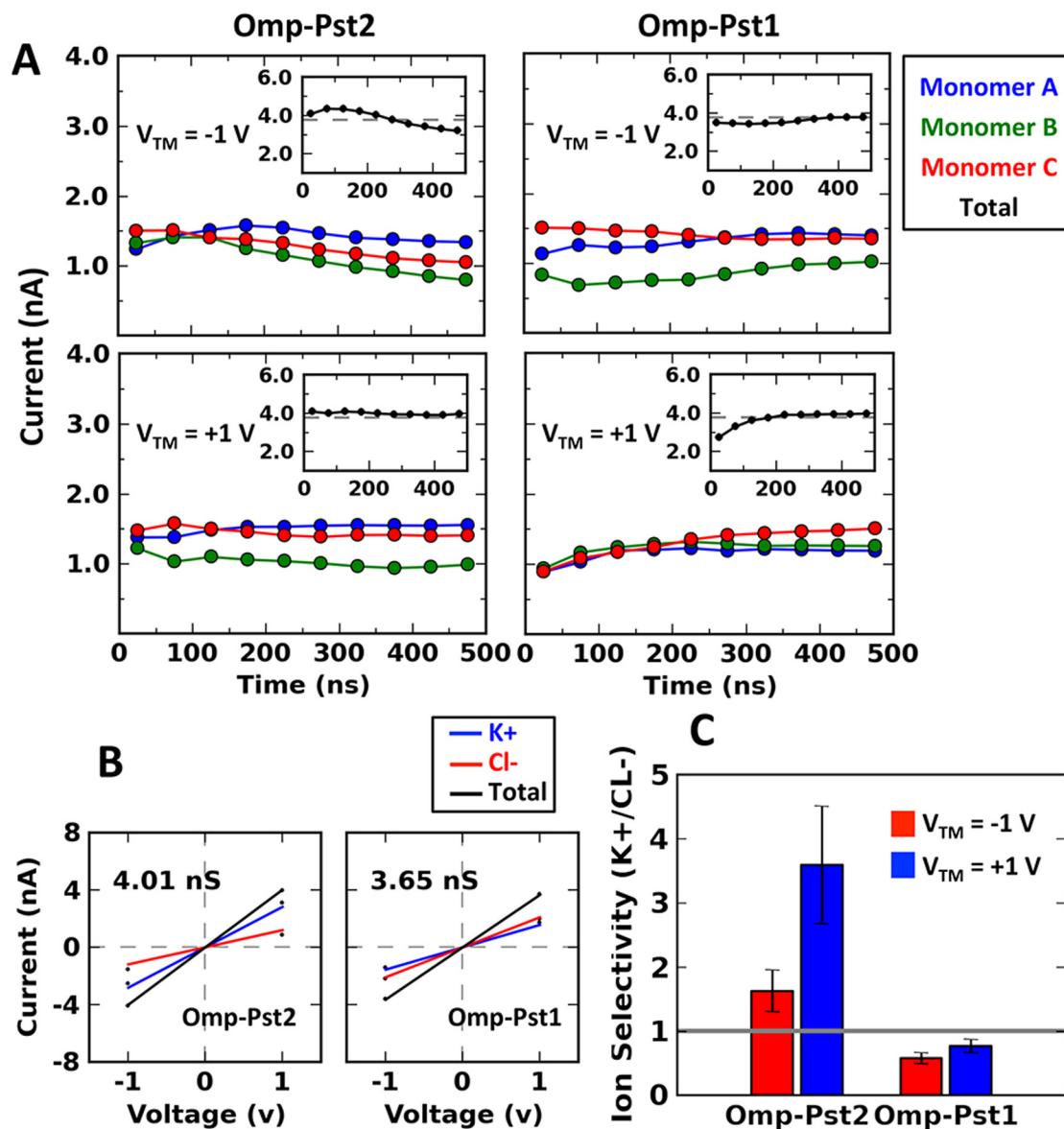
Fig 2. The calculated current, conductance and ion selectivity from MD simulations. (A) The currents are calculated every 50 ns monomer-wise and the total channel currents are shown in in-set panels in comparison to the experimentally determined values (dash lines). (B) The conductances of the porins' channel are obtained from the slope of their I-V curve. The raw channel conductances are shown. (C) The ion selectivity is determined as the ratio of K^+ to Cl^- current. The value shown at each voltage is the averaged ratio from three monomers and the error bar corresponds to the standard deviation among the three.

doi:10.1371/journal.pcbi.1004255.g002

occurs after 84 ns in 112-GA-113, resulting in the opening a highly acidic niche (niche I) between L3 and the barrel wall (Fig 3A). The acidic nature of the niche mainly results from the side chain oxygens of E258, a barrel-wall residue hitherto shielded from the bulk, but also from the side-chain oxygens of N102, T105, T115 and N276. A K^+ ion rapidly (within 0.5 ns) lodges into niche I (Fig 3F), dragging along the side chain of D106. This results in the latter adopting a barrel-facing conformation, thereby reinforcing of the acidic nature of the niche. The change in orientation of D106 propagates to D114, whose side chain draws towards the channel lumen, leading to yet another main chain rearrangement in L3 (~114 ns) (Fig 3C). Originating
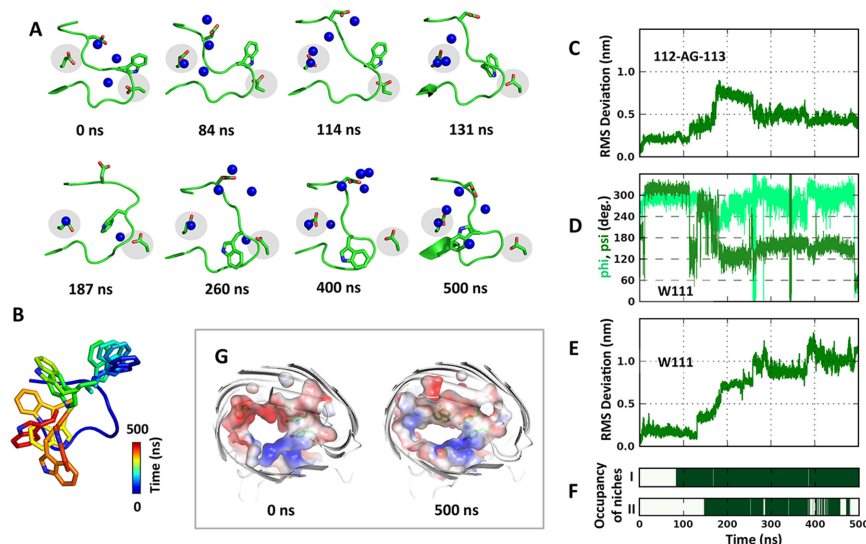
Fig 3. Gating process in Omp-Pst2 monomer B at negative voltage. (A) Snapshots of L3 tip. In each snapshot, residues W104 to D117 are shown in cartoon; W111, D114, E258 and D312 in sticks; and K$^+$ within 3.5 Å of the L3 tip in blue spheres. The acidic niche I (E258) and niche II (D312) are highlighted in gray. (B) W111 movements in every 50 ns. The RMSD of 112-AG-113 (C), the phi/psi angle of W111 (D) and the RMSD of W111 (E) are laid out to demonstrate the sequential events leading to niches exposure and subsequent binding of cations within them (F). G) The electrostatic potential surface at 0 ns and 500 ns. The extent of color scale is ± 100 kT/e. Y95, Y99, A103 and W111 are shown in sticks.

doi:10.1371/journal.pcbi.1004255.g003

in 112-GA-113, these changes rapidly transduce to 111-WGAD-114 (~131 ns) and result in W111 side chain wandering away from the barrel wall (Fig 3D and 3E). W111 movement effects in uncovering D312, a highly conserved barrel wall residue whose side chain oxygens hydrogen bond to the tip of L3 (main chain nitrogens of L110 and W111) in the crystallographic structure of Omp-Pst2. Exposure of D312 side chain generates a second acidic niche (niche II) in which another K$^+$ ion binds ~10 ns latter (Fig 3F). Occupation of this niche effects in unleashing the tip of L3, and most notably, the side chain of W111 (Fig 3B). Originally constrained by Y20, K314 and V334, W111 first positions itself in the middle of L3 (~187 ns), but finally ends up in the channel lumen (~260 ns). There, it imposes steric and hydrophobic hindrance to ions translocation, notably through the formation of a hydrophobic belt by Y95, Y99 and A103 side chains (Fig 3G). In the last 100 ns, translocation of K$^+$ ions is diminished by ~3/4 in monomer B, while that of Cl$^-$ ions by ~1/4 (S5 Fig).

In the two other monomers of the Omp-Pst2 trimer simulated at V$_{TM}$ < 0, a comparable sequence of events is observed, albeit incomplete and spanning a longer time scale. In monomer C, a potassium ion binds in niche I after ~110 ns, following a main chain flip in 112-GA-113 (~80 ns). Similar to that in monomer B, binding of this first K$^+$ ion induces a conformational change in 111-WGAD-114 (~240 ns) that results in the detachment of W111 from the barrel wall (243 ns) and the concomitant opening of niche II. However, binding of a K$^+$ ion in this niche occurs at more than 200 ns latter (~ 453 ns). Thus, D312 side chain remains in its native conformation and migration of W111 side chain toward the channel lumen does not complete (S6 Fig). Accordingly, only a slight reduction of K$^+$ flux is observed, while Cl$^-$ flux remains unaffected. In monomer A, binding of a K$^+$ ion in niche I occurs after 327 ns, and the resulting conformational change in 112-GA-113 after 350 ns. By the end of the simulation time, however, no K$^+$ ion lodges into niche II. W111 consequently stays in place, and ionic fluxes remain steady (S7 Fig). It is interesting to recall that in electrophysiology experiments, gating of the

three monomers in a trimer also occurs sequentially. Thus monomers A, C and B could represent different Omp-Pst2 intermediates in the process of gating.

Steadier attachment of L3 prevents gating in Omp-Pst2 at $V_{TM} > 0$ V

No voltage gating was observed in the simulation of Omp-Pst2 at $V_{TM} > 0$. This observation is consistent with experimentally observed asymmetrical gating behaviour [10, 36, 37]. Trajectory analysis reveals that it is the stronger stabilization of L3 at $V_{TM} > 0$ that impeaches gating. In short, a main chain rearrangement in 112-GA-113 leads to exposure of E258 and concomitant binding of K^+ ions in niche I after ~340, 20 and 95 ns in monomers A, B and C respectively. In the two latter, main chain rearrangements in W111 (after 210 and 340 ns in monomers B and C, respectively) precede binding of K^+ ions in niche II (after 245 and 351 ns in monomers B and C, respectively). Nevertheless, K^+ binding to niche II is less stable at $V_{TM} > 0$ and gating is hence not observed (S8–S10 Figs).

Two factors are responsible for the reduced gating sensitivity of Omp-Pst2 at $V_{TM} > 0$. First and most importantly, the HBN anchoring L3 to the barrel wall is more robust at $V_{TM} > 0$ than at $V_{TM} < 0$ (Fig 4A), owing to a more favourable orientation of acidic side chains. At $V_{TM} > 0$, the acidic residues on Omp-Pst2 L3 are indeed facing toward the barrel wall, facilitating interactions with non-L3 residues. Major stabilizing interactions include: i/ a salt-bridge between E119 and R126; ii/ alternating hydrogen bonds between D117 and either Y99 or N102; and iii/ an hydrogen bond between D114 and Y294 before the main chain rearrangements in 112-AG-113 occurs (Fig 4B). In strong contrast, L3 acidic residues adopt outward conformations in the simulation at $V_{TM} < 0$, which prevents them from forming hydrogen bonds or salt-bridges with neighbouring residues. Secondly, that the transit of K+ ions is energy favoured at $V_{TM} > 0$ and that these ions thus transit faster across the CZ furthermore diminishes
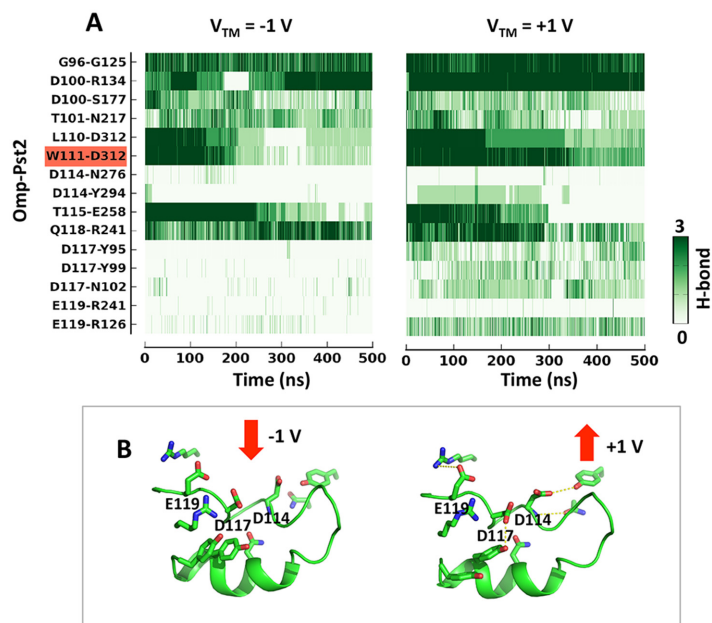
Fig 4. **Comparison of hydrogen-bonding network on Omp-Pst2 L3 at two voltages.** A) Hydrogen bonds on L3 as a function of time. The color scale indicates whether the hydrogen bond is seen in 0, 1, 2 or 3 monomers of the trimer. The hydrogen bond W111-D312, which anchors L3 tip to barrel wall, is highlighted. B) Snapshots of Omp-Pst2 L3 at 200 ns at $V_{TM} = +/- 1$ V. The three charged residues D114, D117, E119, and their hydrogen-bonding residues are shown in sticks.

their likelihood of forming stable interaction with D312. Their intermittent binding to niche II does not trigger the repositioning of W111 side chain.

L3 fastening prevents gating in Omp-Pst1

From a structural point of view, Omp-Pst1 shares the critical features of two acidic niches under L3, with E266 and D321 (equivalent to Omp-Pst2 E258 and D312) being the main contributors to niche I and II, respectively. Likewise, an aromatic residue is found at its L3 tip, *viz.* W114 (equivalent to W111 in Omp-Pst2). Yet, gating was not observed in Omp-Pst1 on the time-scale of our simulations, regardless of the directionality of the transmembrane potential. Accordingly, the HBN holding L3 attached to the barrel wall, W114-D321, remained unaffected throughout all simulations ([Fig 5A](#)). These observations are in faithful agreement with experimental data, which established a higher Vc for Omp-Pst1 than Omp-Pst2 ([Table 1](#) and [S11 Fig](#)).

At $V_{TM} < 0$, binding of a K^+ ion in niche I (~200 ns) occurs in monomer A, where it results in a conformational jump of L3 residues 115-AG-116 (equivalent to 112-GA-113 in Omp-Pst2) toward the extracellular side. In monomers B and C, however, neither binding of a K^+ ion in niche I nor a conformational change in L3 is observed. Niche II meanwhile remains unoccupied in all three monomers ([S12](#)–[S14](#) Figs). At $V_{TM} > 0$, binding of a K^+ ion in niche I is observed in monomers A and B (after ~196 and ~254 ns, respectively), which precedes a conformational change in 115-AG-116 (after ~300 and ~500 ns, respectively). But again, niche II remains unoccupied in all three monomers ([S15](#)–[S17](#) Figs). Thus at both V_{TM}, and in all three Omp-Pst1 monomers, D321 remains covered by the side chains of L113 and W114. The tip of L3 is therefore kept fastened to the barrel wall, and W114 maintains its native, open-state conformation.
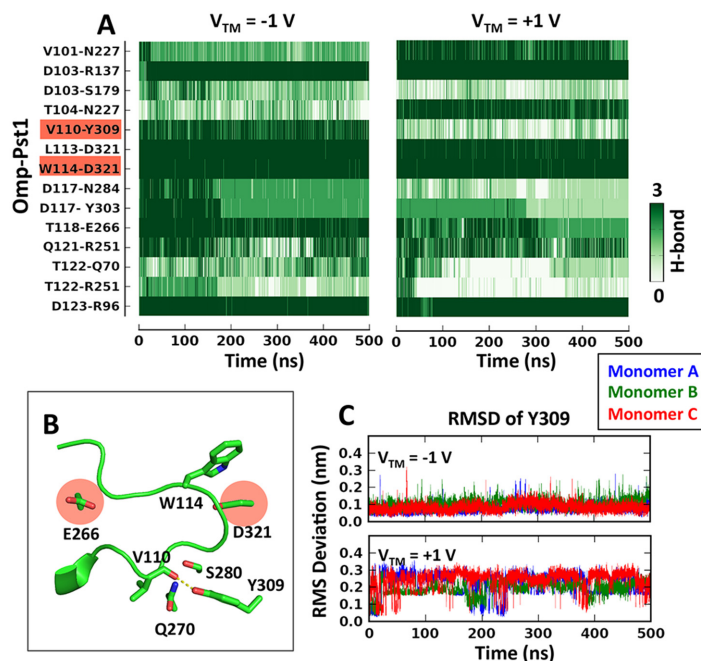
Fig 5. Hydrogen-bond network on Omp-Pst1 L3. (A) Hydrogen-bonds on L3 as a function of time. The color scheme is the same as in [Fig 4A](#). Hydrogen bonds V110-Y309 and W114-D321 are highlighted. (B) Structure of Omp-Pst1 L3. The hydrogen bond between V110 and Y309 highlighted in panel A is labeled out in dash lines. (C) RMS Deviation of Y309 as a function of time in three monomers at $V_{TM} = +/- 1$ V.

doi:10.1371/journal.pcbi.1004255.g005

The discrepancy in the voltage sensitivity can be rationalized by a comparative analysis of Omp-Pst1 and Omp-Pst2 structures. In Omp-Pst2, the tip of L3 is attached to the barrel wall solely through hydrogen bonding of L110 and W110 main chain nitrogens to D312, whereas the presence of Q270, S280 and Y309 in Omp-Pst1 contributes three additional hydrogen bonds that manifestly increase the energy barrier of exposing the acidic niches (Fig 5B). The lower sensitivity to voltage of Omp-Pst1 (S18 Fig) is thus encoded in the HBN holding L3 attached to the barrel wall. Of note, we also observed asymmetry in HBN resilience in simulations of Omp-Pst1. At $V_{TM} > 0$, and not at $V_{TM} < 0$, the hydrogen bond between Y309 and V110 is disrupted at the end of the simulation. Therefore, Omp-Pst1 could gate faster at this V_{TM} (Fig 5C). Opposed asymmetries in voltage sensitivity were reported earlier for *E. coli* OmpF and PhoE [10].

Discussion

This study reports on four 0.5 μs time-scale simulations conducted on the two porins from *P. stuartii*, *viz*. Omp-Pst1 and Omp-Pst2, at different transmembrane potentials. Under application of a negative transmembrane potential, we observed partial gating in one monomer of Omp-Pst2 (monomer B). Trajectory analysis revealed that a sequential changes on L3, including loop rearrangement and exposure of the hitherto hidden acidic niches, leads to protrusion of W11 side chain in the channel lumen. The presence of this large indol ring in the middle of the CZ hinders ion transit and results in the conductance of the monomer being decreased by ~50%. Based on curve fitting ($I(t) = a \times e^{-b \times t}$) to the calculated currents, we estimate that the time required for full closure is about tens of microseconds. Direct comparison from experiments under similar transmembrane potentials ($V_{TM} = \pm 1$ V) is not available, as lipid membranes do not withstand application of high voltages in experiments. However, we note that it was experimentally demonstrated that the time required for a bacterial porin to gate fully decreases exponentially as the applied voltage increases [6, 38]. Thus the estimated closing constant of Omp-Pst2 could be plausible. In the rest of our voltage-applied systems, stronger attachment of L3 loop onto the barrel wall was observed and the porins of study failed to undergo gating. We thus propose that the strength of this hydrogen bond network determines voltage sensitivity in the two porins from *P. stuartii*.

Based on our simulations, the most critical residues for porins (Omp-Pst2/1) gating are the acidic niches residues E258/E266 and D312/D321, on the one hand, and W111/W114 on the other hand. Sequence alignment with *E. coli* porins of known structures shows good conservation of these residues. First, all *E. coli* porins feature an aspartic acid at the position equivalent to D312 in Omp-Pst2 (niche II; *viz*. D312, D315 and D302 in OmpF, OmpC and PhoE, respectively). While E258 is not strictly conserved in terms of sequence position, negatively charged residues emanating from the barrel wall are found at other locations behind the L3 loop in *E. coli* porins, where they could contribute to an equivalent of niche I (E296 in OmpF; E260 and D299 in OmpC; E248 and D287 in PhoE) (S19B and S19C Fig). Also, an aromatic residue is found at the L3 tip of all *E. coli* porins (F118, F110 and F111 in OmpF, OmpC and PhoE, respectively) (S19A Fig). That residues critical for the voltage-gating of Omp-Pst2 are highly conserved in *E. coli* porins suggests that our gating model could apply to them as well. Furthermore, the lower sensitivity to transmembrane potential of OmpF, OmpC and PhoE (~155, ~185 and ~135 mV, respectively) correlates with the higher stabilization of their L3 loop onto the barrel wall. *E. coli* porins indeed all feature an additional glutamic acid at the L3 tip (E117, E109 and E110 in OmpF, OmpC and PhoE, respectively), which reinforces the attachment of their L3 tip to the barrel wall by one (Y22 in PhoE) or two hydrogen bonds (Y22/Y22 and Y310/Y313 in OmpF/OmpC). Thus, our proposal that it is the strength of the HBN attaching the tip of L3 onto the

barrel wall that determines the likelihood of gating—and thus the sensitivity to voltage—is supported by examination of *E. coli* porins structures and by their Vc.

Further support to our proposed model for gating comes from mutagenesis data gathered on OmpF, which, similar to Omp-Pst2, is cation-selective. Replacement of acidic residues L3 (E117C) and niches residues (D312N, E296L, E296A and E296Q) by neutral ones, or stabilization of L3 by disulphide-bridge tethering onto the barrel wall (between E117C and A333C) [19, 22] both leads to increased Vc in OmpF. Reversely, replacement of basic residues in the anti L3 region (K16A, K16D, R42C, R82C, R132A, and R132D) [17, 18] leads to decreased Vc, as expected from a heavier trafficking of cations at the CZ—and thus an easier binding behind L3. That disulphide-tethering of L3 onto the barrel-wall does not suppress gating but merely increases the required voltage [20] is in accordance with our observation that gating does not require major conformation changes in L3, but a mere protrusion of an aromatic side chain in the channel lumen (here, W111 from Omp-Pst2). It needs to be acknowledged that fitting into our gating model mutagenesis data from anion-selective PhoE is less straightforward. While the critical residues are conserved (S19D Fig), mutagenesis data are pointing to the opposite direction, as discussed earlier [10, 15]. Mutation of residues involved in the attachment of the L3 tip to the barrel wall (E110C) or in the constitution of the acidic niche under L3 (E302C) indeed induce a decrease in Vc, while mutations of anti-L3 residues (R37C, R75C, R37C/R75C, K18C) all provoke an increase in Vc [15]. We believe that similar calculations need to be conducted on PhoE to provide an atomic level understanding of its possibly peculiar gating behaviour.

A tormenting question is whether voltage gating is a mere experimental artefact or underlies a functionally relevant regulatory mechanism. In early days, it was proposed that voltage gating could be a means by which porins that are mistakenly inserted into the inner membrane keep in the closed state [39, 40], because the Donnan potential of the outer membrane is $\leq$ -30 mV [39], while the inner membrane displays a transmembrane potential of about 160–200 mV (*i.e.* a value close to the Vc of most porins). Yet, the observation that Omp-Pst2 displays a strong propensity to gate (low Vc) suggests that this porin could, in the physiological context, rest in the gated state. That the gating propensity is asymmetric, and that this asymmetry correlates with the transportation of cations in an unfavourable direction—*i.e.* against the gradient of transmembrane potential—furthermore raises the question as to whether voltage gating conceals a role, for this porin, in the regulation of the cationic content of the periplasm. In humans, the primary habitat of *P. stuartii*, is the urinary tract, where the ammonium ($NH4^+$) concentration is high. As *P. stuartii* features a urease activity that degrades urea into ammonia and carbonate, the higher propensity of Omp-Pst2 to transport cations from the intracellular to the extracellular side could participate in cleansing the bacterial periplasm of abounding cations. That Omp-Pst2 display a strong propensity to gate when the cationic flux occurs from the extracellular to the intracellular side furthermore suggests an active participation in the regulation of cationic fluxes across the outer-membrane. As new contributions of porins to bacterial development are discovered [41, 42], the functional meaning of voltage gating requires to be re-visited. In this context, molecular dynamics simulations hold the promise of allowing functional insights at the atomic level of resolution, as shown by the present work.

Methods

System setup

The crystal structure of Omp-Pst1 and Omp-Pst2 were solved at 3.3 Å and 2.2 Å respectively (PDB code 4D64 and 4D65 respectively). The crystal packing revealed an organization as dimers of trimers, *viz.* two symmetric, face-to-face trimers. Chain A, B, and C of the crystal

structures were taken out and used as starting models for the simulations. To create the lipid bilayer whereto embed our porins during the simulations, we used dimyristoylphosphatidyl-choline (DMPC), as this lipid is of adequate length to model the thickness of a bacterial outer-membrane and has been used in a number of simulations studies on other bacterial porins [25, 43]. The bacterial outer-membrane is asymmetric, featuring lipopolysaccharides (LPS) on its extracellular leaflet. In our simulations, we did not use LPS, given that both experimental data collected on Omp-Pst1 and Omp-Pst2 reconstituted in LPS-containing bilayers and studies on other porins [44] established that the translocation properties of porins are not influenced by the presence of LPS. The trimeric structure of Omp-Pst1 and Omp-Pst2 were thus inserted into a pre-equilibrated lipid bilayer consisting of 512 DMPC by using the Perl script Inflate-GRO [45]. After the insertion, 58 DMPC were deleted, on the basis of steric clashes with the protein. In the final configuration, the area per lipid (APL) reached 60 Å^2. Lipid-embedded Omp-Pst1 and Omp-Pst2 were then wrapped with 51,943 and 51,976 water molecules, respectively, in a cubic simulation box of $13.7 \times 13.7 \times 13.7$ nm^3. Potassium and chloride ions were added to reach a salt concentration of 1 M, and adjusted to provide neutral simulation systems. The standard protonation state at neutral pH was used for charged residues.

Molecular dynamics simulation

Molecular dynamics simulations were performed using GROMACS 4.5 package [46], and all-atom CHARMM force field for proteins [47] and lipids [48]. The TIP3P model [49] was used for water molecules. In all simulations, periodic boundary conditions were used in x, y and z directions. Electrostatic interactions were computed using the particle mesh Ewald (PME) method [50]. A Fourier spacing of 0.11 nm was used to avoid spurious drifts in the center of mass of the system [28, 30]. The LINCS method [51] was used to restrain bond lengths, allowing integration steps of 2 fs and updating of the neighbor list every 5 fs (cut-off distance of 1.2 nm). Lennard-Jones and Coulomb cut-off distances were set to 1.4 and 1.2 nm, respectively.

To prepare the simulation systems, we used the following procedure. First, the initial configurations of the lipid-embedded Omp-Pst1 and Omp-Pst2 were optimized by four steps of energy minimization, during which positional restrains were imposed on i/ all none-hydrogen atoms, ii/ main-chain atoms, iii/ Cα atoms and iv/ no atoms. Thereby, maximum forces lesser than 100 kJ. mol^{-1}.nm^{-1} was attained. The two systems were then thermalized to 310 K in six steps of NPT ensemble, each lasting 500 ps. In the NPT ensembles, the pressure was kept constant at 1 bar independently on the x-y plane (containing the lipid bilayer) and the z-axis direction (normal to the lipid bilayer) by semi-isotropic coupling to a Parrinello-Rahman barostat with τ_P = 1.0 ps and a compressibility of 4.6×10^{-5} bar [52], while the temperature was maintained at the target temperatures (50 K, 100 K, 150 K, 200 K, 250 K, and 310 K) by weakly (τ_T = 0.1 ps) coupling lipids, protein and solvent separately to a V-rescale thermostat [53]. Each system was then subjected to another 1 ns NVT ensemble at 310 K. After equilibration, the two systems were coupled to a homogenous electrostatic field E aligned with the z-axis, allowing for the simulations with an artificial transmembrane potential (E = V_{TM}/L_Z) of either +1 or -1 V (extracellular to intracellular). As for controls, we also subjected the Omp-Pst1 and Omp-Pst2 simulation systems to NVT ensembles in the absence of an electrostatic field (V_{TM} = 0 V). Simulations at V_{TM} = 0 V were carried out for 100 ns while those at $V_{TM} \neq 0$ for 500 ns each. A recapitulation of the simulations is given in S1 Table.

Data analysis

Net ion permeation events and residency times within the channels were calculated using g_flux tool [54]. Ions that bound in niche I and II and the occupancy of the two niches were

counted using the GROMCAS tool of g_select. Ions were required to move from one side of the lipid to the other to count as a complete permeation event. The selectivity and conductance of Omp-Pst1 and Omp-Pst2 were determined by calculating the current-voltage relationship under different applied electric fields. In each simulation, the current contributed either by K^+ or Cl^- ions was determined through linear regression of the net ion crossing at every time interval of Δt = 50 ns. At each voltage, the total current was the sum of K^+ and Cl^- currents, and conductances were calculated as the slope of the current-voltage curves [55]. Voltage-specific ion selectivity was calculated by using the ratio of K^+ and Cl^- current at each voltage. Simulated ion diffusion coefficients were calculated from our 100 ns simulations at V_{TM} = 0. Diffusion coefficients obtained for K^+ and Cl^- were 1.83 cm^2/s and 1.86 cm^2/s in the simulation of Omp-Pst1, and 1.72 cm^2/s and 1.95 cm^2/s in the simulation of Omp-Pst2. The ratio of the experimentally determined diffusion coefficients (1.96 cm^2/s for K^+ and 2.02 cm^2/s for Cl^- [56]) to the calculated ones was used to get the corrected conductance. In practice, the K^+ and Cl^- currents were scaled by the ratio before calculation of the slope of the I-V curves. Ion densities within the channels (S4 Fig) were calculated using the density calculation module in MDAnalysis tool [57]. Hydrogen-bonding network analysis was performed using VMD (Figs 4A and 5A). Sequence alignments were performed using CLUSTALW. PhoE residue numbering was adjusted to fit the nomenclature used in previous papers [10, 15, 18].

Electrophysiology experiment setup

Planar lipid bilayers were formed according to the monolayer technique of Montal and Mueller [58]. The bilayer was formed across a hole that was about 50 μm in diameter in a 25 μm thick polytetrafluoroethylene (PTFE) film. A lipid bilayer was prepared by spreading 1 μL of a 5 mg/mL solution of 1,2-diphytanoyl-sn-glycero-3-phosphocholine in a solvent mixture of n-pentane in the aperture. Ag/AgCl electrodes were used to detect the ionic currents. The electrode on the *cis* side of the cell was grounded, whereas the other one on the *trans* side was connected to the headstage of an Axopatch 200B amplifier. Purified detergent-solubilized porins (1 ng/mL) were added to the *cis* side of the chamber in presence of 1M KCl, 20mM PO_4 pH 4 and inserted into the bilayer membrane by applying a 150–200 mV voltage. The recordings were made after diluting the same chamber with 1M KCl, 10mM HEPES pH 7.

Supporting Information

S1 Fig. RMS fluctuation. The root mean square fluctuation of protein main-chain atoms was calculated from the 500 ns trajectory in the voltage-applied systems and 100 ns in the non-voltage ones. Blue, green and red lines represent the values in monomer A, B and C respectively. Chain assignment was taken from the crystal structures. The L3 region is highlighted out in gray.
(TIF)

S2 Fig. Fluctuation of extracellular loops. The movements of extracellular loops were projected to the 1st eigenvector of the whole protein in each system. Snapshots were taken every 100 ns.
(TIF)

S3 Fig. Net ion permeation. The cumulative number of K^+ or Cl^- crossing events in each monomer is traced as function of time. In each panel, blue, green and red lines represent crossing events in monomer A, B and C respectively.
(TIF)

S4 Fig. Ion density maps within the channel. The ion density was averaged from the first 100 ns simulations. Heavy ion densities are observed in the constriction zone of Omp-Pst1 and both constriction zone and extracellular vestibule of Omp-Pst2. The red and blue contour surfaces are the Cl- and the K+ ions density of 0.003 Å^{-3} respectively. Each β-barrel denotes one of the three monomers.
(TIF)

S5 Fig. Currents in Omp-Pst2 monomer B at negative voltage. Blue and red dots denote values for K$^+$ and Cl$^-$ respectively. Black dots are the totally currents of K$^+$ and Cl$^-$ combined. Currents were calculated every 50 ns.
(TIF)

S6 Fig. L3 movements of Omp-Pst2 monomer C at negative voltage. (A) Snapshots of L3 tip. In each snapshots, residues W104 to D117 are shown in cartoon; W111, D114, E258 and D312 in sticks; and K$^+$ within 3.5 Å of the tip in blue spheres. The acidic niche I (E258) and niche II (D312) are highlighted in gray. (B) W111 movements taken every 50 ns. The RMSD of 112-AG-113 (C), the phi/psi angle of W111 (D) and the RMSD of W111 (E) are laid out to show the sequential events of exposure and binding of the two niches under L3 (F).
(TIF)

S7 Fig. L3 movements of Omp-Pst2 monomer A at negative voltage. (A) Snapshots of L3 tip. In each snapshots, residues W104 to D117 are shown in cartoon; W111, D114, E258 and D312 in sticks; and K$^+$ within 3.5 Å of the tip in blue spheres. The acidic niche I (E258) and niche II (D312) are highlighted in gray. (B) W111 movements taken every 50 ns. The RMSD of 112-AG-113 (C), the phi/psi angle of W111 (D) and the RMSD of W111 (E) are laid out to show the sequential events of exposure and binding of the two niches under L3 (F).
(TIF)

S8 Fig. L3 movements of Omp-Pst2 monomer A at positive voltage. (A) Snapshots of L3 tip. In each snapshots, residues W104 to D117 are shown in cartoon; W111, D114, E258 and D312 in sticks; and K$^+$ within 3.5 Å of the tip in blue spheres. The acidic niche I (E258) and niche II (D312) are highlighted in gray. (B) W111 movements taken every 50 ns. The RMSD of 112-AG-113 (C), the phi/psi angle of W111 (D) and the RMSD of W111 (E) are laid out to show the sequential events of exposure and binding of the two niches under L3 (F).
(TIF)

S9 Fig. L3 movements of Omp-Pst2 monomer B at positive voltage. (A) Snapshots of L3 tip. In each snapshots, residues W104 to D117 are shown in cartoon; W111, D114, E258 and D312 in sticks; and K$^+$ within 3.5 Å of the tip in blue spheres. The acidic niche I (E258) and niche II (D312) are highlighted in gray. (B) W111 movements taken every 50 ns. The RMSD of 112-AG-113 (C), the phi/psi angle of W111 (D) and the RMSD of W111 (E) are laid out to show the sequential events of exposure and binding of the two niches under L3 (F).
(TIF)

S10 Fig. L3 movements of Omp-Pst2 monomer C at positive voltage. (A) Snapshots of L3 tip. In each snapshots, residues W104 to D117 are shown in cartoon; W111, D114, E258 and D312 in sticks; and K$^+$ within 3.5 Å of the tip in blue spheres. The acidic niche I (E258) and niche II (D312) are highlighted in gray. (B) W111 movements taken every 50 ns. The RMSD of 112-AG-113 (C), the phi/psi angle of W111 (D) and the RMSD of W111 (E) are laid out to show the sequential events of exposure and binding of the two niches under L3 (F).
(TIF)

S11 Fig. Gating of Omp-Pst1 and Omp-Pst2 in planar lipid bilayer. Representative ion current trace and their corresponding histograms show three-step voltage gating of Omp-Pst1 at -199 mV (A) and Omp-Pst2 at -50 mV (B). Buffer conditions: 1M KCl, 10 mM HEPES at pH 7. (TIF)

S12 Fig. L3 movements of Omp-Pst1 monomer A at negative voltage. (A) Snapshots of L3 tip. In each snapshots, residues W107 to D120 are shown in cartoon; W114, D117, E266 and D321 in sticks; and K^+ within 3.5 Å of the tip in blue spheres. The acidic niche I (E266) and niche II (D321) are highlighted in gray. (B) W111 movements taken every 50 ns. The RMSD of 115-AG-116 (C), the phi/psi angle of W114 (D) and the RMSD of W114 (E) are laid out to show the sequential events of exposure and binding of the two niches under L3 (F). (TIF)

S13 Fig. L3 movements of Omp-Pst1 monomer B at negative voltage. (A) Snapshots of L3 tip. In each snapshots, residues W107 to D120 are shown in cartoon; W114, D117, E266 and D321 in sticks; and K^+ within 3.5 Å of the tip in blue spheres. The acidic niche I (E266) and niche II (D321) are highlighted in gray. (B) W111 movements taken every 50 ns. The RMSD of 115-AG-116 (C), the phi/psi angle of W114 (D) and the RMSD of W114 (E) are laid out to show the sequential events of exposure and binding of the two niches under L3 (F). (TIF)

S14 Fig. L3 movements of Omp-Pst1 monomer C at negative voltage. (A) Snapshots of L3 tip. In each snapshots, residues W107 to D120 are shown in cartoon; W114, D117, E266 and D321 in sticks; and K^+ within 3.5 Å of the tip in blue spheres. The acidic niche I (E266) and niche II (D321) are highlighted in gray. (B) W111 movements taken every 50 ns. The RMSD of 115-AG-116 (C), the phi/psi angle of W114 (D) and the RMSD of W114 (E) are laid out to show the sequential events of exposure and binding of the two niches under L3 (F). (TIF)

S15 Fig. L3 movements of Omp-Pst1 monomer A at positive voltage. (A) Snapshots of L3 tip. In each snapshots, residues W107 to D120 are shown in cartoon; W114, D117, E266 and D321 in sticks; and K^+ within 3.5 Å of the tip in blue spheres. The acidic niche I (E266) and niche II (D321) are highlighted in gray. (B) W111 movements taken every 50 ns. The RMSD of 115-AG-116 (C), the phi/psi angle of W114 (D) and the RMSD of W114 (E) are laid out to show the sequential events of exposure and binding of the two niches under L3 (F). (TIF)

S16 Fig. L3 movements of Omp-Pst1 monomer B at positive voltage. (A) Snapshots of L3 tip. In each snapshots, residues W107 to D120 are shown in cartoon; W114, D117, E266 and D321 in sticks; and K^+ within 3.5 Å of the tip in blue spheres. The acidic niche I (E266) and niche II (D321) are highlighted in gray. (B) W111 movements taken every 50 ns. The RMSD of 115-AG-116 (C), the phi/psi angle of W114 (D) and the RMSD of W114 (E) are laid out to show the sequential events of exposure and binding of the two niches under L3 (F). (TIF)

S17 Fig. L3 movements of Omp-Pst1 monomer C at positive voltage. (A) Snapshots of L3 tip. In each snapshots, residues W107 to D120 are shown in cartoon; W114, D117, E266 and D321 in sticks; and K^+ within 3.5 Å of the tip in blue spheres. The acidic niche I (E266) and niche II (D321) are highlighted in gray. (B) W111 movements taken every 50 ns. The RMSD of 115-AG-116 (C), the phi/psi angle of W114 (D) and the RMSD of W114 (E) are laid out to show the sequential events of exposure and binding of the two niches under L3 (F). (TIF)

177

S18 Fig. Gating of Omp-Pst2 at -20 mV in planar lipid bilayer. Upper panel: the ion current trace; Lower panel: the corresponding histograms of the current trace. Buffer conditions: 1M KCl, 10 mM HEPES at pH 7.
(TIF)

S19 Fig. Sequence and structure conservation between Omp-Psts and the *E. coli* general diffusion porins. A) Sequence alignment of L3 of Omp-Pst1, Omp-Pst2, OmpF, OmpC and PhoE. Identical residues are highlighted in red and similar residues in gray. The residue that the blue triangle points out is the conserved aromatic residue at L3 tip. B) L3 tip of OmpF, OmpC and PhoE. The conserved aromatic residues are shown in sticks; the glutamic acid and the residue(s) it form hydrophone-bonding(s) with in sticks; and the main contributors of the acidic niches beneath L3 in sticks and highlighted in gray.
(TIF)

S1 Table. System configurations.
(DOCX)

Acknowledgments

Author Contributions

Conceived and designed the experiments: YX JPC WS HJ. Performed the experiments: WS HB MW CN. Analyzed the data: WS JPC. Wrote the paper: WS JPC.

References

1. Cowan SW, Schirmer T, Rummel G, Steiert M, Ghosh R, Pauptit RA, et al. Crystal structures explain functional properties of two E. coli porins. Nature. 1992; 358:727–733. PMID: 1380671

2. Baslé A, Rummel G, Storici P, Rosenbusch JP, Schirmer T. Crystal Structure of Osmoporin OmpC from E. coli at 2.0 Å. J Mol Biol. 2006; 362:933–942. PMID: 16949612

3. Karshikoff A, Spassov V, Cowan SW, Ladenstein R, Schirmer T. Electrostatic properties of two porin channels from Escherichia coli. J Mol Biol. 1994; 240:372–384. PMID: 8035460

4. Pezeshki S, Chimerel C, Bessonov AN, Winterhalter M, Kleinekathofer U. Understanding ion conductance on a molecular level: an all-atom modeling of the bacterial porin OmpF. Biophys J. 2009; 97:1898–1906. doi: 10.1016/j.bpj.2009.07.018 PMID: 19804720

5. Mathes A, Engelhardt H. Voltage-dependent closing of porin channels: analysis of relaxation kinetics. J Membr Biol. 1998; 165:11–18. PMID: 9705978

6. Jones CM, Taylor DM. Voltage gating of porin channels in lipid bilayers. Thin Solid Films. 1996; 284–285:748–751.

7. Xu G, Shi B, McGroarty EJ, Ti Tien H. Channel-closing activity of porins from Escherichia coli in bilayer lipid membranes. BBA Biomembranes. 1986; 862:57–64. PMID: 2429702

8. Lakey JH, Pattus F. The voltage-dependent activity of Escherichia coli porins in different planar bilayer reconstitutions. Eur J Biochem. 1989; 186:303–308. PMID: 2480894

9. Morgan H, Lonsdale JT, Alder G. Polarity-dependent voltage-gated porin channels from Escherichia coli in lipid bilayer membranes. BBA Biomembranes. 1990; 1021:175–181. PMID: 1689179

10. Samartzidou H, Delcour AH. E.coli PhoE porin has an opposite voltage-dependence to the homologous OmpF. EMBO J. 1998; 17:93–100. PMID: 9427744

11. Todt JC, McGroarty EJ. Acid PH decreases OMPF and OMPC channel size in vivo. Biochem Biophys Res Commun. 1992; 189:1498–1502. PMID: 1482362

12. Nestorovich EM, Rostovtseva TK, Bezrukov SM. Residue Ionization and Ion Transport through OmpF Channels. Biophys J. 2003; 85:3718–3729. PMID: 14645063

13. Delcour AH, Adler J, Kung C, Martinac B. Membrane-derived oligosaccharides (MDO's) promote closing of an E. coli porin channel. FEBS Lett. 1992; 304:216–220. PMID: 1377642

14. Basle A, Iyer R, Delcour AH. Subconductance states in OmpF gating. Biochim Biophys Acta. 2004; 1664:100–107. PMID: 15238263

15. Van Gelder P, Saint N, Phale P, Eppens EF, Prilipov A, van Boxtel R, et al. Voltage sensing in the PhoE and OmpF outer membrane porins of Escherichia coli: role of charged residues. J Mol Biol. 1997; 269:468–472. PMID: 9217251

16. Basle A, Qutub R, Mehrazin M, Wibbenmeyer J, Delcour AH. Deletions of single extracellular loops affect pH sensitivity, but not voltage dependence, of the Escherichia coli porin OmpF. Protein Eng Des Sel. 2004; 17:665–672. PMID: 15469993

17. Bredin J, Saint N, Mallea M, De E, Molle G, Pages JM, et al. Alteration of pore properties of Escherichia coli OmpF induced by mutation of key residues in anti-loop 3 region. Biochem J. 2002; 363:521–528. PMID: 11964152

18. Saint N, Lou KL, Widmer C, Luckey M, Schirmer T, Rosenbusch JP. Structural and functional characterization of OmpF porin mutants selected for larger pore size. II. Functional characterization. J Biol Chem. 1996; 271:20676–20680. PMID: 8702817

19. Phale PS, Schirmer T, Prilipov A, Lou KL, Hardmeyer A, Rosenbusch JP. Voltage gating of Escherichia coli porin channels: role of the constriction loop. Proc Natl Acad Sci U S A. 1997; 94:6741–6745. PMID: 9192635

20. Bainbridge G, Mobasheri H, Armstrong GA, Lea EJ, Lakey JH. Voltage-gating of Escherichia coli porin: a cystine-scanning mutagenesis study of loop 3. J Mol Biol. 1998; 275:171–176. PMID: 9466900

21. Eppens EF, Saint N, Van Gelder P, van Boxtel R, Tommassen J. Role of the constriction loop in the gating of outer membrane porin PhoE of Escherichia coli. FEBS Lett. 1997; 415:317–320. PMID: 9357991

22. Phale PS, Philippsen A, Widmer C, Phale VP, Rosenbusch JP, Schirmer T. Role of charged residues at the OmpF porin channel constriction probed by mutagenesis and simulation. Biochemistry. 2001; 40:6319–6325. PMID: 11371193

23. Tieleman DP, Berendsen HJ. A molecular dynamics study of the pores formed by Escherichia coli OmpF porin in a fully hydrated palmitoyloleoylphosphatidylcholine bilayer. Biophys J. 1998; 74:2786–2801. PMID: 9635733

24. Im W, Roux B. Ion permeation and selectivity of OmpF porin: a theoretical study based on molecular dynamics, Brownian dynamics, and continuum electrodiffusion theory. J Mol Biol. 2002; 322:851–869. PMID: 12270719

25. Im W, Roux Bt. Ions and Counterions in a Biological Channel: A Molecular Dynamics Simulation of OmpF Porin from Escherichia coli in an Explicit Membrane with 1M KCl Aqueous Salt Solution. J Mol Biol. 2002; 319:1177–1197. PMID: 12079356

26. Varma S, Chiu SW, Jakobsson E. The influence of amino acid protonation states on molecular dynamics simulations of the bacterial porin OmpF. Biophys J. 2006; 90:112–123. PMID: 16183883

27. Roux B, Allen T, Berneche S, Im W. Theoretical and computational models of biological ion channels. Q Rev Biophys. 2004; 37:15–103. PMID: 17390604

28. Aksimentiev A, Schulten K. Imaging alpha-hemolysin with molecular dynamics: ionic conductance, osmotic permeability, and the electrostatic potential map. Biophys J. 2005; 88:3745–3761. PMID: 15764651

29. Roux B. The membrane potential and its representation by a constant electric field in computer simulations. Biophys J. 2008; 95:4205–4216. doi: 10.1529/biophysj.108.136499 PMID: 18641071

30. Faraudo J, Calero C, Aguilella-Arzo M. Ionic partition and transport in multi-ionic channels: a molecular dynamics simulation study of the OmpF bacterial porin. Biophys J. 2010; 99:2107–2115. doi: 10.1016/j.bpj.2010.07.058 PMID: 20923644

31. Tran QT, Mahendran KR, Hajjar E, Ceccarelli M, Davin-Regli A, Winterhalter M, et al. Implication of porins in beta-lactam resistance of Providencia stuartii. J Biol Chem. 2010; 285:32273–32281. doi: 10.1074/jbc.M110.143305 PMID: 20667831

32. Danelon C, Suenaga A, Winterhalter M, Yamato I. Molecular origin of the cation selectivity in OmpF porin: single channel conductances vs. free energy calculation. Biophys Chem. 2003; 104:591–603. PMID: 12914905

33. Biro I, Pezeshki S, Weingart H, Winterhalter M, Kleinekathofer U. Comparing the temperature-dependent conductance of the two structurally similar E. coli porins OmpC and OmpF. Biophys J. 2010; 98:1830–1839. doi: 10.1016/j.bpj.2010.01.026 PMID: 20441746

34. Modi N, Barcena-Uribarri I, Bains M, Benz R, Hancock RE, Kleinekathofer U. Role of the Central Arginine R133 toward the Ion Selectivity of the Phosphate Specific Channel OprP: Effects of Charge and Solvation. Biochemistry. 2013.

35. Modi N, Benz R, Hancock REW, Kleinekathöfer U. Modeling the Ion Selectivity of the Phosphate Specific Channel OprP. J Phys Chem Lett. 2012; 3:3639–3645.

36. Berrier C, Coulombe A, Houssin C, Ghazi A. Fast and slow kinetics of porin channels from Escherichia coli reconstituted into giant liposomes and studied by patch-clamp. FEBS Lett. 1992; 306:251–256. PMID: 1633882

37. Berrier C, Besnard M, Ghazi A. Electrophysiological characteristics of the PhoE porin channel from Escherichia coli. Implications for the possible existence of a superfamily of ion channels. J Membr Biol. 1997; 156:105–115. PMID: 9075642

38. Bishop ND, Lea EJ. Characterisation of the porin of Rhodobacter capsulatus 37b4 in planar lipid bilayers. FEBS Lett. 1994; 349:69–74. PMID: 7519149

39. Nikaido H. Molecular basis of bacterial outer membrane permeability revisited. Microbiol Mol Biol Rev. 2003; 67:593–656. PMID: 14665678

40. Sen K, Hellman J, Nikaido H. Porin channels in intact cells of Escherichia coli are not affected by Donnan potentials across the outer membrane. J Biol Chem. 1988; 263:1182–1187. PMID: 2447086

41. Prehna G, Zhang G, Gong X, Duszyk M, Okon M, McIntosh LP, et al. A protein export pathway involving Escherichia coli porins. Structure. 2012; 20:1154–1166. doi: 10.1016/j.str.2012.04.014 PMID: 22658749

42. Ritter A, Com E, Bazire A, Goncalves Mdos S, Delage L, Le Pennec G, et al. Proteomic studies highlight outer-membrane proteins related to biofilm development in the marine bacterium Pseudoalteromonas sp. D41. Proteomics. 2012; 12:3180–3192. doi: 10.1002/pmic.201100644 PMID: 22965736

43. Kutzner C, Grubmuller H, de Groot BL, Zachariae U. Computational electrophysiology: the molecular dynamics of ion channel permeation and selectivity in atomistic detail. Biophys J. 2011; 101:809–817. doi: 10.1016/j.bpj.2011.06.010 PMID: 21843471

44. Wiese A, Schroder G, Brandenburg K, Hirsch A, Welte W, Seydel U. Influence of the lipid matrix on incorporation and function of LPS-free porin from Paracoccus denitrificans. Biochim Biophys Acta. 1994; 1190:231–242. PMID: 8142421

45. Kandt C, Ash WL, Tieleman DP. Setting up and running molecular dynamics simulations of membrane proteins. Methods. 2007; 41:475–488. PMID: 17367719

46. Hess B, Kutzner C, van der Spoel D, Lindahl E. GROMACS 4: Algorithms for Highly Efficient, Load-Balanced, and Scalable Molecular Simulation. J Chem Theory Comput. 2008; 4:435–447.

47. MacKerell AD, Bashford D, Bellott M, Dunbrack RL, Evanseck JD, Field MJ, et al. All-atom empirical potential for molecular modeling and dynamics studies of proteins. J Phys Chem B. 1998; 102:3586–3616. doi: 10.1021/jp973084f PMID: 24889800

48. Feller SE, Yin D, Pastor RW, MacKerell AD Jr. Molecular dynamics simulation of unsaturated lipid bilayers at low hydration: parameterization and comparison with diffraction studies. Biophys J. 1997; 73:2269–2279. PMID: 9370424

49. Jorgensen WL, Chandrasekhar J, Madura JD, Impey RW, Klein ML. Comparison of simple potential functions for simulating liquid water. J Chem Phys. 1983; 79:926–935.

50. Darden T, York D, Pedersen L. Particle mesh Ewald: An N· log (N) method for Ewald sums in large systems. J Chem Phys. 1993; 98:10089.

51. Hess B, Bekker H, Berendsen HJ, Fraaije JG. LINCS: a linear constraint solver for molecular simulations. J Comput Chem. 1997; 18:1463–1472.

52. Martonak R, Laio A, Parrinello M. Predicting crystal structures: the Parrinello-Rahman method revisited. Phys Rev Lett. 2003; 90:075503. PMID: 12633242

53. Bussi G, Donadio D, Parrinello M. Canonical sampling through velocity rescaling. J Chem Phys. 2007; 126:014101. PMID: 17212484

54. Beckstein O, Sansom MSP. The influence of geometry, surface character, and flexibility on the permeation of ions and water through biological pores. Phys Biol. 2004; 1:42. PMID: 16204821

55. Hogg DW, Bovy J, Lang D. Data analysis recipes: Fitting a model to data. arXiv preprint arXiv:10084686. 2010.

56. Hille B. Ion channels of excitable membranes: Sinauer Sunderland, MA; 2001.

57. Michaud-Agrawal N, Denning EJ, Woolf TB, Beckstein O. MDAnalysis: A toolkit for the analysis of molecular dynamics simulations. J Comput Chem. 2011; 32:2319–2327. doi: 10.1002/jcc.21787 PMID: 21500218

58. Montal M, Mueller P. Formation of bimolecular membranes from lipid monolayers and a study of their electrical properties. Proc Natl Acad Sci U S A. 1972; 69:3561–3566. PMID: 4509315

180